The University of Leeds

Faculty of Medicine and Health

Leeds Institute of Cardiovascular and Metabolic Medicine

LICAMM

Rab46-dependent trafficking in endothelial cells requires calcium release from NAADP-sensitive channels

Ryan David Murray BSc (Hons), MSc (MedSci)

March 2025

Thesis is submitted to the University of Leeds in accordance with the requirements for the degree of Doctor of Philosophy (PhD)

Funded by the British Heart Foundation

Intellectual Property and Publication Statements

(i) I confirm that the work submitted is my own and that appropriate credit has been duly given where reference has been made to the work of others.

(ii) This copy has been supplied on the understanding that it is copyright material and that no quotation from this thesis may be published without proper acknowledgement.

(iii) “The right of Ryan David Murray to be identified as the sole author of this work has been asserted by Ryan David Murray by the *Copyright, Designs and Patents Act 1988.”*

Acknowledgements

It is hard to believe I am writing this heartfelt thank you after starting university in Dundee all those years ago! This PhD journey has been made possible by the incredible support system of friends and family who kept me going.

Firstly, a massive thank you to my principal supervisor, Dr. Lynn McKeown. Your unwavering kindness and motivation throughout my studies were invaluable. Thank you for being there through the ups and downs, for your guidance, and for those much-needed after-work chats. I will always be grateful for your belief in me and will deeply miss being part of the McKeown lab.

Thank you also to Prof. David Beech for your ongoing support and for always lending an ear.

To the wonderful LICAMM BHF group, thank you for the daily lunchtime chats and the much-needed moral support. Jess, Eva, Hannah, Anna, Cella, Daisie, Beth, Kasia, Emily, and Michael, your endless laughter got me through it all – our friendship means the world.

To the past and present McKeown lab members, Harriet, where do I even begin? You have been the best support, from emotional coffees to countless repeated experiments and all the laughs in between. Melissa, though our time was shorter, I know you will do amazing – thank you.

My amazing Liverpool best friends, Sophie, Elle, Regan, and Emma, your unconditional love and countless visits over the last three years kept me going. You are the best friends a person could ask for! Sláinte to you all.

To Hannah, Ellie, and Alison, my "troops," thank you for always being there and encouraging me on this academic adventure. Chloe, your light always brightened my day, and I am eternally grateful for your kindness. Grá. Jen, your constant support, and ability to pick me up after lab setbacks were invaluable – thank you. Rory, thank you for the lifts, friendship, and pints! You are a good egg.

My dearest partner, Cameron, thank you for being my rock and for your unwavering support through those long train journeys. I am so grateful for your help in keeping me on track.

To my incredible Mum, Dad, Aunties, Grandpa, and Papa, thank you for being there every step of the way throughout these nine university years. Your wisdom, uplifting words, support, and family moments have been cherished.

Bethany, Liam, Julie M, Jason, Julie Mc, Noah, Lee, Sandra, and Billy, thank you for being the best second family anyone could ask for over the last seven years. It is a true blessing to have you all.

Finally, my deepest gratitude to the British Heart Foundation for their invaluable support and funding. Without it, this research would not have been possible. I am honoured to have benefited from their commitment to advancing cardiovascular health.

Abstract

The endothelium plays a vital role in haemostasis yet is susceptible to dysfunction. This vascular bed contains a monolayer of cells capable of modulating inflammation. Endothelial cells (ECs) contain potent, bioactive cargo stored within specific storage organelles termed Weibel-Palade bodies (WPBs). These contain the pro-thrombotic and pro-inflammatory mediators, angiopoietin-2 (Ang2) and P-selectin which are differentially released in response to vasoactive stimuli. Thrombin (released after vascular injury) or histamine (immunogenic assault) promote WPB cargo release and WPB dysregulation can contribute to an adverse environment, as evidenced in cardiovascular disease.

Rab46 has been shown to localise to Ang2-positive WPBs and is implicated in the regulation of differential cargo release. Rab46 is necessary for the acute immunogenic histamine, but not thrombin, trafficking of these WPBs to the Microtubule Organising Centre (MTOC). This retrograde movement of Rab46 is dependent on dynein motor interactions yet occurs independently of Ca^{2+}. The detachment of Rab46 from the MTOC is a Ca^{2+}-dependent process where Ca^{2+} binds the EF-hand domain of Rab46 and this source of Ca^{2+} has been the subject of ongoing investigation. Histamine stimulation elicits a rapid upregulation of nicotinic acid adenine dinucleotide phosphate (NAADP) within ECs, which is a potent second Ca^{2+} messenger that targets small, acidic intracellular Ca^{2+} stores on the endo-lysosomal system.

Nicotinic acid adenosine dinucleotide phosphate (NAADP) has been shown to indirectly bind via accessory proteins to various lysosomal Ca^{2+} channels, Two-pore channel 1 (TPC1), Two-pore channel 2 (TPC2) and Transient potential receptor mucolipin 1 (TPRML1) and are candidates for the modulation of Ca^{2+} signals generated via NAADP to refill or empty the lysosomal Ca^{2+} pool. Activation of these channels can elicit global Ca^{2+} rises in cells through Ca^{2+}-induced- Ca^{2+} release (CICR) exploiting the ER Ca^{2+} pool as a mechanism to potentiate Ca^{2+} efflux from lysosomes. Understanding the Ca^{2+} channels involved in Rab46 dispersal from the MTOC is crucial for elucidating how ECs modulate their secretory response, particularly Ang2 secretion.

Table of Contents

List of Figures

List of Tables

Abbreviations

AGE	Advanced glycation end-products
Ang2	Angiopoietin-2
CRAC	Calcium-Release-Activated Calcium
CVD	Cardiovascular disease
cDNA	Complementary DNA
ER	Endoplasmic reticulum
EBM-2	Endothelial cell basal medium
FBS	Foetal bovine serum
FCS	Foetal calf serum
GDF	GDI-displacement factor
GDI	GDP-dissociation inhibitor
GFP	Green fluorescent protein
GAP	GTPase activating protein
GDP	Guanosine diphosphate
GEF	Guanosine nucleotide exchange factor
hAEC	Human aortic endothelial cells
HMW	High molecular weight
HUVEC	Human umbilical vein endothelial cells
IP_3	Inositol trisphosphate
k/d	Knockdown
KO	Knockout
MTOC	Microtubule organising centre
MLIV	Mucolipidosis type IV
Na^+	Sodium
NADP	Nicotinamide adenine dinucleotide phosphate
NAADP	Nicotinic acid adenine dinucleotide phosphate
NAFLD	Non-alcoholic fatty liver disease
NSE	NAADP-synthesising enzymes
$PI(3,5)P_2$	Phosphatidylinositol 3,5-bisphosphate
PFA	Paraformaldehyde
PBS	Phosphate buffered saline

RT-qPCR	Quantitative reverse transcription polymerase chain reaction
REP	Rab escort protein
RabGGT	Rab-Geranylgeranyl transferase
Rab	Ras-associated binding proteins
siRNA	Short interfering RNA
SNP	Single nucleotide polymorphism
SNARE	Soluble NSF Receptor
SOCE	Store-operated Ca^{2+} entry
STIM1	Stromal interaction molecule 1
TGN	Trans-Golgi network
tPA	Tissue plasminogen activator
VEGF	Vascular endothelial growth factor
VWD	von Willebrand disease
vWF	von Willebrand factor
WPBs	Weibel-Palade bodies
WT	Wild type

Publications and Communications

Publications

Cheng, C.W., Pedicini, L., Alcala, C.M., Deligianni, F., Smith, J., **Murray, R.D**., Todd, H.J., Forde, N., McKeown, L., 2025. RNA-seq analysis reveals transcriptome changes in livers from Efcab4b knockout mice. *Biochemistry and Biophysics Reports* 41, 101944.

Murray, R.D., Rose, M., Miteva, K.T., Beech, D.J., McKeown, L., 2025. Two-pore channel protein 2-mediated calcium release promotes angiopoietin 2 secretion by regulating Rab46-dependent Weibel-Palade body trafficking. *bioRxiv* 2025.03.03.641167; DOI: https://doi.org/10.1101/2025.03.03.641167.

Communications

The role of NAADP-dependent calcium release on Rab46 activity in endothelial cells. L. McKeown, **RD. Murray**, DJ. Beech, K. Miteva. 16th International Meeting of the European Calcium Society (ECS), Cork, Ireland (2022) **Poster**.

Rab46 function in endothelial cells requires NAADP-dependent calcium release. **RD. Murray**, L. McKeown, DJ. Beech, K. Miteva. Gordon Research Conference on Calcium Signalling (GRC), Lucca, Italy (2024) **Poster.**

Chapter. 1

Introduction

1.1 Endothelial cells (ECs)

1.1.1 EC function

The endothelium comprises a cellular monolayer that constitutes the innermost lining of the vasculature. Playing a crucial role in maintaining vital organ health and homeostasis, it operates dynamically to control vascular tone, angiogenesis, and haemostasis (Braun et al. 2017). Through modulation of these processes, it can maintain the anti-thrombotic/pro-thrombotic interface. Endothelial cells (ECs) play a pivotal role in vascular responses such as serving as the primary interface for the invagination of immune cells entering sites of infection as well as representing the primary cell type necessary for the process of new blood vessel formation (i.e. angiogenesis) (Figure 1.1) within the vasculature (Young, 2012). Beyond their role as dynamic regulators of vascular tone and haemostasis, ECs demonstrate remarkable morphological plasticity that has a direct impact on their functionality. They are explicitly exposed to blood flow and align in the direction of flow to minimise shear stress, however, at bifurcations (regions of disturbed flow) or in response to pathogenic stimuli (histamine or thrombin) they can alter their phenotype which can contribute to endothelial cell dysfunction (Hennigs et al. 2021; Chiu and Chien, 2011; Russo et al. 2020).

Due to the nature of the harsh environment endothelial cells are exposed to, it is no surprise that they are highly susceptible to dysfunction in disease. Alterations in cell surface molecule expression or morphology of endothelial cells play central roles in the pathogenesis and progression of various clinical conditions, be that cardiovascular in the case of heart failure, hypertension, or stroke or metabolic in that of diabetes, peripheral vascular disease, and kidney disease (Nishigaki et al. 2013). As a result of these pro-inflammatory conditions, the endothelium can degrade and become more permeable, allowing for infiltration

of inflammatory cells into the vessel lumen, which can lead to the initiation of signalling cascades that can promote plaque formation, a precursor to heart attacks and strokes (Buckley & Ramji, 2015). This intricate interplay between EC function, environment and morphology underpins their crucial role in modulating vascular health and preventing disease outcomes. This chapter aims to highlight the crucial role of ECs in the context of Ca^{2+} signalling and the trafficking of a novel large intracellular GTPase, Rab46. Firstly, I will discuss the physiology of the endothelium when its function is compromised by disease, highlighting conditions such as atherosclerosis and inflammation caused by thrombosis.

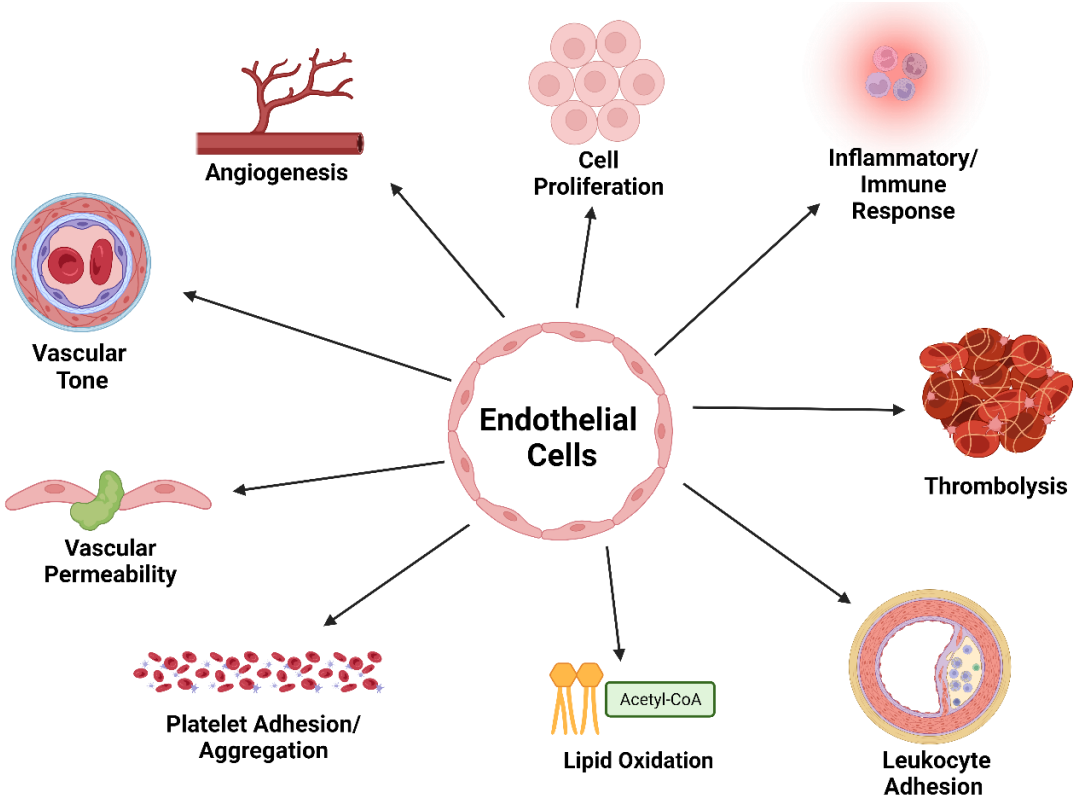

Figure 1.1 Physiological functions of ECs. ECs perform a plethora of functions in the body, with the most important being the maintenance of vascular tone, modulating the permeability of the vascular bed and growth processes such as vascular neo-angiogenesis, to form new blood vessels.

1.1.2 EC dysfunction

One of the most prominent downstream conditions affecting the endothelium is atherosclerosis. This condition is characterised by the build-up of fatty plaque deposits on the luminal surface of large blood vessels such as the aorta. The condition can be accelerated in the presence of cellular stress, and we now know that this condition shares prominent similarities to cardiovascular complications identified in diabetic individuals (Poznyak et al. 2020). These similarities include an increased production of advanced glycation end-products (AGEs) and oxidative stress which are known contributors to the clinical manifestation of cardiovascular disease (Hegab et al. 2012). In addition to endothelial dysfunction, increased secretion of von Willebrand Factor (vWF), observed in atherosclerosis can lead to platelet adhesion at sites of endothelial damage, further contributing to plaque formation. These elevated levels of vWF can initiate vascular remodelling, whereby vessels change in response to injury, worsening the outcome of the disease and this clinically has been associated with an increased risk of cardiovascular events such as heart attacks and stroke (Gragnano et al. 2017; Wu et al. 2017).

In healthy vessels, the endothelium modulates an equilibrium between opposing vasoactive factors that maintain vascular tone. Tilting this balance to be less haemostatic, induces an upregulation in vasoconstrictive components such as endothelin-1 (ET-1) and promotes thickening of the vessel lumen, thus promoting a hypertensive environment (Sandoo et al. 2010). There is evidence of EC damage within the vascular network in patients with hypertension however, it is not known for certain whether this is what directly drives EC dysfunction (Rajendran et al. 2013). Thrombosis is a highly inflammatory condition whereby processes such as angiogenesis are upregulated, leading to a rise in the release of Ang2. Under these pro-inflammatory conditions, the endothelium will release Ang2 to restore haemostasis through upregulation of neo-angiogenesis (formation of new blood vessels) and this plays a great deal of strain on the endothelium, thus is a highly monitored process to ensure the angiogenic response to tissue repair is controlled (Hinsbergh, 2011). P-selectin, a potent cell adhesion molecule, is also implicated in this inflammatory pathway, where it assists in the recruitment of leukocytes at sites of inflammation, such

as that of a thrombus. These potent bioactive cargoes are crucial in the modulation of endothelial cell dysfunction and serve as markers of inflammatory disease (Vandendries et al. 2004). ECs are multifactorial and are not only involved in the regulation of haemostasis, but also have active roles in maintaining vessel permeability, regulating tight junctions mediating the proliferation of vascular smooth muscle cells, and contributing to fibrinolysis in disease models, via tissue plasminogen activator (tPA) secretion (De Pablo-Moreno et al. 2022; Mussbacher et al. 2022). Thus, we scientists and clinicians can use the endothelium as a model to characterise the degree of deterioration in cardiometabolic health with disease and with increasing targeted research against EC dysfunction we are ever closer to developing future cardiovascular therapeutics. The various pro-inflammatory mediators discussed above are collectively stored in EC-specific storage organelles termed Weibel-Palade bodies (WPBs) and I will now provide context on how these differentially release their cargo in response to stimuli.

1.2 Weibel-Palade bodies (WPBs)

ECs contain unique secretory cellular organelles termed Weibel-Palade bodies (WPBs) that contain haemostatic, pro-angiogenic and inflammatory mediators. Close to 60 years ago, Edward Weibel and George Palade made an unexpected discovery whilst routinely investigating rat pulmonary arterial tissue under electron microscopy. They identified small, rod-shaped striated organelles measuring 0.5-5 μm localised to the cytoplasm of endothelial cells, which contained fine tubules enrobed in a tight-fitting membrane (Weibel & Palade,1964). Their discovery was initially note but gained significant attention in the 1990s when the Wagner group identified WPBs as the principal storage organelle for the haemostatic protein, von Willebrand Factor (vWF) which promotes platelet plug formation at sites of vessel injury (Figure 1.2). Using pro-vWF cDNA expression, they identified that the rod-shaped phenotype of WPBs was due to the multimeric storage of vWF and that pro-vWF is pivotal in the formation of vWF storage granules within ECs (Wagner, 1991). WPBs contain diverse and vital cargo that constitute both pro-thrombotic and pro-angiogenic responses, such as P-selectin (leukocyte adhesion), angiopoietin-2 (angiogenesis) and interleukin-8 (neutrophil recruitment) (Texier et al. 2023).

The biogenesis and regulation of these emergency response vesicles is essential for understanding vascular function in both health and disease. I will briefly discuss the biogenesis of WPBs and how vWF plays a crucial role in this pathway.

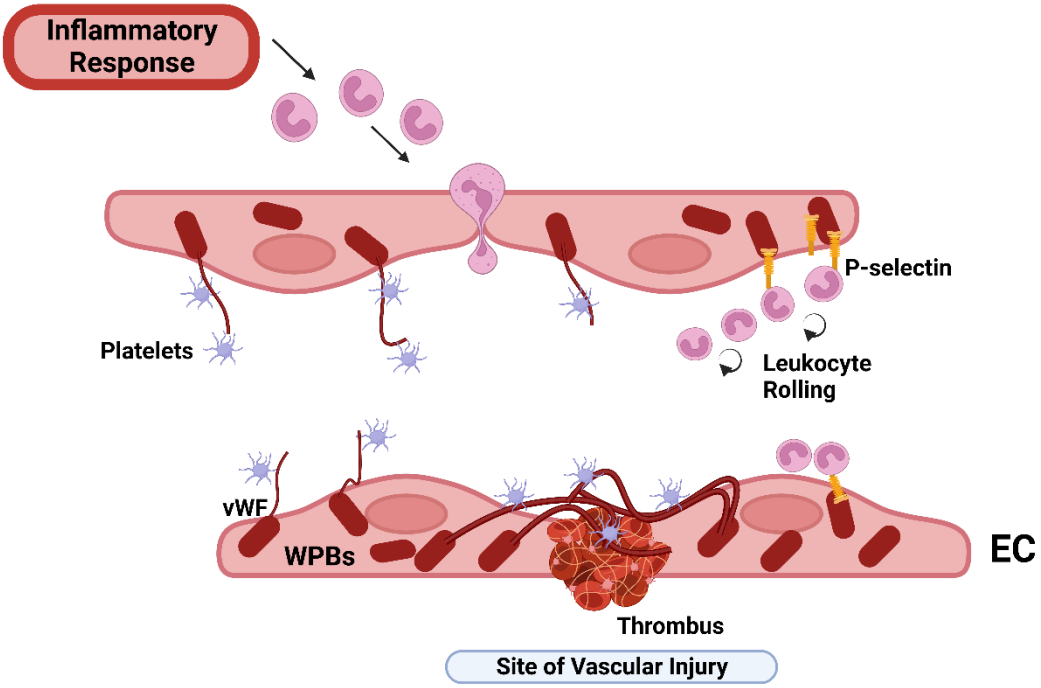

Figure 1.2 EC response to acute vascular injury. Inflammatory signals within the endothelium are detected by individual cells that then actively send out signals to recruit circulating leukocytes to the site of injury and bind to P-selectin at the cell surface, exocytosed from WPBs. These leukocytes then undergo rolling along with platelets that stick to vWF strings that are secreted from these WPBs. These then initiate platelet plug formation around the thrombus to prevent an acute thrombotic episode.

1.2.1 WPB cargo

WPBs are vascular first-aid kits containing a plethora of pro-inflammatory and pro-thrombotic cargo that are secreted from WPBs in a highly regulated process. This tight control is paramount as inappropriate or excessive release could have a detrimental effect on the endothelium. A summary of the various

cargo localised within WPBs is highlighted in Table 1.1. The process of cargo recruitment to WPBs is complex and is controlled by a complex interplay of signalling pathways.

1.2.1.1 vWF

WPBs are made in response to the expression of vWF, and this protein in the largest constituent protein located within WPBs. This large multimeric protein is synthesised in the endoplasmic reticulum (ER) and then inserted at a site within the Golgi apparatus where it undergoes multimerization, glycosylation and packaging. How it is packaged determines the size and shape of the final WPB (Ferraro et al. 2014; Valentijn et al. 2013). The ultra-large vWF multimers (preferentially selected for WPBs) are stored in a compact, folded coil conformation. Its functions upon exocytosis include the deployment of vWF strings, which unfurl to tether platelets and circulating vWF to arrest bleeding, as well as the establishment of the platelet plug at the site of vessel injury. The recruitment of vWF to WPBs is related to the expression of the TGN-associated AP-1 adaptor protein, which is crucial in the initial formation of WPBs at the Golgi (Nightingale et al. 2013).

1.2.1.2 P-selectin

vWF is considered a major driving force in the recruitment of P-selectin and Ang2 to WPBs. P-selectin is involved in the recruitment and adhesion of leukocytes by mediating the ‘rolling’ of leukocytes along the endothelium to sites of vascular inflammation. It is mutually stored within its activating ligand, P-selectin glycoprotein ligand-1 (PSGL-1), which upon release resides on the surface of leukocytes to facilitate adhesion (McEver, 2015; Escopy & Chaikof, 2024). The luminal domain of P-selectin has been shown to directly interact with D’-D3 domains of vWF to allow for sufficient incorporation into WPBs (Michaux et al. 2006). whilst multimerization of vWF is taking place, the formation of tubules creates a favourable environment where the Golgi favours the co-packaging of other mutually exclusive cargo to the WPB, demonstrating WPB heterogeneity, of which I will discuss later.

1.2.1.3 Ang2

Ang2 is a member of the Ang family, playing vital roles in angiogenesis and it is an antagonist for angiopoietin-1 (Ang1), whereby it acts to inhibit Ang1-directed Tie-2 signalling, which is a crucial pathway in the stabilisation of vascular beds (Hu and Cheng, 2009). In the context of the vasculature, Ang1 and Ang2 operate in a complement to maintain vascular function and vessel integrity. Early in-vitro studies found that Ang2 was both an antagonist and agonist of Tie-2 receptor signalling and was capable of modulating EC migration, survival, and the formation of new vascular networks (Jones et al. 2001; Shim et al. 2007). Ang2 is stored in an immobilised state bound to vWF inside WPBs where it has a generational half-life of around 18 hrs, making it a moderately stable protein in this conformation (Texier et al. 2023). The retention of Ang2 within WPBs permits immediate deployment in response to physiological stimulus, which emphasises its role in maintaining endothelial function, through striking a balance between pro- and anti-inflammatory signalling (Breevoort et al. 2012; Tirapelli et al. 2006). Ang2 is also thought to engage in direct interaction with vWF upon recruitment. Ang2 is said to become entrapped, associated with the growing vWF multimers during the maturation of WPBs (Texier et al. 2023). These cargo are potently bioactive and have opposing roles upon secretion, where for example, Ang2 has a functional role in the regulation of the angiogenic switch, causing a destabilisation of mature blood vessels, leading to an upregulation of neo-angiogenesis, and this is particularly apparent in response to release of vasoactive factors such as VEGF (Lugano et al. 2019).

1.2.1.4 Other cargo

In addition to the main cargo (vWF, Ang2 and P-selectin), the potent vasoconstrictor, Endothelin-1 (Table 1.1) is also stored with WPBs. It is packaged into WPBs during immature WPB formation in the Golgi, however, the exact method of recruitment is subject to further investigation (Valentijn et al. 2011). The primary and most well-known function of Endothelin-1 is its ability to constrict vessels, thereby maintaining blood pressure and regulating blood flow to various tissues. It is also implicated in angiogenesis, whereby it can contribute to the recruitment of inflammatory cells and modulate the secretion of

other vasoactive mediators (Banecki et al. 2023). These pro-inflammatory mediators have consequences clinically upon their release into the vasculature of which I will now provide evidence.

Table. 1.1 WPB constituent cargo

Protein	Functional Role
vWF	Haemostasis[6]
P-Selectin	Inflammation, leukocyte adhesion[7]
Interleukin 8 (IL-8)	Inflammation, granulocyte adhesion[8]
Angiopoeitin-2 (Ang2)	Inflammation, maintaining haemostasis[9,10]
Endothelin-1	Vasoconstriction[11,12]
CD63/LAMP-3	Cell adhesion/migration[13]
Tissue-type plasminogen activator (tPA)	Fibrinolysis[14,15]
Eotaxin-3	Eosinophil recruitment[16,17]
Osteoprotegerin	Vascular homeostasis[18]

1.2.2 Clinical significance of WPBs

Due to the extensive list of cargo contained within these small intracellular vesicles, it is no surprise that they are the subject of multiple disease pathologies. It is important to note here that the large haemostatic protein vWF is crucial for the biogenesis and maintenance of WPBs, thus, experimental depletion of vWF from ECs prevents WPB from forming (Mojzisch & Brehm, 2021). von Willebrand disease (VWD), is the world's most common bleeding disorder, with around every 10 in 100,000 people affected by the condition and is characterised by the inability of vWF to be produced and secreted on demand, preventing the initiation of primary haemostasis (Bharati & Prashanth, 2011). The disease can present with multiple phenotypes and various point mutations can directly affect vWF synthesis and lead to symptomatic VWD. The aetiology of the disease presents in one of three forms, the most common of these being Type 1, which is considered quantitative and mild resulting in a reduced serum level of vWF in the patient's blood. Type 2 is split into four

distinct categories (2A, 2B, 2M, and 2N) and is defined as the presence of dysfunctional vWF, highlighting a qualitative defect. Both Type 1 and Type 2 are autosomal dominant conditions, however, the defining clinical manifestation between them is the aberration of clotting in Type 2 leading to moderate bleeding. The rarest presentation is Type 3 which is denoted by autosomal recessive inheritance and accounts for less than 5% of all cases of VWD. It has detrimental quantitative effects on vWF expression i.e., a complete or near total loss of vWF (Ng et al. 2015). This can lead to serious internal bleeding and has a remarkably similar clinical aetiology to haemophilia, which can lead to misdiagnosis as noted by a case study highlighted in the Cote d'Ivoire population (Adjambri et al. 2020).

In addition to VWD, cargo such as Endothelin-1 has been shown to play roles in the pathogenesis of hypertension. Endothelin-1 is one of the most potent vasoconstrictors, and excessive release of this can lead to a narrowing of the arteries across the vasculature, forcing the heart to work even harder to pump blood around the body (Schiffrin, 2001). The excessive binding of Endothelin-1 to its receptor (ETA) leads to sustained vasoconstriction. This rise in blood pressure can lead to progression from hypertension to left ventricular hypertrophy, whereby the heart is pumping at a higher resistance, leading to an increased workload. Over time, this chronic elevation in Endothelin-1 leads to the thickening of the heart wall, terminating in the increased risk of heart failure (Banecki et al. 2023; Titus & Marappa-Ganeshan, 2023).

WPBs when activated normally mobilise P-selectin to the cell surface, where its primary role is to attach platelets and regulate their aggregation. Following this, it is internalised and broken down. However, conditions, such as atherosclerosis can lead to chronic release as characterised by the exacerbated recruitment of leukocytes to the vessel wall contributing to the formation of fatty streaks in the vessel lumen as well as the progression toward plaque formation, a major risk factor in a thrombotic episode associated with atherosclerosis (Valentijn et al. 2011). Studies have shown that this increased leukocyte adhesion can also destabilise platelets, leading to the formation of a pro-thrombotic environment, a risk factor for the development of ischemic stroke (Merten & Thiagarajan, 2000).

Ang2, when secreted from activated WPBs, can cause various downstream cellular effects, from modulating the de-stabilisation of Ang1 from the Tie-signalling pathway to working in concert with VEGF signalling to promote EC migration, characterised in atherosclerosis (Lobov et al. 2002). This can occur in coordination with response to vasoactive stimuli, such as thrombin, which induces an all-out vascular response in EC. Thrombin activates Ang2 to promote a pro-thrombotic, pro-atherogenic response, for example, in the event of thrombosis, whereby cells would need to undergo vascular remodelling. In the presence of thrombin, cells will release all their Ang2 to assist in the braking of vessel rupture or assist in the migration of cells to promote the assembly of new vessels (Lane et al. 2005; Huang et al. 2002). Angiopoietins play a huge role in disease, especially cancers, due to the dense vascular makeup of tumours. A major effort thus far investigating anti-angiogenic therapeutics has focused on anti-VEGF therapy, however, cancers are resistant to this due to complexities in the Tie-2/Ang2 signalling axis. Thus, studying angiogenic responses in an immune context may shed light on potential downstream therapeutics for vascular conditions (Pafumi et al. 2015; Bergers et al. 2008).

1.2.3 WPB biogenesis

WPBs are a heterogeneous population which confers a functional plasticity on them, important in the context of differential cargo secretion. Our lab has shown that at sites of vessel bifurcation (disturbed flow), there are changes in the morphology of WPBs and their cargo within these vascular beds is altered (e.g. increased WPBs containing Ang2) (Money et al. 2023). This in turn, confers alterations to the functioning of WPBs, i.e. vWF string length varied significantly in low oscillatory shear stress (disturbed flow) regions, thus are more prothrombotic and supports formation of atherosclerotic plaques. The initial biogenesis of WPBs is a tightly regulated process driven by various factors such as the recruitment of the vital cargo at the trans-Golgi network (TGN) and a secondary recruitment of critical integral and peripherally associated membrane proteins (Rab27a, Rab3D) to WPBs, driven by the AP1/AP3 membrane proteins and the formation of di-sulphide bonds and cleavage of the vWF pro-peptide (Cutler, 2008). vWF is synthesised in ECs as a single pre-polypeptide in the TGN and as mentioned above contains a high concentration of cysteine

residues that contribute to disulphide bridging. This leads to a multimerization of vWF subunits, resulting in glycosylation to produce a pro-vWF subunit ready for storage (Nightingale et al. 2013). Following synthesis, the vWF is then packaged up and transported to storage organelles, WPBs in ECs. This packaging of vWF requires the formation of vWF multimers that can be assembled into a tubule, permitting a 100-fold compaction of vWF into the premature WPB. At this point, the multimeric vWF tubules induce the formation of membrane protrusions from the TGN, leading to the vesicles budding off and allowing the formation of the premature WPB. Evidence has highlighted that there could be a degree of homotypic fusion during this multimerization step, which could contribute to their heterogeneity (Valentijn et al. 2008). Following maturation and the immobilisation of vWF within, WPBs can then begin to recruit further cargo, of which I will now go into detail.

1.2.4 WPB docking and fusion events

In the cell, there are a variety of proteins that collectively tether, dock and fuse WPBs to the plasma membrane. I will only briefly outline these here to provide scope as to how tightly regulated this process is within the cell. One of the first to be discovered was RalA back in 2001, by the Voorberg lab and they found that mutant expression of this protein significantly upregulated the release of stimulus-induced vWF (Leeuw et al. 2001). It was later discovered that RalA could form a tethering complex that could interact with Soluble NSF Attachment Protein Receptors (SNAREs) which permits the fusing of two membranes and binds with Ras-associated binding (Rabs) proteins to coordinate fusion events. Munc13-4 and Munc18c, (members of the SM protein group involved in exocytosis whereby they act as Ca^{2+} sensors to prime vesicles for fusion with the cell membrane) have also shown promising interactions with WPBs regarding their ability to regulate vWF exocytosis through binding to syntaxins (a.k.a. Q-SNAREs) by inducing functional changes in their conformation. It has been shown that HUVECs can express these Munc proteins and through immunofluorescence (IF) imaging demonstrated strong colocalization with WPBs (Zografou et al. 2012). Recent developments are looking at a complex of proteins known as annexin A2-S100A10 as being necessary for vWF secretion, however, due to its lipid and calcium (Ca^{2+}) -binding capacity, it is postulated to

have a role in late fusion/exocytosis at the plasma membrane, however, this role remains to be elucidated further (Knop et al. 2004). It should be made clear, that although there have been significant advances in the understanding of tethering and fusion of WPBs at the plasma membrane and the related protein complexes required to drive these, we are still puzzled by the process of docking at the sites of exocytosis in the endothelium and are continuously developing our understanding of small (and now large) GTPases in the overall control of these processes. As such, these Rab proteins are the master regulators of cell membrane physiology, acting at various points along the system from the formation of organelles right through to exocytotic machinery control. We know from the data to date that the interpretation of findings from functional studies looking at WPB secretion of vWF should be interpreted with caution, as I have discussed above, there are a plethora of proteins and complexes that interact at various stages with WPBs to modulate their activity. The introduction of large GTPases (e.g. Rab46) and their functional N-terminal EF-hand domains are offering promising insights into this highly regulated and spatial-temporal distribution of WPBs and their ability to differentially secrete cargo of which I will now provide evidence of how these function in ECs.

1.2.5 WPB cargo exocytosis

WPBs have been labelled ‘emergency vascular toolkits’ in the past and this title still stands as it accurately describes the ability of these organelles to detect a disturbance within the vasculature and be one of the first respondents to vessel injury. An important example of this would be the ability of WPBs to dock to the plasma membrane and allow exocytosis of the multimerised form of vWF to allow for platelet adhesion during a thrombotic episode (Bierings et al. 2019).

The precise mechanism by which WPBs expel their contents is not fully understood, however, over the last 15 years, there has been a great progression in developing a reasonable depth of knowledge on how the interaction of the WPB changes in the extracellular environment allows for exocytotic machinery to be deployed in a regulated manner. vWF, being the largest multimerised protein residing within WPBs can be secreted in one of three ways; constitutive, basal, or regulated (da Silva & Cutler, 2016).

Basal release refers to a continuous, low-level release of cargo from WPBs that will occur even in the absence of stimuli. This process is not highly regulated by the endothelium and is thought to be triggered by the fusion of a small portion of WPBs to the plasma membrane, occurring in response to spontaneous changes in ion flux or vesicle trafficking (Nightingale et al. 2013). Physiologically, the most important cargo secreted at these basal levels is low-molecular-weight vWF, where a constant baseline level circulates to maintain vessel integrity and modulate haemostasis in the local cellular environment (Rusu et al. 2018).

Constitutive secretion does not occur with WPBs and is centred around the secretion of low molecular weight vWF and is subsequently expelled at the basolateral face of the endothelium. It is described classically, as an ongoing release that is not under tight, regulatory control. Many groups have classified basal and constitutive release under the same umbrella term, however, the purpose of this steady release of cargo is responsible for maintaining a constant level of vasoactive factors in the blood, to stabilise the immediate vicinity surrounding the endothelium (da Silva et al. 2016; Nightingale et al. 2013).

1.2.6 Regulated WPB cargo secretion

Regulated cargo secretion is evoked by various EC secretagogues including histamine, thrombin, and VEGF. Raising the intracellular Ca^{2+} concentration in response to stimuli drives downstream effector activation, many of which are Ca^{2+}-sensitive proteins that regulate various steps in exocytosis e.g. anchoring of WPBs (cortical actin), tethering (Anx2) and fusion of WPBs (SNARE complexes) (Bagur & Hajnoczky, 2017). Ca^{2+}-raising stimuli such as shear stress and hypoxia can also evoke WPB trafficking toward the plasma membrane, where they are exocytosed and are involved in mediating downstream inflammation (Rusu et al. 2018; Billaud et al. 2014).

The release of cargo from WPBs must be tightly regulated to ensure that downstream off-target effects are minimised. Upon injury, there is a critical need for the release of high molecular weight (HMW) vWF upon vascular insult, as a loss of vWF multimers can result in a bleeding cascade, characterised clinically in the manifestation of Type 2A and 2B von Willebrand disease (Horiuchi et al. 2019). Packing of multimerized vWF and further maturation of WPBs takes

place at the TGN; however, their maturation continues long after their scission from this region of the cell and is assisted by Rab27a, a GTPase that is usually associated with lysosomal secretagogues where its effector proteins link organelles in the vicinity to cortical actin filaments (Alzahofi et al. 2020). One key finding by the Nightingale lab (Nightingale et al. 2009), found that HUVECs deficient in Rab27a had WPBs that contained less highly multimerised vWF than control, which upon stimulation released shorter vWF strings. This data suggested that Rab27a serves as a modulator of the process of WPB maturation, which this process is dependent on the spatial distribution of WPBs within the cell. Rab27a serves as a braking mechanism to prevent the release of immature vWF by anchoring WPBs to filamentous actin, allowing full maturation. Further activation of WPBs by example, thrombin, then leads to the release of WPBs from this anchoring and allows exocytic fusion with the plasma membrane to promote the secretion of vWF into the extracellular space and to sites of vascular injury.

Other secretagogues cause cellular rises in cAMP, i.e. vasopressin which causes release of mature WPBs that are docked at the plasma membrane, and immature WPBs are trafficked to the microtubule organising centre (MTOC). This is a weaker form of secretion as compared to that of Ca^{2+}-raising stimuli and clinically, drugs such as desmopressin are used in von Willebrand Disease (VWD) to increase circulating blood levels of vWF (Beltran et al. 2023; Kaufmann et al. 2000).

1.2.7 Differential WPB cargo secretion from ECs

Regulation of differential cargo secretion occurs at the apical surface of the endothelium and results in the propulsion of high molecular weight vWF from WPBs (Rusu & Minshall, 2018). The result of large multimers of vWF being released initiates the assembly of vWF strings on the apical edge of the endothelium that can bind platelets and arrest vessel injury (Bierings et al. 2019). The propulsion of vWF from the plasma membrane is promoted by the formation of an actin ring evoked by secretagogues released during vascular injury, such as thrombin (Nguyen et al. 2020; Rondaij et al. 2004). Through modulation by Rho, actin is recruited to the WPB fusion sites where it can form

rings or coats that squeeze and cover WPBs as they undergo cargo exocytosis (Mietkowska et al. 2019).

Another form of WPB cargo exocytosis is the ‘lingering kiss.’ This phenomenon occurs when the WPB fusion pore opens and remains so for around 80 seconds, permitting cargo exocytosis, before resealing. This does not permit the propulsion of HMW vWF but is thought to permit the release of small molecules (low molecular weight vWF and endothelin) and prevents the release of pro-thrombotic or pro-angiogenic, larger cargo (Babich et al. 2008). The kiss and run, where WPBs open to the plasma membrane for a short space of time before being internalised, further prevents the release of any vWF (Valentijn et al. 2011).

One interesting characteristic of WPBs is their ability to alter their cargo recruitment and secretion based on their cellular environment and this is critical in their role as initial response vesicles (Hordijk et al. 2024). They can modulate the expression of their cargo to be more haemostatic, inflammatory or angiogenic in response to the variable stimulus being applied to them. From data published within our lab we observe that upon stimulation of HUVECs with histamine, we observe two spatially distinct subpopulations of WPBs that contain either P-selectin or Ang2, undergoing differential trafficking events (Miteva et al. 2019). This immunological stimulus prevents WPBs containing Ang2 from being exocytosed whilst P-selectin-positive WPBs will migrate to the periphery of the cell, where P-selectin is released to attract leukocyte migration. The Ang2-positive WPBs (Figure 1.3) migrate in a retrograde fashion towards the Microtubule Organising Centre (MTOC), whereby they cluster, suggesting a potential braking mechanism to arrest cargo secretion. We do not observe these effects with thrombin stimulation as this physiological stimulus induces an ‘all-out’ vascular response, upon which all WPBs can expel their contents. This differential trafficking pathway is dependent on microtubules and is regulated by a complex formed between a novel Rab GTPase, Rab46 and dynein. Rab46 acts as a dynein adaptor and its GTPase activity allows it to form a complex with dynein upon histamine stimulation, thus promoting WPB migration toward the MTOC (Pedicini et al. 2021). Rab46 is a Rab GTPase and considering its importance in this pathway is the focus of research in the lab.

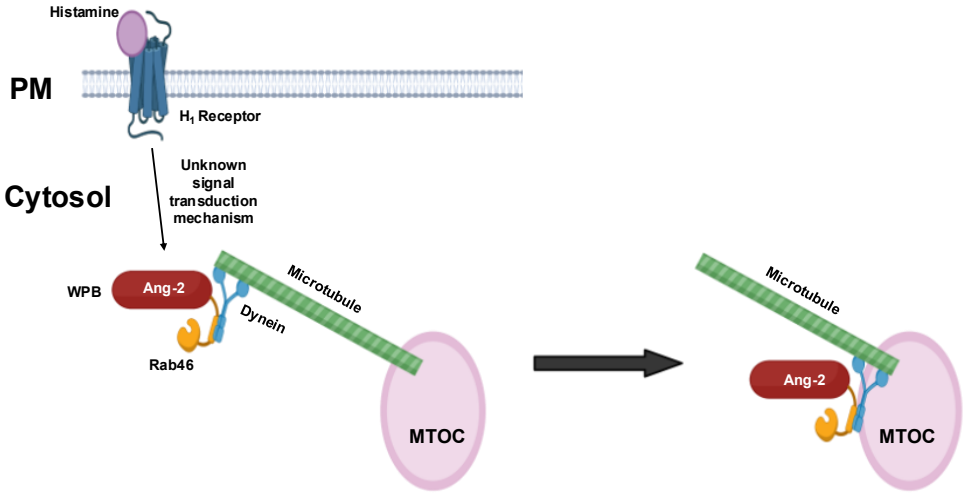

Figure 1.3 Acute histamine stimulation results in retrograde trafficking of Rab46 and WPBs containing Ang2 to the MTOC. Histamine binds to the H_1R causing an intracellular rise in NAADP, eliciting the retrograde trafficking of Rab46 in a dynein-dependent mechanism with Ang2-positive WPBs to the MTOC where they are held during the stimulus.

1.3 Rab GTPases

1.3.1 Rab GTPase function

Rab GTPases comprises the largest sub-group within the Ras superfamily of GTPases. They are widely regarded as the 'master regulators' of intracellular trafficking and oversee all events regarding the movement of vesicles. Specifically, Rab GTPases regulates processes such as endocytosis and exocytosis of vesicles. For instance, Rab5 is crucial in the formation of the early endosome and Rab7 is pivotal in the maturation of the late endosome before it terminates as a lysosome (Wandinger-Ness et al. 2014; Hyttinen et al. 2013).

Within the human species, there are approximately 60 members of the Rab GTPase family already identified, and they are spatially and temporally distributed within various membranes (Stenmark, 2009). Rab GTPases have been identified to be critical for inter-organellar membrane crosstalk (Table 1.2) via their effector proteins which range from kinases and adaptor proteins to

phosphatases, and this is integral to modulating immune and hormonal processes across various cell types and in multiple disease models (Waschbusch & Khan, 2020; Pylypenko et al. 2018). For example, Rab GTPases are crucial for antigen presentation within immune cells and are responsible for insulin signalling in metabolic tissues such as the pancreas (Prashar et al. 2017). The spatial and temporal distribution of Rab GTPases ensures that trafficking of vesicles occurs in the correct location and at the right time. This is crucial as Rabs interact with effector proteins (dynein, SNAREs etc) that drive the movement of vesicles along microtubules or tether them to membranes (through geranylgeranyl modifications) to facilitate correct spatial-temporal membrane fusion which is critical to their function (Hutagalung & Novick, 2011; Horgan & McCaffery 2011).

1.3.2 Rab GTPase regulation

Rab GTPases follow a cyclic pathway of activation and inactivation (Figure 1.4) which controls their ability to operate as molecular ‘on-off’ switches and this is known as the Rab GTPase cycle (Stenmark, 2009). They contain two independent switch regions (I and II) that determine the specificity of the nucleotide-dependent functioning of Rab proteins, acting through the gamma-phosphate of GTP. In the resting state, Rab proteins have a disordered appearance at the switch region, and these undergo very precise conformational changes when the GTPase is bound to GTP, which allows for the binding of effector proteins to initiate downstream protein activation and thus migration of the Rab GTPase throughout the cytosol (Pylypenko et al. 2018; Homma et al. 2021). This conformational change that permits the exchange of GDP for GTP is mediated by guanine-nucleotide exchange factors (GEFs) and these are normally localised to specific intracellular membranes, providing spatial and temporal controls over Rab GTPase activation (Goldberg,1998; Homma et al. 2020). The Rab GTPase cycle is mediated by various cellular factors and as one is aware, Rab proteins readily oscillate between the cytosol and target membranes. The concentration of GTP is at a high concentration (~1 mM) within the cell, which accounts for the high-affinity binding of GTP once GDP is released. The activated Rab protein can then specifically interact with effector proteins to promote the trafficking of intracellular vesicles. GTPase

accelerating proteins (GAP) initiate hydrolysis of Rab from its GTP-to-GDP-bound form. The inactive Rab then becomes a substrate for GDP-dissociation inhibitor (GDI) which sequesters Rab to the cytoplasm. Here, the GDI-displacement factor (GDF) is required to mediate the displacement of GDI to allow Rab to reinsert itself back into the cycle (Brighouse et al. 2010).

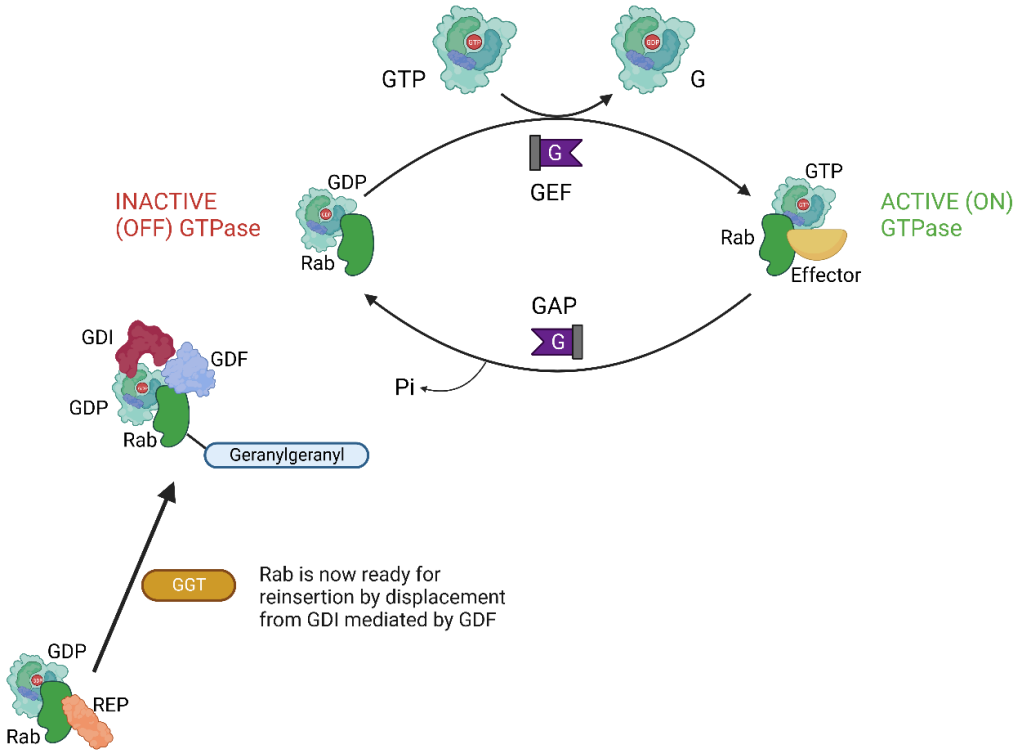

Figure 1.4 Rab GTPase prenylation and the Rab GTPase cycle. All Rab GTPases exist in either a GDP-bound, off or GTP-bound on conformation. This cycling between on and off is controlled by a variety of effector proteins. In the GTP-bound form, GAPs initiate hydrolysis of GTP converting Rabs to a GDP-bound off state. Here, The Rab protein is targeted by GDI and removed from the cycle, where it is held, until such a time that activation is needed. The Rab protein will be recruited back to the cycle via REPs that will undergo geranyl-geranyl modification by GGTs to prepare the Rab protein for re-entry, where GDF mediates the displacement of GDI and subsequently allows the Rab to enter the cycle again. This is where GEFs catalyse the exchange of GDP for GTP, thus activating the Rab protein, allowing effector protein binding to allow downstream signalling to take place.

1.3.3 Large Rab GTPases

The GTPase superfamily of proteins all share a variety of common and distinct structural domains that inevitably denote their function (Bourne et al. 1991). GTPases are ancient and have been throughout evolutionary history a highly conserved group of proteins across a species-wide distribution (Atkinson, 2015). Within this superfamily, exist a subfamily of Rab GTPases (Table 1.2) that do not conform to the usual Rab GTPase structure. They are twice the size of regular Rabs due to the presence of extra domains. The Rab domain is critical in the function of Rabs to act as molecular ‘on and off’ switches, however, these extra domains confer additional protein-protein interaction sites to large Rabs, allowing them to interact with a greater range of effector proteins (Agola et al. 2011). Whilst small Rab GTPases are associated with the movement of cargo between specific locales or regulate the integration of Rabs with membranes, large Rab GTPases tend to be involved in general membrane dynamics, such as cell signalling (Ca^{2+}-mediated events) or cytoskeletal organisation in response to trafficking (Stenmark et al. 2009). In addition to this, large Rab GTPases, are modulated not only by their respective effector proteins but also by proteins in their immediate vicinity. Rab44 is an example of this, where it is highly expressed in mast cells, where it assists in the process of degranulation, however, in addition to this, the extra domains at its C-terminus allow it to regulate retrograde transport of pigment-containing organelles in melanocytes (Kadowaki et al. 2021; Maruta & Fukuda, 2022). I will now discuss the discovery of the novel, large Rab GTPase, Rab46 and its relationship with the differential trafficking of WPBs in ECs.

Table 1.2 Large Rab GTPase functions and cellular distribution

Protein	Cellular Distribution	Functions	Binding Proteins	Phenotypes/ Aetiology
Rab44-L	Mast cells	Degranulation	VAMP8	↓ Anaphylaxis (Tsukuba et al. 2021) Nickel-induced hypersensitivity (Noguromi et al. 2023)
Rab45-L	Epithelial cells Cancer cells	Unknown Tumour suppressor	Dynein-dynactin	Unknown
Rab45-S	Germ cells	Unknown	Rab45/RASEF (oligomer)	Unknown
CRACR2A	T-cells	Transport of Vav1+ vesicles	Vav1	Impaired Th1 differentiation
Rab46	Endothelial cells (Tube formation)	Transport of WPBs to/from the MTOC	Dynein-dynactin Na^+/K^+ ATPase subunit alpha-1	Periodontal diseases/ Cancer metastasis/ NAFL, NAFLD, Cardiovascular system defects

1.4 Rab46

Most Rab proteins are around 20-25 kDa in size and are defined by their GTPase domain (Srikanth et al. 2017; Wilson et al. 2015). In 2015 a study by Wilson et al. discovered the EC-specific large Rab GTPase, now known as Rab46. It was proved that a longer variant of the CRAC channel modulator, CRACR2A (CRACR2A-L; 95kDa) was expressed in both murine T cell and

human models. This longer variant (Rab46) contained the same domains as CRACR2A at the N-terminus but also had a large, C-terminal conserved Rab domain (Figure 1.5). This discovery potentiated further exploration of this newly discovered CRACR2A long variant, and it was found to be similar in size to Rab44 and Rab45 and contained two functional Ca^{2+}-sensing EF-hands (N-terminus), a coiled-coiled domain and a Rab domain at the C-terminus), thus, leading to it being named Rab46.

1.4.1 Rab46 and WPBs

The role of Rab46 is crucial in the context-dependent trafficking of WBPs. Rab46 is responsible for regulating the histamine-evoked trafficking of Ang2-positive WPBs to the MTOC, where they are held until Ca^{2+} becomes available. Our lab has shown that the retrograde trafficking of Rab46 to the MTOC is a Ca^{2+}-independent process, however, it is assisted by interactions with the motor protein dynein. Rab46 is a direct dynein adaptor, whereby it binds with the dynein/dynactin complex in a Ca^{2+}-independent manner to assist in the trafficking of WPBs to the MTOC. Rab46 is an unconventional Rab in that it contains a pair of EF-hands, a coiled-coil domain, and a Rab GTPase domain and within the context of this histamine-evoked trafficking, it is the presence of a long coiled-coil domain that serves as an important site for interactions with dynein (Pedicini et al. 2021). The subsequent detachment of Rab46 and WPBs containing Ang2 away from the MTOC following stimulation is a Ca^{2+}-dependent process. At the N-terminus of Rab46, resides two functional Ca^{2+} -binding motifs (EF-hands) and Ca^{2+} binding to these EF-hands elicits WPB release and secretion of Ang2. As mentioned earlier these extra domains present on large Rab GTPases allow for more complex regulatory controls and explain how large Rabs like Rab46, integrate multiple signalling pathways (e.g. Ca^{2+} signalling).

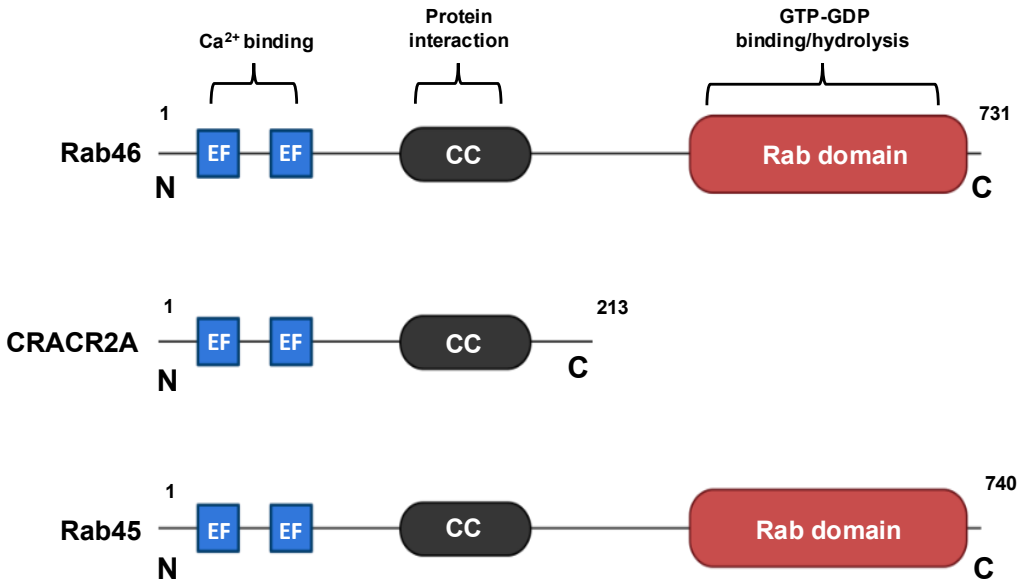

Figure 1.5 Structural differences in large Rab GTPases. Large Rab GTPases are characterised by their C-terminal Rab domain which is highly evolutionary conserved. It is this Rab domain that confers the 'on-off' switch phenotype to this family of proteins. The interesting area of the protein that is crucial to this thesis is the N-terminal EF-hand domain. Rab GTPases have 2 of these as they are crucial Ca^{2+} binding domains where Ca^{2+} released from stores is capable of binding to and eliciting detachment of the protein from the MTOC.

1.4.2 Rab46; EF-hand domain

The EF-hand Ca^{2+} binding domain is one of the most highly conserved protein sequences within animal cells, with around 1,000 in existence and they help to facilitate the binding of free Ca^{2+} ions and convert ionic signals into mechanistic action. Despite this elevated level of sequence conservation, EF-hand proteins conduct multiple functions from Ca^{2+} sensors; transducing signals, to Ca^{2+} modulators, which can determine the duration of Ca^{2+} signals or serve as mediators of Ca^{2+} homeostasis (Nelson et al. 2002). The large Rab GTPases are complex intracellular trafficking proteins, where Ca^{2+} binding states play a key role in their spatial and temporal locations within cells. One study investigated the role of Rab44 in the subcellular localisation and formation of

organelles found in WT cells and those expressing dominant mutations of the EF-hand domain (hT847N) localised Rab44 to the cytosol. Mutations in the EF-hand or coiled-coil domain of Rab44 induced a loss of localisation to the plasma membrane (Ogawa et al. 2020). This confirmed that the EF-hand domain is required for the partial translocation of Rab44 to the PM following an influx of Ca^{2+}, and the coiled-coil domain is necessary for localisation and organelle formation.

The EF-hands of Rab46 is located at its N-terminus, previous work from other members of the lab has shown that Ca^{2+} binding to this EF-hand domain is essential for the dispersal of Rab46 from the MTOC following stimulation with histamine (Miteva et al. 2019; Pedicini et al. 2021). Work conducted in our lab identified that of the two EF-hand domains present on Rab46, only the 2^{nd} domain was functional and that by Ca^{2+} binding, induces a conformational change in the structure of Rab46 eliciting dispersal from the MTOC (Wiktor, 2024). The interaction between dynein and Rab46 was initially hypothesised by our group to be a Ca^{2+}-dependent process. Work by Pedicini et al investigated the Rab46 interactome and identified the dynein heavy chain (DHC) as a key interaction site (Pedicini et al. 2021). The dynein adaptor associated with Rab11, FIP3, was identified in 2009 and is structurally similar to that of Rab46 with two EF-hands, followed by coil-coil domains (Horgan and McCaffrey, 2009). Pedicini et al revealed a 22.9% sequence alignment similarity between Rab46 and Rab11FIP3 and omics analysis revealed two conserved alanine residues (A227 and A555) of which A227 was identified at the N-terminal of Rab46's coil-coiled domain and A555 with the Rab domain (Pedicini et al. 2021). These data suggested that the conservation of these residues was important in the binding of Rab46 to dynein. Studies in T-cells have reported that Ca^{2+} binding to the EF-hands was responsible for the interaction between Rab46 and dynein (Wang et al. 2019). They demonstrated that through abolishing the Ca^{2+} gradient in T-cells, the interaction between dynein and dynactin and subsequently Rab46 was lost. Our lab has also shown that the chelation of intracellular Ca^{2+} in HUVECs using BAPTA-AM, does not inhibit the dynein-dependent retrograde trafficking of Rab46 to the MTOC in ECs. Furthermore, a mutant of Rab46 that is unable to bind Ca^{2+} ($Rab46^{EFmut}$) was recruited to WPBs containing Ang2 that

rapidly trafficked to the MTOC, even in the absence of stimulation with histamine. Our lab was able to evaluate through IP pulldown experiments using this Rab46 EF-hand mutant and an inactive GFP-N658I Rab46 mutant (that does not bind to the DHC), that the Rab46-dynein interaction was not dependent on Ca^{2+}. This was due to the presence of a distinct band when immunoblotting for the DHC in the $Rab46^{EFmut}$ fraction (460 kDa) that was not observed in the N685I mutant or GFP control (Pedicini et al. 2021). This data confirmed that the interaction between Rab46 and dynein is Ca^{2+}-independent in ECs. Dispersal of Rab46 is dependent on the active role of the 2^{nd} EF-hand binding Ca^{2+}. Where this Ca^{2+} comes from is subject to investigation of which I will now discuss candidate Ca^{2+} stores believed to play a vital role in this pathway.

1.5 EC Ca^{2+} signalling

1.5.1 Store-operated Ca^{2+} entry (SOCE)

The major store of Ca^{2+} within the cell is the endoplasmic reticulum (ER) and the majority of Ca^{2+} signalling is controlled via the process of store-operated Ca^{2+} entry, a mechanism that relies on the translocation of proteins from one membrane to another that triggers store depletion and Ca^{2+} re-filling (Peterson & Fedirko, 2001). The main trigger for SOCE is the activation of GPCRs which leads to the production of IP_3 from $PI(4,5)P_3$ by PLC which then binds to IP_3Rs on the ER membrane leading to a major Ca^{2+} store depletion within the lumen of the ER. This depletion is detected by stromal interaction molecule 1 (STIM1), an ER-bound transmembranous protein that contains an EF-Ca^{2+} binding domain, which upon depletion leads to a dissociation of the EF-hand domain on STIM1 and Ca^{2+} inducing a conformational change in the structure of STIM1 exposing oligomerisation domains that cause an aggregation of multiple STIM1 molecules to form complexes. This forces a translocation of STIM1 to the ER-PM junction (Figure 1.6) where it binds to the PM-bound Ca^{2+} channel, Orai1, which forms a putative pore region upon STIM1 binding at the N-terminus, allowing a free and rapid influx of Ca^{2+} ions into the ER lumen. This process continues until such at time that the ER Ca^{2+} pool has been replenished. After

this, STIM1 oligomers will dissociate from one another with Ca^{2+} binding the EF-hand domain to inactivate the protein. The last stage is the closure of the putative pore region of Orai1, terminating Ca^{2+} ion uptake. This form of Ca^{2+} signalling plays a key role within endothelial cells in the context of histamine stimulation. The process of small lysosomal Ca^{2+} release can trigger the amplification of global Ca^{2+} release from the ER, via CICR, thus it is clear that there is a cross-talk between the two signalling pathways and that they may operate independently but functionally are very much linked.

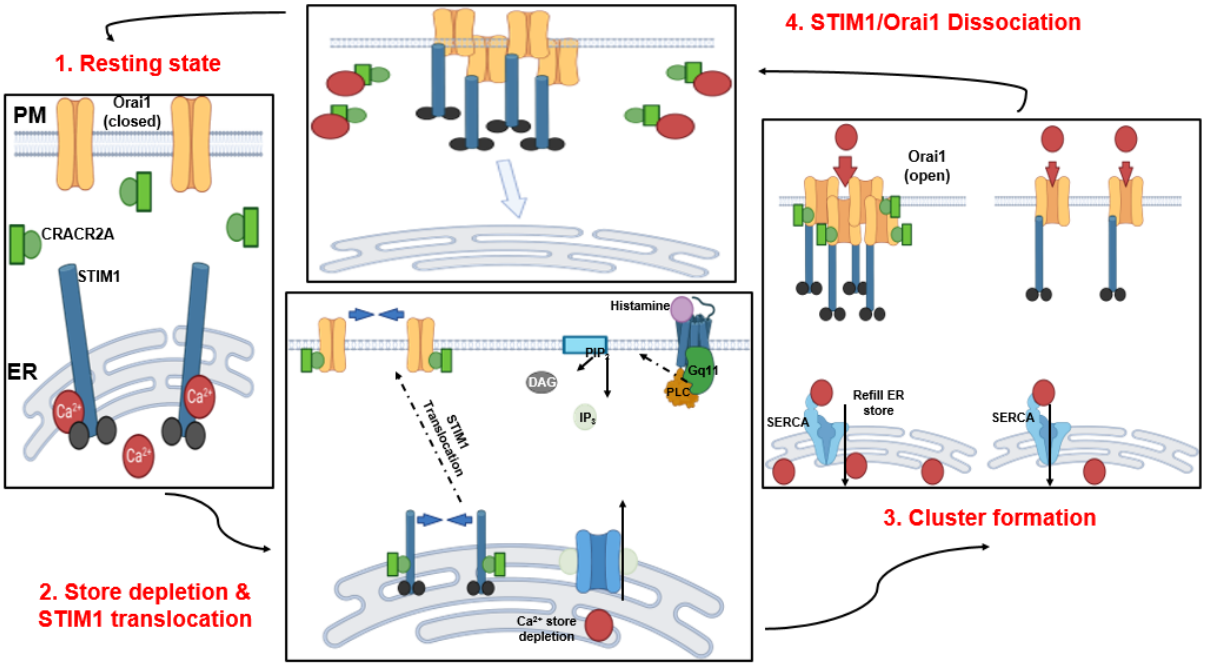

Figure 1.6 Store-operated Ca^{2+} entry (SOCE) mechanism of action. In the resting state, STIM1 remains bound to the ER membrane and Orai1 is in the pore-closed conformation. Upon ER Ca^{2+} store depletion, there is a subsequent translocation of STIM1 to the PM where it binds to Orai1 eliciting cluster formation of multiple Orai1 channels that then open to allow a rapid influx of Ca^{2+} into the cytosol. This Ca^{2+} is then actively transported by the SERCA pump to refill the ER stores. Upon completion of refilling, STIM1 dissociates from Orai1, and the clusters disperse. The last part of the cycle to occur is the closure of the Orai1 cation pore, signalling the termination of SOCE.

1.5.2 IP_3 mediated globalisation of Ca^{2+} signals

The process of SOCE is tightly regulated and for Ca^{2+} signals to be meaningful, they must be tightly coordinated. The IP_3 pathway is crucial in the generation of downstream signals of multiple cell surface receptors, especially those coupled to G proteins. This occurs in conjunction with the activation of PLC to diffuse IP_3 into the cytosol and produce DAG which remains plasma membrane-bound and activates PKC (Bagur et al. 2017; Lock & Parker, 2020). IP_{31}-mediated Ca^{2+} release is often initially observed locally in regions of the cells near the ER, where IP_3 receptors (IP_3Rs) are standalone and the initial Ca^{2+} 'blips' (Figure 1.7) are sufficient to induce clustering of IP_3Rs on the ER membrane (Thillaiappan et al. 2017). The globalisation of IP_3-mediated Ca^{2+} signals is not by diffusion of cytosolic Ca^{2+} alone as this is too slow to induce rapid globalisation. Thus, the ryanodine receptor (RyR) is crucial for amplifying the calcium-induced-calcium release (CICR) pathway, albeit they are activated by cytosolic Ca^{2+} itself.

This signalling operates in the form of a positive feedback loop that rapidly amplifies the Ca^{2+} signal by inducing Ca^{2+} 'puffs' that activate more and more RyRs which then elicits a Ca^{2+} 'wave' across the ER network fully globalising the response (Farrell et al. 2003; Fill & Copello, 2002). There are physiological benefits to coordinating IP_3-mediated signals and their globalisation, from fast processes such as muscle contraction to rapid release of neurotransmitters or hormones, CICR can elicit the mobilisation of vesicles across a larger area of the plasma membrane (Kuo & Ehrlich, 2015). The most vital function of CICR is its ability to operate as a thresholding mechanism. This works by preventing weak IP_3 signals from causing widespread cellular responses, ensuring that only large and relevant stimuli lead to global rises in intracellular Ca^{2+} (Ivanova et al. 2024).

SOCE is a crucial part of EC machinery, however, considering that both histamine and thrombin evoke SOCE, histamine must evoke a distinct signal that allows Rab46-dependent dispersal of WPBs from the MTOC. Therefore, NAADP-mediated Ca^{2+} signals from lysosomal stores have been shown to mediate localised responses and previous studies (Favia et al. 2014; Esposito

et al. 2011) have implicated NAADP-evoked Ca^{2+} release in histamine signalling. Here, I describe the NAADP-sensitive Ca^{2+} pathway.

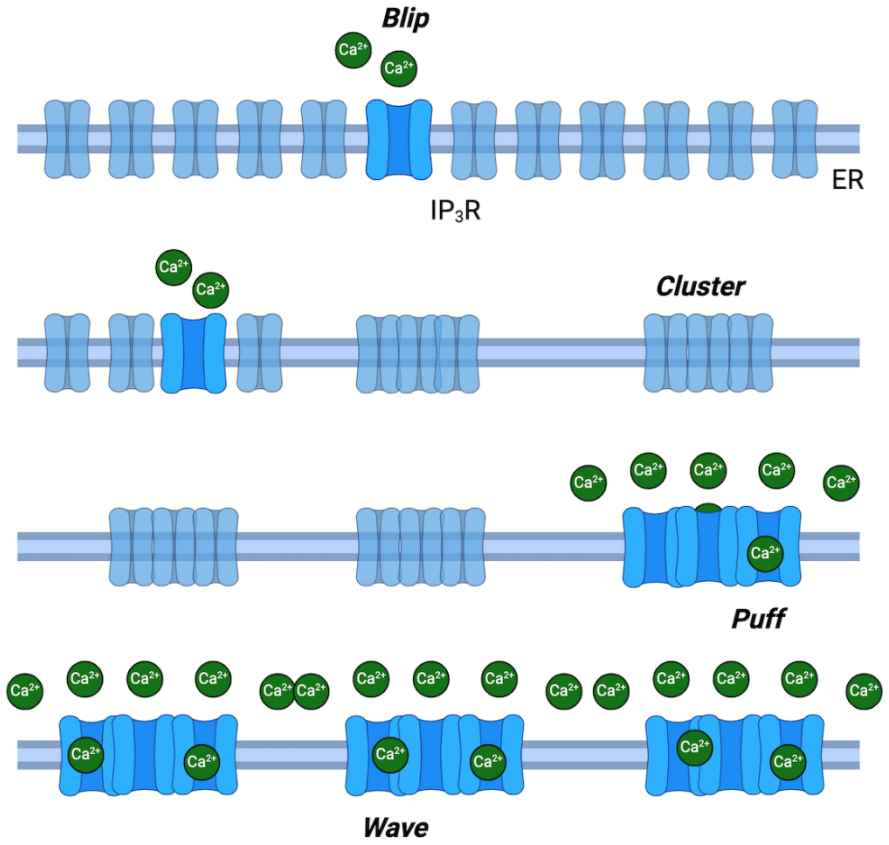

Figure 1.7 IP_3-mediated Ca^{2+} signalling and the various stages of signal potentiation. Initial Ca^{2+} signals elicited via IP_3 are usually in the case of Ca^{2+} blips from immobilised IP_3Rs on the PM. These initial signals are exacerbated through a positive feedback loop in which RyRs cause an amplification of these localised signals through CICR and potentiate Ca^{2+} puffs. From here, the subsequent recruitment of more IP_3Rs to the ER membrane, increases the RyR rate of activation, eliciting full-scale Ca^{2+} waves across the entire ER membrane, fully globalising the signal.

1.5.3 Lysosomal Ca^{2+} stores

1.5.3.1 Lysosomes

The term ‘lysosome’ (from the Greek: ‘digestive body’) was first coined in 1955 by Christian de Duve during an investigation into the characterisation of glucose 6-phosphate in the rat liver (de Duve, 2005). This name was given due to the

newly discovered organelle containing a high concentration of soluble hydrolases, which housed the capability to degrade various cellular debris (nucleic acids, lipids, carbohydrates etc). Lysosomes were deemed nothing more than cellular recycling centres, capable of digesting unwanted waste and serving as a storage site for said debris. However, it has come to light in the last 20 years, that these small organelles may have much more complex and characterised roles within cell biology (Bonam et al. 2019; Yang et al. 2018). We now know that lysosomes serve as small stores for crucial ions involved in cell signalling (Ca^{2+}, H^{+}, Na^{+}, K^{+}) and help to modulate cell homeostasis through various enzymatic processes with the lysosome that induce recycling events such as cell death, chaperone-mediated autophagy, macromolecular degradation (Appelqvist et al. 2013).

The morphology of lysosomes is ubiquitous across most eukaryotic cells, comprising of an acidic lumen, containing specific hydrolases and membrane proteins to which the structure is bound and maintained. Most lysosomes are > 1 μm in diameter and they are limited by a singular 7-10 nm phospholipid bilayer which is home to around 25 membrane proteins for various functions (Saftig et al. 2010). Lysosomes are the product of a long chain of maturation processes (Figure 1.8) in which small dense bodies within the endocytic and autophagic pathways are transported, synthesised, and enveloped into the product, the lysosome. Initially, lysosomal proteins are resorbed into early endosomes/recycling endosomes from the *trans*-Golgi network (TGN). These proteins undergo modifications further developing the vesicle into a late endosome, also known as a multivesicular body. This early lysosome undergoes a fusion event with the late endosome to form an endo-lysosome After subsequent maturation and development, the final end-product lysosome is then able to re-form and break away.

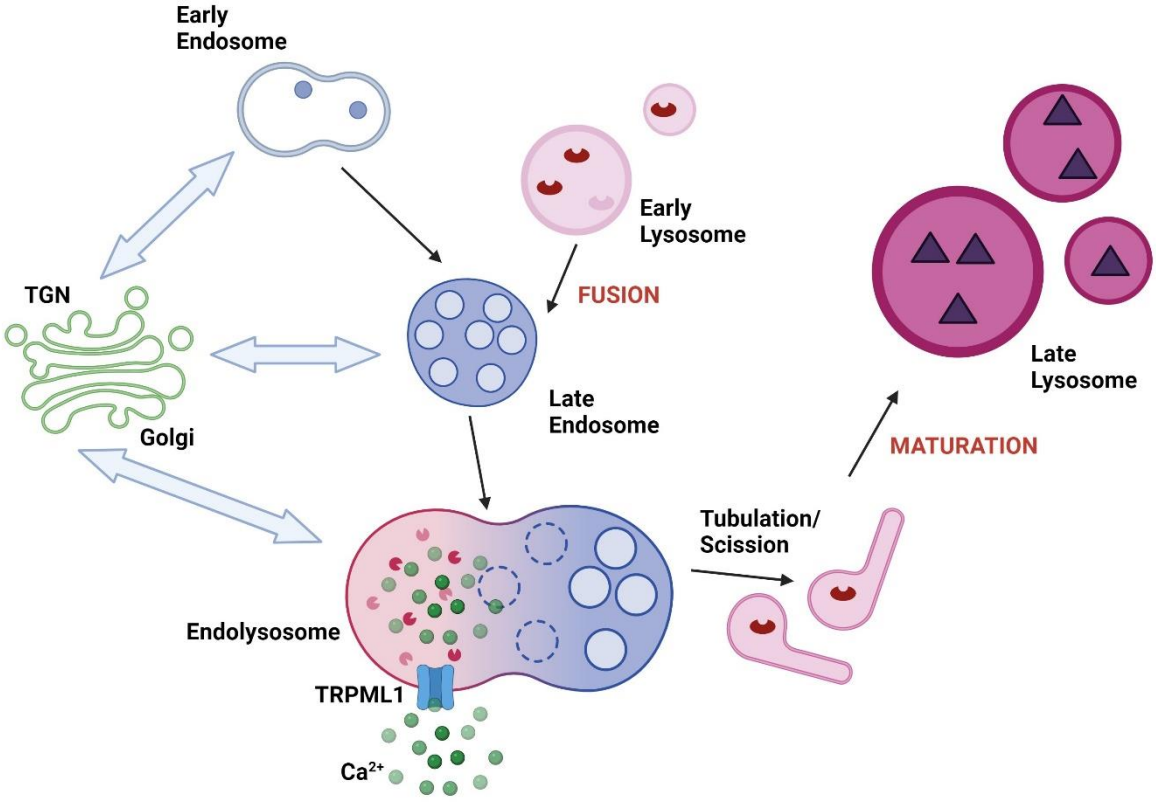

Figure 1.8 Lysosomal biogenesis is a well-coordinated process. Endocytic lysosomal reformation (ELR) is regulated by TRPML1, PIKfyve, and Ca^{2+}. PIKfyve converts PtdIns3P to PtdIns(3,5)p2, which activates TRPML1 to regulate lysosomal Ca^{2+} efflux which is required for lysosomal tubulation to allow for lysosome maturation from the late-endosome to endo-lysosome to the end stage, the fully matured lysosome.

The process of lysosomal maturation has been studied in detail and various proteins and complexes have been identified as key players in this process. The fusion of early lysosomes with the late endosome is modulated by SNAP REceptor (SNARE) proteins. These are expressed on the plasma membrane of the lysosome and allow for stability during the docking and fusion event. HOPS proteins (hVps41 & hVps39) are critical for the docking of late endosomes to endo-lysosomes and through a Ca^{2+} exocytosis event, the fusion of the two bodies takes place. End-stage lysosomes are then formed through various

protein retrieval and condensation steps which decapitate endosomal-associated membrane proteins (Pols et al. 2013).

1.5.3.2 Discovery of NAADP

Until the early 2000s, the lysosome was recognised as just another piece of cellular recycling machinery, capable of modulating processes such as protein degradation and autophagy. It was not until 2001 that breakthroughs were made in Ca^{2+} signalling from small intracellular organelles. The first evidence of NAADP-mediated Ca^{2+} signalling was identified in sea-urchin egg homogenates, where fractionation of these showed a contaminant of NADP, which subsequently became known as the secondary Ca^{2+} mobiliser, NAADP (Lee et al. 2001). Following this discovery, scientists have sought to understand how NAADP-mediated Ca^{2+} signals are altered in the presence of pro-inflammatory stimuli, such as histamine and thrombin.

1.6 NAADP-sensitive channels

The channel(s) through which Ca^{2+} is released from lysosomes (Figure 1.9) in response to the second messenger NAADP, had remained an elusive subject until the last two decades. Recent evidence has pointed to the role of the lysosomal two-pore channels (TPCs), specifically TPC1 and TPC2 as potentially endo-lysosomal cation channels responsible for the release of Ca^{2+} in response to NAADP-mediated signalling (Ruas et al. 2015; Jha et al. 2014; Galione et al. 2009). Another lysosomal membrane-bound channel, TRPML1, belonging to the transient receptor potential mucolipin (TRPML) family has been shown to play a role in the modulation of Ca^{2+} signals related to NAADP and is implicated in cardiovascular disease (Cheng et al. 2010; Li & Li, 2023). This thesis will attempt to highlight these three channels in detail, looking at various agonists of the channels, the relationship between histamine stimulation on the NAADP-evoked Ca^{2+} response and the effect of siRNA knockdown on the spatial and temporal distribution of Rab46 as well as the Ca^{2+} release. This data will help to push the frontier of intracellular acidic-store Ca^{2+} release and will aim to shed light on whether these channels play a role in Ca^{2+}-dependent detachment of Rab46 and Ang2 positive WPBs following histamine stimulation.

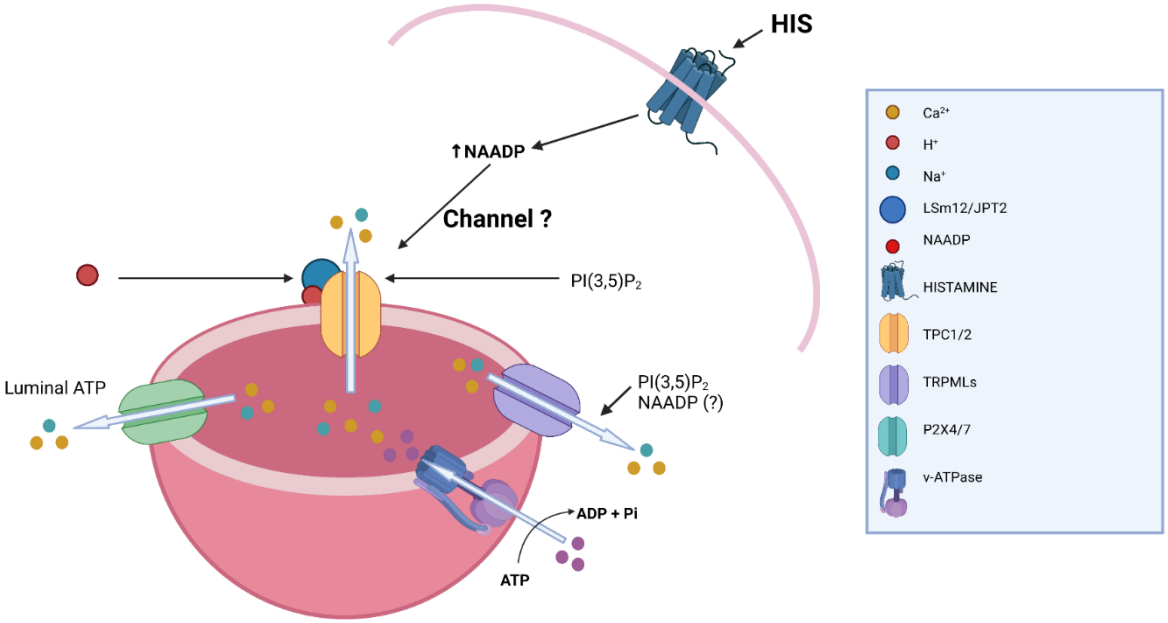

Figure 1.9 Lysosomal cation channels and their ion flux in response to NAADP. Schematic demonstrating the various forms of lysosomal cation channels and their associated ion fluxes in response to NAADP-mediated Ca^{2+} signalling evoked by acute stimulation with histamine. Na^{+}, Ca^{2+}, K^{+}, and H^{+} are among the most routinely transported ions across TPC1/2, and TRPML1. P2X4/7 participate in the transport of luminal ATP, and v-ATPase, hydrolyses ATP to ADP + Pi. These channels are homeostatic and maintain the luminal pH gradient for normal lysosomal functions.

1.6.1 Two-pore channels (TPCs)

The two-pore channels (TPCs) are a class of Ca^{2+} and Na^{+} -permeable cation channels expressed ubiquitously within the endo-lysosomal system. They are ancient members of the voltage-gated superfamily of proteins but can be controlled through both voltage and ligand gating, however, are equally activated by the secondary Ca^{2+} mobiliser, NAADP (Jha et al. 2015). The ability of these channels to permit both Ca^{2+} and Na^{+} ions to promote a non-selective phenotype as well as being able to control Na^{+} flux via gating by $PI(3,5)P_2$ (Patel et al. 2022). TPCs have been shown to control apoptotic, autophagic and fusion/fission events within the endo-lysosomal system and these functions rely on the correct establishment of a Ca^{2+} gradient within these acidic organelles

(Jha et al. 2014). Research has highlighted the agonist selectivity of TPCs to coordinate varying ion fluxes in response to agonist activation, thus conferring agonist selectivity on these channels (Yuan et al. 2022; Gerndt et al. 2020). The evolution of the structure of these channels is interesting, in that they are believed to be descendants of a shaker-like precursor Ca^{2+}/Na^{+} channel that eventually gave rise to a two-domain protein with each domain containing six transmembrane regions. The first four regions (S1-S4) depict the voltage-sensing domain for channel activation and S5-S6 creating the channel pore for ion flux (Rahman et al. 2015; Patel et al 2022). The relationship between Ca^{2+} released from TPCs and binding of this Ca^{2+} to Rab46 remains elusive, however, it is probable that these localised Ca^{2+} signals elicited by histamine, cause a complex formation at the lysosomal membrane to coordinate dispersal of Rab46 and Ang2-positive WPBs from the MTOC.

1.6.2 Two-pore channel protein 1 (TPC1)

Two-pore channel 1 (TPC1) is a voltage- and ligand-gated cation channel encoded by the *TPCN1* gene and is localised to early and late endosomes; however, it is observed within the cytosol of lysosomes. Multiple studies have investigated the distribution of this channel within the endolysosomal system, looking at the proteome of purified lysosomes and through subcellular fractionation of the endo-lysosome (Ayagama et al. 2021; Castonguay et al. 2017). TPC1 is capable of fluxing Na^{+} and Ca^{2+} ions, of which Ca^{2+} is the preferential ion within the endo-lysosomal system, however, the channels are permeable to monovalent ions such as H^{+} and K^{+} in which protons were the most permeable ion (Pitt et al. 2014). Researchers have argued that TPC1 is a voltage-gated channel capable of activation through depolarisation of the membrane resulting in an open-pore conformation (Wang et al. 2012; Zhang et al. 2019). Ligand-gated activation of TPC1 is crucially activated by $PI(3,5)P_2$ where the expression of this ligand is enriched on endo-lysosomes and lysosomes, whereby $PI(3,5)P_2$ binds directly to the channel to activate it and promote Na^{+} permeability (Boccaccio et al. 2014). Recent advances in lysosomal Ca^{2+} studies have highlighted, albeit less consistently observed, that NAADP activates TPC1, either through upregulation of $PI(3,5)P_2$ signalling or independently. Studies have concluded that this TPC1/NAADP axis is mediated

firstly by membrane potential, such hyperpolarisation of the channel resulted in a significant increase in affinity or TPC1 for NAADP (Rybalchenko et al. 2012). This evidence highlights a unique property of TPC1, describing its ability to regulate NAADP-induced Ca^{2+} oscillations, a sort of lysosomal homeostatic mechanism, which is in line with my hypothesis of TPC1 as a modulator of lysosomal Ca^{2+} that helps to coordinate the actions of other lysosomal cation channels, such as TPC2. TPC1-mediated Ca^{2+} release from endo-lysosomes is implicated in a variety of intracellular processes, from the trafficking of early endosomes to assisting the maturation of endo-lysosomes through fusion events with the autophagosome to promote autophagy which is crucial for the activation of acid hydrolases (Ca^{2+} sensitive) that break down cellular proteins (Afghah et al. 2019).

1.6.3 Two-pore channel protein 2 (TPC2)

Two-pore channel 2 (TPC2) belongs to the TPC family of ion channels alongside TPC1 (discussed above) and TPC3, a pseudogene in humans. Again, similar to TPC1, TPC2 is voltage-gated, but can also be gated by ligands, such as NAADP, with primary permeability to Ca^{2+} and Na^{+} ions, however, it can allow permeation of protons and K^{+}, albeit at lesser rates (Lopez et al. 2012). It maintains the same two pore-forming domain phenotype as observed in TPC1, and it is this unique pore structure that confers unique gating and pharmacological properties to the channel (Feijoo-Bandin et al. 2016). Surprisingly, the location of TPC2 within the endolysosomal system is in a membrane-bound state on lysosomes, whereas TPC1 is more associated with the plasma membrane and late endosomes, various colocalization studies using LAMP1 (a lysosomal membrane-bound protein) have discovered significant co-localisation of TPC2 and LAMP1 (Marchant & Patel, 2016). The gating of TPC2 through depolarisation is subject to debate in the field, due to the difficulty in gaining access to the lysosomal membrane potential, however, patch-clamp studies have shown that depolarising the lysosomal membrane, activates TPC2 to flux Ca^{2+} out of the lysosome (Ruas et al. 2015). A significant volume of research in the field has been centred around the role of TPC2 being directly involved in the NAADP-mediated Ca^{2+} release from lysosomes, and that NAADP is a key mediator of this rise in intracellular Ca^{2+} release. The binding

site of NAADP to TPC2 was unknown until the Patel group where able to show that NAADP uses two accessory binding proteins, Jupiter microtubule associated homolog 2 (JPT2) and lik-Sm protein 12 (LSM12) (Marchant et al. 2022). These small accessory proteins serve as a bridging mechanism through which NAADP binds to TPC2 at its cytosolic side to elicit the release of luminal Ca^{2+}. One of the most interesting discoveries in the last few years has been that NAADP acts as a potentiator of the channel, where NAADP sensitises the channel to other stimuli. These other stimuli come in the form of two novel agonists of TPC2, TPC2-A1-N and TPC2-A1-P. As the names infer, TPC2-A1-N mimics the effects of NAADP binding and switches the channel to bias the efflux of Ca^{2+} ions from the lysosomal lumen in the cytosol. The opposite is that of TPC2-A1-P, whereby it mimics $PI(3,5)P_2$ binding and causes a rapid Na^+ efflux via TPC2 (Gerdnt et al. 2020; Yuan et al. 2023). This biasing capability has highlighted these compounds as powerful tools for studying the architecture and function of TPC2. I have proposed that TPC2 is the candidate channel through which NAADP-mediated Ca^{2+} release fluxes, allowing binding of this Ca^{2+} to the EF-hand domain of Rab46, eliciting dispersal of the protein from the MTOC, following histamine stimulation.

1.6.4 Transient receptor potential mucolipin 1 (TRPML1)

TRPML1 belongs to the TRP superfamily of ion channels and there exist three isoforms of the channel in mammals, however, TRPML1 remains the most characterised and to date, has been regarded as the primary lysosomal cation channel (Puertollano & Kiselyov, 2009). It is primarily localised to lysosomes, late endosomes, and endo-lysosomes, with documented evidence of expression at the ER, but this is not a defining feature of the channel. TRPML1 is regarded as a non-selective cation channel, permeable to Ca^{2+}, Na^+ and K^+, with Ca^{2+} serving as the main cation flux (Samie and Xu, 2011). Unlike TPC1 and TPC2, TRPML1 appears to be gated via low luminal pH within lysosomes, where channel activity is most active between pH 4.5-5.5, compared to neutral. The role of NAADP in modulating ligand activation of the channel is not well reported, and studies have looked at intraluminal Ca^{2+} as a potential gating mechanism through the vesicular fusion of SNAREs to lysosomes, however, the role of Ca^{2+} gating is less clear-cut (Ruas et al. 2015, Bhattacharjee et al.

2024). From the clinical perspective, the role of TRPML1 is highly regulated, where mutations in *MCOLN1* can lead to Mucolipidosis type IV (MLIV), a lysosomal storage disease, whereby processes such as autophagy are dysregulated leading to a build-up of lipids within lysosomes, causing neurological and ophthalmological issues (Park et al. 2015). This highlights the critical role of TRPML1 in the regulation of lysosomal homeostasis and Ca^{2+} is believed to have a very direct role in this pathway. Again, as per the mechanisms discussed earlier surrounding TPC1/2 mediated Ca^{2+} release, TPRML1 Ca^{2+} release is mediated by NAADP and is distinct from that of IP_3/RyR-mediated Ca^{2+} release. This spatial distinction of Ca^{2+} signals on the lysosome, vs the ER, leads to localised Ca^{2+} signals that can be potentiated through CICR, to induce SOCE, sometimes referred to as two-step Ca^{2+} signalling (Faris et al. 2018; Brunetti et al. 2024).

Altogether, it is clear that these three endo-lysosomal cation channels share a common denominator, in that they all are capable of fluxing Ca^{2+} and releasing this ion from lysosomal stores, and they can all be gated by the potent Ca^{2+} mobilising agent NAADP. This thesis will aim to study these three channels in greater detail to understand their signalling dynamics alongside how the channels can be activated using potent agonists to study Ca^{2+} signalling. With Rab46 function in endothelial cells relying on intracellular localised Ca^{2+} signals from NAADP-mediated channels, the transport of Ca^{2+} ions across these three channels is responsible for the Ca^{2+}-dependent dispersal of Rab46 and WPBs from the MTOC following acute immunogenic stimulation.

1.7 NAADP; ‘trigger hypothesis’

The mechanisms through which Ca^{2+} responses are mediated in lysosomes are complex and require coordination of multiple signalling pathways and channels within the endo-lysosomal network. At rest, lysosomes exist in an equilibrium-like fashion regarding maintaining Ca^{2+} concentration on either side of the lysosomal lumen. From a signalling perspective, this modality is modulated through the actions of TPRML1 and ATPases on the membrane that actively pump out and flux through Ca^{2+} ions to maintain the acidity of the lysosome

around pH 4.5 (Xiong & Xhu, 2016; Bhattacharjee et al. 2024). The activation of lysosomes by NAADP is not a new school of thought, however, more recently it has been shown that NAADP does not bind directly to small lysosomal cation channels, it uses small binding proteins, JPT2 and LSM12 to indirectly bind to Ca^{2+} channels such as TPC2 (Gunaratne et al. 2023). Through this indirect binding of NAADP, there is a sudden activation of the lysosome, resulting in an efflux of Ca^{2+} through one of these undefined lysosomal membrane channels into the cytosol of the cell. From here, the sufficient release of Ca^{2+} and the concurrent increase in NAADP signalling is detected, eliciting the Ca^{2+} 'trigger' (Figure 1.10). This trigger response leads to the amplification of the NAADP-evoked Ca^{2+} signal via CICR, leading to ER store depletion, which activates SOCE through translocation of STIM1 to Orai1 leading to a rapid influx of Ca^{2+} into the cell via the SERCA pump to refill the ER stores.

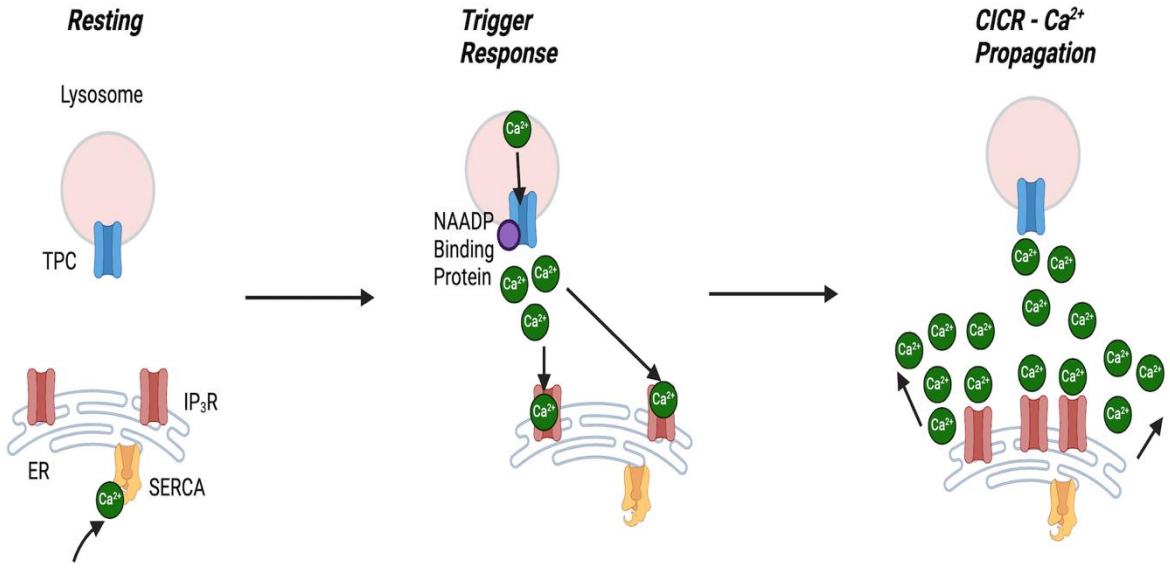

Figure 1.10 Ca^{2+} mobilisation from NAADP-mediated stores; 'trigger hypotheses. Lysosomal Ca^{2+} release is mediated by NAADP, where small, localised release of Ca^{2+} from an endo-lysosomal channel elicits propagation of the Ca^{2+} signal through the involvement of IP_3 and its receptor, IP_3R. This propagation is referred to as CICR and is a crucial mechanism in Lysosomal-ER Ca^{2+} cross-talk.

It is very apparent that these NAADP-evoked Ca^{2+} responses are highly localised and are specific to the endo-lysosomal system. The relationship between histamine-evoked Ca^{2+} signals within the system is well characterised and previous lab members have shown that Ca^{2+} release from NAADP-dependent stores results in small, highly localised Ca^{2+} responses, and at these low concentrations of histamine, there is a cycling of Rab46 and Ang2-positive WPBs through the cytosol of the cell, leading to a spatial distribution of the protein due to the increase in the production of NAADP. NAADP is a self-inhibitory protein at high concentrations, and this is due to the presence of two binding sites on the NAADP receptor, one with a high affinity and one with a low binding affinity. When NAADP binds to the high-affinity site, it triggers a huge surge in Ca^{2+} release however, as this saturates, NAADP starts to bind at the low-affinity site which induces a conformational change in the receptor, inhibiting further release of Ca^{2+}. The exact mechanisms that control this pathway are poorly understood, but this mechanism is crucial in preventing Ca^{2+} overload within cells, which could lead to cellular toxicity (Galione, 2019). This process of self-desensitisation is what is observed when cells are stimulated with high concentrations of histamine (30 μM). The rise in NAADP is so rapid, that it induces no further release of Ca^{2+} from lysosomes due to self-inhibition, hence, the EF-hand on Rab46 is unable to bind cytosolic Ca^{2+}, causing clustering of the protein at the MTOC with Ang2 containing WPBs. Altogether this evidence suggests a close and highly localised Ca^{2+} signalling pathway specific to histamine-evoked Ca^{2+} responses, evoking Ca^{2+} responses from endo-lysosomal stores that can have global effects on the cell through potentiation from ER involvement.

With Ca^{2+} being a pivotal intracellular messenger controlling a plethora of cellular functions, the influx and efflux of Ca^{2+} from lysosomal stores rely on cross-talk with other organelles to regulate a multitude of localised processes. In the early 1990s, NAADP was found to be a potent signalling molecule that could mobilise the release of Ca^{2+} from stores independently and insensitive to IP_3 and cADPR (Lee et al. 1995). Later, the lysosomal Ca^{2+} pool was found to reside at around 0.5 mM in concentration, which compared to the free cytosolic concentration (100 nM) is around 5000-fold higher (Christensen et al. 2002;

Churchill et al. 2002). Studies have attempted to characterise the establishment of the lysosomal Ca^{2+} gradient and the mechanism through which it is modulated. Early evidence suggested an unidentified Ca^{2+}/H^{+} proton exchanger; however, more recent evidence has pointed to small lysosomal membrane proteins playing a significant role in maintaining lysosomal homeostasis through activation of the mTOR and TFEB pathways (Morgan et al. 2011; Xiong & Zhu, 2016).

Lysosomes serve as highly concentrated intracellular Ca^{2+} stores, with studies questioning the mechanism(s) through which lysosomes replenish their Ca^{2+} pool. Advances in molecular biology have highlighted an ER-lysosomal cross-talk mechanism as the route for this refilling process. A 2016 study highlighted that the ER Ca^{2+} stored via SOCE maintains the Ca^{2+} concentration within lysosomes and this is independent of lysosomal pH. A rise in lysosomal pH triggered a rapid influx of Ca^{2+}, however, this was challenged after they found that inhibition of ER- Ca^{2+} refilling prevented the reuptake of Ca^{2+} into the lysosome (Garrity et al. 2016). Similarly, one group identified a cross-talk between the ER and lysosome concerning Ca^{2+} exchange. They decided to investigate the inflammasome, where lysosomotropic agents are established activators. They found that SOCE was coupled to a rapid efflux of K^{+} and when this was inhibited using pharmacology, there was a subsequent reduction in ER Ca^{2+} and a failure of lysosomal Ca^{2+} recovery (Kang et al. 2024). A 2014 paper highlighted a relationship between Ca^{2+}-activated potassium channels that take form in non-excitable cells (e.g. ECs, cancer cells). They postulated a role of K^{+} efflux potentiating SOCE through a mechanism known as hyperpolarisation-accelerated Ca^{2+} influx (Gueguinou et al. 2014). Although much is still to be learned surrounding Ca^{2+} refilling in the lysosome, these links to K^{+}-induced Ca^{2+} influx via SOCE (from the ER stores) provide context regarding ER-lysosomal cross-talk and with this being involved with the inflammasome, there is a high probability of a connection between the immunogenic histamine stimulus and the complexes that form to facilitate this ER-lysosomal refilling mechanism.

1.8 NAADP antagonists

To effectively study the associated Ca^{2+} dynamics, a potent and selective inhibitor of NAADP was discovered through a visual drug screening (Naylor et al. 2009). The study used mouse pancreatic beta cells to confirm that Ned-19 specifically inhibited NAADP-evoked Ca^{2+} signals. Ned-19 has been shown to confer equal selectivity for blockade of both two-pore channel protein 1 (TPC1) and two-pore channel protein 2 (TPC2), both of which are small endo-lysosomal Ca^{2+} channels believed to be involved in NAADP-mediated Ca^{2+} release from small, acidic stores (Ruas et al. 2015). Galione et al. were the first to identify the self-inhibitory nature of NAADP, demonstrating that as the concentration of NAADP rises within cells, it reaches an auto-inhibitory level (Galione et al. 2011). As the NAADP concentration rises in the cell, so does the cytosolic Ca^{2+} concentration. Our lab has hypothesised that it is this rise in cytosolic Ca^{2+} detected by the EF-hand domain of Rab46 which elicits the dispersal of Rab46-positive WPBs from the MTOC following acute stimulation with histamine. In this thesis I will explore the effect of Ned-19 inhibition of TPC1/2 on the histamine-evoked Ca^{2+} response in hAECs and whether inhibition of NAADP, alters Rab46 distribution in this cell type.

Tetrandrine is a plant-derived alkaloid that was initially discovered in Japan in 1928 and later confirmed in 1935 to be a plant-derived medicine (Liu et al. 2016). It was not until 1995 that tetrandrine was identified as a potent Ca^{2+} channel blocker (Wang & Lemos, 1995). It has been shown to confer selectivity for TPC2 over TPC1(Alharbi & Parrington, 2025; Morgan et al. 2022). However, studies have highlighted that it can be linked to TPC1 blockade (Huang & Hong, 1998). The reason tetrandrine has become a popular target for NAADP-mediated Ca^{2+} blockade is the low concentration (< 5 μM) required for effective inhibition of TPC2-mediated Ca^{2+} release. This is in comparison with Ned-19 and other pharmacological TPC2 blockers such as nifedipine and verapamil that block at high concentrations and thus make tetrandrine a promising target for viral therapy and the study of intracellular Ca^{2+} dynamics from TPC2 (Genazzani et al 1997; Rahman et al. 2014).

Recent computational modelling of TPC2 has suggested that tetrandrine interacts with distinct hydrophobic residues within the pore region of TPC2 (specifically the S5-S6 linker) which contributes to its selective blockade of this channel. With this, tetrandrine has been attributed to preferring TPC2 blockade over TPC1. This is due to amino acid changes in the S5-S6 and pore loop of TPC2 creating a favourable binding pocket for tetrandrine (Heister & Poston, 2020; Patel et al. 2022). Studies within the field have highlighted the potential of therapeutic uses for tetrandrine through analogue screening. One group stripped tetrandrine of its bis benzylisoquinoline structures and unveiled a heightened potency and selectivity for TPC2 blockade, the group attributed this outcome to be beneficial in preventing cancer cell proliferation and impairing proangiogenic responses in endothelial cells, compared to tetrandrine alone (Muller et al. 2021).

1.9 NAADP agonists

One of the most interesting discoveries in the last few years has been that NAADP acts as a potentiator of the TPC2 channel, where NAADP sensitises it to other stimuli. These stimuli come in the form of two novel agonists of TPC2, TPC2-A1-N and TPC2-A1-P. As the names infer, TPC2-A1-N mimics the effects of NAADP binding and switches the channel to bias the efflux of Ca^{2+} ions from the lysosomal lumen in the cytosol. The opposite is that of TPC2-A1-P, whereby it mimics $PI(3,5)P_2$ binding and causes a rapid Na^{+} efflux via TPC2 (Gerdnt et al. 2020; Yuan et al. 2023). This biasing capability has highlighted these compounds as powerful tools for studying the architecture and function of TPC2. I have proposed that TPC2 is the candidate channel through which NAADP-mediated Ca^{2+} release fluxes, allowing binding of this Ca^{2+} to the EF-hand domain of Rab46, eliciting dispersal of the protein from the MTOC, following histamine stimulation.

1.10 Summary

This chapter provides a comprehensive overview of the indispensable contribution of endothelial cells to the maintenance of haemostasis. It highlights the key relationship between Rab46 and its EF-hand Ca^{2+} binding domain in the context of histamine-stimulus coupled trafficking of Rab46 to the MTOC with Ang2-positive WPBs. Rab46 serves as a sensor for Ca^{2+} released from a highly specific endo-lysosomal locale and this is pivotal in the regulation of this protein *in vivo,* especially in the context of cardiovascular disease. Understanding this novel NAADP-mediated Ca^{2+} signalling territory will open new avenues for potential therapeutics for lysosomal storage diseases and will provide mechanistic insight into how large Rab GTPases coordinate highly localised Ca^{2+} signals from acidic organelles to potentiate these via CICR into global Ca^{2+} responses involving ER Ca^{2+}. Research is required to establish which endo-lysosomal channel(s) coordinate these Ca^{2+} signals responsible for the detachment of Rab from the MTOC, an area that provides the basis for this thesis.

1.11 Aims and Objectives

Hypothesis

NAADP-mediated Ca^{2+} release from endo-lysosomal Ca^{2+} channels is responsible for the detachment of Ang2-positive WPBs from the MTOC following acute immunogenic stimulation.

Aim

The aim of this project is to identify the candidate ion channel(s) located on endo-lysosomes as the primary source of Ca^{2+} responsible for the detachment of Rab46 and Ang2-positive WPBs from the MTOC following acute immunogenic stimulation with histamine.

Understanding the highly localised Ca^{2+} signals, mediated via NAADP through these channels using a pharmacological approach will provide an insight in to the level of contribution of Ca^{2+} has in the regulation of Rab46 dependent trafficking of Ang2 and WPBs in the context of immunogenic stimulation. Insights into the mechanisms that underlie these physiological changes will aid the development of therapeutic targets for the treatment of cardiovascular diseases.

Objectives

1. Observe the inhibitory effects of Ned-19 on NAADP-mediated Ca^{2+} signalling and distribution of Rab46.
2. Characterise the novel TPC2 agonist, TPC2-A1-N in ECs in the context of histamine stimulation.
3. Explore the effects of endo-lysosomal Ca^{2+} channel knockdown on the histamine-evoked and TPC2-A1-N-mediated Ca^{2+} response.
4. Investigate the relationship between inflammatory disease and SNPs significantly associated with Rab46.

Chapter. 2

Methodology

2.1 Reagents

Table 2.1 List of common reagents

Product	Solvent	Stock concentration	Working concentration	Supplier
BAPTA-AM	DMSO	25 mM	10 + 20 µM	Bio-techne®
DMSO	N/A	N/A	1:1000	Honeywell® Research Chemicals
Fura-2-AM	DMSO	1 mM	2 µM	Invitrogen (Thermo Scientific™)
Histamine	DH_2O	100 mM	0.1 µM – 300 µM	Sigma Aldrich ®(Merck)
Hoechst 33342	DDH_2O	10 mg/mL	1: 1000	Cell Signalling Technologies
PA-127	DMSO	10%	1:1000	Sigma Aldrich® (Merck)
PFA	PBS	4%	4%	Alfa Aesar / Thermo Scientific™
PMA	DMSO	5 mM	1 µM	Sigma Aldrich®(Merck)
RO2959	DMSO	10 mM	10 µM	MedChem Express LLC
Tetrandrine	DMSO	5 mM	5 µM	Santa-Cruz Biotechnologies
Thapsigargin	DMSO	5 mM	1 µM	Sigma Aldrich®(Merck)
Thrombin	DH_2O	200-250 U/ml	0.1U/ml	Thermo Scientific™
TPC2-A1-N/P	DMSO	100 mM	5 µM – 100 µM	MedChem Express LLC
Ned-19	DMSO	100 mM	100 µM	Bio-techne®
Yoda-1	DMSO	10 mM	2 µM	Bio-techne®

2.2 Cell culture

2.2.1 HUVEC

Pooled human umbilical vein endothelial cells (HUVEC) from PromoCell® were harvested and subsequently cultured in endothelial cell basal medium (EBM-2) supplemented with endothelial growth medium-2 supplement pack (PromoCell®) to produce working complete media (EGM-2). Cells were incubated in a humidified incubator at 37°C and 5% CO_2. Cells were then passaged twice weekly and passages 1 through 5 were used for experimental purposes.

2.2.2 hAEC

Primary human aortic endothelial cells (hAEC) from PromoCell® were harvested and subsequently cultured in endothelial cell basal medium (EBM-2) supplemented with endothelial medium supplement pack MV2 (PromoCell®) to produce working complete media (EMV-2). Cells were incubated in a humidified incubator at 37°C and 5% CO_2. Cells were then passaged twice weekly and passages 1 through 5 were used for experimental purposes.

2.3 Immunocytochemistry (ICC)

Cells were incubated in an Ibidi® µ-Slide 8-well^{HIGH} slide on day one (300 µL max vol./50,000 cells per well). On day two, media was aspirated and 300 µL EGM-2/EMV-2 was added and incubated at 37°C, 5% CO_2 in a humidified incubator. On day three, media was aspirated. Cells being stimulated had 300 µL of [1X] M199+HEPES media added per well and incubated at 37°C, 5% CO_2 for 1 hr before stimulation to serum starve the cells. If inhibitors were being used in the assay, 30 mins into this 1 hr serum starve, inhibitors were reconstituted in [1X] M199+HEPES to the desired concentration and added onto cells for 30 mins before stimulation. Cells were then washed 1x with PBS. If stimulating, compounds diluted to working concentrations were prepared in M199+HEPES and added to cells for 10 mins. 4% paraformaldehyde (PFA) was then added to each well to fix cells and left for 10 minutes at room temperature.

Wells were then washed 3x with PBS and permeabilized with 0.1% Triton for 10 mins. Wells were washed 3x with PBS and subsequently treated with respective primary antibodies (1°) (Table 2.2) at the required dilution for 1 hr at room temperature. Washing with PBS was then repeated a further 3x to remove any unbound 1° antibody. Fluorescently labelled Alexa Fluor secondary antibodies (2°) were then prepared (Table 2.3) at the desired concentration and left on cells for 30 mins in dark conditions. Cells were then washed 3x with PBS to remove unbound 2° antibody. The nucleus was then stained using Hoechst 33342 at [1:1000 PBS] and left for 7 mins to incubate at room temperature in the dark. A further 2x washes with PBS were conducted before 4 drops per well of Invitrogen® Prolong Gold Mountant was added, covered with foil, and stored at 4°C until ready for microscopy.

Table 2.2 Primary antibodies for immunofluorescence

Primary antibody	Species	Dilution	Manufacturer	Lot. number
Anti-vWF	Human	1:200	Abcam	AB778
Anti-Angpoietin-2	Goat	1:200	Bio-techne®	AF623
Anti-CRACR2A	Rabbit	1:300	Antibodies.com	A89955
Anti-CRACR2A	Rabbit	1:300	Proteintech®	15206-1-AP
Anti-Pericentrin	Rabbit	1:300	Abcam	AB28144

Table 2.3 Secondary antibodies for immunofluorescence

Secondary antibody	Species	Dilution	Manufacturer	Lot. number
Fluorescein (FITC-488) Anti-Goat IgG	Goat	1:300	Jackson ImmunoResearch Europe LTD	705-095-147
Alexa Fluor 488 Anti-Rabbit Fab Frag	Rabbit	1:300	Jackson ImmunoResearch Europe LTD	711-547-003
Alexa Fluor 594 Anti-Mouse IgG	Mouse	1:300	Jackson ImmunoResearch Europe LTD	715-585-150
Alexa Fluor 488 Anti-Rabbit IgG	Rabbit	1:300	Jackson ImmunoResearch Europe LTD	711-545-152
Alexa Fluor 594 Anti-Rabbit IgG	Rabbit	1:300	Jackson ImmunoResearch Europe LTD	715-585-152

2.4 Microscopy

2.4.1 Widefield deconvolution microscopy

The CellSens deconvolution system (Olympus) was used throughout to image cells plated on Ibidi® µ-Slide plates on an Olympus IX-83 inverted microscope. For Z-stack imaging, 10-focal planes were sectioned at 0.2 µm per Z-stack per image and were taken on a Photometrics-BSI camera device. Re-iterative deconvolution (5x) was performed using an advanced maximum likelihood algorithm to rebalance out-of-focus light (deconvolution) from one focal plane of

the Z-stack to another. The filters used on the Olympus IX83 camera were as follows, DAPI; GFP, and RFP. The objective used was a 60x/1.4 oil. All images were taken at ambient room temperature and image acquisition, and further processing was conducted using the CellSens Olympus software before transfer to storage.

2.4.2 Image processing and analysis

All maximum projection (intensity) images were generated using the CellSens (Olympus) software before being transferred to ImageJ Fiji for analysis. ImageJ macros (see appendix) were used for the quantification of Rab46 distribution and WPB counts.

2.4.3 WPB counts

Image channels were split, and the background was subtracted from the DAPI/RFP channels. A local threshold was set and subsequently followed by particle analysis (WPB Count macro, see appendix) to determine the number of WPBs per image. Five images per condition, per repeat, were analysed.

2.4.4 Rab46 distribution

The intracellular distribution of Rab46 and the relative particle intensity were determined using a customised macro (Rab46 Distribution macro, see appendix) Briefly, an 8-bit image was loaded into ImageJ Fiji. Image channels were then split, and the background was subtracted from the DAPI/GFP channels. A binary mask of the DAPI channel was created using a default threshold. Background noise was subtracted using the median filter and a distance map was generated using the StarDist 2D plugin (https://imagej.net/plugins/stardist) to estimate the cell edges. The GFP channel was duplicated to sample the un-modified pixel intensity of Rab46. Each channel was then segmented using the Max Entropy threshold and the distance and intensity of each particle from the nucleus was measured. I programmed the macro to automatically export the results tables with distance (Min) and intensity values per particle (IntDen) to an Excel file for each image, with 5-10 images (60x magnification) analysed per experimental condition. The Min and IntDen values were then imported to GraphPad Prism 9. Distance (Min) values

ranged from 0 px (nucleus-black) to 255 px (periphery-white). This spectrum of values was then binned into 3 distinct regions: Perinuclear (x < 2 μm); Intermediate (2 μm < > 5 μm); and Periphery (x > 5 μm), where x is defined as the distance from the nucleus to the cells peripheral edge (Figure 2.1). The integrated intensity was then normalised to the total fluorescence of the image (TIF). The mean values were calculated for each area and averaged amongst all the images per condition. The mean values amongst all biological repeats were presented in GraphPad Prism 9 as bar-plots depicting mean ± SEM, whereby the Y-axis denotes the ‘normalised integrated intensity (as a ratio of TIF) and the X-axis denotes the distance from the nucleus displayed as the binned signal into the three subcellular regions described above.

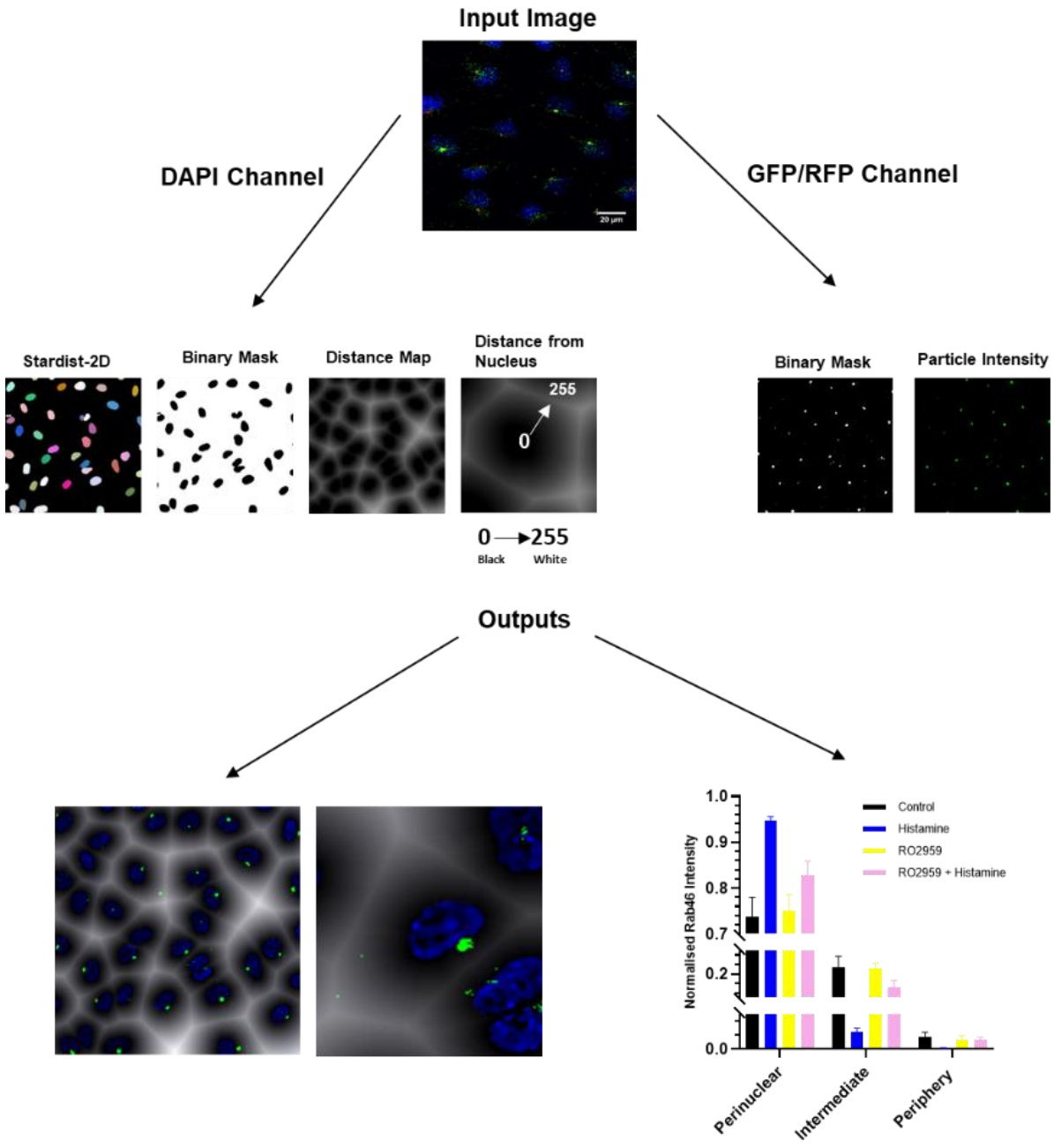

Figure 2.1 ImageJ macro workflow. Images were loaded into ImageJ. All channels were split and binary masks of those were generated. A distance map was produced on the DAPI channel where the pixels were replaced with a greyscale value from 0-255 (black-white), respectively. Distance from the nucleus of each particle was measured across three distinct areas and the respective particle intensity was noted alongside its corresponding map location. The outputs (distance (Min) and intensity (IntDen) were exported to GraphPad to obtain normalised intensity ratios, plotted as bar charts, where the x-axis is the cellular location and the y-axis, is normalised intensity as a ratio.

2.5 RT-qPCR

2.5.1 RNA extraction

HUVEC and hAEC cells were plated on a 6-well plate to a concentration of 250,000 cells per well and grown to confluency with daily media changes (2 ml/well). Total RNA was then extracted using a High Pure Total RNA Isolation Kit (Roche®) as per the manufacturer's protocol. In summary, the cell culture medium was aspirated, and the cells were washed with ice-cold PBS before shearing with 200 µl lysis buffer per well, adding this to a spin column. For each sample, 90 µl DNase incubation buffer I and 10 µl of DNase enzyme were added to the spin column before incubating and undergoing centrifugation. Following three intermediary wash steps, the RNA was collected using ~50 µl elution buffer, and then quantified on a DeNovix Nanodrop, before being stored at -80ºC or used immediately in RT-qPCR.

2.5.2 Reverse Transcription PCR

Complimentary DNA (cDNA) was initially synthesised using a High-Capacity RNA-to-cDNA RT Kit (Roche®). RNA was measured on nanodrop and diluted in nuclease-free water to 100 ng/µl before being mixed with 5 µl 2x RT buffer, 1 µl 20x RT enzyme mix, and nuclease-free water to create a final reaction volume of 10 µl. Non-reverse transcribed control samples were prepared and evaluated. The samples were mixed thoroughly, centrifuged (1000 rcf for 1 min), and then placed in a BioRad® T100 thermal cycler according to parameters listed below (Table 2.4), resulting in cDNA that was then diluted in 30 µl nuclease-free water to give a final volume of 40 µl cDNA ready for use in qPCR or short-term storage at 4ºC.

Table 2.4 Thermal cycler – BioRad® T100 setup

Temperature (ºC)	Time (hh:mm:ss: ss)
(1) 25	00:00:30
(2) 37	01:00:00
(3) 95	00:05:00
(4) 4	∞

2.5.3 qPCR

RT-qPCR was conducted using the LightCycler® 480 SYBR Green 1 Master Mix (Roche®) on a LightCycler® 96 (Roche®). Each reaction was set to have a final volume of 20 µl. This contained: 10 µl of 2x the LightCycler® 480 SYBR Green 1 Master (containing FastStart Taq DNA Polymerase, reaction buffer, dNTP mix (with dUTP instead of dTTP), SYBR Green 1 dye, and MgCl2), 1.5 µl forward primer (0.75 µM), 1.5 µl reverse primer (0.75 µM), 2 µl cDNA, and 5 µl nuclease-free water. Real-time qPCR primers (Table 2.5) were designed using the Primer3-BLAST tool (http://www.ncbi.nih.gov/tools/primer-blast/). DNA amplification commenced using the template described below (Table 2.6) and the relative abundance of target genes amplified by RT-qPCR was calculated relative to the housekeeping genes, GAPDH and ß-Actin. These genes were selected as they participate in glycolysis and cytoskeletal integrity, respectively. Based on these ubiquitous activities, their expression was not readily altered by the immunological histamine stimulus (Shasby et al. 2002).

Table 2.5 – RT-qPCR primers

Target	Primer Sequence (5’ – 3’)
h-GAPDH	Unknown
h-ß-Actin	Unknown
h-Rab46	**F:** 5’ GGTCATCCTTGCCTACG 3’ **R:** 5’ GCTCGCATGAGATCAAGT 3’
h-TPC1	**F:** 5’ TGGCTTTGAAAGGGAGCTCAAAC 3’ **R:** 5’ CCGCCATTTTTGCTAGGTAGCTC 3’
h-TPC1 (AS/S)	**F:** 5’ GCATTTTCCTGGACTGT 3’ **R:** 5’ AGACTCAGGCAGGTTCTGGA 3’
h-TPC2	**F:** 5’ GGTTGCTTGGGTTGTGCATT 3’ **R:** 5’ CTCACTGCAGGTAGACAGCC 3’
h-TRPML1	**F:** 5’ AGTGCCTGTTCTCGCTCATC 3’ **R:** 5’ CCGGGATGCTTGATGGTGTC 3’

Table 2.6 qPCR template – LightCycler® 96 (Roche®)

Temperature (°C)	Time (hh:mm:ss: ss)
(1) 95	00:10:00
(2) 95 **(3) 60**	00:00:15 00:01:00 **(x40 Cycles)**
(4) 105 **(5) 37**	00:00:15 00:00:10
(6) 4	∞

2.6 Western blotting

2.6.1 Lysate preparation and BCA protein quantification

Cells were seeded onto a 6-well tissue culture plate (Corning®) at a concentration of 250,000 cells/well in complete media. 24 hrs later the used media was aspirated off and replaced with an ice-cold PBS wash (~500 µl/well) to terminate any cellular reactions and prevent proteolysis. The PBS was then removed carefully and 60 µl lysis buffer (0.5 ml mPER lysis buffer (Thermo Scientific™), 1 µl anti-protease cocktail (Sigma-Aldrich®, P8340), and 10 µl broad-range anti-phosphatase (Sigma-Aldrich®, 524629) added per well. Each well was then scraped vigorously for 15 seconds. Once scraped, the plate was inverted vertically, and the lysate was collected into 1.5 ml Eppendorf tubes and quickly placed back on ice and left to incubate for 30 mins. The lysates were then centrifuged at 12,000 g for 10 mins at 4 °C and the supernatant was collected and stored at -20 °C (0-3 months) or -80 °C (>3 months).

Determination of the protein concentration in each lysate was conducted using the Rapid Gold BCA Kit (A53225, Thermo Scientific™). An Excel template (see appendix) was filled in to provide the appropriate loading volumes depending on gel type and generate the standard protein curve using Bovine Serum Albumin (BSA) as the standard.

2.6.2 Gel loading and transfer

A 4-20% acrylamide gel (BioRad®) was loaded into a Bio-Rad® chamber tank and 1X TGS running buffer (diluted from 10X with dH2O, Bio-Rad®, Table 2.7) was added to the required volume within the tank. 4-8 µl/well of known molecular weight protein ladder (46.5-270 kDa, Abcam, AB234592) was added to desired wells followed by an allocated volume of samples denoted by the results of the Excel template (see appendix) using gel loading tips. The tank was then connected to the Powerpack unit and electrophoresed at a constant voltage of 160V for ~60 mins or until the bromophenol blue band had run out of the gel.

A semi-dry transfer was conducted using Bio-Rad® Trans-blot Turbo alongside the Trans-blot Turbo RTA Mini 0.2 µm PVDF Transfer kit (Bio-Rad®, #1704272). Two stacks were prepared per membrane and soaked for 3 mins beforehand in transfer buffer (10 ml of 5x transfer buffer (Bio-Rad®), 10 ml 100% ethanol, and 30 ml dH_2O, Table 2.7). A pre-cut PVDF membrane was then activated for 15 secs in 100% ethanol, before being soaked in transfer buffer, preventing drying. The gel was then stopped and opened before transferring onto Whatmann paper and transferred onto the stack following the procedure defined on the kit. The transfer was performed using the High molecular weight (HIGH MW) program.

Table 2.7 Western blotting reagents

Solution	Chemical composition
Sample (loading) buffer (4x)	200 mM Tris (pH 6.8), 8% SDS, 40% glycerol, 8% beta-mercaptoethanol, and 0.1% bromophenol blue
Running buffer	25 mM Tris, 192 mM glycine, and 0.1% SDS, pH 8.3
Transfer buffer	48 mM Tris, 39 mM glycine, 0.5% SDS, and 20% methanol
TBS-T	145 mM NaCl, 20 mM Tris-base, 0.5% Tween-20, pH 7.5

2.6.3 Blocking, antibody probing, and imaging

Blocking was performed using 5% skimmed milk powder (VWR Chemicals™) diluted in 1X TBS-T (5 g/100 ml) and placed on a rocker for 1 hr at room temp. Primary (Table 2.8) and secondary antibodies (Table 2.9) were prepared with the primary antibody applied for 24 hr at 4*C on a rocker and secondaries applied for 1 hr on a rocker at room temperature. A 1:1 dilution of Dura/Femto solution (Thermo Scientific™) was applied to the membrane before imaging on the iBright™ FL1500 Imaging System (Invitrogen, Thermo Scientific™).

Table 2.8 Primary antibodies for Western blotting

Primary antibody	Species	Dilution	Manufacturer	Lot. number
Anti-CRACR2A	Rabbit	1:1000	Antibodies.com	A89955
Anti-TPCN1	Rabbit	1:1000	Proteintech®	23758-1-AP
Anti-TPCN2	Rabbit	1:1000	Abcam	AB119915
Anti-TRPMLN1	Rabbit	1:1000	ABCEPTA.com	AP1355-1B-EV

Table 2.9 Secondary antibodies for Western blotting

Secondary antibody	Species	Dilution	Manufacturer	Lot. number
Peroxidase AffiniPure™ F(ab')$_2$ Fragment Donkey Anti-Rabbit IgG (H+L)	Rabbit	1:10,000	Jackson ImmunoResearch Europe LTD	711-036-152
Peroxidase AffiniPure™ Donkey Anti-Mouse IgG (H+L)	Mouse	1:10,000	Jackson ImmunoResearch Europe LTD	715-035-150
beta-Actin [C4], Mouse Monoclonal Antibody	Mouse	1:10,000	Insight Biotechnology LTD	SC-47778

2.7 Intracellular Ca^{2+} measurements – Flexstation

Cells were seeded onto a black, clear-bottom Greiner Bio-One® 96-well plate at a seeding density of 200 µl max vol./15,000 cells per well and placed in a humidified incubated at 37°C, 5% CO_2 for 24 hrs to achieve a confluency. For assays conducted in 0 mM Ca^{2+}, only the compound plate solutions and recording buffer stages contained 0 mM Ca^{2+} SBS + 0.4 mM EGTA, all other steps were conducted using 1.5 mM Ca^{2+} SBS (Table 2.10). The following day, a Fura-2-AM solution (Fura-2-AM (2 µM, 10% pluronic acid (PA-127), 1.5 mM Ca^{2+} SBS) was prepared. The growth media was aspirated and 50 µL of the Fura-2-AM mix was added per well. The plate was then covered with foil and left to incubate for 1 hr at 37°C in a non-humidified, non-CO_2 incubator. The Fura-2-AM mix was aspirated, and wells were washed 2x with 100 µL SBS the 2nd wash was left on (if incubating with inhibitors, this was applied here) and incubated for 30 mins in dark conditions at room temperature to allow the esterase to cleave the -AM. After incubation, wells were aspirated and 80-100 µL recording buffer (SBS, assay dependent) was added to each well. For flex runs where there was only a single addition, 100 µl SBS was added per well and protocols setup as described (Table 2.11). For double compound addition flexes, 80 µl SBS was added per well, and protocols were set as described (Table 2.12).

The change (Δ) in intracellular Ca^{2+} concentration above baseline is identified by the ratio of Fura-2 fluorescence by emission at 340 nm and excitation at 380 nm. This is plotted on a trace as the ratio of change in fluorescence ($\Delta[Ca^{2+}]_i\Delta(340/380)$). After completion, raw data was then processed and baseline subtracted for analysis and presentation on GraphPad Prism 9.

Table 2.10 Standard bath solutions (SBS) for Flexstation

Solution	Chemical composition
0 mM Ca^{2+} SBS	130 mM NaCl, 5 mM KCl, 8 mM glucose, 10 mM HEPES, 1.2 mM $MgCl_2$ (sol.), and 0.4mM EGTA, pH 7.4
1.5 mM Ca^{2+} SBS	130 mM NaCl, 5 mM KCl, 8 mM glucose, 10 mM HEPES, 1.2 mM

	$MgCl_2$ (sol.), and 1.5 mM $CaCl_2$ (sol.), pH 7.4
[3x] 1.5 mM Ca^{2+} SBS (Addback Responses)	130 mM NaCl, 5 mM KCl, 8 mM glucose, 10 mM HEPES, 1.2 mM $MgCl_2$ (sol.), and 4.5 mM $CaCl_2$ (sol.), pH 7.4

Table 2.11 Flexstation acquisition settings (single compound)

Option	Command
Flex	Fluorescence
Wavelengths	Unbound: 380 nm Bound: 340 nm
Excitation wavelengths	Lm1 = 340 nm Lm2 = 380 nm
Emission wavelength	510 nm
Sensitivity	Medium
Runtime	300 secs
Plate type (cells)	96-well Thermo Fisher black clear bottom
Plate type (compounds)	Costar 96 clear – round bottomed
Compound transfer settings:	
Transfers	1 per column
Initial vol. cell plate	100 µL
Pipette height	80 µL
Compound transfer vol.	100 µL
Time point	30 secs (to add treatments)
Titration	Pre-determined 1ul/sec

Table 2.12 Flexstation acquisition settings (dual compound)

Option	Command
Flex	Fluorescence
Wavelengths	Unbound: 380 nm Bound: 340 nm
Excitation wavelengths	Lm1 = 340 nm Lm2 = 380 nm
Emission wavelength	510 nm
Sensitivity	Medium
Runtime	600 secs
Plate type (cells)	96-well Thermo Fisher black clear bottom
Plate type (compounds)	Costar 96 clear – round bottomed
Compound transfer settings:	

Transfers	2 per column
Initial vol. cell plate	80 µL
Pipette height	70 µL
Compound transfer vol.	80 µL
Time point	30 secs (to add 1st treatment) 330 secs (to add 2nd treatment)
Titration	Pre-determined 1ul/sec

2.8 ELISA

2.8.1 Angiopoietin-2 ELISA

hAEC were seeded onto a clear-bottom, Nunc® coated 96-well plate (Thermo Scientific™) at a concentration of 15,000 cells/well, in a total volume of 200 µL EMV2. 24 hours later, cells were serum starved in basal M199 for 1 hr (± inhibitor) before stimulating for 10 mins in 1.5 mM Ca^{2+} SBS. After stimulation, the SBS was collected into Eppendorf's and centrifuged at 500 x g for 5 mins and then used immediately. The samples remained undiluted throughout. The ELISA kit used was a Human Angiopoietin-2 ELISA Kit from Antibodies.com (A77682) and all buffers, and reagents were made by the supplier information. A standard curve was generated from the supplied pre-determined Angpt-2 protein standard. The endpoint was determined by the addition of 50 µL of stop solution and the plate was read within 15 minutes on a Bio-Tek end-point plate reader at 450 nm to determine the optical density. All raw data was then exported to Microsoft Excel before the final analysis was completed on GraphPad Prism 9. To calculate the unknown concentrations of angiopoietin-2, blank-subtracted OD450 values were interpolated against the equation of the line for the standard curve.

2.9 Endothelial cell transfection

2.9.1 siRNA transfection for Ca^{2+} measurements

Primary human aortic endothelial cells (HAEC) (PromoCell®) were seeded onto a 6-well sterile cell culture plate (Corning®) at a concentration of (~200,000 cells/well) dependent on the rate of growth. Cells were plated using 2 ml/well complete endothelial growth medium-2 (EMV2) (PromoCell®) and were incubated in a humidified 5% CO_2 incubator at 37 °C for 24 hrs or until they

reached ~95% confluency before being transfected using Lipofectamine™ 2000. 30 mins before the application of transfection reagents, 800 µl of fresh EMV2 (no antibiotics) was applied to the cells. A 1:3 ratio of siRNA (Table 2.13) (1 µl) and Lipofectamine™ 2000 (3 µl) was used. The EMV2 was then aspirated and replaced with the transfection media mix (100 µl) ([1x] Opti-MEM, Gibco + Lipofectamine and siRNA) and 100 µl EMV2 (no antibiotics). After 6 hrs, the transfection medium was removed and replaced with 2 ml complete EMV2 media per well.

The next morning, cells were washed with 1X PBS, and then 500 µl of 0.05% trypsin + EDTA (0.4 mM) was added to each well of the 6-well plate before incubating for 5 mins to allow cells to detach. Each well was washed with 1.5 ml of complete EMV2 media before resuspending, counting, and plating at a concentration of 15,000 cells/well of a 96-well flex plate (Grenier Bio®) and placed in a humidified incubator at 37 °C, 5% CO_2 for 24 hrs before experimentation the following day.

2.9.2 siRNA transfection for immunofluorescence (IF)

Primary human aortic endothelial cells (HAEC) (PromoCell®) were seeded onto an 8-well µ-slide (Ibidi) at a concentration of 50,000 cells/well. Cells were plated using complete endothelial growth medium-2 (EMV2) (PromoCell®) and were incubated in a humidified 5% CO_2 incubator at 37 °C for 24 hrs or until they reached ~95% confluency before being transfected using Lipofectamine™ 2000. 30 mins before the application of transfection reagents, 130 µL of fresh EMV2 (no antibiotics) was applied to the cells. A 1:3 ratio of siRNA (0.5 µl) (Table 2.13) and Lipofectamine™ 2000 (1.5 µL) was used. 20 µl of the transfection mix ([1x] Opti-MEM, Gibco + Lipofectamine, and siRNA) was then added to the 130 µl media already in the wells. After 6 hrs, the transfection medium was removed and replaced with 300 µl fresh complete EMV2 media per well, with experiments being conducted a maximum of 48 hr after transfection to ensure sufficient knockdown.

Table 2.13 siRNA targeting sequences

Name/Target	Sequence	Supplier
siRNA Negative Silencer® Select	(UGGUUUACAUGUCGACUAA)	Ambion Inc.
EFCAB4B (Rab46) Silencer® Select siRNA	(GUGUGAAGGUCAAAAGAGAtt)	Ambion Inc.
MCOLN1 (TRPML1) Silencer® Select siRNA	N/A	Ambion Inc.
TPCN1 (TPC1) siRNA	N/A	Invitrogen
TPCN2 (TPC2) siRNA	N/A	Invitrogen

2.10 Statistical analysis

All averaged data is presented as the mean ± SEM. Any outliers were detected and then subsequently removed using a Grubb's test and equal variance was established. To determine if the data was extracted from a normally distributed population, a Shapiro-Wilk normality test was performed. When comparing data from two groups (normally distributed) significance was assessed using a two-sample t-test or a one-way (or two-way) ANOVA coupled with the Tukey *post-hoc* test when considering three or more groups of data. Data not extracted from a normally distributed population was evaluated for significance using one of the following: either a Mann-Whitney U test or a Kruskal Wallis test. The test chosen was dependent on the number of groups being considered. The presence of statistical significance was determined to exist at probability $p < 0.05$ (## $< 10^{-15}$, **** < 0.0001, *** < 0.001, ** < 0.01, * < 0.05). Where there are comparisons are represented by ns, no significant differences between groups were observed. GraphPad PRSIM9 and OriginPro22b were used for computing data analysis as well as the presentation of analysed data. n = the number of

independent biological repeats, and N = the number of technical repeats within 1 biological repeat. For immunofluorescence microscopy, each technical repeat per condition included 5-10 individual images.

Chapter. 3

Pharmacological inhibition of NAADP-sensitive Ca^{2+} channels in hAECs impacts histamine-evoked trafficking of Rab46 to the MTOC and Ang2 secretion.

3.1 Introduction

When endothelial cells (HUVEC and/or hAEC) are stimulated using the immunogenic amine histamine, we observe a retrograde translocation of Ang2-positive WPBs towards the MTOC. This movement is dependent on an EF-hand containing Rab GTPase, Rab46, but occurs independently of Ca^{2+} and has been verified in work performed previously (Miteva et al. 2019). The subsequent dispersal of Rab46-tagged WPBs away from the MTOC following histamine stimulation is dependent on Ca^{2+} binding to the EF-hand domain of Rab46. What the source of this Ca^{2+} is has remained unsolved. Here, I have functionally established that the source of this Ca^{2+} required for the release of Rab46 from the MTOC is not the global ER store, but the much smaller, and highly localised lysosomal Ca^{2+} store, which is mediated by the actions of the Ca^{2+} mobilising second messenger, NAADP.

The aim of this chapter is to determine if pharmacological inhibition of NAADP-sensitive channels using Ned-19 affects the dispersal of Rab46 from the MTOC and if this has an impact on histamine-evoked Ang2 secretion. I will use Flexstation Ca^{2+} measurements to look at localised changes in Ca^{2+} fluxes within the cells in response to various stimuli. High-resolution imaging will be used to look at the effects of these stimuli on the clustering of Rab46 and WPBs. This chapter reveals that using the potent NAADP antagonist, Ned-19, it is possible to study the NAADP-mediated Ca^{2+} signals that affect intracellular Ca^{2+} release and the subsequent spatial distribution of Rab46 within hAECs.

3.2 Rab46 is present at the protein level in endothelial cells

To allow for the study of the spatial and temporal distribution of Rab46 in endothelial cells, I validated two commercially available primary antibodies (anti-CRACR2A Rabbit Polyclonal (Figure 3.1A), Antibodies.com and Proteintech® anti-CRACR2A Rabbit Polyclonal (Figure 3.1B) raised against Rab46 using Western blot. In 2015, the work of Wilson et al., showed the first inclination of antibody specificity for Rab46, detecting a single band around 95 kDa in size in HUVEC lysate. To validate this in my hAEC model, I used a lipofectamine-only control and scrambled siRNA control for Rab46 as well as siRNA specific for Rab46 (Figure 3.1C) to check that I could achieve sufficient depletion of Rab46 in-vitro for experimental work and confirm antibody specificity by Western blot. I also included two lanes whereby (1) I overexpressed CRACR2A in hAEC (Figure 3.1A, B) (of which isn't present in EC's), where a clear band was detected around 45 kDa which shows specificity of the antibody for recognising both CRACR2A (short-form primarily found in T-cells) and Rab46 (EC specific) and (2) Rab46 was overexpressed tagged to GFP and again detected a band at 95 kDa (endogenous) and at 110 kDa (GFP-tagged Rab46). Since both blots indicated a reduced protein expression of Rab46 in the siRNA lane (Figure 3.1C) and that only a single band at 95 kDa was detected with both antibodies in the WT samples, it encouraged the next step which was to evaluate these antibodies under immunofluorescence staining protocols to observe the subcellular distribution of Rab46 in hAEC.

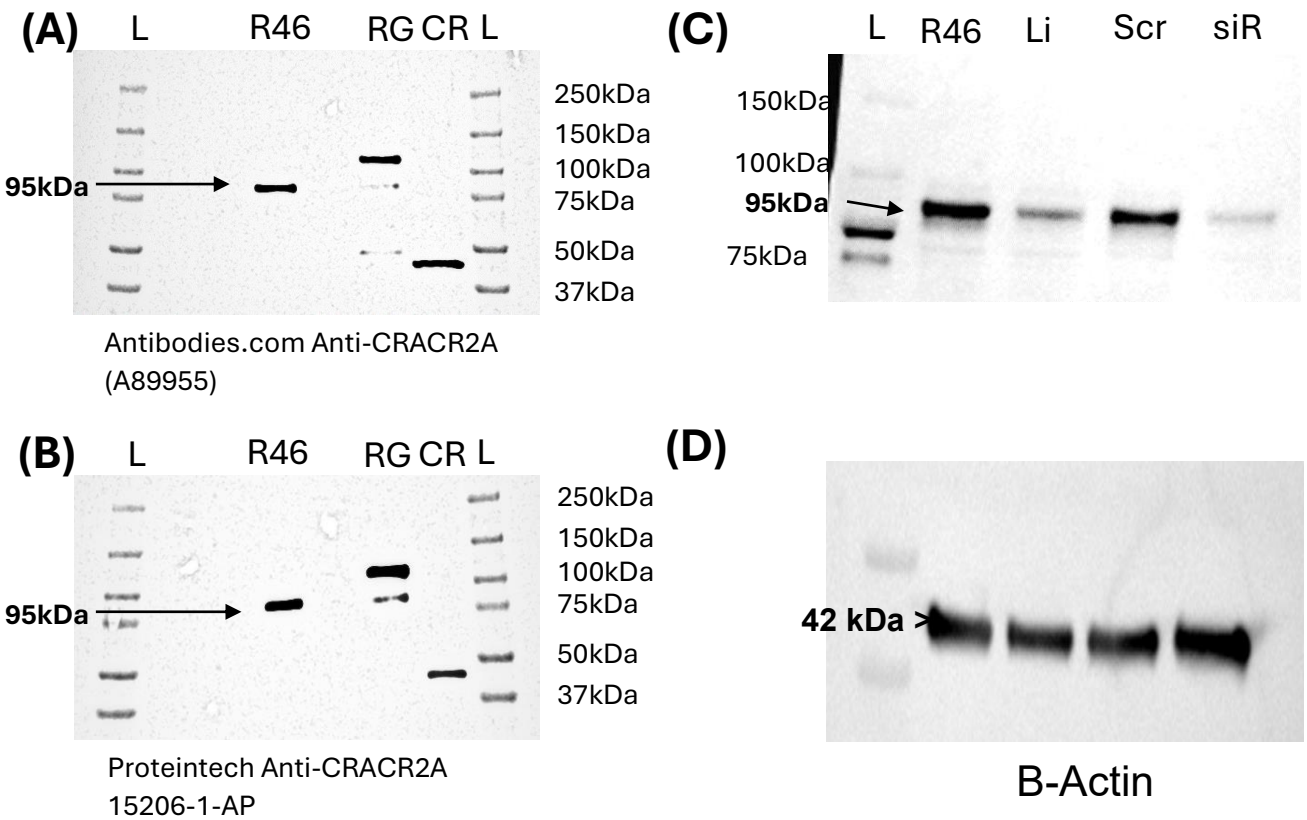

Figure 3.1 Specificity of primary antibodies for Rab46. Representative Western blots highlighting the specificity of both Antibodies.com (A) and Proteintech® (B) anti-CRACR2A commercially available antibodies against Rab46 (A) and (B) show Rab46 overexpression compared to control. (C) Cells depleted of Rab46 using transfection of a siRNA for Rab46 show bands with reduced intensity (R46; 35.5%, siR; 19.7% of β-Actin intensity) as compared to lipofectamine only and siRNA controls (Scr; 28.7%, Lipo; 20.9% of β-Actin intensity). (D) β-actin stain to show equal protein loading and siRNA transfection does not interfere with housekeeper protein expression. Details of the lanes are as follows: L = Ladder, Li = Lipofectamine Only, Sc = Scrambled Control, R46 = Rab46, SiR = siRNA for Rab46, RG = Rab46+GFP, CR = CRACR2A**.** n = 3.

3.3 Histamine evokes a concentration-dependent perinuclear clustering of Rab46 at the MTOC in hAEC

Histamine evokes clustering of Rab46 and WPBs at the MTOC in HUVECs, thus I wanted to determine if histamine-induced retrograde trafficking of Rab46 from the extracellular space to the MTOC in hAECs. hAECs were stimulated before being fixed and stained for Rab46. I have shown concentration-dependent retrograde trafficking of Rab46 to the MTOC in hAEC (Figure 3.2A). An increase in the distribution of Rab46 at the perinuclear region (Figure 3.2B), was evoked when concentrations of histamine exceeded 5 μM. From the distribution analysis conducted (represented as the distance from the nucleus, split into 3 regions) in hAEC treated with histamine, I observed that cells treated with low concentrations of histamine (≤ 0.3 μM) showed a diffuse distribution of Rab46 across the cell and similar when compared to control (Figure. 3.4C). Cells were co-stained with pericentrin to identify the MTOC, and it is apparent that as the histamine concentration increased, Rab46 colocalises with the pericentrin at the MTOC in the perinuclear region of the cell.

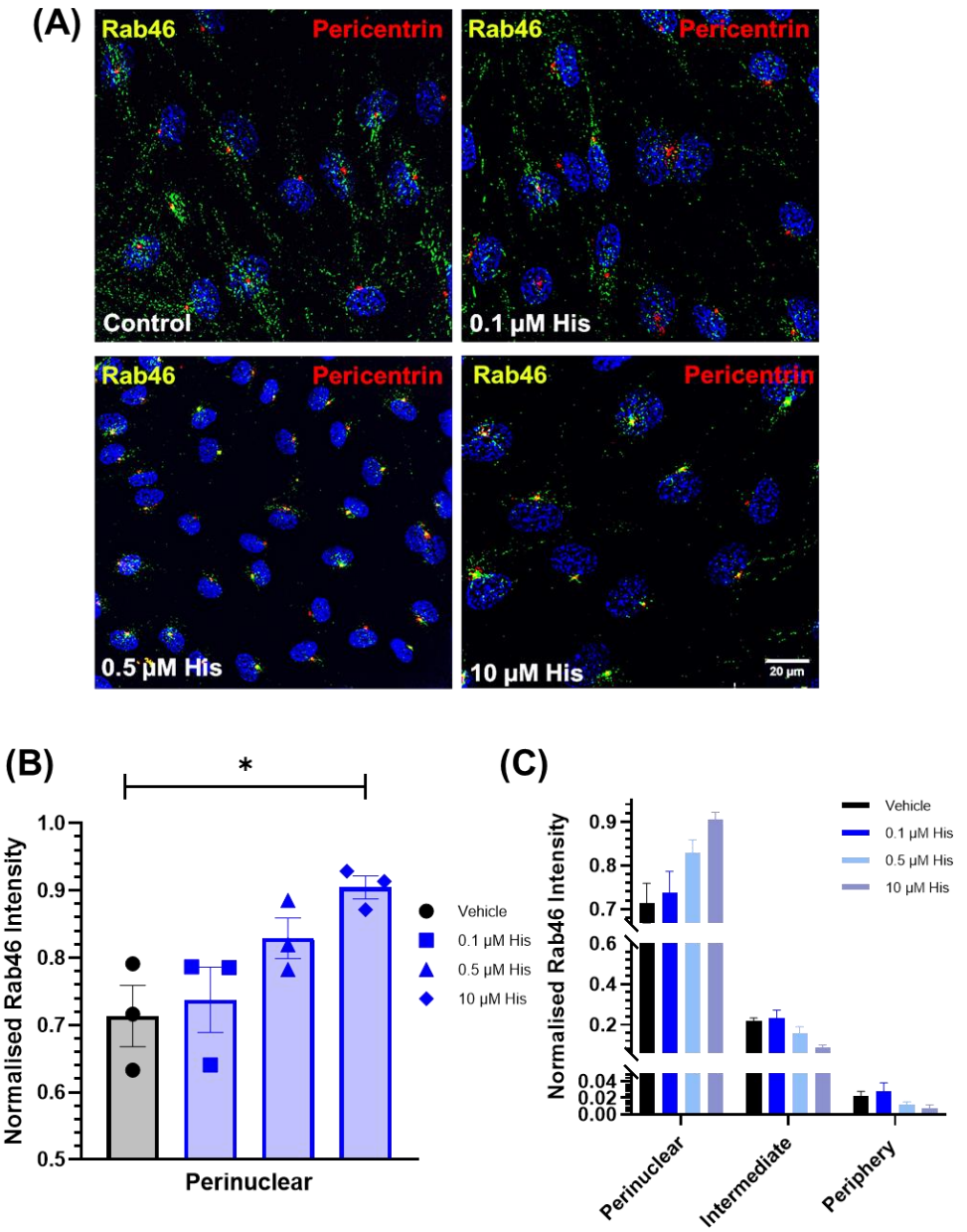

Figure 3.2 Histamine evokes a concentration-dependent clustering of Rab46 at the MTOC. (A) Representative images showing the distribution of Rab46 (green: anti-Rab46), and pericentrin (red: anti-pericentrin) across a range of histamine concentrations (0-10 µM). Hoechst 33342 (blue) shows nuclei. Scale bar = 20 µm. (B) The perinuclear region shows a dose-dependent increase in the clustering of Rab46 at the MTOC. (C) Distribution analysis showing the subcellular distribution of Rab46 across 3 defined regions of the cell, perinuclear (< 2 u µm), intermediate (2 <> 5 µm), and periphery (> 5 µm). Mean (± SEM) was reported as a ratio of the total signal intensity (NIR). * = $p < 0.05$ following One-way ANOVA , n/N = 3/15.

3.4 Movement of Rab46 to the MTOC is Ca^{2+} independent in hAEC

3.4.1 Blockade of Orai1 pore formation by RO2959 does not inhibit the Ca^{2+} response to histamine in hAEC.

To maintain Ca^{2+} homeostasis, cells will modulate their re-uptake of Ca^{2+} to the ER via the SOCE pathway (Daverkausen-Fischer & Prols, 2022). There are two distinct Ca^{2+}-mediated pathways for refilling stores. The most rigorously studied of these is the SOCE pathway which activates in response to a depletion of ER Ca^{2+} which triggers STIM1 translocation from the ER membrane to the PM to form a pore complex with Orai1 to promote an influx of Ca^{2+} into the cell. NAADP-mediated Ca^{2+} was first described by Lee et al. 2005 and is the mechanism by which lysosomal stores release and refill their Ca^{2+} stores. I wanted to block the actions of Ca^{2+} influx through Orai1 to confirm histamine-evoked retrograde trafficking was Ca^{2+}-independent by using the Orai1 channel inhibitor RO2959 (Figure 3.3A, B). First, I confirmed the efficiency of RO2959 in inhibiting the histamine-evoked Ca^{2+} response in my hAEC model.

To determine whether RO2959 inhibited the histamine-evoked Ca^{2+} response I preincubated hAECs with RO2959 or vehicle control before stimulation with 30 μM histamine. I found no significant difference between peak Ca^{2+} responses in both 1.5 mM and 0 mM Ca^{2+} SBS buffer (Figure 3.3C). In the presence of extracellular $Ca^{2+,}$ we see that RO2959 did not affect the peak Ca^{2+} response evoked by histamine (2.656 ± 0.178 v 2.255 ± 0.117, p = ns), however, RO2959 was able to significantly inhibit the sustained Ca^{2+} response in hAEC (Figure 3.3D). In 0 Ca^{2+} the peak Ca^{2+} response (Figure 3.3E) was not affected by the presence of RO2059 in histamine-stimulated cells (2.278 ± 0.189 v 1.903 ± 0.199, p = ns) and I did not observe these inhibitory effects of RO2959 in 0 Ca^{2+} as there was no significant inhibition of the sustained response (Figure 3.3F). These data suggest that RO2959 inhibits the Orai1 channel thus preventing store-operated Ca^{2+} influx but does not inhibit the histamine-evoked release of Ca^{2+} from ER stores, thus showing that the RO2959 compound is active in this cell type.

I evaluated the ability of histamine to evoke Rab46 movement to the MOTC following acute stimulation with histamine in the presence of RO2959 blockade. As hypothesised, I found that pre-incubation with RO29259 had no impact on the histamine evoked retrograde trafficking of Rab46 to the MTOC (Figure 3.4A). When considering the perinuclear distribution of Rab46 upon stimulation with this pharmacology (Figure 3.4B) there was an increase in particle signal intensity in this region in both histamine and histamine + RO2959 conditions suggesting that RO2959 does not impede trafficking events and that Orai1-dependent Ca^{2+} influx is not required. Taking into consideration all three regions of the cell (Figure 3.4C) I observed there was an increased signal intensity of the histamine + RO2959 treated cells in the intermediate and peripheral regions, suggesting that although RO2959 does not impede Rab46 trafficking, it may have some off-target effects that limit the efficacy of histamine to induce complete clustering at the MTOC.

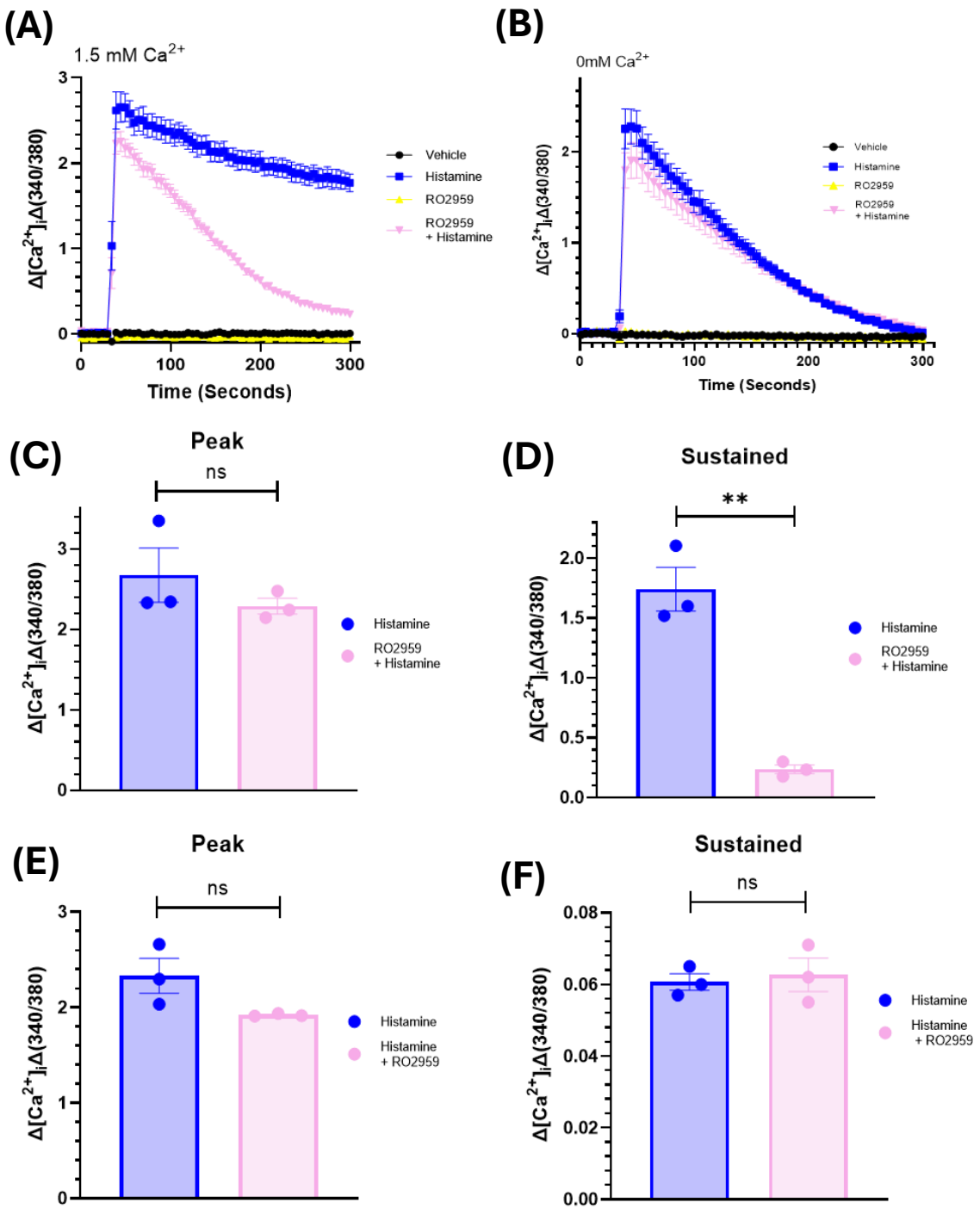

Figure 3.3 RO2959, does not inhibit the histamine evoked Ca^{2+} response. (A) Representative Ca^{2+} trace, cells were treated with 30 µM His and pre-treated for 30 mins with 10 µM RO2959 before stimulation with 30 µM His in 1.5 mM Ca^{2+} SBS buffer. (B) Same conditions as (A) but in 0 mM Ca^{2+} + 0.4 mM EGTA SBS buffer. (C) Peak Ca^{2+} response of (A). (D) Sustained Ca^{2+} response of (A). (E) Peak Ca^{2+} response of (B). (F) Sustained Ca^{2+} response of (B). All mean data plotted as mean ± SEM, n/N = 3/9.

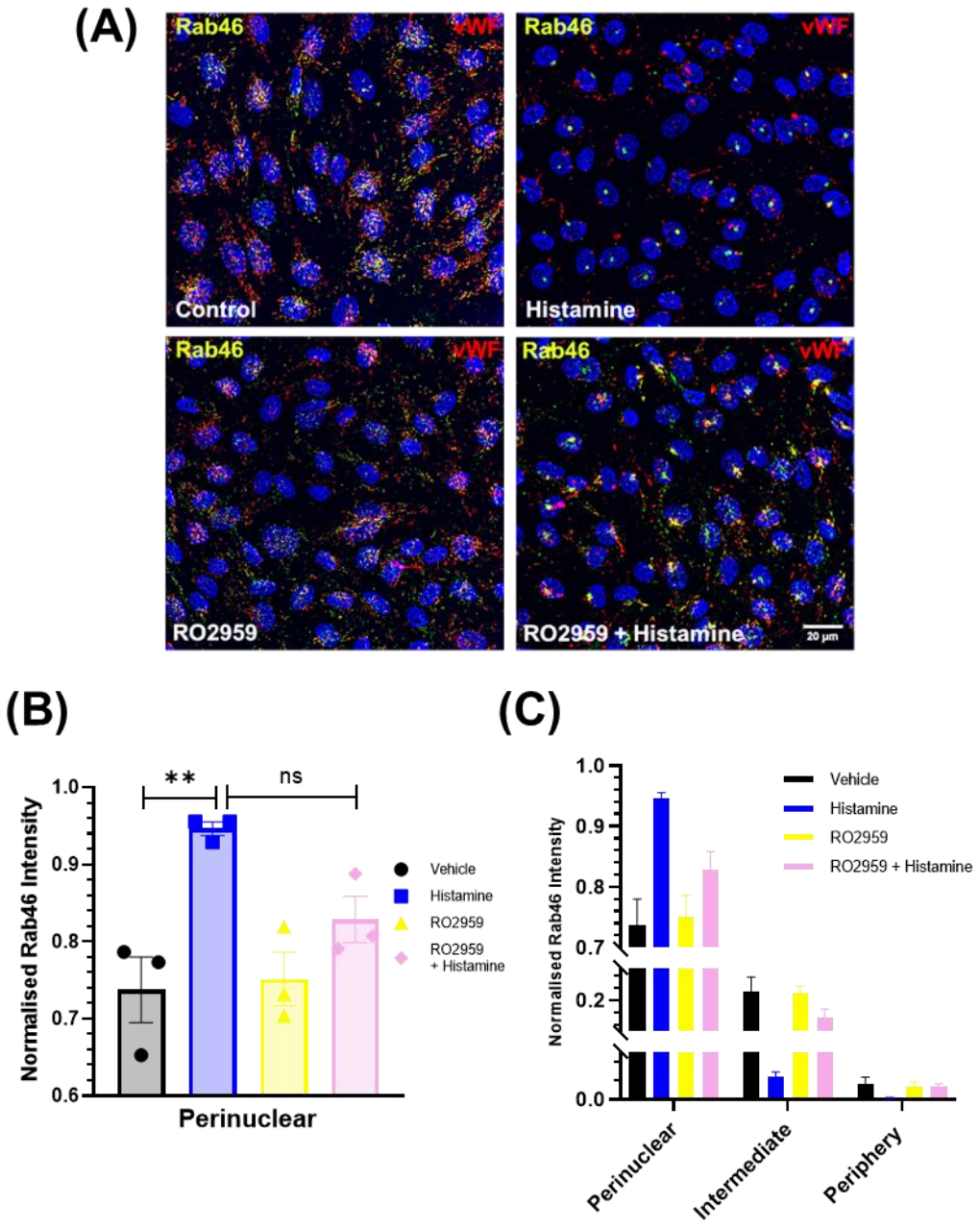

Figure 3.4. Inhibition of Orai1 by RO2959 does not impact Rab46 distribution. (A) Representative images of hAEC inhibited with 10 µM RO2959 for 30 minutes, before 10 mins acute stimulation with 30 µM histamine. Blue = H33342 (nucleus), green = Rab46, red = vWF. (B) Mean data of (A) showing the distribution of Rab46 at the perinuclear region. (C) Mean data of (B) expanded, to show the distribution of Rab46 across all cellular locations. 5 images were taken per condition, across 3 repeats, n = 3 / N = 15, ** = $p < 0.01$ by One-way ANOVA, all mean data plotted as mean ± SEM.

3.4.2 BAPTA inhibits intracellular Ca^{2+} but does not prevent retrograde trafficking of Rab46 to the MTOC

To further confirm that Rab46 retrograde trafficking to the MTOC is a Ca2+-independent process I employed the use of the intracellular Ca^{2+} chelator, BAPTA (used in its -AM form). Firstly, I wanted to determine in a hAEC model that I could effectively deplete the intracellular Ca^{2+} levels and inhibit the histamine-evoked Ca^{2+} response. hAEC were incubated with BAPTA-AM (10 and 20 μM) and subsequently stimulated with either 0.5 μM or 30 μM histamine. I observed in cells pretreated with 10 μM BAPTA (Figure 3.5A, Figure 3.5B) and then stimulated at both 0.5 and 30 μM histamine, there was still residual Ca^{2+} detected by Fura-2 after 5 mins of stimulation. Thus, the decision was made to investigate 20 μM BAPTA-AM as a more efficient concentration. I was able to conclude through optimisation that this concentration was able to sequester the Ca^{2+} response upon stimulation with histamine. Through quantification of the mean data (Figure 3.6C and Figure 3.6D) in hAEC, BAPTA-AM is a potent Ca^{2+} chelator, allowing for the study of Ca^{2+} dependency studies.

It was then necessary to validate that through abolishing the intracellular Ca^{2+} gradient, it was still possible to observe retrograde trafficking of Rab46 to the MTOC. I pre-incubated cells with 20 μM BAPTA-AM before stimulation with histamine and then performed immunofluorescence staining and imaging of Rab46. When cells were stimulated with 30 μM histamine, I observed a complete clustering of Rab46 at the MTOC, which was expected (Figure 3.6A). When cells exposed to 30 μM histamine were pre-incubated with BAPTA-AM, clustering of Rab46 was not inhibited (Figure 3.6B), thus, proving that in the absence of intracellular Ca^{2+}, Rab46 is still capable of undergoing a retrograde trafficking to the MTOC. Across all three cellular locations (Figure 3.6C) there were no differences observed in the overall distribution of Rab46 in or out of the presence of BAPTA-AM, in response to stimulation with histamine, and this movement is a Ca^{2+} independent process.

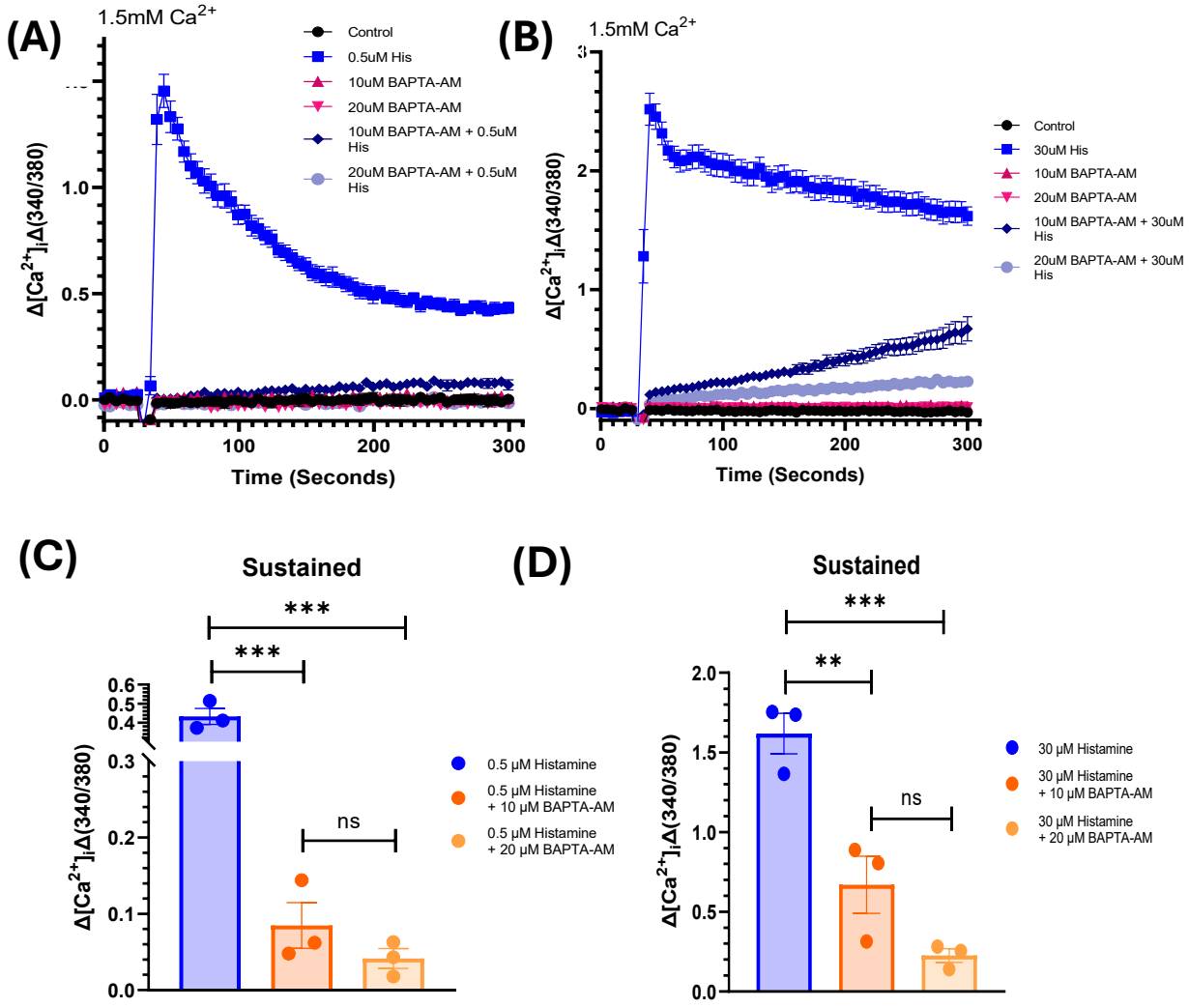

Figure 3.5 BAPTA-AM is a potent chelator and inhibitor of intracellular Ca^{2+} release. (A) Representative Ca^{2+} trace showing acute stimulation of hAEC with 10 and 20 μM BAPTA-AM in combination with 0.5 μM histamine. (B) Representative Ca^{2+} trace showing acute stimulation of hAEC with 10 and 20 μM BAPTA-AM in combination with 30 μM histamine. (C) Mean data of (A), showing the sustained Ca^{2+} response for 0.5 μM histamine. (D) Mean data of (B), showing the sustained Ca^{2+} response for 30 μM histamine. All experiments were conducted in 1.5 mM Ca^{2+} SBS. Mean data plotted as mean ± SEM. Individual dots represent the mean of 1 biological repeat. n/N = 3/9. ** = $p < 0.01$, *** = $p < 0.001$, by One-way ANOVA.

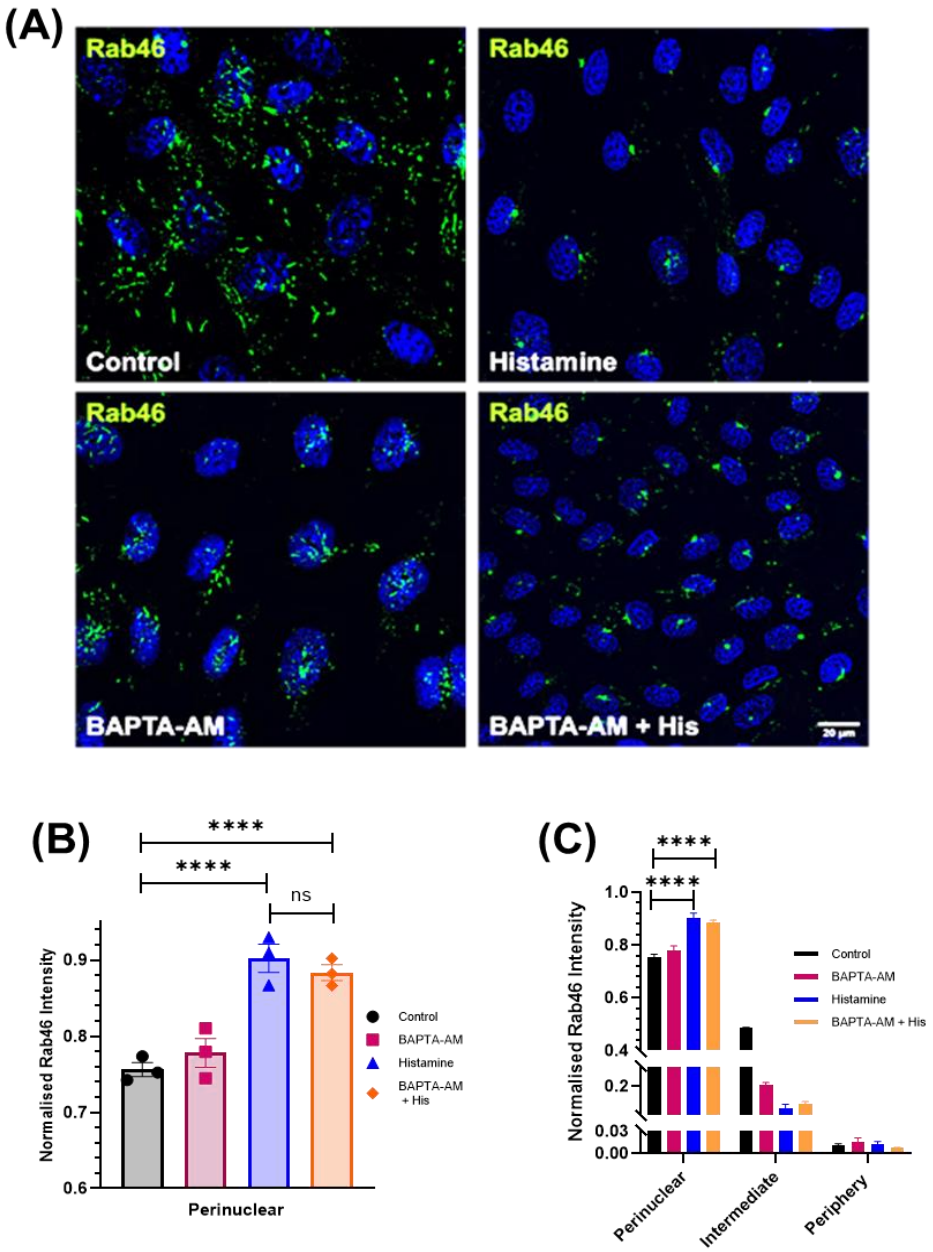

Figure 3.6 BAPTA-AM does not inhibit retrograde trafficking of Rab46 to the MTOC. (A) Representative images showing the distribution of Rab46 under control conditions of when stimulated with ± BAPTA-AM. Blue = H33342 (nucleus), green = Rab46, Scale bar = 20 µm. (B) Analysis and mean data of the perinuclear distribution of (A), showing the normalised Rab46 intensity. (C) Extended mean data analysis of (A) highlighting the three areas of interest, perinuclear, intermediate, and periphery. Control = DMSO, BAPTA-AM = 20 µM, Histamine = 30 µM. 5 images were taken per condition, across 3 repeats, n = 3 / N = 15, **** = $p < 0.0001$ by One-way ANOVA, all mean data plotted as Mean ± SEM.

3.4.3 SERCA pump blocker, thapsigargin is capable of inducing dispersal of Rab46 following histamine stimulation.

Previous research undertaken by Pedicini et al had questioned the role of the Rab46 EF-hand. They discovered it was not necessary for the histamine-induced association with dynein (Pedicini et al. 2021). Srikanth et al have shown that in T-cells, the EF-hand domain plays a key role in the function of CRACR2A, whereby Ca^{2+} binds to the EF-hands to evoke a simultaneous dissociation of proteins that are clustered near the plasma membrane of T-cells (Srikanth et al. 2010). Thereby, it was proposed, that since the N-terminal of Rab46 is the same sequence as CRACR2A, the role of the EF-hand domain may be to regulate the dispersal of WPBs clustered at the MTOC following acute stimulation with histamine. A mutant of Rab46, $Rab46^{EFMut}$ that cannot bind Ca^{2+}, was localised to the MTOC in the absence of stimulation, indicative that Ca^{2+} is not necessary for the trafficking of Rab46 to the MTOC in HUVECs.

EF-hand Ca^{2+} binding domains will bind to any source of local, freely available Ca^{2+} ions (Gifford et al. 2007; Grabarek, 2006). Thus, our group firstly stimulated HUVEC with 30 μM histamine to induce a retrograde trafficking of Rab46-positive WPBs to the MTOC and then forced a global intracellular Ca^{2+} release via the SERCA pump inhibitor, thapsigargin to observe the effect on the distribution of Rab46 (Figure 3.7A). Thapsigargin alone did not impact the trafficking of Rab46, however, it triggered the dispersal of Rab46 from the MTOC (Figure 3.7B), as indicated by an increase in the signal intensity in the peripheral region following thapsigargin stimulation. Although thapsigargin could induce re-distribution of Rab46 following stimulation with histamine, in the case of the EF-hand mutant, this re-dispersal was not observed (Figure 3.7C). Altogether, these data suggest that it is Ca^{2+} binding to the EF-hand domain of Rab46 that is necessary for the dispersal of Rab46 from the perinuclear region following acute stimulation with histamine. Therefore, my aim was to understand the source of this Ca^{2+} signal.

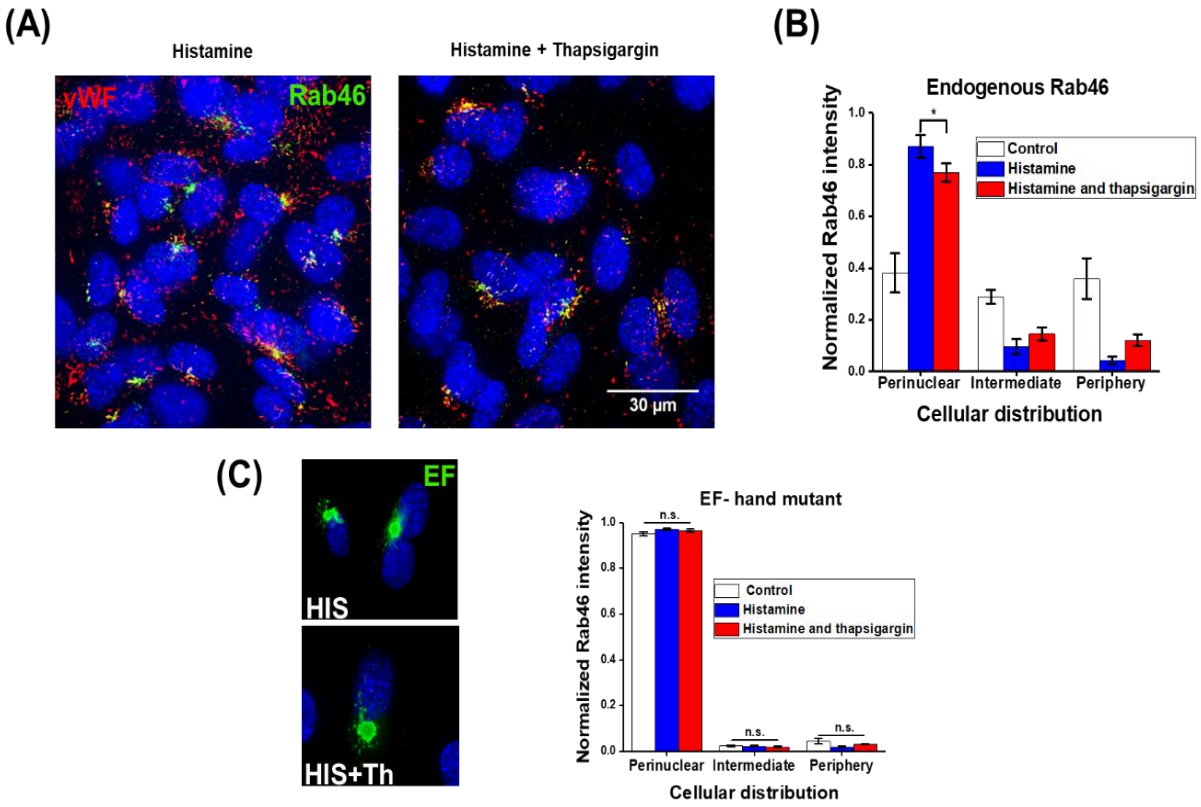

Figure 3.7 Thapsigargin induces Rab46 dispersal following acute histamine stimulation. (A) Representative images taken on an Olympus IX-70 inverted microscope of HUVECs treated with 30 µM histamine for 10 mins alone or subsequently followed by 1 µM thapsigargin and stained for endogenous Rab46 (green) and vWF (red), nucleus (blue). (B) Quantitative analysis of Rab46 distribution across the cell. Scale bar = 30 µm. The bar plot shows the Rab46 signal intensity respective to the cell area, where the mean (± SEM) was described as a ratio of the total fluorescence intensity. n=3/N=30. * p = < 0.05, by one-way ANOVA. Figure adapted from the Miteva et al. 2019, JCB paper, DOI: https://doi.org/10.1083/jcb.201810118. Accessed: March 2025.

3.5 hAECs express the NAADP-sensitive channels, TPC1, TPC2, and TRPML1

3.5.1 Expression at the mRNA level by RT-qPCR

The two-pore channel proteins (TPC1/2) and transient-receptor potential mucolipins (TPRML1/MCOLN1) have previously been identified as candidate ion channels expressed on the membrane of both autosomal and secretory lysosomes that actively release Ca^{2+} from lysosomal stores (Li et al. 2019; Chen et al. 2022; Ruas et al. 2015). In both HUVEC and hAEC, I used RT-qPCR to quantify the expression of these channels at the mRNA level. The data shows TPC1 (Figure 3.8A), TPC2 (Figure 3.8B), and TPRML1 (Figure 3.8C) are expressed in endothelial cells; however, it is apparent that the relative expression of these genes to the housekeeper, GAPDH, is low.

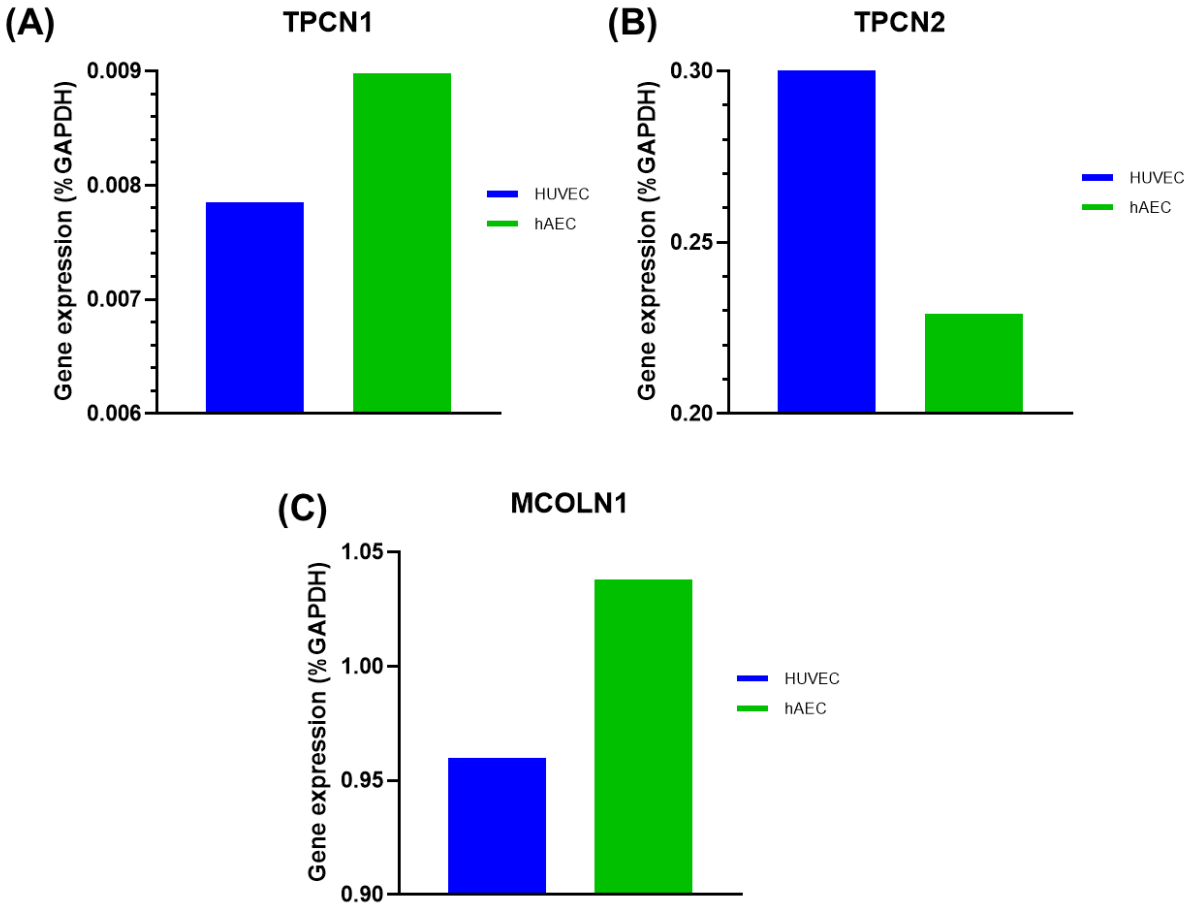

Figure 3.8 HUVEC and hAEC express lysosomal cation channels at the mRNA level. (A) Expression of TPCN1 in HUVEC and hAEC relative to housekeeper, GAPDH (%). (B) Expression of TPCN2 in HUVEC and hAEC relative to the housekeeper, GAPDH (%GAPDH). (C) Expression of MCOLN1 (TRPML1) in HUVEC and hAEC relative to the housekeeper, GAPDH (%GAPDH). Analysis of LightCycler® 96 output from Roche®, displayed as % of the housekeeper, GAPDH. n/N = 1/3.

3.6 Histamine-evoked Ca^{2+} signals are sensitive to Ned-19

I wanted to explore if histamine elicits an NAADP-evoked Ca^{2+} signal by investigating if these signals were sensitive to inhibition by the NAADP channel antagonist, Ned-19. Further to this I wanted to determine if Ned-19 was a potent pharmacological inhibitor of the small endo-lysosomal Ca^{2+} channels, TPC1 and TPC2 as Ned-19 is specific for both channels (Pitt et al. 2014; Jin et al. 2020). I first performed a series of Flexstation Ca^{2+} measurements (Figure 3.9A) to show that there is a dose-dependent increase in the release of Ca^{2+} with histamine and that at all concentrations, Ned-19 inhibits this Ca^{2+} release. At low concentrations of histamine, pre-incubation of the cells with Ned-19 leads to a complete abolishment of the Ca^{2+} response (Figure 3.9B). At higher doses of histamine (30 μM) (Figure 3.9C), there is only a partial inhibition of the Ca^{2+} response. At 0.1 μM histamine, this abolishment of the Ca^{2+} response in cells preincubated with Ned-19 was reflected in the peak (Figure 3.9D) and sustained responses (Figure 3.9E) At 30 μM histamine peak (Figure 3.9F) response was inhibited but was not significantly different from control. The sustained (Figure 3.9G) response was significantly inhibited at 30 μM histamine in cells pre-incubated with Ned-19.

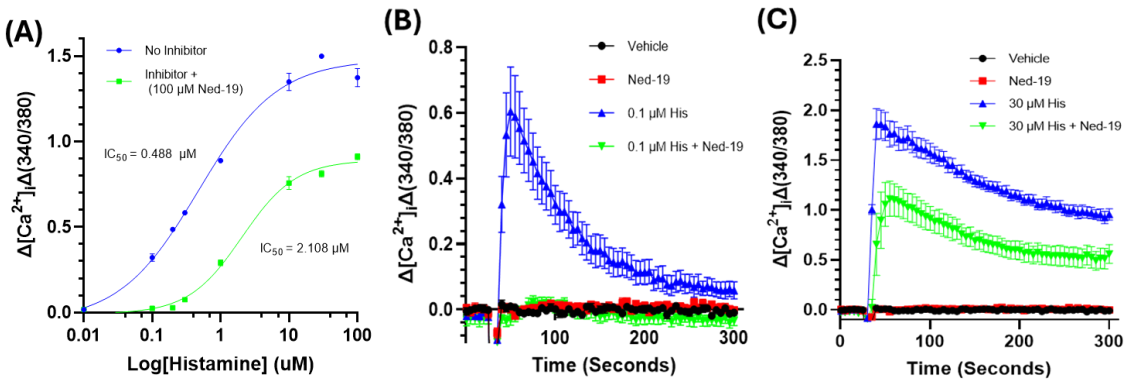

Figure 3.9 Histamine evokes an intracellular Ca^{2+} rise in hAEC and is inhibited by Ned-19. (A) Concentration-response of histamine ± 100 µM Ned-19 in hAEC. (B) Representative Ca^{2+} trace showing complete inhibition of the histamine-evoked Ca^{2+} response by Ned-19 at 0.1 µM histamine. (C) Representative Ca^{2+} trace of hAEC pre-incubated with 100 µM Ned-19 and then acutely stimulated with 30 µM histamine, showing partial inhibition of the histamine-evoked Ca^{2+} response.

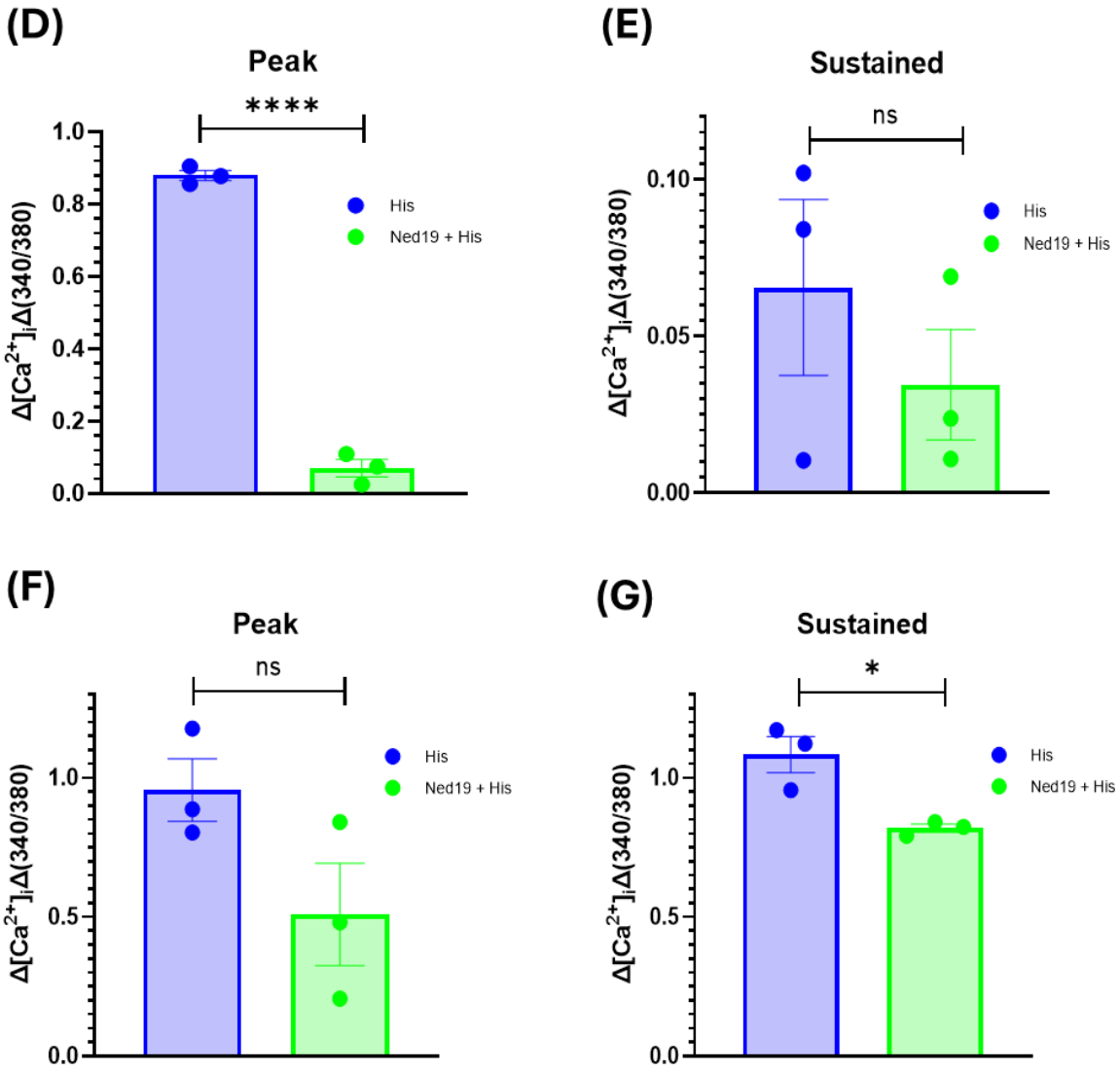

Figure 3.9 Histamine evokes an intracellular Ca^{2+} rise in hAEC and is inhibited by Ned-19 (continued). (D) Peak amplitude mean data of (B) (0.1 µM Histamine). (E) Sustained Ca^{2+} response of (B) (0.1 µM Histamine). (F) Peak amplitude mean data of (C) (30 µM Histamine). (G) Sustained Ca^{2+} response of (C) (30 µM Histamine). Experiments were conducted in 1.5 mM Ca^{2+} SBS buffer. Error bars represent mean ± SEM. n/N 3/9, * $p < 0.05$, **** $p < 0.0001$, ns = not significant, by unpaired t-test.

3.7 Inhibition of NAADP-mediated Ca^{2+} signalling by Ned-19 does not affect the functionally independent Piezo1 channel

To demonstrate that Ned-19 is specific for the inhibition of NAADP-mediated Ca^{2+} channels, I evaluated the effects of Yoda-1, a chemical activator of the plasma membrane mechanosensitive ion channel, Piezo1. The Piezo1 channel is a large, trimeric cation channel capable of active transport of Ca^{2+}, Na^{+}, and K^{+} ions across the cell membrane and is activated in response to changes in shear stress detected by the channel. First, I investigated if Yoda-1 can induce a Ca^{2+} response in hAECs (Figure 3.10A, B). Yoda-1 produced a robust and acute rise in intracellular Ca^{2+} from hAEC, stimulated for 5 mins with increasing concentrations of Yoda-1 (0-10 μM) (Figure 3.10B). This confirmed that hAECs can be activated indirectly in a non-mechanosensitive fashion by Yoda-1, which is to be expected as being aortic cells in nature, they are exposed *in-vivo* to a physiologically pre-determined rate of shear flow.

To demonstrate that Ned-19 had no impact on Ca^{2+} influx through the Piezo1 channel, hAECs were pretreated with Ned-19 before acute stimulation with 2 μM Yoda-1, and fluorescence readings were recorded. The results indicate that Ned-19 does not inhibit the Ca^{2+} rise in response to co-stimulation with Yoda-1 (Figure 3.10C). The mean peak amplitude and the sustained Ca^{2+} response (Figure 3.10D, E, respectively) show no significant differences between conditions. These data indicate that Ned-19 is specific for NAADP-mediated Ca^{2+} rises and that a functionally independent, off-target Ca^{2+} channel, Piezo1 with its direct activator Yoda-1, is not impacted by inhibition of NAADP by Ned-19. Overall, this highlights that Ned-19 is a powerful and specific NAADP-antagonist and is not capable of influencing other Ca^{2+} responses, such as the thrombin signalling pathway, which is at least partially controlled by SOCE.

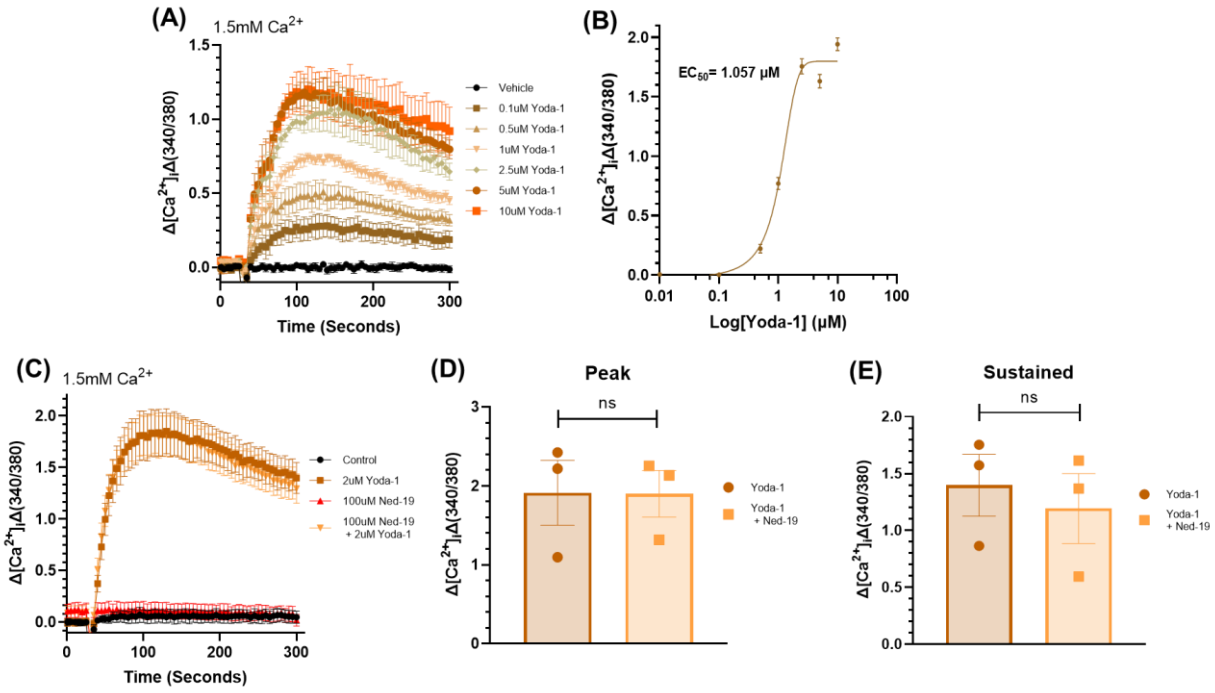

Figure 3.10 Yoda-1 elicits release of Ca^{2+} and Ned-19 does not inhibit this response. (A) Representative Ca^{2+} trace showing dose response of Yoda-1 from 0-10 µM on Molecular Devices Flexstation. Experiments were performed in 1.5 mM Ca^{2+} SBS buffer and cells stimulated with varying concentrations of Yoda-1 (0.1-10 µM) for 5 mins. (B) log transformed Hill equation from (A), EC50 calculated at 11.84 µM, n/N = 3/9. (C) Representative Ca^{2+} trace showing hAEC pre-incubated for 30 mins with Ned-19, before 5 mins acute stimulation with 2 µM Yoda-1. (D) Peak amplitude mean data of (C) to prove no inhibition of the Ca^{2+} response by Ned-19 in the presence of Yoda-1. (E) Sustained mean Ca^{2+} response of (C). Experiments were conducted in 1.5 mM Ca^{2+} SBS buffer. n/N = 3/9, ns = not significant, by unpaired t-test. Error bars represent mean ± SEM.

3.8 Histamine-evoked Ca^{2+} signals alter the distribution of Rab46 in hAECs

Here, I explored the impact of Ned-19 on the distribution of Rab46 upon histamine stimulation. As previously shown, clustering of Rab46/WPBs at the MTOC is not observed when cells are stimulated low concentrations of histamine (where we presume NAADP production allows for freely available Ca^{2+} to bind to the EF-hand domain of Rab46 and release it from the MTOC) (Figure 13A). However, when cells are pre-incubated with Ned-19 and then stimulated with low doses of histamine the Ned-19 competitively blocks NAADP-dependent Ca^{2+} release. Thus, Rab46 that has trafficked to the MTOC,

permit dispersal (Figure 3.11A). At concentrations of histamine, exceeding 30 μM, (where they may already be emptying both the lysosomal and ER Ca^{2+} stores), so that Rab46 has trafficked to the MTOC and remains clustered there as there is no Ca^{2+} available. Therefore, at high doses of histamine, the strong inhibitory effect of Ned-19 is lost. This is due to the self-inhibitory nature of NAADP, and such that Ned-19 is unable to out-compete for the already saturated NAADP and its associated binding sight, thus the Rab46 remains clustered at the MTOC, as also observed in the high histamine control (Figure 3.11A). There was a significant increase in the perinuclear shift of Rab46 (Figure 3.11B) toward the MTOC in the presence of Ned-19 when stimulated with low concentrations of histamine (0.1 μM). Considering the distribution of Rab46 across multiple cellular locations (Figure 3.11C) in cells stimulated with 30 μM histamine, there is a shift in the distribution of particle intensity from the periphery toward the perinuclear region and this shift is not observed in cells stimulated with 0.1μM histamine alone, unless cells have been pre-incubated with Ned-19.

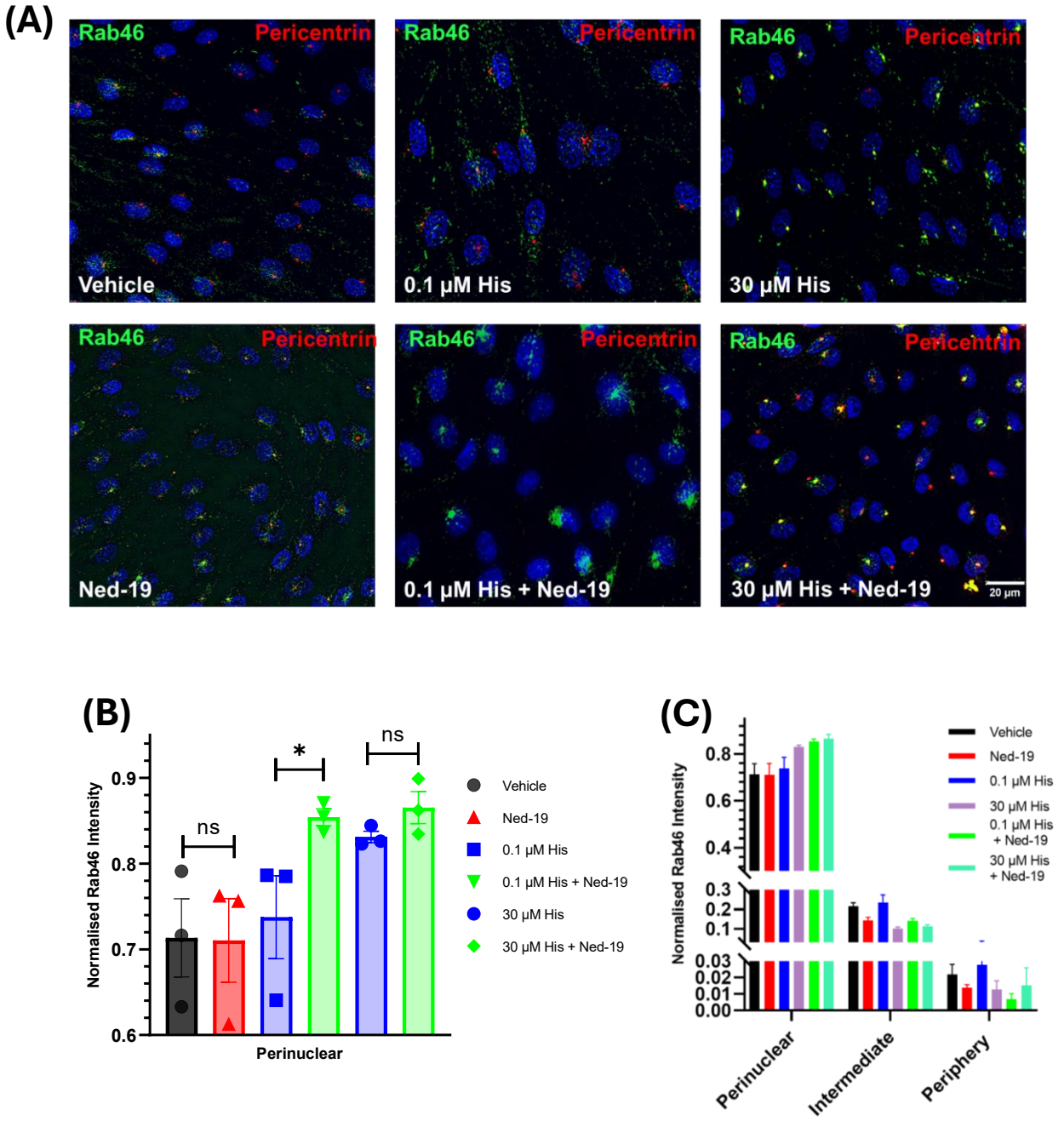

Figure 3.11 Ned-19 inhibition at low concentrations of histamine promotes perinuclear clustering of Rab46 at the MTOC. (A) Representative images of hAEC pre-treated for 30 mins with 100 µM Ned-19, before acute stimulation with either 0.1 or 30 µM histamine for 10 mins, scale bar = 20 µm. (B) mean data of the perinuclear distribution of Rab46 under conditions described in (A). (C) mean data of the complete Rab46 distribution across all three cellular regions, perinuclear, intermediate and periphery from (A). 5 images were taken per condition, across 3 repeats, n = 3 / N = 15, * = $p < 0.05$, all mean data plotted as mean ± SEM.

3.9 Piezo1 operates independently of the NAADP- signalling pathway in hAECs

Having hypothesised that the Ca^{2+} channels responsible for NAADP-mediated Ca^{2+} signalling are not SOCE-related and that the signalling cascades generated from this type of pathway operate independently of SOCE, I wanted to further confirm this using pharmacology tailored to activate the plasma membrane-bound mechanosensitive ion channel, Piezo1. Yoda-1, a synthetically derived agonist of Piezo1 modulates channel activity by enhancing the mechanical sensitivity of the channel.

I hypothesised that hAEC exposed to treatment with Yoda-1 would not induce clustering of Rab46 at the MTOC. To assess this, I exposed hAECs to a dose-response of Yoda-1 ranging from 0-5 μM for 10 mins before fixing and staining as per the methods chapter. As expected, under all conditions, I did not observe (Figure 3.12A) a clustering of Rab46 at the MTOC. There was no significant difference observed in perinuclear Rab46 distribution (Figure 3.12B) and all cellular regions all doses of Yoda-1 showed comparable results for particle intensity (Figure 3.12C). From this, it can be deduced that the Ca^{2+} signalling pathway through Piezo is physiologically distinct from that of NAADP and that this demonstrates that the histamine response is specific to Rab46 and not from other plasma membrane ion channels.

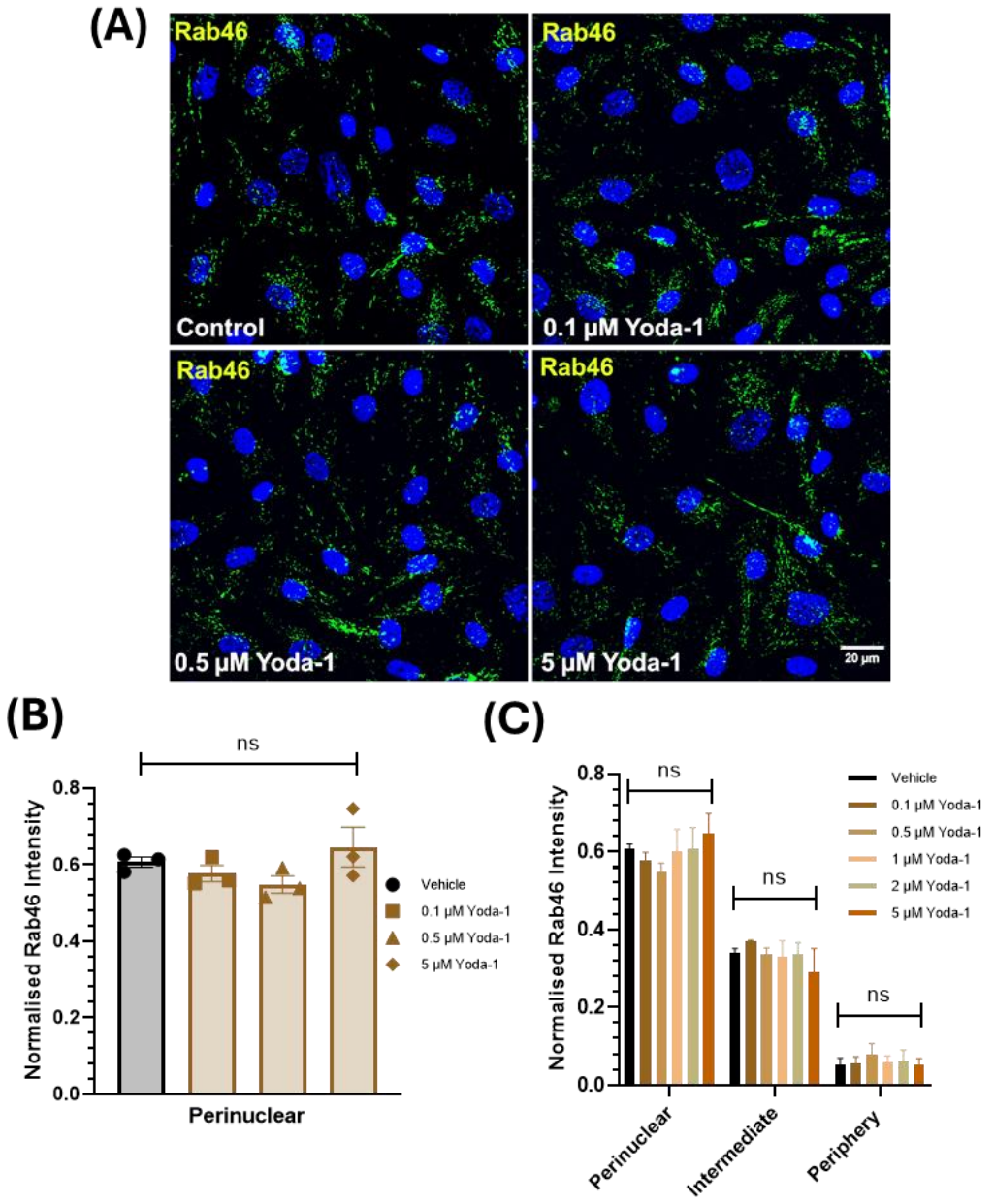

Figure 3.12 Yoda-1 does not induce retrograde trafficking of Rab46 and does not affect the localisation of the protein. (A) Representative images of various concentrations (0.1-5 µM) Yoda-1 in hAEC. Scale bar = 20 µm, representative of all images in (A). Cells were acutely stimulated for 10 mins with Yoda-1 before fixing and staining. Rab46 = green, nuclei = blue (H33342). (B) Mean data of the Rab46 signal intensity at the perinuclear region of the cell. (C) Expanded mean data of (B) showing all three cellular locations, perinuclear, intermediate and periphery. All data is plotted as mean ± SEM. Significance set at $p < 0.05$, ns = not significant by one-way ANOVA, n = 3 / N = 5.

3.10 Plant-derived bis benzylisoquinoline alkaloid, tetrandrine induces clustering of Rab46 at the MTOC

In response to histamine stimulation, the NAADP-mediated Ca^{2+} signals generated can be inhibited by the NAADP antagonist Ned-19. However, Ned-19 confers an equal antagonistic selectivity for both TPC1 and TPC2. I used the plant-derived Ca^{2+} channel blocker, tetrandrine, known to confer greater selectivity for TPC2 (Heister & Poston, 2020), to further investigate and distinguish between the channels whether it was TPC2 that had the greatest effect on these NAADP-mediated Ca^{2+} signals and whether they are responsible for Rab46 spatial distribution following stimulation. It must be noted that tetrandrine can antagonise both NAADP and IP_3-mediated Ca^{2+} signalling. Recent evidence shows that TPC2 can confer selective ion-conductance bias via agonist binding, with NAADP leading to a greater influx of Ca^{2+} conductance and $PI(3,5)P_2$ leading to a rise in intracellular Na^+ conductance.

Tetrandrine confers selectivity for the blockade of voltage-gated Ca^{2+} channels, however, it has been shown to have small off-target effects on TPC1 and L-type Ca^{2+} channels, thus, it is not completely selective for TPC2 vs Ned-19 (Sakurai et al. 2015). With NAADP-mediated signalling inducing a surge in the TPC2 Ca^{2+} ion conductance, I wanted to experimentally assess the effects of this compound on Rab46-mediated Ca^{2+} signalling in the context of trafficking and dispersal of Rab46-positive WPBs from the MTOC.

Firstly, I performed a concentration-response to histamine, applying a fixed concentration of tetrandrine (5 μM) (Figure 3.13A, B). At all concentrations of histamine (0-30 μM) pre-treatment for 30 min with 5 μM tetrandrine before stimulation leads to inhibition of the Ca^{2+} response. I observed the greatest inhibitory effects of tetrandrine at high concentrations of histamine (Figure 3.13A, B) which was not expected as at these high doses the production of NAADP is high and would in the context of Ned-19, negate its effects. Cells preincubated with tetrandrine and then exposed to low concentrations (0.1 μM) of histamine do not exhibit the complete inhibition of the Ca^{2+} response observed in Ned-19 treated cells but instead show a much faster decline to zero in the Ca^{2+} response as compared to histamine alone (Figure 3.13C). Cells pre-

treated with 5 μM tetrandrine and stimulated with 30 μM histamine exhibited similar responses (Figure 3.13D) to those observed with Ned-19 at these high concentrations of histamine. We can infer from this, that it is likely that there is channel compensation from TPC1 supplementing Ca^{2+} release that may be preventing complete inhibition of the Ca^{2+} responses at both low and high concentrations of histamine. Mean peak amplitude data show that at low concentrations of histamine, tetrandrine does not significantly impede histamine-evoked Ca^{2+} release (Figure 3.13E, F), however at high concentrations I observed a significant inhibition of the Ca^{2+} response in tetrandrine-treated cells. There was a significant effect of tetrandrine on the sustained Ca^{2+} response in hAEC (Figure 3.13G, H), demonstrating that its effects are delayed due to its mode of activation. Tetrandrine has a complex pharmacological makeup and the signalling pathways through which it is modulated could play a role in this delay.

To further question the effect of tetrandrine on the distribution of Rab46, I employed the use of immunofluorescence imaging of hAECs exposed to a pre-treatment of 5 μM tetrandrine, before stimulation with histamine (Figure 3.14A). At low histamine concentrations, cells exposed to pre-treatment with tetrandrine showed clustering of Rab46 in the perinuclear region compared to no clustering in the histamine-only condition (Figure 3.14B). This is in line with the findings accredited to the use of Ned19, in which at low concentrations of histamine, tetrandrine can block NAADP-mediated Ca^{2+} signals, thus locking Rab46 at the MTOC following stimulation with low doses of histamine. Similarly, at high doses of histamine (30 μM), cells pre-treated with 5 μM tetrandrine exhibit an identical distribution of Rab46 as compared to control cells (30 μM histamine only). At this high concentration, the production of NAADP within the cell negates the effects of tetrandrine having any further effect on clustering. The overall distribution of Rab46 across the cell (Figure 3.14C) matched my findings with Ned-19, thus securing tetrandrine as a potential TPC2-specific inhibitor. One observation to note is that cells pre-treated with the pharmacology, do exhibit a stronger, more clustered distribution around the MTOC as compared to untreated cells. From this, we can conclude that tetrandrine mechanistically functions in a manner like that of Ned-19 and can be used as a tool to

investigate NAADP-mediated Ca^{2+} responses, specifically in the context of histamine stimulation. With the drug conferring greater sensitivity for TPC2, it may possess therapeutic potential in vivo and has already been evaluated in various cancers.

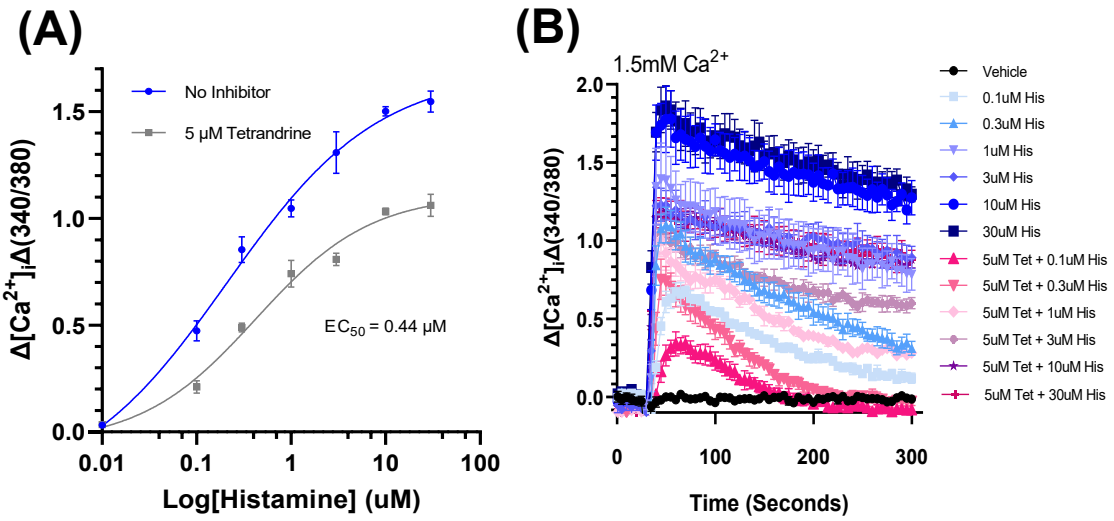

Figure 3.13 Tetrandrine elicits inhibition of the histamine-evoked Ca^{2+} response, like Ned-19. (A) Concentration-response curves of histamine alone (0.1-30 µM) and of hAEC pre-treated for 30 min with 5 µM tetrandrine followed by acute 10 min stimulation with histamine (0.1-30 µM), plotted using the Hill Equation. (B) Representative Ca^{2+} traces (A). n/N = 3/9.

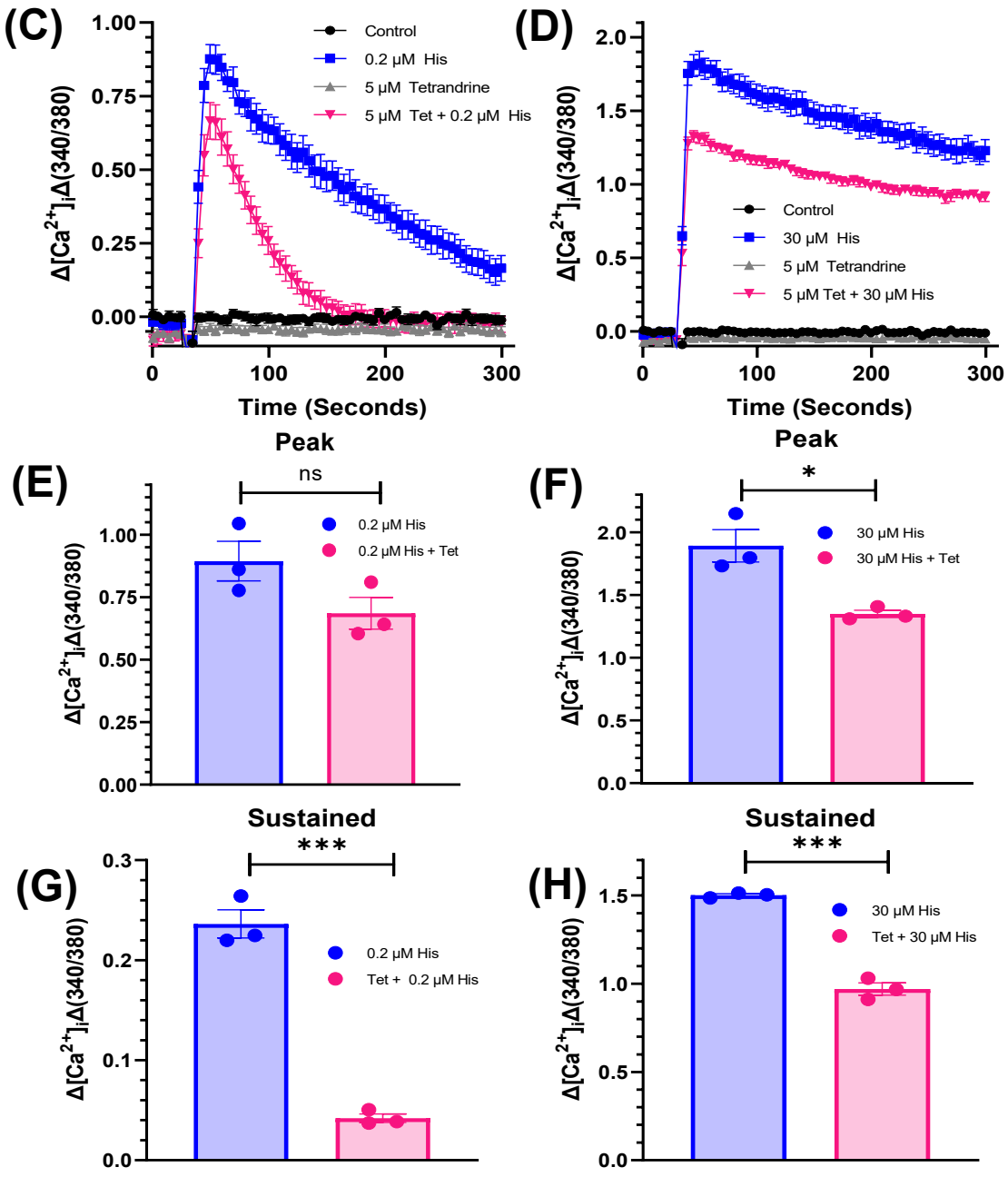

Figure 3.13 Tetrandrine elicits inhibition of the histamine-evoked Ca^{2+} response, like Ned-19 (continued). (C) Representative Ca^{2+} trace of 0.2 µM histamine ± 5 µM tetrandrine. (D) Representative Ca^{2+} trace of 30 µM histamine ± 5 µM tetrandrine. (E) Peak amplitude mean data of (C). (F) Peak amplitude mean data of (D). (G) Sustained Ca^{2+} response as mean data of (C). (H) Sustained Ca^{2+} response of mean data of (D). All mean data were plotted as mean ± SEM, and all experiments were conducted in 1.5 mM Ca^{2+} SBS buffer. ns = not significant, * = $p < 0.05$, *** = $p < 0.001$ by unpaired t-test, n/N = 3/9.

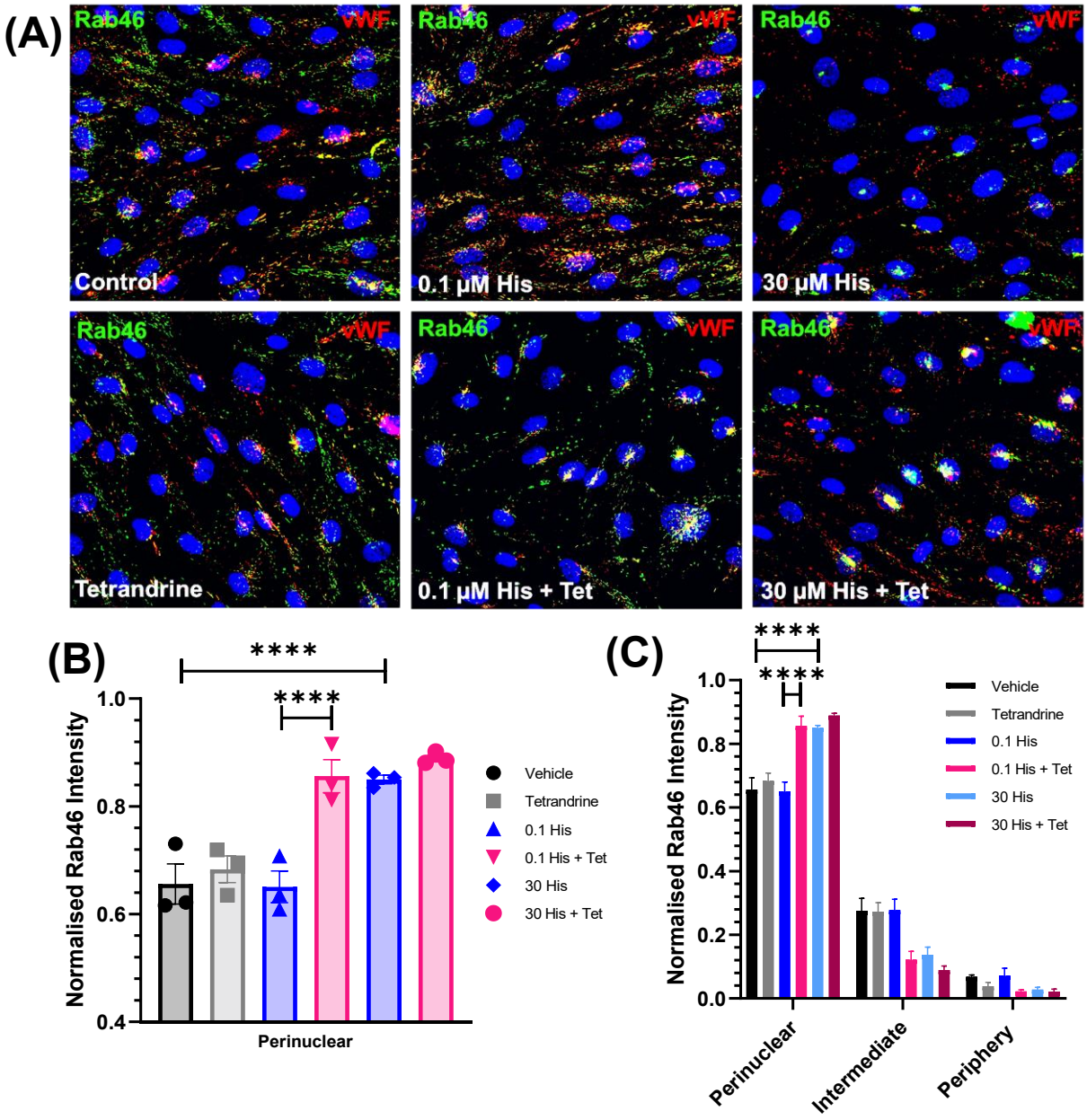

Figure 3.14 Tetrandrine elicits perinuclear clustering of Rab46 at low concentrations of histamine. (A) Representative images of hAEC pre-treated with 5 µM tetrandrine for 30 mins before acute stimulation with 0.1 or 30 µM histamine. Green = Rab46, red = vWF and blue = nuclei (H33342 stain). Vehicle = DMSO, Scale bar = 20 µm applies to all images in (A). (B) mean data of the perinuclear distribution of Rab46. (C) Expanded mean data of (B) showing Rab46 distribution across all three cellular locations, perinuclear, intermediate, and periphery. The data is plotted as the ratio of the total fluorescence intensity. All data in (B) and (C) are presented as mean ± SEM, where **** = $p < 0.0001$, by one-way ANOVA.

3.11 Secretion of angiopoietin-2 is inhibited by Ned-19, particularly at low concentrations of histamine

Angiopoietin-2 is a Tie-2 pathway ligand that is stored within WPBs and can be rapidly exocytosed following stimulation. It is known that Ang2 is one of the prominent cargos stored in an immobilised state within WPBs, bound to vWF and is mutually exclusive from P-selectin storage within the same organelles. The secretory pathway responsible for the exocytosis of Ang2 into the vascular system is poorly understood. However, it is known that it can act to modulate the Ang1 activity in the circulation, a pathophysiological consequence that requires further exploration.

In the context of Rab46 distribution, it is those WPBS that contain Ang2 that are retrogradely trafficked to the MTOC following stimulation with histamine. In the context of an immune stimulus, such as histamine, a release of Ang2 is not warranted, and thus, it leads to the hypothesis that Rab46 may be acting as a braking mechanism to prevent this pro-inflammatory protein from being released and thus is acting to maintain a haemostatic balance. To investigate the effect of varying concentrations of histamine on the release of Ang2 from hAEC and whether inhibition of the NAADP-evoked Ca^{2+} release by Ned-19 inhibited the release of Ang2. I performed an Ang2 ELISA whereby hAEC were acutely treated with various pharmacological reagents in the presence or absence of Ned-19. The ‘media’ was then collected and analysed to determine the release of Ang2. For this assay, I devised a positive control (100 μM His + 1U/ml Thr – Combo) that would allow for the maximal release of Ang2 from the cells. This was selected over PMA, as it was physiologically closer to what would be observed *in-vivo* following vascular injury. Thus, all data is presented as a percentage of the total release by the combo. From the results below (Figure 3.15) there is release of Ang2 evoked by 0.1 μM histamine which is not significantly increased by 30 μM (as we have shown previously in HUVECS) (Miteva et al. 2019). Cells pre-incubated with the NAADP antagonist, Ned-19 inhibit the release of Ang2. It is also clear that the inhibitory effects of Ned-19 on Ang2 secretion are most prominent at low concentrations of histamine, and this is in line with previous findings that at high concentrations of histamine, we have

already reached a saturation point in terms of the concentration of endogenous NAADP, and thus further inhibition of this pathway via Ned-19, does not negate the release of Ang2 as potently.

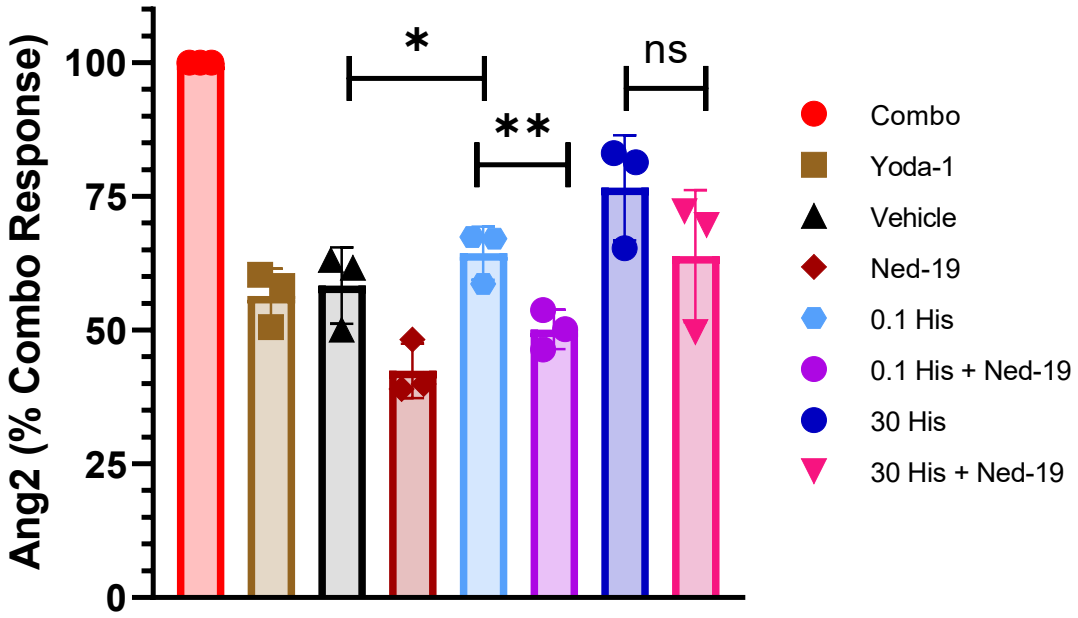

Figure 3.15 Inhibition of NAADP-mediated Ca^{2+} signalling by Ned-19 prevents release of angiopoietin-2. Mean data of ELISA used to measure the release of Ang2 from hAECs. Data was first calculated as the release of Ang2 (pg/ml) and then converted to a % of the combo response. Cells were pre-incubated with Ned-19 for 30 min during the cell starvation step in M199 and then acutely stimulated for 10 min with stimuli in 1.5 mM Ca^{2+} SBS. This was then collected, centrifuged at 500 x g and then the supernatant was collected for analysis. All data is reported as mean ± SEM, where ns = not significant, * = $p < 0.05$, ** = $p < 0.01$, n/N = 3/9.

3.12 Discussion

NAADP-mediated Ca^{2+} release in endothelial cells is a pivotal regulator of intracellular Ca^{2+} signalling pathways. It is still poorly understood exactly how NAADP evokes Ca^{2+} responses within cells and the mechanisms by which cells initiate NAADP-mediated Ca^{2+} responses are cell-type dependent. Understanding where the Ca^{2+} required for the dispersal of Rab46 from the MTOC comes from is crucial to underpinning the ubiquitous function of Rab46 as a Ca^{2+}-sensing protein. I have shown in two endothelial cell types, that acute stimulation with histamine can evoke a rise in intracellular Ca^{2+} and that this release of Ca^{2+} can be inhibited using the NAADP-antagonist, Ned-19. Esposito and colleagues successfully demonstrated in human EA.hy926 cells that application of Ned-19, completely abolished H_1R-induced Ca^{2+} currents but not those induced by thrombin (Esposito et al. 2011). I confirmed this in an aortic endothelial cell model and established that the mechanism by which hAEC deduce localised intracellular Ca^{2+} signals evoked by histamine is by the Ca^{2+} mobilising messenger NAADP and is not controlled by SOCE. Using a chelator of intracellular Ca^{2+}, BAPTA-AM I have shown that removal of cytosolic Ca^{2+} does not prevent trafficking of Rab46 to the MTOC and using the Orai1 pore blocker, RO2959, SOCE (prevents refilling by the ER) is not required for this trafficking. However, it is the Ca^{2+} sensing EF-hand domain of Rab46 that plays a crucial role in the dispersal of the protein from the MTOC following acute physiological stimulation.

Miteva showed that in the presence of the NAADP-antagonist, Ned-19, cells pre-treated and then acutely stimulated with thrombin showed a small but insignificant impact on intracellular Ca^{2+} release at low doses (0.07U/ml), whilst at high doses (1.25/2.5U/ml) there was no effect on the Ca^{2+} release evoked by thrombin (Miteva PhD Thesis, 2021). This work showed that Ned-19 did not impact the efficacy of the thrombin response and had no effect on the time-to-peak response. Thus, indicating that thrombin-evoked intracellular Ca^{2+} release is not mediated by NAADP-sensitive stores. In addition, the mechanism by which Ned-19 inhibits the release of intracellular Ca^{2+} appears to be concentration-dependent in context with histamine stimulation. Low concentrations of histamine show the most profound inhibition of the NAADP-

mediated Ca^{2+} response. At these concentrations, the endogenous levels of NAADP being produced are low, such that the cell Ca^{2+} is still released from the NAADP channels, allowing for binding to the EF-hand of Rab46-inducing dispersal. It has been previously shown that H_1R agonists rapidly increase the release of NAADP in ECs after only 5 minutes of the stimulus being applied (Esposito et al. 2011). This time aligns with the observation that Rab46 and WPBs cluster at the MTOC under these conditions. Thus, it is likely that this clustering of Rab46 at the MTOC at high (30 μM) concentrations of histamine is because NAADP is a self-limiting compound and that at such high concentrations is capable of preventing localised Ca^{2+} release from the lysosomal system, and subsequent binding to the EF-hand domain or Rab46, culminating in the prevention of release from the MTOC and perinuclear clustering of Rab46.

I then wanted to confirm that Ca^{2+} channels on the plasma membrane do not play an active role in this signalling pathway, and I used the Piezo1 agonist, Yoda-1 to demonstrate this. Application of Yoda-1 to hAECs showed a concentration-dependent rise in intracellular Ca^{2+}, however, Yoda-1 did not affect the distribution of Rab46 at any cellular location. I then evaluated whether inhibiting NAADP-mediated Ca^{2+} signals via Ned-19 would inhibit the Yoda-1 response. As hypothesised, Ned-19 inhibition did not inhibit the Yoda-1 response, thus, Ned-19 is a specific tool that can be used in the study of NAADP-mediated Ca^{2+} signalling and it is not influenced by Ca^{2+} channels on the PM, operating via SOCE in a functionally independent manner.

Knowing that the histamine-evoked Ca^{2+} release I was observing was in fact from an NAADP-mediated Ca^{2+} store, it became clear that understanding through what channels within the endo-lysosomal system was this Ca^{2+} responsible for the release of Rab46 from the MTOC coming from. Early studies involving sea urchin egg homogenates helped to identify 3 candidate ion channels located on endo-lysosomes, TPC1, TPC2, and TRPML1 (Lee et al. 2005; Galione et al. 2009). They demonstrated that within a sub-fraction of homogenate, NAADP-evoked Ca^{2+} release persisted even when the ER Ca^{2+} pool was ablated using the SERCA pump inhibitor, thapsigargin. TPC1 and TPC2 were originally proposed as functional NAADP receptors (Calcraft et al.

2009). The Galione group countered this with a double knock-out mouse model (*Tpcn1/2*$^{-/-}$) and upon single-cell patch clamp analysis concluded that NAADP regulation must be conferred by an accessory binding protein (Ruas et al. 2015). In 2021, Patel and colleagues were able to definitively say that TPCs were not the binding sites for NAADP and that NAADP was bound to these targets via specific binding proteins (JPT2 and LSM12) (Patel et al. 2021).

Ned-19 was initially thought to be an indirect inhibitor of NAADP due to its inherent structure; however, it has been shown to confer an equal selectivity for both TPC1 and TPC2 (Naylor et al. 2009). I have shown that at low concentrations of histamine, the effects of Ned-19 are more profound, due to the availability of free Ca^{2+} present in the cytosol, coming from TPCs as at these low concentrations of histamine, there is not sufficient Ca^{2+} release from these unknown channel(s) to propagate a global Ca^{2+} response via CICR. Evidence in the field points to TPC2 as the most probable candidate channel (TPC2, showing implications in vascular neo-angiogenesis) for Ca^{2+} release resulting in Rab46 dispersal (Favia et al. 2014). I wanted to look at a more specific inhibitor of TPC2, which led to the implementation of the plant alkaloid, tetrandrine.

Tetrandrine, in hAECs has similar effects to Ned-19, however, mean peak amplitude data for tetrandrine, demonstrated that its ability to inhibit NAADP-mediated Ca^{2+} release was initially delayed and, instead, observed as a sustained Ca^{2+} response. This implied the initial peak Ca^{2+} response could be via TPC1 or another lysosomal Ca^{2+} channel nearby. Recent advances in virology have explored the anti-viral properties of tetrandrine and have found that it is through TPC2 that these antiviral effects are observed (Grimm et al. 2020). This led to my hypothesis that TPC1 could be a Ca^{2+} release channel responsible for maintaining Ca^{2+} homeostasis, and that it could modulate the activity of other endolysosomal Ca^{2+} channels. Using the double TPC1/2 knockout mouse model from Anthony Galione's lab was work that I was keen to pursue in the context of stimulation with histamine, however, time constraints did not allow for this collaboration to take place.

In response to histamine, there are two sub-populations of WPBs that are differentially trafficked with mutually exclusive cargo either to the plasma

membrane (containing P-selectin) or the MTOC with Rab46 containing Ang2. Functional studies have confirmed that stored Ang2 may have important implications downstream of processes like angiogenesis, due to its long half-life (> 18 hrs) and that increasing concentrations of histamine does not elicit a concentration-dependent increase in Ang2 secretion (Fiedler et al. 2004; Miteva et al. 2019). I questioned whether inhibition of NAADP-mediated Ca^{2+} signalling by Ned-19 could abolish the release of Ang2. I found that inhibition of histamine-evoked Ca^{2+} release by Ned-19 via ELISA concurrently inhibited the release of Ang2 and yet again, this was most prominent at low concentrations of histamine.

The ability of Rab46 to operate as a functional Ca^{2+} sensor in endothelial cells poses its candidature for the title of emergency vascular brake. In the context of an immunological response, such as that of histamine, cells inhibit the release of vast quantities of pro-inflammatory (vWF) or pro-angiogenic (Ang2) factors into the extracellular environment. Thus, it poses the question, is Rab46 serving as a braking mechanism to prevent an ‘all-out’ response, like that we see with thrombin, and can we physiologically interrupt this signalling pathway with pharmacological inhibition of NAADP-mediated Ca^{2+} release? Albeit, not in the cardiovascular context, however, potential therapeutic benefits of Ned-19 have been identified in the context of parasitic infections such as malaria. Where Ned-19 interferes with the blood stage development of the parasite, whereby inhibition of the NAADP-mediated Ca^{2+} release prevents spontaneous Ca^{2+} oscillations that can promote the development of the parasite from early to late trophozoite (Suarez-Cortez et al. 2017; Arendse et al. 2021).

In summary, I have shown that the Ca^{2+} response evoked by histamine is sensitive to inhibition of NAADP channels (TPC1/2), but the cation Piezo1 agonist Yoda-1 is not. Pharmacological inhibition of Ca^{2+} release from these lysosomal channels induces clustering of Rab46 at the MTOC, preventing dispersal and is more prevalent at low histamine concentrations. I now want to explore the relationship between low and high concentrations of histamine on Ca^{2+} mobilisation and Rab46 trafficking using a functional agonist of the TPC2 channel, TPC2-A1-N.

Chapter. 4

TPC2-A1-N is a potent activator of TPC2, highlighting context with histamine stimulation

4.1 Introduction

The Patel et al. group identified that the TPC2 channel can undergo segregated cation fluxes, whereby the channel possesses the ability to modulate Na^+ and Ca^{2+} fluxes. They demonstrated that TPC2 could regulate its cation permeability differentially via its native ligands, NAADP and $PI(3,5)P_2$. Through the discovery of a novel channel agonist, TPC2-A1-N, one can now mimic the action of NAADP to selectively bias the channel to select fast-inducting Ca^{2+} signals via TPC2 (Yuan et al. 2022). I will explore activation of TPC2 using the potent agonist, TPC2-A1-N to study the effect on Rab46 distribution and the effects that overactivation of the channel has alongside the application of a histamine stimulus. Until this point, I have used antagonists of NAADP, thus, using an agonist I would expect to observe opposing results, providing further evidence that TPC2 provides the critical Ca^{2+} signal for dispersal of Rab46 from the MTOC.

From evidence previously published, I have hypothesized that TPC2 is the target Ca^{2+} store necessary for the dispersal of Rab46 from the MTOC. I have previously shown that hAEC exposed to high concentrations of histamine will undergo retrograde trafficking of Rab46 to the MTOC and remain clustered there. I wanted to determine whether activating TPC2, using TPC2-A1-N, could force Ca^{2+} release via TPC2, which would in turn initiate the dispersal of Rab46 from the MTOC.

4.2 TPC2-A1-N elicits activation of TPC2 through bias-selectivity for release of Ca^{2+} in HUVEC and hAECs.

To study the channel activity of TPC2, it was necessary to identify a pharmacological activator that would bind in a discrete manner away from the NAADP binding site. TPC2-A1-N, the Ca^{2+} bias TPC2 activator, selectively mimics the actions of NAADP, by forcing the TPC2 channel to remain in the open conformation to allow for efflux of Ca^{2+} from the lysosome. TPC2-A1-P was used as a control, as it is selectively biased for the Na^{+} current acting through the $PI(3,5)P_2$ pathway and does not elicit a Ca^{2+} response in hAEC but is only active at high doses in HUVECs (non-specific effects). I initially assessed the effects of these compounds on Ca^{2+} release using Flexstation Ca^{2+} measurements and found that for both TPC2-A1-N (not TPC2-A1-P) there was a robust Ca^{2+} response at concentrations exceeding 50 μM (Figure 4.1A, B, C). I have shown that when HUVECs are co-stimulated with TPC2-A1-N and -P together there is a potentiation of the Ca^{2+} response, compared to the N-compound alone (Figure 4.1D). These findings agree with those of Patel and show that TPC2-A1-N is a powerful agonist of the TPC2 channel and can be used as a candidate drug to target Ca^{2+} responses specifically aligned with that channel's activity.

Low concentrations of TPC2-A1-N (<10 μM) do not elicit a rise in intracellular Ca^{2+} (Figure 2A, B). As compared to HUVEC, the Na^{+} -selective TPC2-A1-P compound elicits no Ca^{2+} response in hAEC (Figure 2C, D). TPC2-A1-N (>30 μM) evokes a concentration-dependent rise in Ca^{2+} in hAEC (Figure 2A, E). These findings support work from other labs that TPC2-A1-N can be used as an agonist of TPC2 channel activity, and that TPC2 can operate as an ion switch, capable of modulating ion fluxes via influences from these compounds.

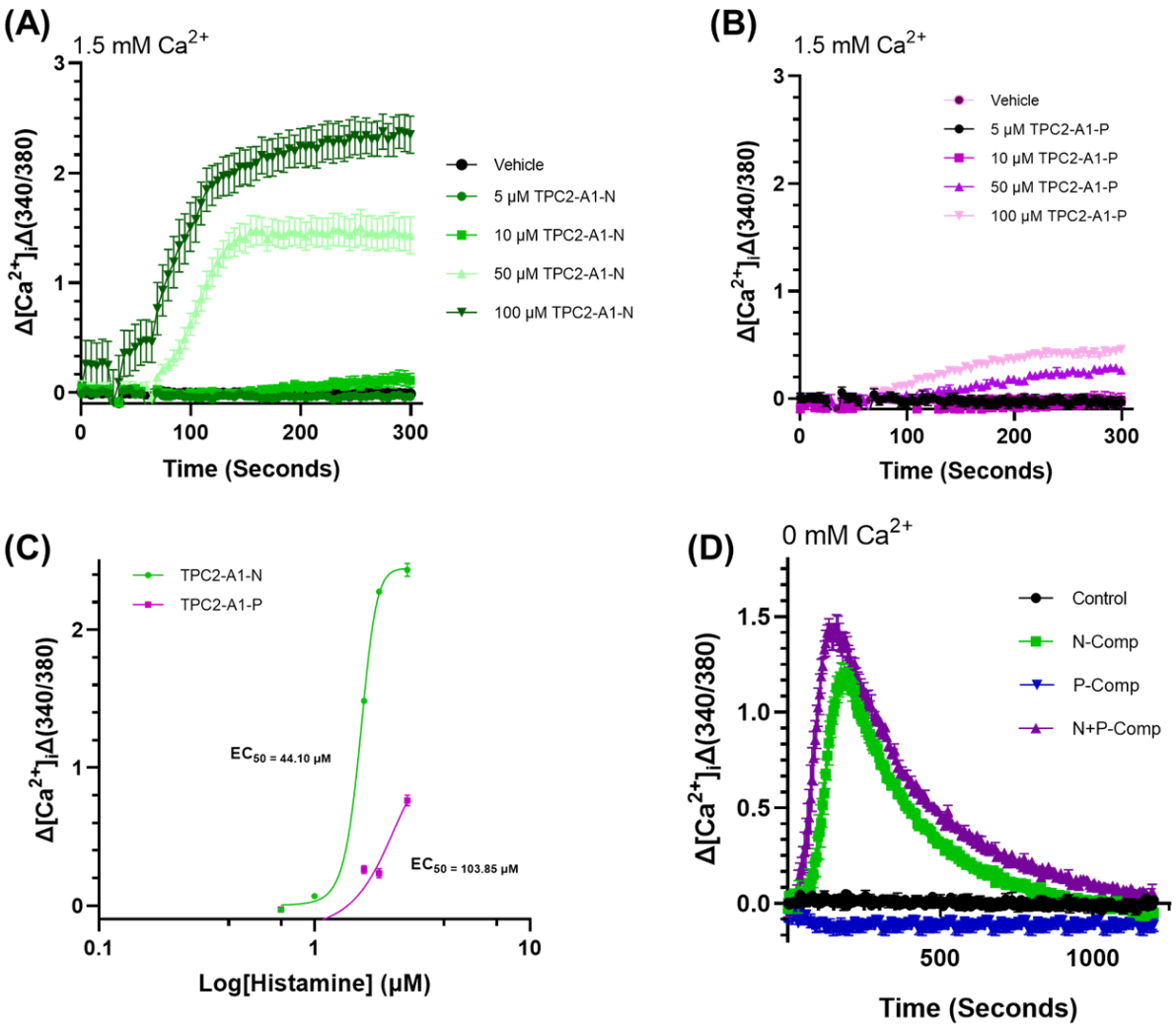

Figure 4.1 TPC2-A1-N and TPC2-A1-P elicit robust Ca^{2+} responses in HUVECs. (A) Representative Ca^{2+} trace showing concentration-response of TPC2-A1-N (5-500 μM). (B) Representative Ca^{2+} trace showing concentration-response of TPC2-A1-P (5-500 μM). (C) Concentration-response curves for (A) and (B) were plotted using the Hill Equation. (D) Representative Ca^{2+} trace showing potentiation of the Ca^{2+} response when both TPC2-A1-N and –P are applied in co-stimulation. (A)-(C) performed in 1.5 mM Ca^{2+} SBS buffer. (D) performed in 0 mM Ca^{2+} SBS buffer + 0.4 mM EGTA. n/N = 3/9 for (A)-(C), 1/3 for (D).

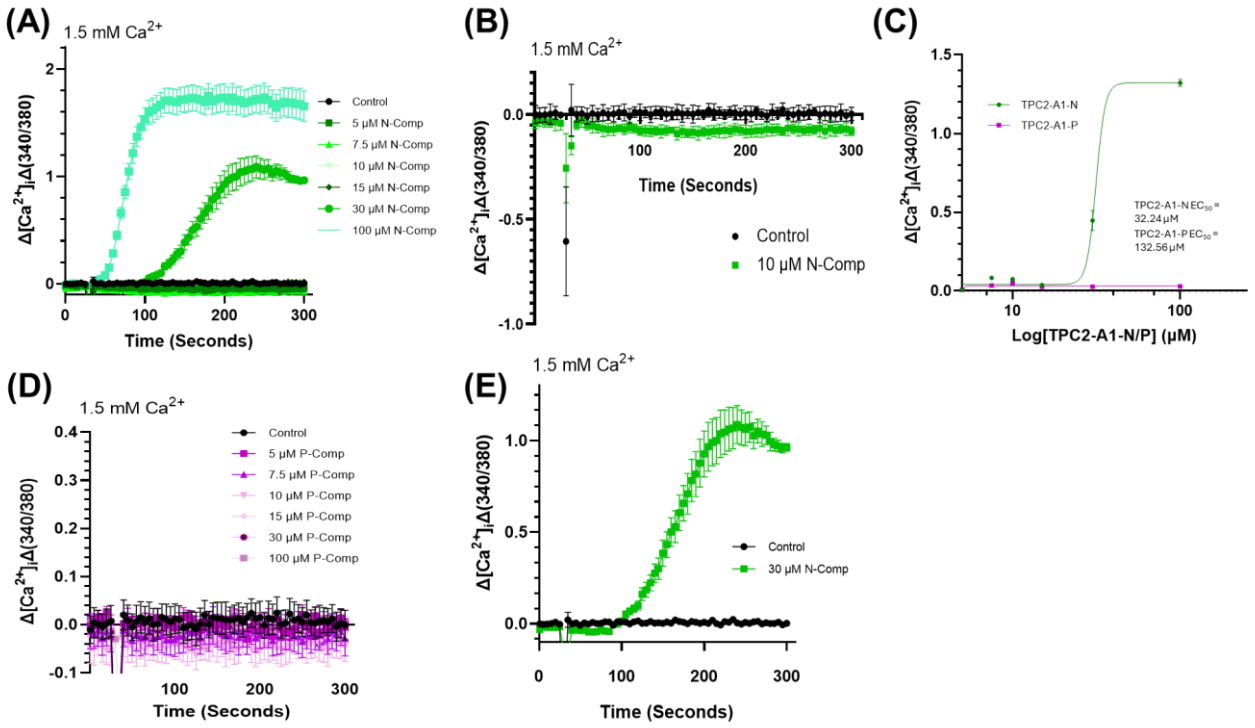

Figure 4.2 TPC2-A1-N, but not TPC2-A1-P elicits a robust Ca^{2+} response in hAECs. (A) Representative Ca^{2+} trace showing a concentration-response of TPC2-A1-N (5-100 µM). (B) Representative Ca^{2+} trace of 10 µM TPC2-A1-N. (C) Concentration-response curves for TPC2-A1-N and –P plotted using the Hill Equation. (D) Representative Ca^{2+} trace showing concentration-response of TPC2-A1-P (5-100 µM), showing no response at all concentrations. (E) Representative Ca^{2+} trace of 30 µM TPC2-A1-N. All experiments were conducted in 1.5 mM Ca^{2+} SBS buffer. n/N = 3/9.

4.3 TPC2-A1-N and histamine at high concentrations elicit both lysosomal and ER Ca^{2+} store depletion

To understand if TPC2 evokes the local Ca^{2+} signal necessary for Rab46 detachment from the MTOC, I first considered the concentration of TPC2-A1-N and histamine that would enhance the histamine signal without triggering ER-store depletion. The sensitivity of Flexstation measurements would not be sufficient to detect small localised Ca^{2+} signals released from lysosomal stores. Therefore, I hypothesised, that at high concentrations of TPC2-A1-N, the signal observed is global, equal to lysosomal store depletion, and sufficient to trigger a CICR response. To investigate this theory, the cells were stimulated with 30 µM of TPC2-A1-N followed by 30 µM histamine (Figure 4.3A). Compared to the vehicle control, a significant inhibition of the mean peak amplitude and sustained response was observed when cells were pretreated with TPC2-A1-N (Figure 4.3B, C). The data suggests TPC2-A1-N has evoked CICR where ER stores have already started to deplete. Understanding that high concentrations of TPC2-A1-N and histamine deplete both lysosomal and ER Ca^{2+} stores, I wanted to test whether a high concentration of histamine (30 µM) also depletes both stores, so that subsequent stimulation with 30 µM TPC2-A1-N could not evoke Ca^{2+} release. To do this, I first simulated hAECs with 30 µM histamine for 1 min before application of 30 µM TPC2-A1-N (Figure 4.3D). I observed no potentiation of the histamine-evoked Ca^{2+} response, and this was indicative that these high concentrations of histamine have caused store depletion, thus, the rate of refilling lags behind the effects of applying another Ca^{2+} secretagogue such as TPC2-A1-N.

4.4 Low concentrations of TPC2-A1-N evokes a localised Ca^{2+} response

As shown in Figure 4.2, a low concentration of TPC2-A1-N does not evoke a global Ca^{2+} response in the time I observe histamine signalling. To determine whether 10 μM TPC2-A1-N evokes a localised Ca^{2+} response, which is unable to be detected by using Flexstation measurements. I hypothesised that a localised Ca^{2+} flux could induce CICR in the presence of histamine. I pretreated cells with histamine (0.5 μM) before treating them with 10 μM TPC2-A1-N (Figure 4.4). When compared to vehicle control, 10 μM TPC2-A1-N evoked a Ca^{2+} peak in cells pretreated with histamine. This data indicated that when applied alone, 10 μM TPC2-A1-N alone is not sufficient to evoke CICR, but it may trigger a localised response that is not visible using Flexstation measurements. Histamine (when applied at concentrations that do not deplete stores) permits a complex formation whereby the TPC2 channels are in closer proximity with one another, allowing for the potentiation of the Ca^{2+} response, via CICR.

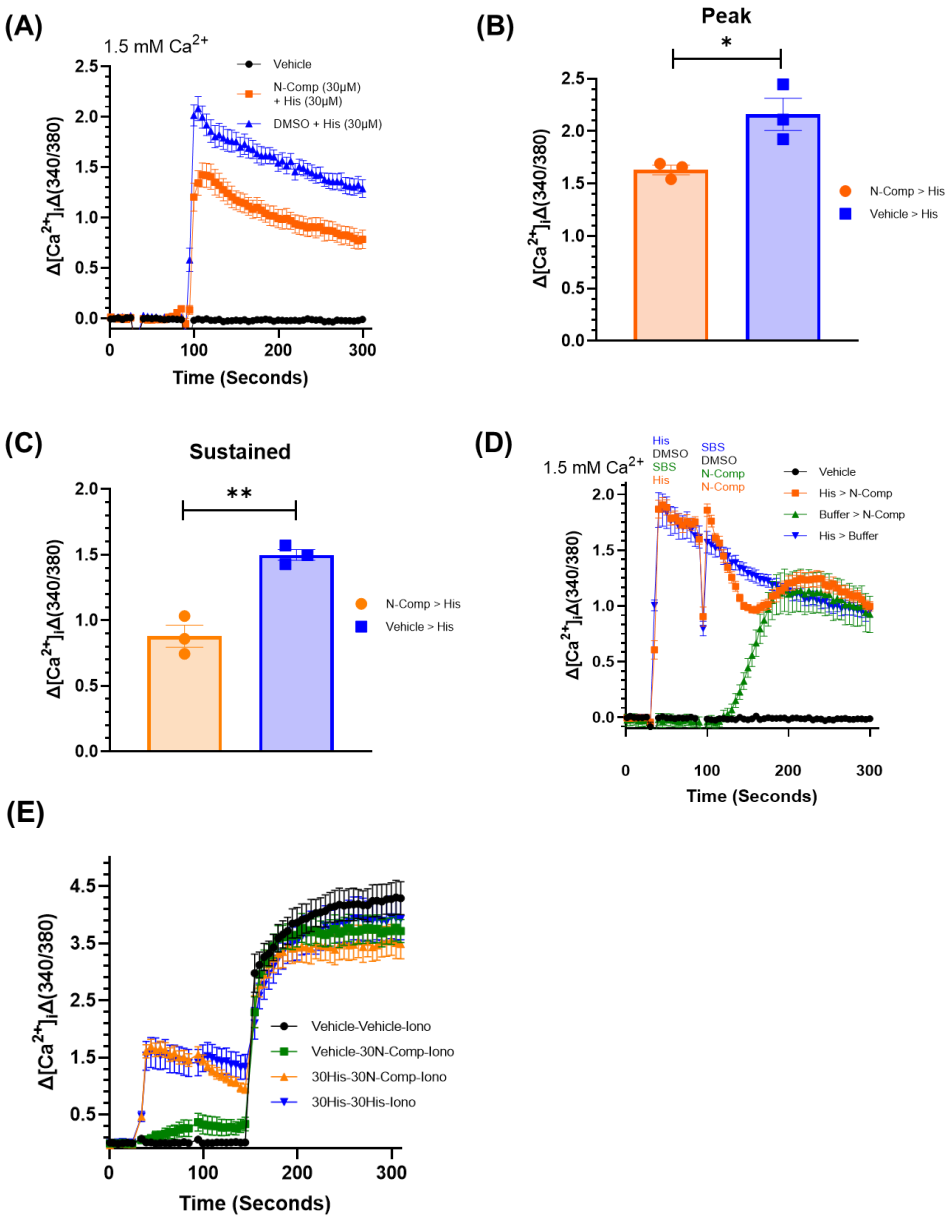

Figure 4.3 High concentrations of TPC2-A1-N depletes both lysosomal and ER Ca^{2+} stores, activating CICR. (A) Representative Ca^{2+} traces of hAEC were stimulated with 30 μM TPC2-A1-N at 30 s and then stimulated with 30 μM histamine at 90 s. (B) Mean peak amplitude data of (A). (C) Sustained Ca^{2+} responses of (A). (D) Representative Ca^{2+} trace showing no potentiation of the histamine evoked Ca^{2+} release in hAEC stimulated with 30 μM histamine at 30 secs and then followed by the addition of 30 μM TPC2-A1-N at 90 s. (E) Ionomycin stimulation to determine the maximal response from the Fura-2 loaded cells. Mean data plotted as mean ± SEM. n/N = 3/9, * = $p < 0.05$, ** = $p < 0.01$ by unpaired t-test.

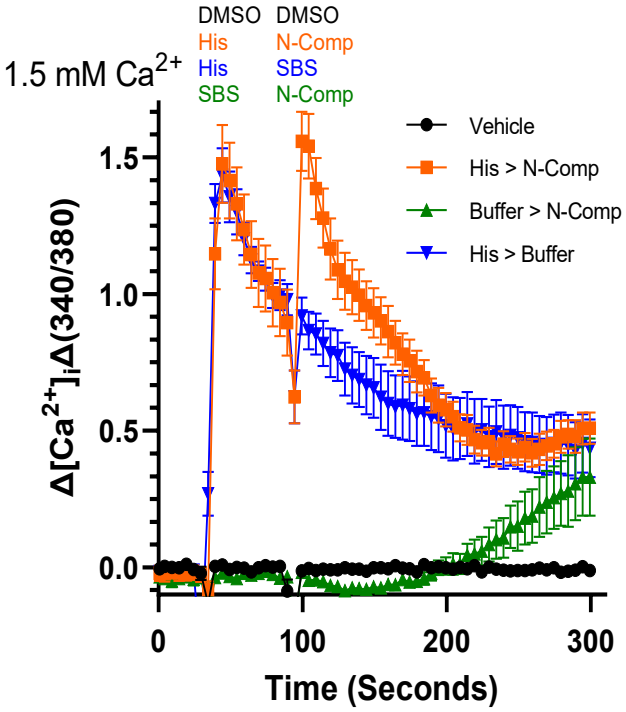

Figure 4.4 TPC2-A1-N context with histamine is lost when ER stores are initially depleted. Representative Ca^{2+} trace of dual addition Flexstation recording showing potentiation of the histamine-evoked Ca^{2+} release in hAEC stimulated with 0.5 µM his at 30 s and then 10 µM TPC2-A1-N at 90 s. Vehicle = DMSO, Buffer = SBS. All experiments were conducted in 1.5 mM Ca^{2+} SBS buffer. n/N = 3/9, plotted as mean ± SEM.

4.5 Simultaneous additions of TPC2-A1-N and histamine potentiated the sustained Ca^{2+} response

I have shown that by applying 10 μM TPC2-A1-N after sub-maximal histamine, it is possible to observe potentiation of the Ca^{2+} response, but not possible at higher concentrations when ER stores have already been depleted. I hypothesised that the simultaneous addition of 10 μM TPC2-A1-N and histamine could potentiate the release of Ca^{2+}. In the presence of extracellular Ca^{2+}, the simultaneous addition of 0.5 μM histamine and 10 μM TPC2-A1-N (Figure 4.5A) had no significant impact on Ca^{2+} rise as compared to histamine only (Figure 4.5A-C). However, the presence of extracellular Ca^{2+} in the SBS buffer may mask the true response. In the absence of extracellular Ca^{2+}, the simultaneous addition of 0.5 μM histamine and 10 μM TPC2-A1-N significantly increased the sustained response evoked by histamine only, but not the peak response (Figure 4.6A-C). This indicated in the presence of Ca^{2+}, there is a Ca^{2+} influx which is masking the effect. In the absence of Ca^{2+}, the initial release from intracellular stores is equally evoked by histamine alone or by histamine and TPC2-A1-N, However, the persistent opening of the TPC2 channel by TPC2-A1-N continues to evoke Ca^{2+} release.

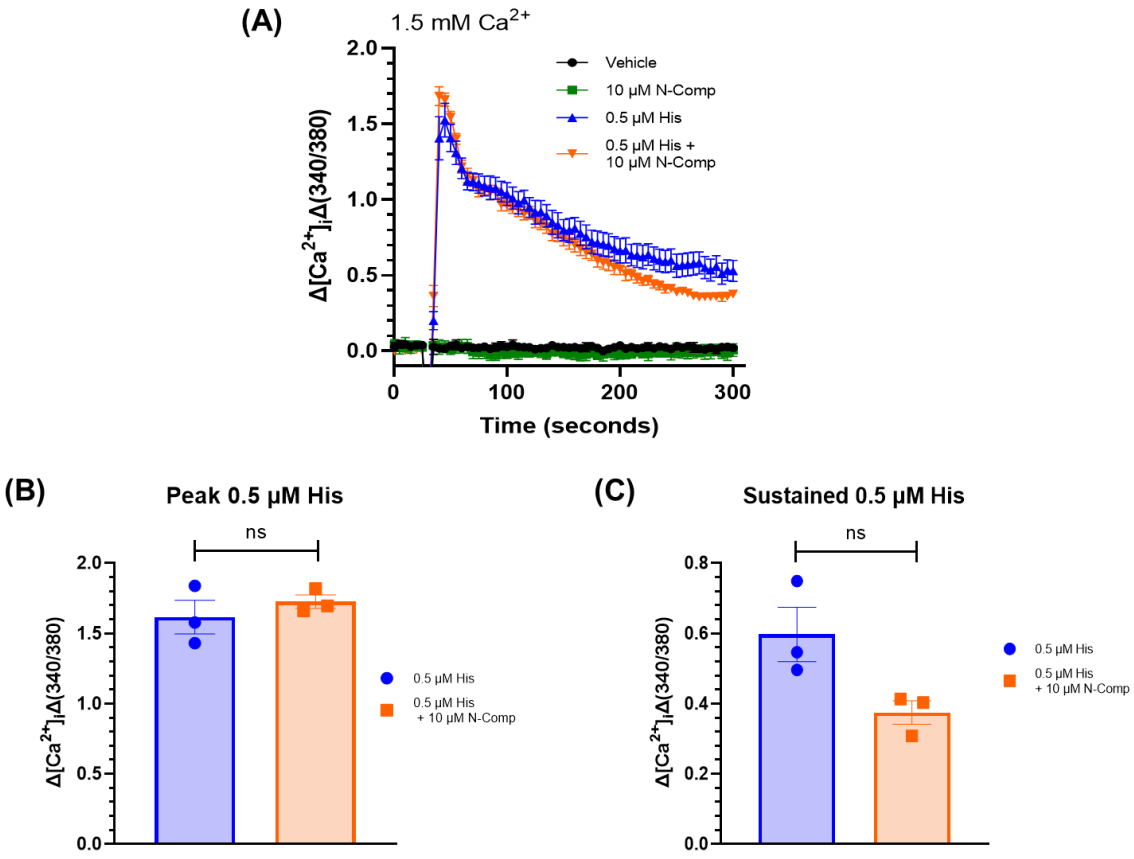

Figure 4.5 Simultaneous addition of low concentrations of His and TPC2-A1-N induces a partial potentiation of the Ca^{2+} response. (A) Representative Ca^{2+} trace of showing hAEC co-stimulated with 0.5 µM His and 10 µM TPC2-A1-N. (B) Peak mean amplitude data of (A). (C) Sustained Ca^{2+} responses for (A). N-Comp = TPC2-A1-N. All experiments were conducted in 1.5 mM Ca^{2+} SBS buffer. n/N = 3/9. ns = not significant, by unpaired t-test.

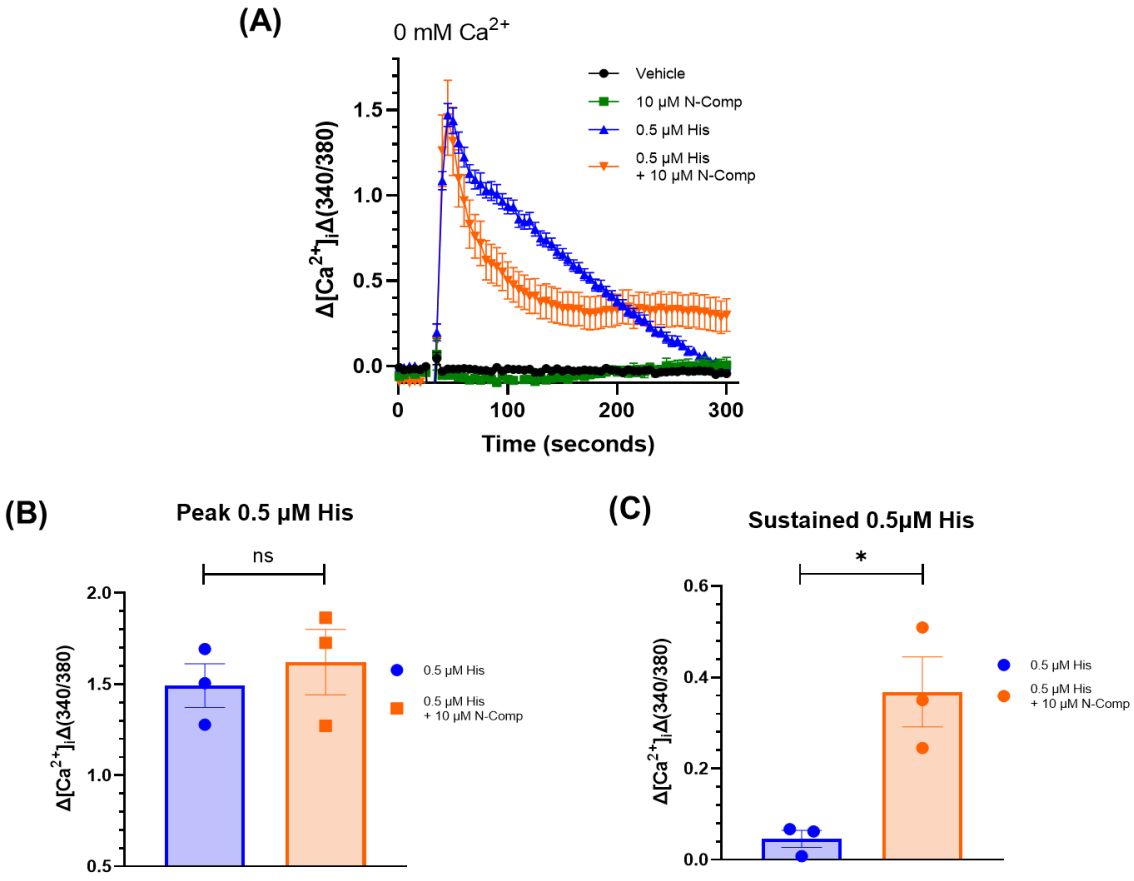

Figure 4.6 Simultaneous additions of low concentrations of histamine and TPC2-A1-N elicit a sustained Ca^{2+} response in the presence of no extracellular Ca^{2+}. (A) Representative Ca^{2+} trace of showing hAEC co-stimulated with 0.5 µM His and 10 µM TPC2-A1-N, with sustained Ca^{2+} response after acute stimulation. (B) Peak mean amplitude data of (A). (C) Sustained Ca^{2+} responses for (A). N-Comp = TPC2-A1-N. All experiments were conducted in 0 mM Ca^{2+} SBS buffer supplemented with 0.4 mM EGTA. n/N = 3/9. ns = not significant, * = $p < 0.05$, by unpaired t-test. All data is plotted as mean ± SEM.

4.6 Simultaneous additions of histamine and TPC2-A1-N evoke the dispersal of Rab46 from the MTOC

Intracellular Ca^{2+} measurements established the feasibility of characterizing TPC2 channel agonist effects in vitro, revealing that low concentrations of TPC2-A1-N potentiate localized Ca^{2+} responses with histamine co-stimulation, prompting an investigation into whether this potentiation enhances Rab46 dispersal from the MTOC. I treated hAEC with 0.5 μM histamine in the presence and absence of 10 μM TPC2-A1-N and then quantified Rab46 intracellular distribution (Figure 4.7A). TPC2-A1-N stimulation alone did not evoke trafficking of Rab46 to the MTOC, nor did it reduce the intensity of the Rab46 signal, however, it did significantly inhibit histamine-evoked clustering of Rab46 at the MTOC compared to histamine alone (Figure 4.7B). Across all three regions (Figure 4.7C) it is clear that there is not a peripheral shift in the intensity of the Rab46 signal in cells stimulated with both histamine and TPC2-A1-N. In agreement with my Flexstation data, this distribution analysis indicates that the enhanced rise in intracellular Ca^{2+} evoked by the simultaneous activation of TPC2 has potentiated the detachment of Rab46 from the MTOC.

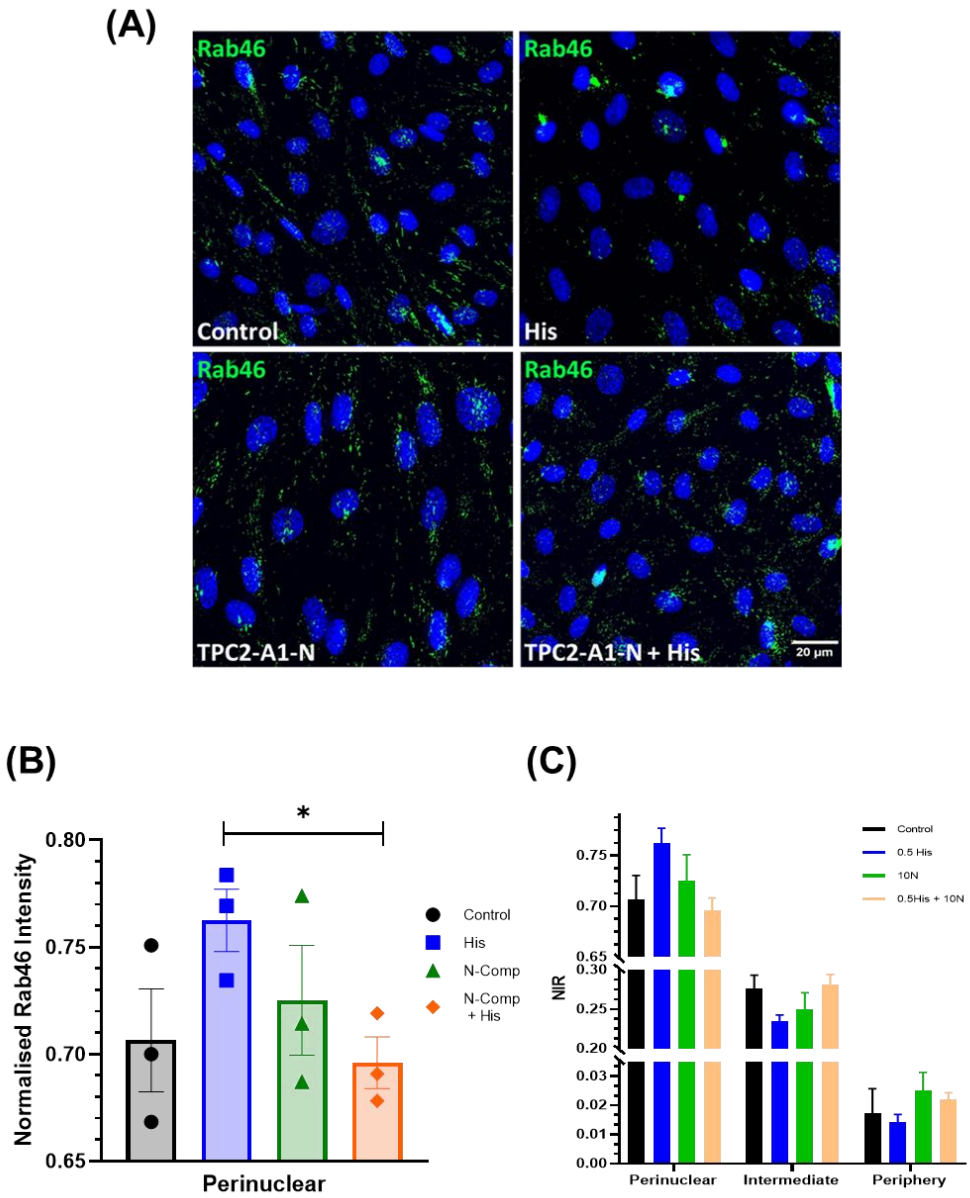

Figure 4.7 Simultaneous addition of low concentrations of histamine and TPC2-A1-N induces dispersal of Rab46 from the perinuclear region. (A) Representative images of hAECs stimulated with either 0.5 µM histamine, 10 µM TPC2-A1-N alone or in co-stimulation. Rab46 is stained green, nucleus is stained blue with H33342. Scale bar = 20 µm for all images in (A). (B) Particle intensity analysis of (A) shows the perinuclear distribution of Rab46 as a ratio of the total image fluorescence. (C) Expanded particle analysis of (B) showing all three cellular regions, perinuclear, intermediate, and periphery. Control = DMSO, His = 0.5 µM, N-Comp = 10 µM TPC2-A1-N. All data was plotted as mean ± SEM, n/N = 3/15, * = $p < 0.05$ by one-way ANOVA.

4.7 Co-stimulation with histamine and TPC2-A1-N potentiates secretion of Ang2

The data suggests release of Ca^{2+} via TPC2 mechanisms is sufficient to induce the dispersal of Rab46 from the MTOC. It has previously been shown that Rab46 is responsible for regulating the trafficking of Ang2-positive WBs to the MTOC in response to histamine stimulation (Miteva et al. 2019) and this limits Ang2 secretion from within ECs as compared to the thrombin-enhanced histamine response (that causes an all-out release). Thus, I wanted to determine the functional relevance of the Ca^{2+}-mediated dispersal of Rab46 from the MTOC and investigate the role of endo-lysosomal Ca^{2+} channels on histamine-evoked Ang2 secretion. I questioned whether the potentiation of the TPC2-dependent Ca^{2+} release by simultaneous stimulation with histamine and TPC2-A1-N would potentiate the secretion of Ang2. While neither 10 μM or 30 μM TPC2-A1-N independently evoked secretion (Figure 4.8) of Ang2 (levels similar to basal vehicle control), stimulation of hAECs with histamine and TPC2-A1-N significantly increased secretion of Ang2 when compared to histamine (0.5 μM) alone. As per my initial hypotheses, the data in this chapter identify TPC2-A1-N as a potent, physiologically active agonist of TPC2. I have demonstrated that histamine evokes retrograde trafficking of Rab46 (and WPBs containing Ang2) to the MTOC where Ca^{2+} released from TPC2 plays a significant role in eliciting the dispersal of Ang2-positive WPBs and Rab46 from microtubules.

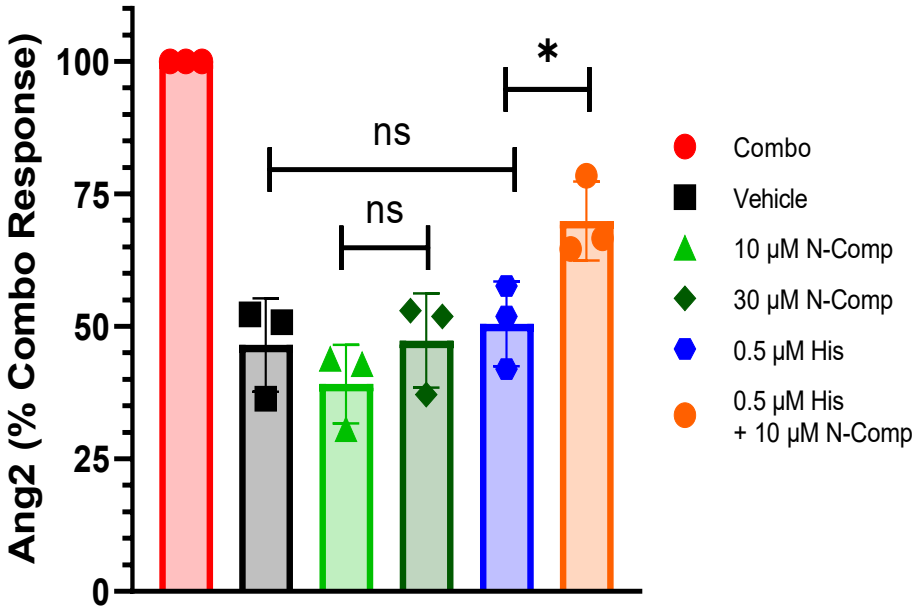

Figure 4.8 Simultaneous addition of low concentrations of histamine and TPC2-A1-N elicits increased secretion of angiopoietin-2 in hAECs. (A) Mean data from Ang2 ELISA, showing hAECs stimulated with Combo (200 U/μL thrombin + 100 μM histamine), Vehicle (DMSO), 10N (10 μM TPC2-A1-N), 30N (30 μM TPC2-A1-N), 0.5 His (0.5 μM histamine), and co-stimulation 0.5 μM histamine + 10 μM TPC2-A1-N. Data reported as mean ± SEM in (A). n/N = 3/9, ns = not significant, * = $p < 0.05$, by one-way ANOVA.

4.8 Discussion

The lysosomal two-pore channel 2 (TPC2) is a member of the TPC family that is characterised by its prominent localisation to late-endosomes and lysosomes. It possesses like TPC1, two homologous domains (I and II) that assemble to form a functional ion pore, through which the conductance of Ca^{2+} can be achieved. The ability of TPC2 to contribute to localised Ca^{2+} rises near lysosomes (most often in response to a stimulus) which can then go on to potentiate global cytosolic Ca^{2+} rises is due to its spatial and temporal Ca^{2+} dynamics (Patel et al. 2011). As with all these small, mobile lysosomal Ca^{2+} channels (excluding TPRML1; diffusion within the membrane is limited) they are potential candidates for Ca^{2+} release channels affecting the intracellular distribution of Rab46, due to their Ca^{2+} signals influencing lysosomal positioning. I hypothesised that with this coordinated movement of lysosomes, Rab46 and these channels upon stimulation with histamine would allow the local release of Ca^{2+} and for this Ca^{2+} to bind to the EF-hand domain of Rab46 causing detachment from the MTOC. TPC2 is gated by NAADP, where NAADP binding proteins (and LSM12) have been shown to mediate the binding of NAADP to TPC2, however, to date, the binding site on TPC2 remains uncharacterised (Gunaratne et al. 2023). This NAADP-mediated Ca^{2+} signalling is crucial in the coordination of small lysosomal signals potentiating into global responses in the context of an immunogenic stimulus such as histamine.

With TPC2 being identified as a strong candidate ion channel, I used another pharmacological approach, this time, an agonist of TPC2, TPC2-A1-N that was developed through analogue screening techniques. TPC2-A1-N is a potent agonist of the channel, which possesses the ability to bypass the need for NAADP activation and modulation of channel activity. The role of this agonist is to leave TPC2 in a long-lasting open conformation, through which Ca^{2+} efflux is achieved. The development of a Na^{+} -selective agonist, TPC2-A1-P permits mimicking of $PI(3,5)P_2$ where it preferentially induces Na^{+} efflux from TPC2. The discovery of these compounds showed that TPC2 operates like a cation-switch, with the capability of these compounds to bias the efflux of one ion over another (Gerndt et al. 2020; Yuan et al. 2024). I have used this pharmacology to explore the effects of TPC2 activation on the histamine-evoked Ca^{2+} release by

NAADP-mediated signals and the distribution of Rab46 in response to this channel activation.

Firstly, I confirmed that in endothelial cells, TPC2-A1-N evoked a robust Ca^{2+} response in both HUVEC and hAEC. I hypothesised that TPC2-A1-P would not produce a Ca^{2+} response due to its ability to promote a Na^{+} efflux, however, it is clear in HUVEC that at high concentrations I evoked a small rise in intracellular Ca^{2+} that was not observed in hAEC. This could be due to differential expression and abundance of TPC2 in HUVEC vs hAEC, where I observed increased expression of TPC2 in HUVEC with RT-qPCR. Patel et al. are credited with identifying the potentiated effects of adding them in a co-stimulus model, where they demonstrated that an acute stimulation with both TPC2-A1-N and TPC2-A1-P simultaneously induced an increased Ca^{2+} response in HeLa cells, due to a preferential bias for switching TPC2 for being even more selective for Ca^{2+} over Na^{+} (Yuan et al. 2022; Yuan et al. 2024). I have been able to show in HUVEC that TPC2 is capable of biasing Ca^{2+} release through dual stimulation with TPC2-A1-N and -P. Time restraints within the lab led to this not being evaluated in my hAEC model.

At low concentrations of TPC2-A1-N (10 μM), I observed no Ca^{2+} rise within the same timeframe as histamine stimulations. However, at these low concentrations, when applied in co-stimulation with histamine (0.5 μM) I observed that the N-compound could potentiate the histamine-evoked Ca^{2+} rise. These data highlighted, that 10 μM TPC2-A1-N alone may induce a localised release of lysosomal Ca^{2+} (from TPC2) which is not detectable using Flexstation-based assays as the responses are below the detection limits. However, cells stimulated with low concentrations of histamine (evoked a localised Ca^{2+} rise from lysosomes) and then stimulated with 10 μM TPC2-A1-N showed potentiation of the Ca^{2+} response is through release from the ER Ca^{2+} store. Hence, I observed a further rise in the Ca^{2+} response. The opposite is observed at high concentrations of histamine (30 μM) or TPC2-A1-N whereby ER stores are already depleted, hence the addition of a high concentration of TPC2-A1-N (30 μM) fails to potentiate Ca^{2+}. Recent evidence suggests TPC2 sensitises IP_3Rs to Ca^{2+} release evoked by TPC2-A1-N and that through this pathway TPC2-A1-N bypasses NAADP to synergise with IP_3 to coordinate local

Ca^{2+} signals and evoke globalisation of this small Ca^{2+} response (Yuan et al. 2024). Work conducted by Yuan and Patel, has focused on single-cell electrophysiology, and although this allows for control over cell conditions. I believe that having a comprehensive approach, such as Flexstation measurements allows for a more physiologically relevant representation due to ECs requiring confluence. Here, I present work that characterises TPC2-A1-N in the context of histamine stimulus in ECs and investigate the effects of TPC2 activation of the release of Ang2.

Now understanding that TPC2-A1-N is capable of bypassing NAADP agonism to evoke intracellular Ca^{2+} release, I questioned whether it was a form of lysosomal-ER crosstalk that was regulating these localized physiological Ca^{2+} signals. To test this, I used simultaneous additions of 10 μM TPC2-A1-N in combination with increasing concentrations of histamine (0.1-10 μM) and observed the presence of extracellular Ca^{2+} (1.5 mM Ca^{2+} SBS buffer) at low concentrations of histamine (0.5 μM) there was a slight, but not significant potentiation of the histamine + TPC2-A1-N evoked Ca^{2+} release compared to control (histamine only). I have shown that there is no further potentiation of Ca^{2+} release by TPC2-A1-N in hAEC when applied alongside histamine. This disagrees with the work of the Patel group, as they show that TPC2-A1-N may be capable of synergising with IP_3 (produced by the cell in response to histamine) to amplify the Ca^{2+} signals generated by TPC2, however, I believe this might not be a universal response and could be cell-type specific. Despite this slight synergism I observed at 0.5 μM + 10 μM N, I could not confidently conclude this was a true response since there still could be residual Ca^{2+} in the extracellular space from the buffer interfering with the ER-refilling process. Thus, I turned to using a 0 mM Ca^{2+} model and discovered an interesting response of hAEC to stimulation with low histamine and low concentration of TPC2-A1-N when added simultaneously. Again, there was no potentiation of the mean peak histamine + TPC2-A1-N evoked Ca^{2+} response. Nonetheless, I observed a significant difference between control and histamine + N in the sustained Ca^{2+} response. In 0 mM Ca^{2+} conditions, it is unusual to observe sustained Ca^{2+} responses, due to the complete depletion of the ER stores, and with no-refilling, I expected under all conditions for the responses to fall to zero.

This was not the case in those cells subjected to simultaneous addition of low concentrations of histamine and low concentrations of TPC2-A1-N (0.5 μM and 10 μM, respectively). To answer this phenomenon is complicated, but it is possible that due to TPC2 being forced to stay in an open conformation, the imbalance in Ca^{2+} inside and outside, forces the cell to enter a survival mode, where it uses emergency Ca^{2+} pools, mitochondrial Ca^{2+}. There have been multiple studies that highlight in various situations, mitochondria can release Ca^{2+} as a last resort. This is intricately linked with cell death due to the sudden efflux of Ca^{2+} through the mitochondrial permeability transition pore (mPTP) causing apoptotic signalling cascades (Montero et al. 2001; Baumgartner et al. 2009).

Ang2 secretion was shown to be potentiated upon co-stimulation with histamine and TPC2-A1-N at low doses (0.5 μM and 10 μM, respectively). Forcing TPC2 to remain open, causes a rapid efflux of Ca^{2+} in combination with histamine, which I have shown on its own releases a small amount of Ang2 that cannot be potentiated by increasing the histamine concentration. It is probable that when the two pharmacological agents are applied simultaneously the surge in the release of more Ca^{2+} from both lysosomal and ER Ca^{2+} stores is sufficient to trigger the release of Rab46 and thus WPBs containing Ang2 from the MTOC allowing an increase in secretion. The time for the secretion of Ang2 I have observed is short (10 min). I used this time to allow for direct comparison with Flexstation and IF imaging data, however most studies investigating Ang2 in a stimulus-dependent context have applied compounds for 24 hr or more, hence, this could explain why I only observe minor changes above basal secretion (Ferraro et al. 2019). Ang2 is a large glycoprotein, and experiments have shown that cells prioritise controlling production over reliance on stability once the final protein is made and stored, thus its detection by ELISA may be hindered by this (Huang et al. 2002). For this reason, it provides justification for my use of a powerful positive control (combo) consisting of thrombin and elevated levels of histamine to mimic an all-out vascular response, which would occur within a noticeably brief time *in-vivo*, to normalise my ELISA responses to.

Altogether, the data in this chapter highlights the potent Ca^{2+} permeable TPC2 agonist, TPC2-A1-N as a powerful tool for the study of intracellular Ca^{2+}

signalling mediated by NAADP, through pharmacological mimicking of the second messenger in the context of TPC2. I have demonstrated that efflux of Ca^{2+} through this channel can be potentiated in response to histamine stimulus and that prolonged opening of the channel can elicit sustained Ca^{2+} responses. It is possible to elucidate from the data that low concentrations of the agonist elicit a local, small release of Ca^{2+} from lysosomes and that at concentrations exceeding 30 μM, it is possible to globalise the response leading to CICR via ER Ca^{2+} pool depletion. Ang2, a constitutively active cargo stored within Rab46-positive WPBs appears to have increased secretion when subject to co-stimulation with histamine and TPC2-A1-N. This further strengthens the argument that the release of Ang2 in the context of an immune stimulus, is reliant on Ca^{2+} release from small lysosomal stores. TPC2 along with other members of the lysosomal cation channel family have been identified as having important roles in viral vector translocation and cancers (Chi et al. 2024). Thus, it is probable that targeting this channel with TPC2-A1-N could confer therapeutic potential downstream.

Chapter. 5

Endo-lysosomal Ca^{2+} stores are actively involved in NAADP-mediated Ca^{2+} signalling.

5.1 Introduction

Having used a pharmacological approach to demonstrate the roles of TPC1/2 and TRPML1 in the dispersal of Rab46 from the MTOC following stimulation with histamine, I wanted to use channel-specific siRNA to understand how the reduced expression of each channel affects NAADP-mediated Ca^{2+} release.

Within the literature, there are multiple reports of cross-talk between intracellular organelles, and the endo-lysosomal system is no exception. Work has been published on the relationship between ER-lysosomal cross-talk pathways, one of the most probable being the idea of a 'trigger hypothesis,' whereby, a small, localised release of Ca^{2+} through lysosomal Ca^{2+} channels, triggers, and amplification of the signal via CICR, thus triggering the release of Ca^{2+} from the ER (Lee et al. 2019; Morgan et al. 2021). Following on from the results in the previous chapter, I postulated whether TPC1/2 and TRPML1 are capable of this type of communication with one another. TPC1 may have luminal cation homeostatic function, in that it is responsible for maintaining the Ca^{2+} current and ensuring that this is kept in check (Larisch et al. 2016). TPC2 has become a 'hot-topic' channel in this histamine-evoked Ca^{2+} release pathway, due to the context in which it operates with the TPC2 channel agonist, TPC2-A1-N, and its ability to operate as a cation switch, where it can bias Ca^{2+} currents over Na^{+} currents (Gerndt et al. 2020; Yuan et al. 2022). TRPML1 is a unique channel, which it has been isolated as having a direct cardiovascular function in nitric oxide release by eliciting a global rise in intracellular Ca^{2+} in cerebrovascular cells (Brunetti et al. 2024). In this chapter, I wanted to explore the effect of knocking down these three endo-lysosomal cation channels individually on

histamine and TPC2-A1-N-induced Ca^{2+} release. Following this work, I decided to briefly consider the effect of TPC2 knockdown on histamine-evoked Rab46 cellular distribution and Ang2 secretion.

5.2 siRNA knockdown of TPC1/2 and TRPML1 can be successfully induced in hAECs.

Before Ca^{2+} measurements were recorded, it was necessary to validate that commercially available antibodies for TPC1/2 and TRPML1 were target-specific, and that knockdown of the channels was feasible. hAECs underwent lipofectamine transfection with siRNA specific to each channel, alongside siRNA controls. Rab46 was used as a positive control (Figure. 5.1A), as the antibodies and siRNA for this protein had been validated previously (Pedicini et al. 2021; Miteva et al. 2019). Endogenous expression of all three channels in hAECs was observed under control conditions and expression was successfully reduced in siRNAs conditions (Figure. 5.1B, C, D). After imaging, all blots were then stripped and underwent further washing and probing with beta-actin to ensure equal protein loading across samples. These data suggest that I could explore intracellular Ca^{2+} channel dynamics in hAECs using these siRNAs.

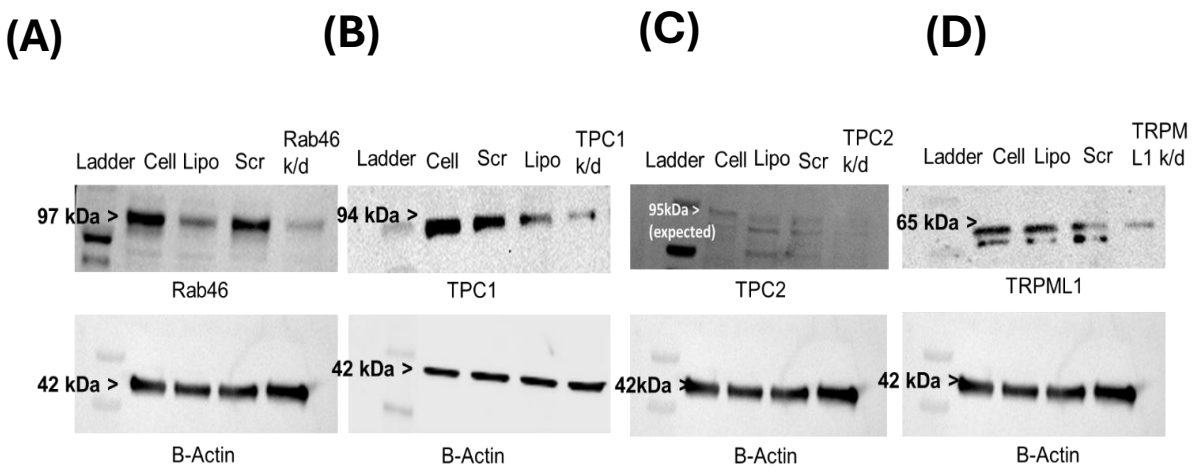

Figure 5.1 Antibody and siRNA-induced knockdown validation of TPC1, TPC2, and TRPML1 in hAECs. (A) Western blot showing the anticipated band at 97 kDa for Rab46 and subsequent reduction in protein intensity (Cell; 20.4%, Rab46 k/d; 5.4% of β-Actin intensity) upon k/d. (B) Western blot showing the anticipated band at 94 kDa for TPC1 and subsequent reduction in protein intensity (Cell; 62.9%, TPC1 k/d; 26.0% of β-Actin intensity) upon siRNA transfection (knockdown: k/d), β-actin remained constant across all conditions. (C) Western blot showing the anticipated band at 95 kDa for TPC2 and subsequently a reduction in protein intensity (Cell; 47.0%, TPC2 k/d; 32.9% of β-Actin intensity) in the upon k/d, β-actin remained constant across all conditions. (D) Western blot showing the anticipated band at 65 kDa for TRPML1 and subsequently a reduction in protein intensity (Cell; 54.1%, TRPML1 k/d; 21.0% of β-Actin intensity) in the upon k/d, β-actin remained constant across all conditions. n = 1, all samples underwent protein quantification before loading to ensure equal protein loading across all blots for comparison. Ladder = protein ladder, Cell = untransfected cell lysate, Scr = scrambled siRNA, Lipo = lipofectamine only, k/d = channel knockdown.

5.3 Transfection of hAECs using Lipofectamine® 2000 does not impede histamine-evoked Ca^{2+} release

Before achieving channel knockdown and measuring Ca^{2+} channel dynamics, it was vital to ensure that transfection using Lipofectamine® 2000 did not affect the release of intracellular Ca^{2+} evoked by histamine. Although lipofectamine has long been considered a stable and effective tool for transfection in endothelial cells, optimization of the concentration of lipofectamine and the ratio of siRNA to this medium, was crucial to evaluate before the application of acute stimuli. I assessed the effects of lipofectamine alone and in combination with histamine (30 μM). I was able to demonstrate that in hAECs, transfection with lipofectamine did not inhibit the histamine-evoked Ca^{2+} release (Figure. 5.2A). Transfection did not negate the mean peak Ca^{2+} response (Figure 5.2B) or interfere with the sustained Ca^{2+} response in this cell line (Figure 5.2C).

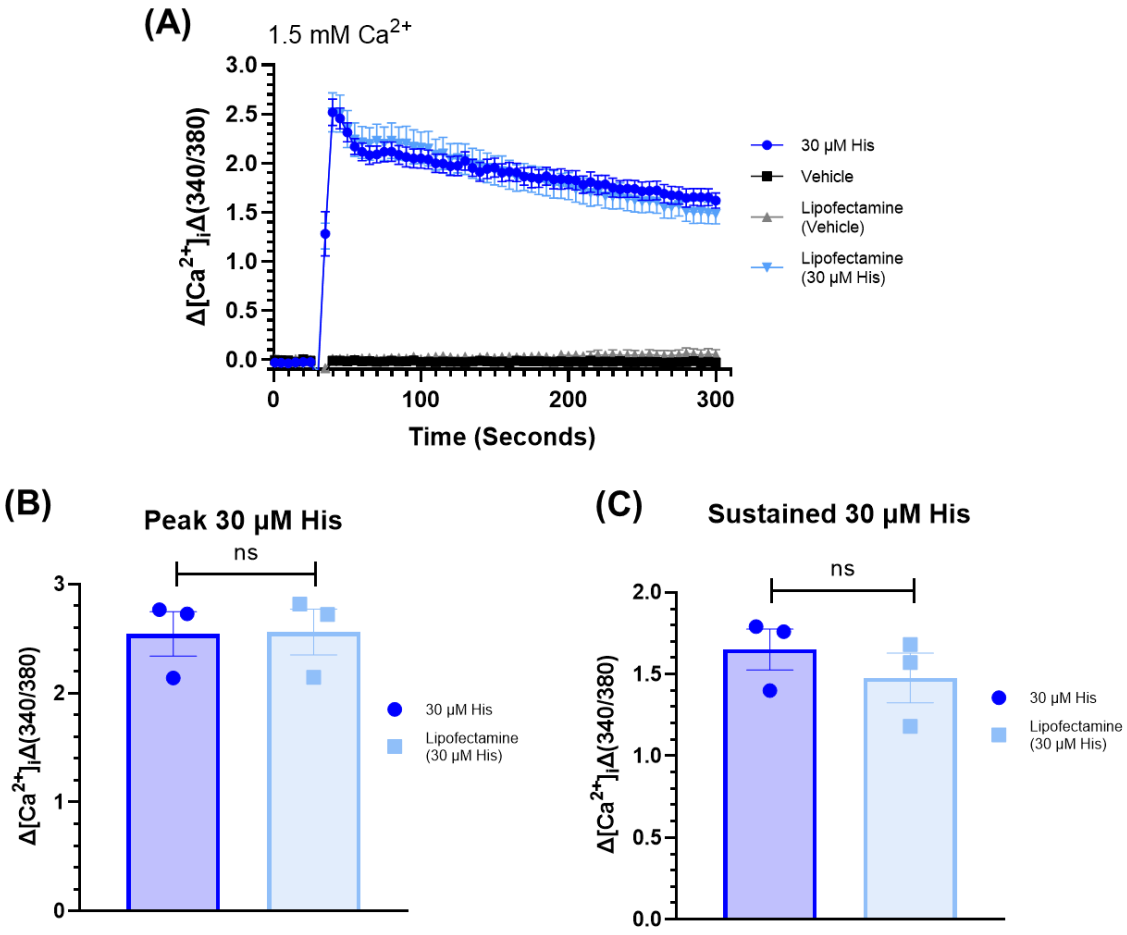

Figure 5.2 Lipofectamine transfection does not negate histamine-evoked Ca^{2+} responses. (A) Representative Ca^{2+} trace showing stimulation of hAECs stimulated with either 30 µM His or vehicle in or out of the presence of transfection for 48 h by Lipofectamine® 2000 (ratio 1:3). (B) Mean peak amplitude data of (A). (C) Sustained Ca^{2+} response mean data of (A). Vehicle = DMSO. All experiments were conducted in 1.5 mM Ca^{2+} SBS buffer. Data plotted as mean ± SEM. Ns = not significant, by unpaired t-test. n/N = 3/9.

5.4 TPC1 knockdown inhibits histamine-evoked Ca^{2+} rises at low concentrations

The two-pore channel proteins (TPCs) are ancient, highly conserved cation channels that reside uniquely within acidic intracellular organelles, such as lysosomes. Studies have demonstrated that they are targets of NAADP, which mobilises Ca^{2+} from these acidic stores (Lin-Moshier et al. 2014; Capel et al. 2015). TPC1 has two variant isoforms and is colocalised to endosomes (early and late) and lysosomes. Researchers claim that TPC1 and TPC2 operate independently of each other (Ruas et al. 2014). I questioned this in endothelial cells, due to the proximity of these channels to one another and the lack of drug targets commercially available capable of agonising or antagonising TPC1. It has been shown that TPC1 knockout in mice is not embryonic lethal, however, it does disrupt normal immune function and promotes abnormal Ca^{2+} signalling, hence I hypothesised that this channel serves as a modulator of lysosomal homeostasis (Mallmann & Klugbauer, 2020). To study the effect of TPC1 knockdown on the histamine-evoked Ca^{2+} release, I used intracellular Flexstation Ca^{2+} measurements to acutely stimulate hAECs with histamine in siTPC1-targeted cells vs control.

At high concentrations of histamine (30 μM) there was no effect on the peak Ca^{2+} response by knockdown of TPC1 (Figure. 5.3A, B).). I observed, however, that knockdown of TPC1, induced a potentiation of the sustained response (Figure 5.3A,C). TPC1 knockdown induced a significant inhibition of Ca^{2+} rise in hAECs stimulated with low concentrations (0.1 μM) of histamine (Figure. 5.3D), but not the sustained response (Figure 5.E).

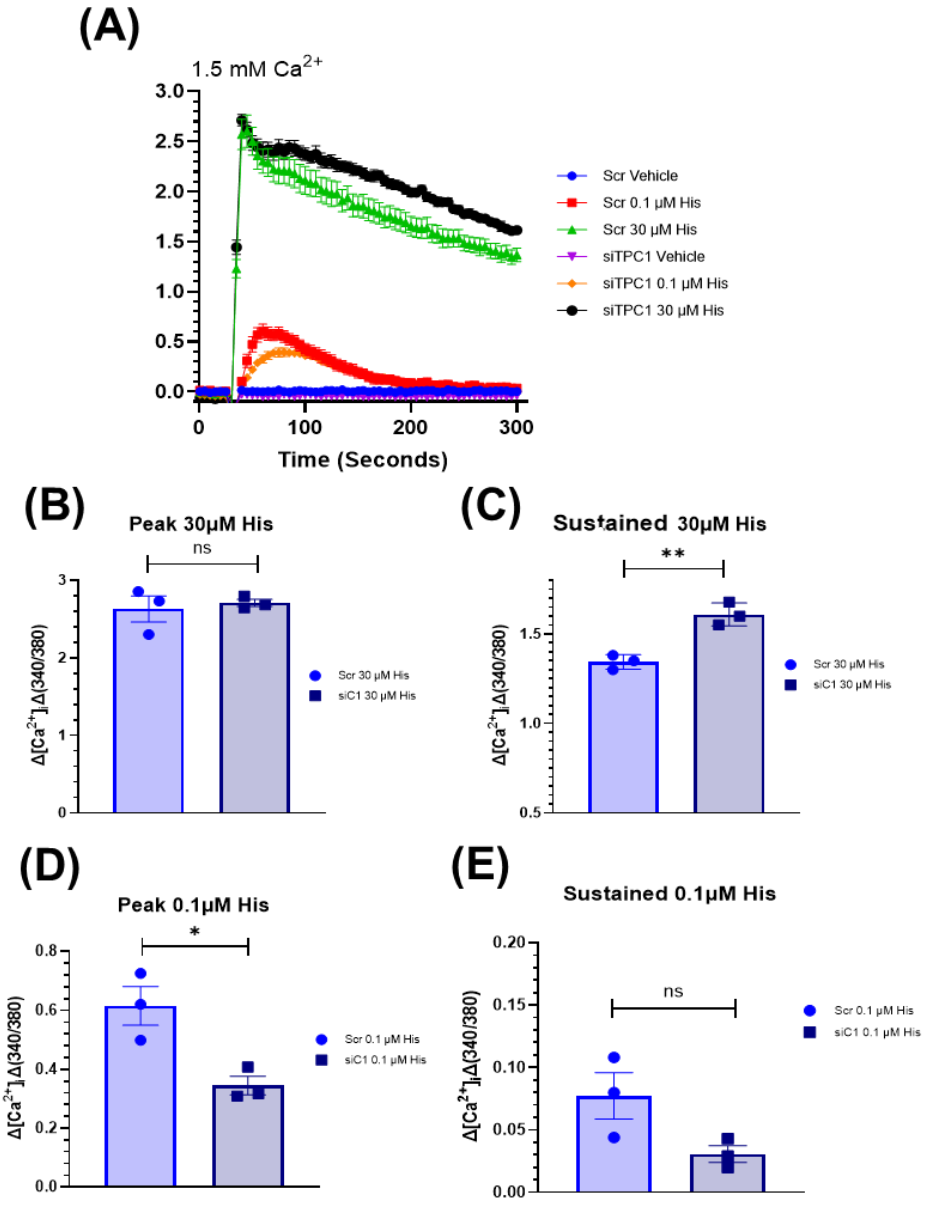

Figure 5.3 TPC1 knockdown potentiates the sustained Ca^{2+} response at high histamine concentrations and depletes Ca^{2+} release at low concentrations. (A) Representative Ca^{2+} traces showing acute stimulation of hAEC with 0.1 or 30 µM histamine in siRNA control versus acute stimulation with TPC1 knockdown. (B) Mean peak amplitude data of 30 µM histamine from (A). (C) Sustained Ca^{2+} responses of 30 µM histamine from (A). (D) Mean peak amplitude data of 0.1 µM histamine from (A). (D) Sustained Ca^{2+} responses of 0.1 µM histamine from (A). Scr = scrambled controls, siC1 = k/d TPC1. All experiments were conducted in 1.5 mM Ca^{2+} SBS buffer. Data reported as mean ± SEM. n/N = 3/9, ns = not significant, * = $p < 0.05$, ** = $p < 0.01$, by unpaired t-test.

5.5 Knockdown of TPC2 significantly impairs the histamine-evoked Ca^{2+} release in hAECs

TPC2 is ubiquitously expressed across multiple cell types within humans and is the most widely studied of the three channels, due to its ability to operate as a cation switch. Agonists of the channel, TPC2-A1-N/-P can alter the Ca^{2+} and Na^{+} currents through a bias mechanism for Ca^{2+} efflux. Evidence from the Patel and Galione groups has highlighted TPC2 to be a strong candidate for mediation of NAADP Ca^{2+} signalling, with the identification of the agonists listed above, but also through the identification of NAADP binding proteins (JPT2 and LSM12), which allowed for in-depth analysis of NAADP activation of TPCs. A recent study identified a close relationship between TPC2 and IP_3Rs in their ability to coordinate very localised Ca^{2+} signals in the lysosome and propagate these into global Ca^{2+} signals via the release of Ca^{2+} from the ER (Yuan et al. 2022). Thus, it is apparent that TPC2 is a strong candidate ion channel, capable of deducing NAADP-mediated Ca^{2+} signals and setting the context for the propagation of these signals into global, amplified responses.

Here, I monitored intracellular Ca^{2+} dynamics to study the effects of TPC2 knockdown on histamine-evoked Ca^{2+} signalling. I hypothesized that at both low (0.1 μM) and high (30 μM) concentrations of histamine, I would observe inhibition of the Ca^{2+} response, and this was observed experimentally as shown (Figure 5.4A). At both 30 μM histamine, the peak (Figure 5.4B) and sustained (Figure 5.4C) responses were inhibited by knockdown of TPC2. At 0.1 μM histamine, I again observed a significant inhibition of the peak Ca^{2+} response (Figure 5.4D), and the sustained response (Figure 5.4E), however, this was not significantly different from to control. These findings highlight that the TPC2-mediated Ca^{2+} release plays a role in eliciting the histamine-evoked Ca^{2+} response and loss of this channel could impair ER-lysosomal cross-talk.

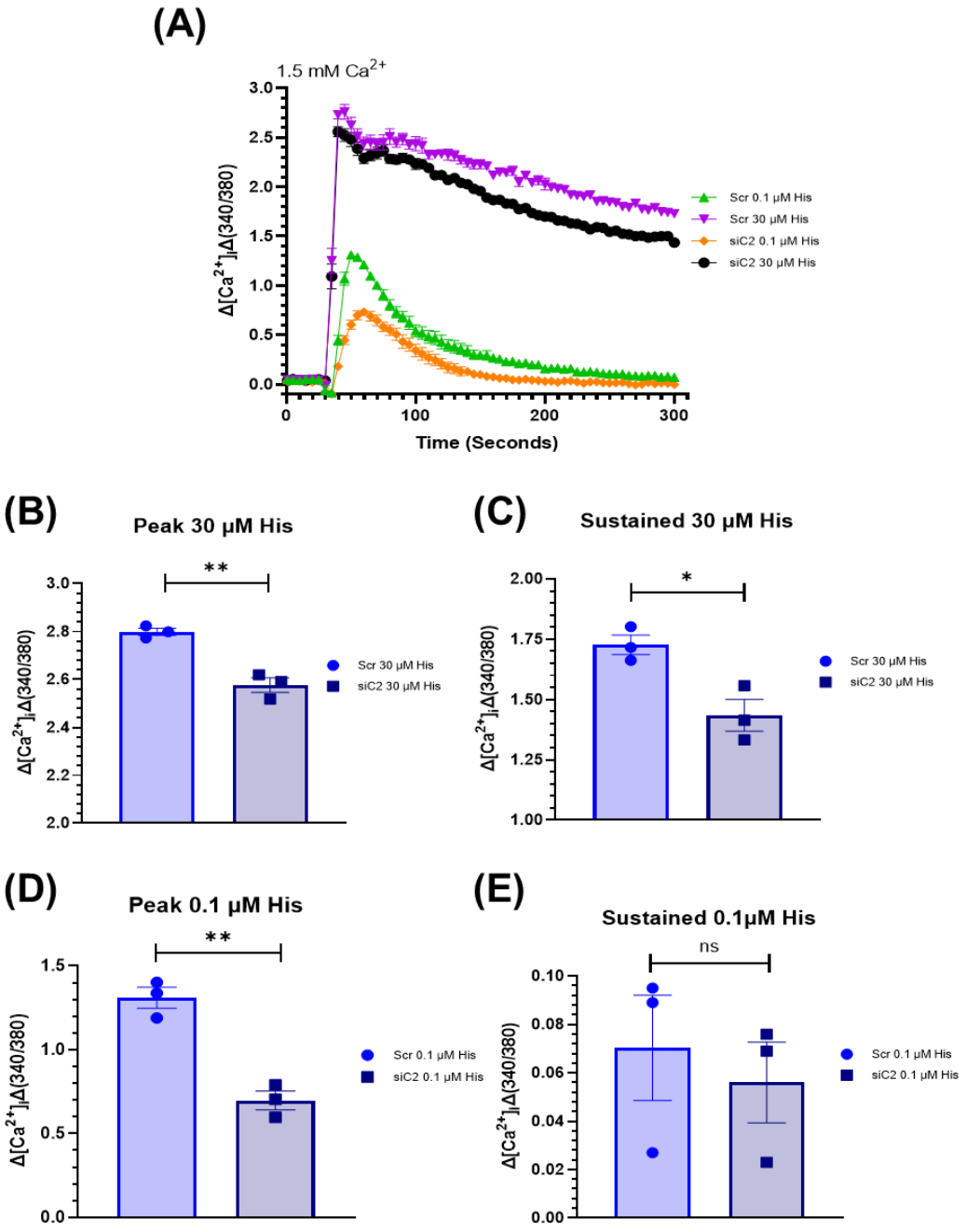

Figure 5.4 Knockdown of TPC2 inhibits intracellular histamine-evoked Ca^{2+} release. (A) Representative Ca^{2+} traces showing acute stimulation of hAECs with 0.1 and 30 µM histamine ± TPC2 channel knockdown. (B) Mean peak amplitude data of (A) for 30 µM histamine. (C) Sustained Ca^{2+} responses for 30 µM histamine of (A). (D) Mean peak amplitude data of (A) for 0.1 µM histamine. (E) Sustained Ca^{2+} responses of (A) for 0.1 µM histamine. Scr = siRNA control, siTPC2 = k/d TPC2. All experiments were conducted in 1.5 mM Ca^{2+} SBS buffer. Data plotted as mean ± SEM, n/N = 3/9. ns = not significant, * = $p < 0.05$, ** = $p < 0.01$, by unpaired t-test.

5.6 TRPML1 knockdown inhibits the histamine-evoked Ca^{2+} response at low concentrations

TRPML1 is a member of the transient receptor potential (TRP) family of proteins and possesses unique characteristics that isolate it from that of the endo-lysosomal TPCs. Firstly, TRPML1 is exclusively restricted to the lysosomal membrane and has been intricately linked to playing a pivotal role in mitochondrial Ca^{2+} homeostasis (Peng et al. 2020). Unlike TPC1/2, TPRML1 is the only known lysosomal Ca^{2+} channel to modulate mitochondrial Ca^{2+} dynamics, via contact sites between mitochondria and lysosomes. Although, in this thesis, I have not considered mitochondrial Ca^{2+} signalling, it is important to highlight that TRP channels have clear, independent signalling pathways to that of TPC1/2. Knowing that TRPML1 and other members of the TRP family of proteins are implicated in lysosomal storage disorders, such as Mucolipidosis type IV (MLIV), I believe that probing their Ca^{2+} dynamics could shed light on potential therapeutics. I applied the same pharmacology as used in TPC1 and TPC2 within the chapter (0.1 and 30 μM histamine) and observed the effects of knockdown of TRPML1 on these responses. At high concentrations (30 μM) of histamine, TRPML1 knockdown did not affect the histamine-evoked Ca^{2+} release (Figure 5.5A) and there were no differences in the mean peak amplitude (Figure 5.5B) and the sustained Ca^{2+} response (Figure 5.5C). Again, at low concentrations of histamine (0.1 μM), I observed a significant inhibition of the mean peak histamine-evoked Ca^{2+} response (Figure 5.5D), however, there was no significant difference between control and knockdown in the sustained Ca^{2+} response (Figure 5.5E).

Together, so far, this data on the three lysosomal Ca^{2+} channels in this thesis, point to a hypothesis that knockdown of lysosomal cation channels, significantly affects the localised Ca^{2+} release, characterised by NAADP, and that there is potential for a compensation of Ca^{2+} release through TPC1/2 that is independent of TPRML1.

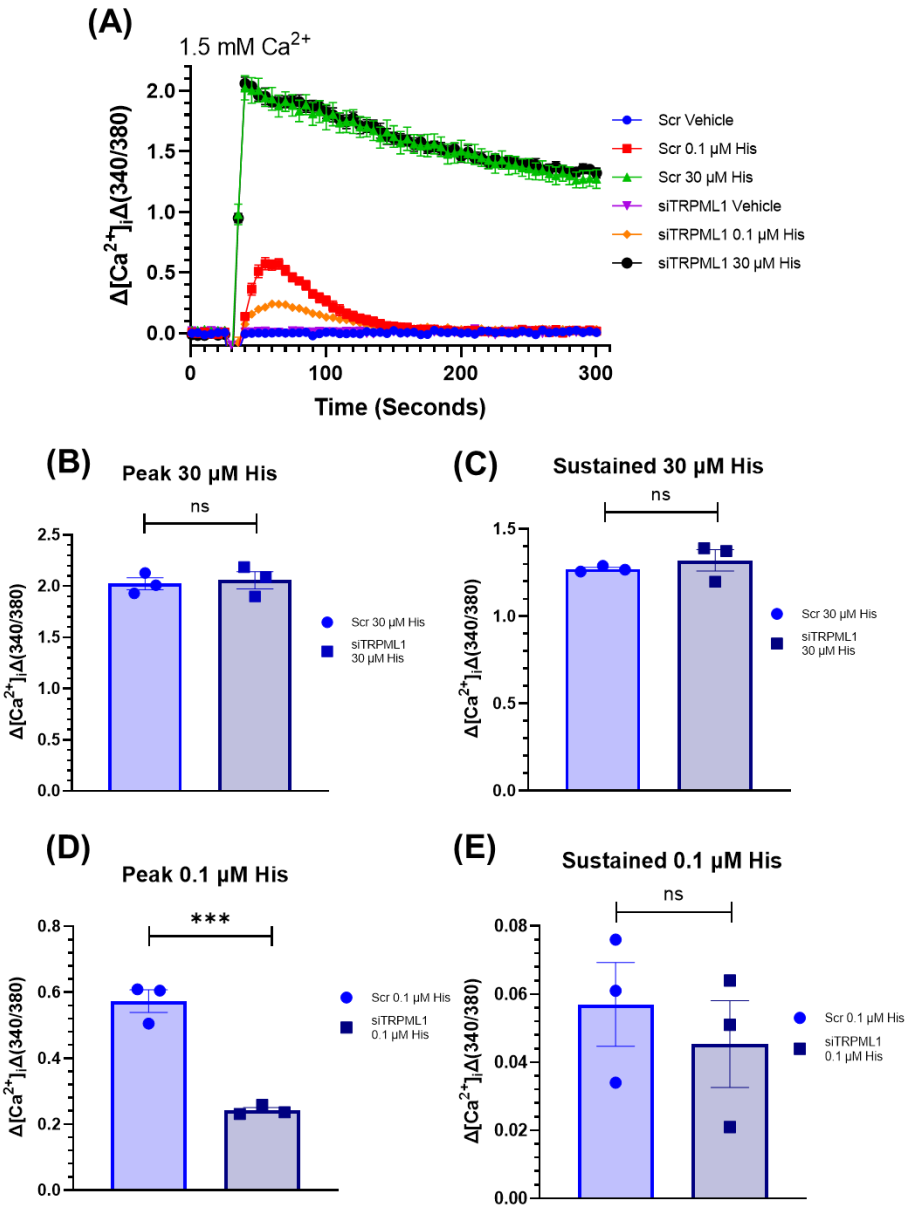

Figure 5.5 Knockdown of TRPML1 in hAEC evokes an inhibition of the histamine-evoked Ca^{2+} release at low concentrations. (A) Representative Ca^{2+} traces of hAEC transfected with siRNA for knockdown of TRPML1 versus control and acutely stimulated with either 0.1 or 30 µM histamine. (B) Mean peak amplitude data for 30 µM histamine of (A). (C) Sustained Ca^{2+} responses for 30 µM histamine of (A). (D) Mean peak amplitude data of (A) showing 0.1 µM histamine stimulation. (E) Sustained Ca^{2+} responses of (A) at 0.1 µM histamine. Scr = siRNA control, siTPRML1 = k/d TRPML1. All Data was collected in 1.5 mM Ca^{2+} SBS buffer, where data is presented as mean ± SEM. n/N = 3/9, ns = not significant, *** = $p < 0.001$, by unpaired t-test.

5.7 Knockdown of TPC1 alters Ca^{2+} dynamics in hAECs stimulated with TPC2 agonist, TPC2-A1-N

With the evidence supplied earlier that TPC1 and TPC2 may mechanistically operate independently of each other, with variety in ion flux, they are functionally linked in terms of their Ca^{2+} currents. Previous work has shown that the loss of both isoforms of TPC1 can have serious implications in protein trafficking events within the lysosome, which are not observed with the loss of TPC2 (Castonguay et al. 2017). Furthermore, this highlights the potential for TPC1 and TPC2 to function as compensatory Ca^{2+} stores in the event of loss or reduction of expression of one of the channels. Here I employed the use of the TPC2-A1-N agonist of TPC2 to observe whether knockdown of TPC1 would alter the Ca^{2+} dynamics of the TPC1 channel in response to acute stimulation with TPC2-A1-N. hAECs were plated 24 h before transfection with siRNA specific for TPC1, before being acutely stimulated 48 h later with either 10 or 30 μM TPC2-A1-N versus control (scrambled). Here I have shown that at low concentrations (10 μM) of TPC2-A1-N, there is again no global Ca^{2+} response exhibited at this concentration (Figure 5.6A). For the mean peak Ca^{2+} data, as expected, there was a large transient rise in intracellular Ca^{2+} at 30 μM in both control versus knockdown conditions, and knockdown of TPC1, did not negate the effects of TPC2-A1-N (Figure 5.6B). However, around 110 s after acute stimulation, I observed a second intracellular Ca^{2+} rise, which was significantly exacerbated in the TPC1 knockdown cells at 30 μM TPC2-A1-N (Figure 5.6C). When considering the sustained Ca^{2+} response at both 10 and 30 μM TPC2-A1-N, there were no significant differences between control and siTPC1 cells (Figure 5.6D, E). It is probable here, that in the case of TPC1 knockdown, the rate of ER-refilling is impacted, due to the loss of the channel, thus, TPC2 is kept in an open conformation depleting the ER stores faster. As siRNA knockdown does not cause complete loss of the channel, it could be that the remaining TPC1 channels are capable of sensing a depletion in Ca^{2+} and propagating a signal to force further release of Ca^{2+} from the ER through an amplification of their local signals via IP_3.

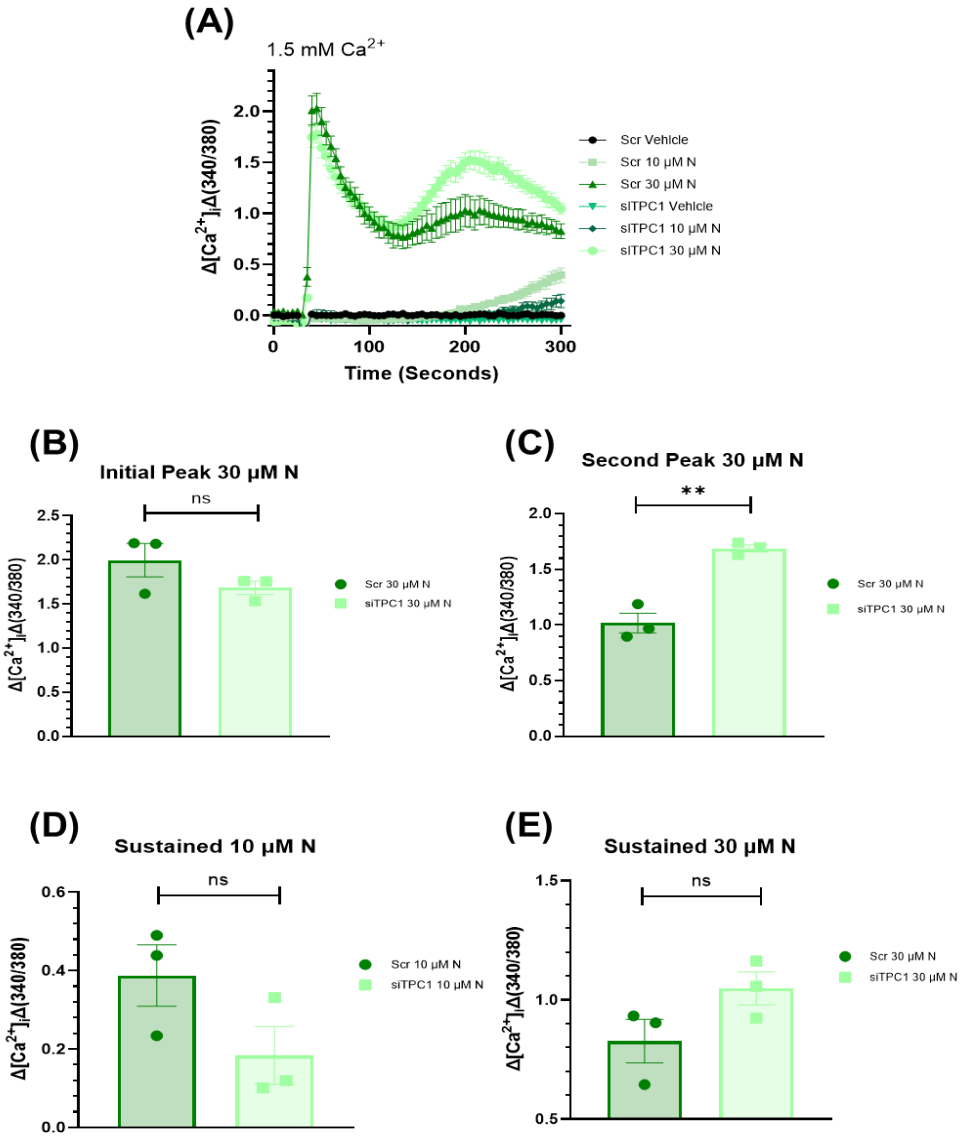

Figure 5.6 Knockdown of TPC1 induces a secondary Ca^{2+} spike in hAEC stimulated with TPC2 agonist, TPC2-A1-N. (A) Representative Ca^{2+} traces of hAECs acutely stimulated with 10 and 30 μM TPC2-A1-N in control (Scr) versus TPC1 knockdown cells. (B) Mean peak amplitude data of (A) for 30 μM TPC2-A1-N, showing an initial non-significant difference in peak Ca^{2+} response. (C) Mean peak amplitude data of (A) for 30 μM TPC2-A1-N, show a distinct resurgence in Ca^{2+} release, which is significantly potentiated in hAEC with TPC1 knockdown. (D) Sustained Ca^{2+} response data for (A) of 10 μM TPC2-A1-N. (E) Sustained Ca^{2+} response data for (A) of 30 μM TPC2-A1-N. All data plotted as mean ± SEM, with all experiments conducted in 1.5 mM Ca^{2+} SBS buffer. Scr = siRNA control, siTPC1 = k/d TPC1, n/N = 3/9. ns = not significant, ** = $p < 0.01$, by unpaired t-test.

5.8 Knockdown of TPC2 significantly depletes Ca^{2+} release evoked by TPC2-A1-N

TPC2-A1-N was discovered in 2020 and since its discovery, has become well-reported to be specific for the TPC2 channel target. My primary goal here was to demonstrate that knockdown of TPC2, would result in reduced expression at the protein level of the channel, which would correspond to a lower efficacy of TPC2-A1-N at eliciting a Ca^{2+} response in hAECs. Using Flexstation intracellular Ca^{2+} measurements, I have shown that in response to channel, knockdown using a siRNA specific for TPC2, upon acute stimulation with 30 μM TPC2-A1-N there was a significant inhibition of the Ca^{2+} response in cells with TPC2 knockdown (Figure 5.7A) in cells where TPC2 was specifically depleted by siRNA there was a significant decrease in the mean peak amplitude (Figure 5.7B) of the Ca^{2+} response versus control. This loss of Ca^{2+} release was also reflected in the sustained Ca^{2+} response (Figure 5.7C). I can deduce from this data that reduced expression of TPC2, negatively impacts Ca^{2+} release evoked by TPC2-A1-N, but does not completely inhibit the response.

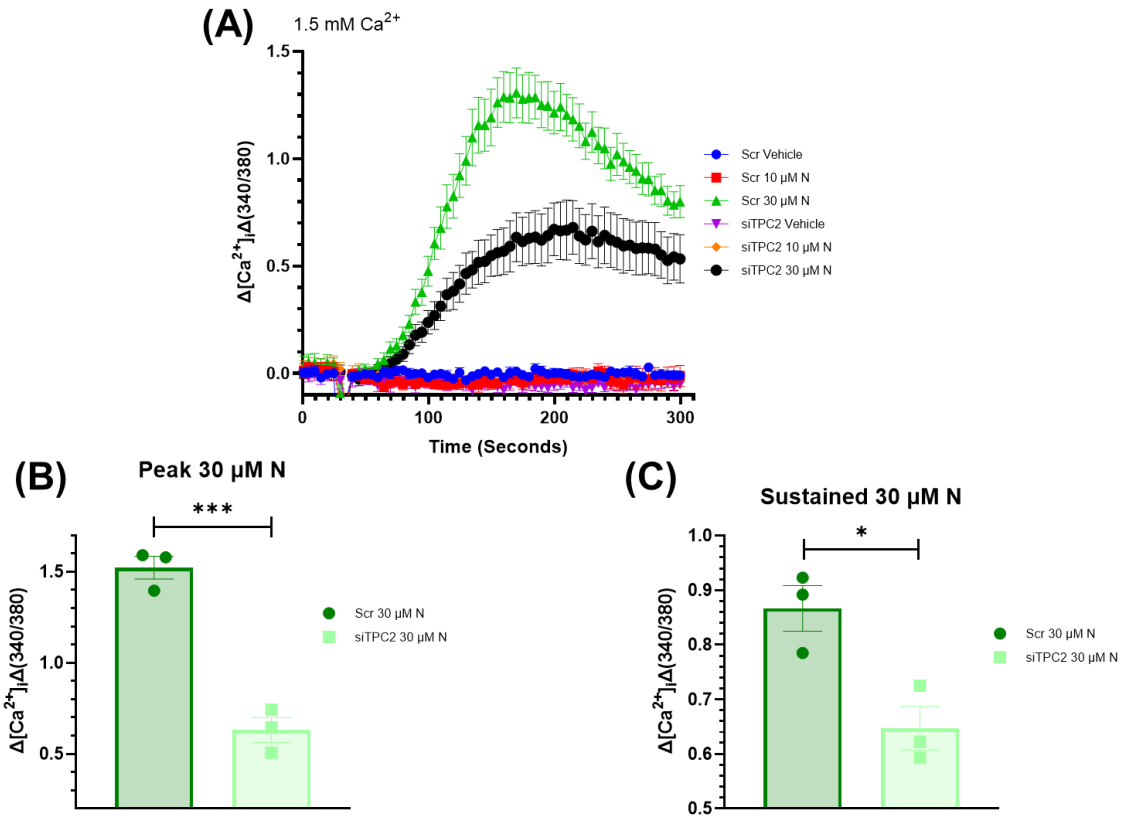

Figure 5.7 Knockdown of TPC2, inhibits intracellular Ca^{2+} release elicited by the TPC2 agonist, TPC2-A1-N. (A) Representative Ca^{2+} traces of hAECs acutely stimulated with 10 or 30 μM TPC2-A1-N in control (Scr) versus hAECs that have undergone transfection to knockdown TPC2. (B) Mean peak amplitude data of (A) showing a drastic inhibition of the TPC2-A1-N-evoked Ca^{2+} response in hAECs that are expressing less of the channel under stimulation with 30 μM TPC2-A1-N. (C) Sustained Ca^{2+} responses of (A) showing significant inhibition of the Ca^{2+} response following stimulation with 30 μM TPC2-A1-N. All data was plotted as mean ± SEM, in 1.5 mM Ca^{2+} SBS buffer, n/N = 3/9. Where * = $p < 0.05$, *** = $p < 0.001$, by unpaired t-test.

5.9 Knockdown of TRPML1 potentiates peak and sustained Ca^{2+} responses in hAEC

One of the major functions of TRPML1 is to regulate trafficking events and prevent lysosomes from becoming too acidic, maintaining ionic homeostasis (Schmiege et al. 2017). The activity of TRPML1 is mediated by the Ca^{2+} and proton gradients within the lysosomal lumen and the cytosol. Previous publications have highlighted the relationship between TRPML1 and TPC1 communicating via ER-lysosomal contact sites, hence, TRPML1 is a strong candidate channel for NAADP-mediated Ca^{2+} signalling. Here, I determined if the depletion of TRPML1 protein impacted the Ca^{2+} response evoked by TPC2-A1-N. hAECs stimulated with either 10 or 30 μM TPC2-A1-N. The results show that in both control and TRMPL1 knockdown cells at 10 μM TPC2-A1-N, there was no Ca^{2+} response observed (Figure 5.8A), which we observed previously (Chapter. 2 Figure 4.4A). At 30 μM TPC2-A1-N, there is a transient increase in the Ca^{2+} rise in both knockdown and control cells, with no significant difference being observed in the mean peak Ca^{2+} amplitude (Figure 5.8B). There was, however, an increase in the sustained Ca^{2+} response in those cells subjected to TRPML1 knockdown (Figure 5.8C).

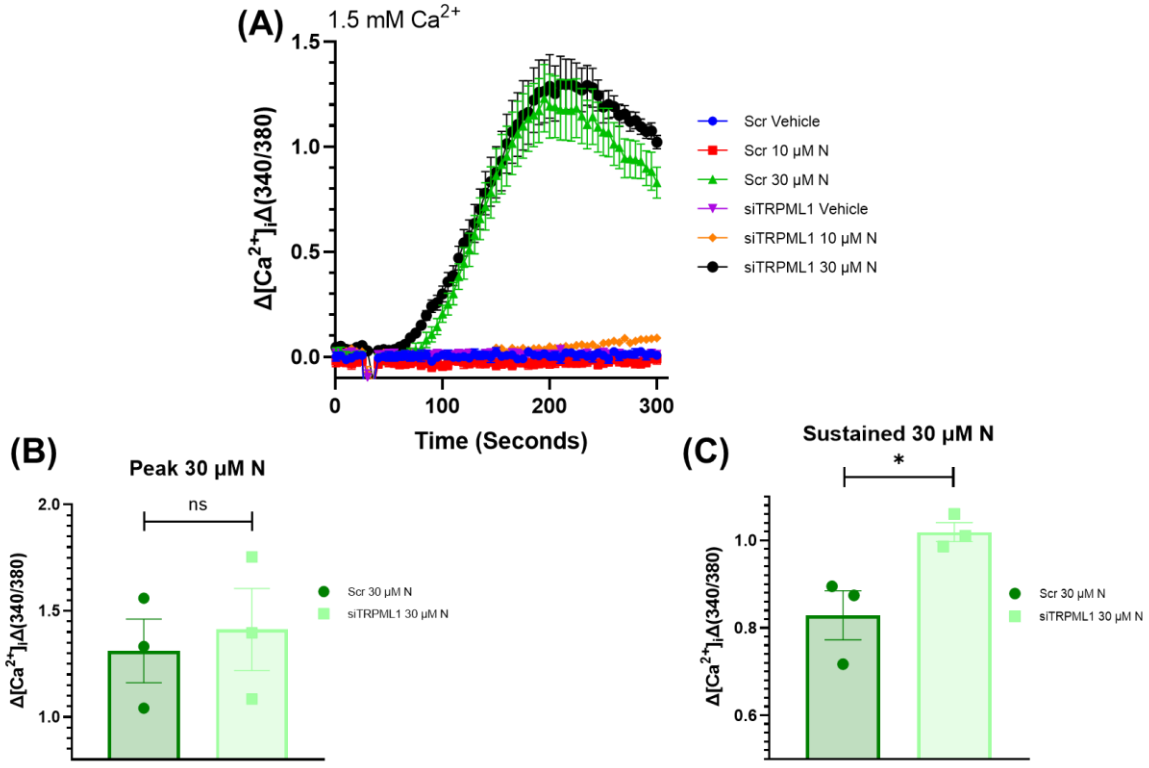

Figure 5.8 Knockdown of TRPML1 results in an inhibition of the sustained Ca^{2+} response following stimulation with TPC2-A1-N. (A) Representative Ca^{2+} traces of hAEC with knockdown of TRPML1 versus control (Scr) and acutely stimulated with 10 or 30 µM TPC2-A1-N. (B) Mean peak amplitude data of (A) for 30 µM TPC2-A1-N showing no inhibition of the peak Ca^{2+} response. (C) Mean data of sustained Ca^{2+} responses of (A) for 30 µM TPC2-A1-N showing inhibition of the sustained response following acute stimulation. Scr = siRNA controls, siTRPML1 = k/d TRPML1. All data were plotted as mean ± SEM, with experiments conducted in 1.5 mM Ca^{2+} SBS buffer. n/N = 3/9. Where ns = not significant, * = $p < 0.05$, by unpaired t-test.

5.10 TPC2 knockdown does not affect Rab46 trafficking to and from the MTOC upon stimulation with histamine

Following on from the intracellular Ca^{2+} data shown above and from evidence within the literature, it was likely that TPC2 was a strong candidate channel for being directly involved in the Rab46 dispersal mechanism linked to histamine-evoked Ca^{2+} release. hAECs were transfected with specific siRNA for TPC2 or control and then fixed and stained for Rab46, to investigate the spatial and temporal distribution across the cell when acutely stimulated with 0.1 and 30 μM histamine. In TPC2-depleted cells stimulated with 0.1 μM histamine the clustering of Rab46 at the MTOC was comparable to control (Figure 9A). At 30 μM histamine, in TPC2 knockdown cells, these cells behaved similarly to the control (30 μM, untransfected) in that there was perinuclear clustering was observed and was not lost in the absence of TPC2 (Figure 5.9A). When considering the relative distribution of Rab46 at the perinuclear region, TPC2 knockdown cells behaved similarly to that of control, where there was a concentration-dependent increase in clustering at the perinuclear region and knockdown of TPC2 did not evoke clustering of Rab46 at the MTOC upon stimulation with 0.1 μM histamine (Figure 5.9B). The distribution of Rab46 across all cell areas (Figure 5.9C) highlights that there are similar levels of Rab46 detected in the intermediate and peripheral regions across all conditions when comparing knockdown to control. This data together, suggests that loss (or reduced expression) of TPC2 does not affect the histamine-evoked cellular distribution of Rab46 in hAECs.

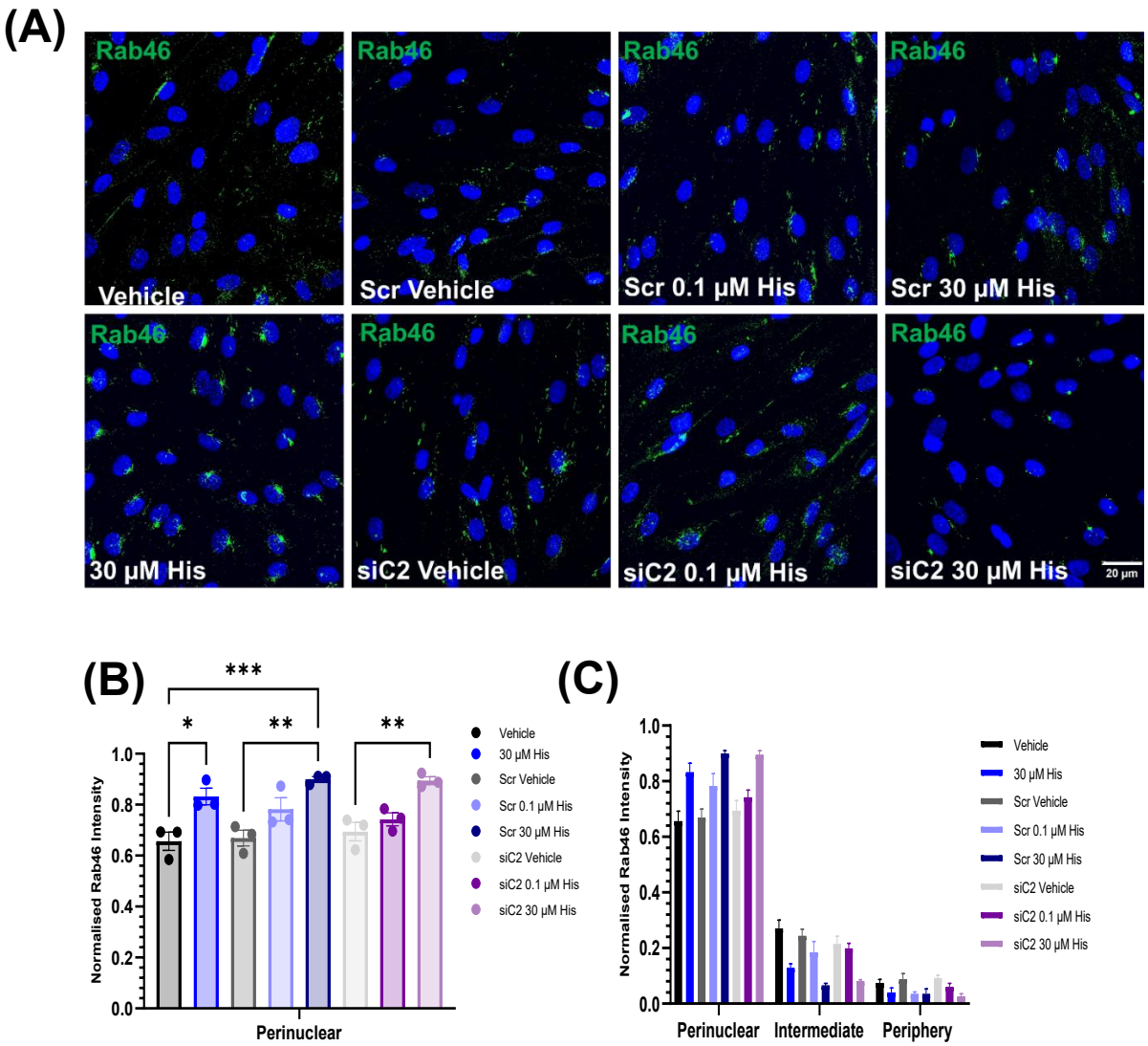

Figure 5.9 Knockdown of TPC2 does not affect perinuclear trafficking and clustering of Rab46 following histamine stimulation. (A) Representative images of hAECs acutely stimulated for 10 mins with histamine (0.1 and 30 µM), DMSO, in control cells (Scr) or with TPC2 knocked down (siC2). Scale bar = 20 um for all images in (A), green = Rab46, blue = nuclei (H33342). (B) Mean particle intensity data of (A) showing the Rab46 distribution in the perinuclear region of the cells. (C) Expanded mean data analysis of (B) showing all three intracellular locations for particle intensity of Rab46, perinuclear, intermediate, and periphery. All data is plotted as mean ± SEM. n/N = 3/15. where * = $p < 0.05$, ** = $p < 0.01$, and *** = $p < 0.001$, by one-way ANOVA.

5.11 TPC2-A1-N elicits a concentration-dependent increase in secretion of Ang2 with TPC2 inhibiting the histamine-evoked Ca^{2+} release

To understand if TPC2 played a role in the histamine-evoked Ang2 secretion, I performed an Ang2 ELISA in hAECs transfected with TPC2-targeted siRNA or control. I used a positive control that would elicit full secretion of Ang2 and mimic an all-out vascular response (Combo; 100 μM histamine and 200 U/μL thrombin) and normalised to the combo. This was nicknamed Combo and consisted of 100 μM histamine added in combination with 200 U/μL thrombin, and all ELISA data gathered was normalised to the combo. ELISA evidence as predicted, showed that when TPC2 was knocked down in hAEC there was an inhibition of the histamine-evoked Ang2 secretion (Figure 5.10). Together, this data shows that Ang2 secretion is sensitive to activation of the small lysosomal Ca^{2+} channel, TPC2 and that reduced expression of this channel hinders the release of Ang2.

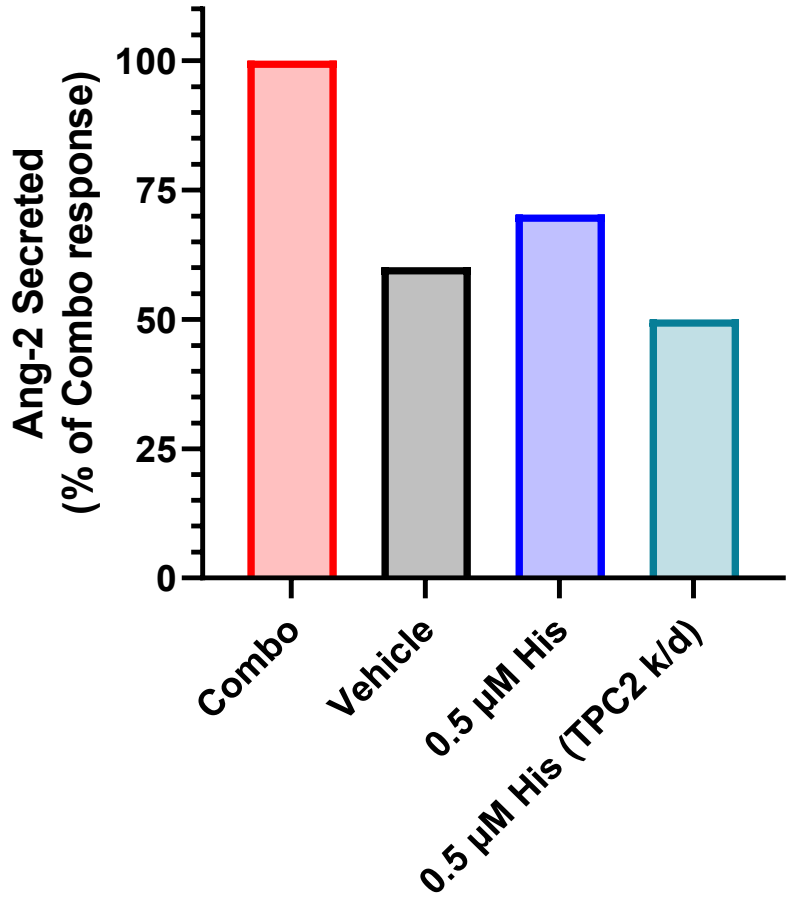

Figure 5.10 Knockdown of TPC2 inhibits release of Ang2. ELISA for Ang2 secretion showed an inhibition of the release of Ang2 in hAEC stimulated with 0.5 µM histamine with TPC2 knockdown, as compared to siRNA control cells. Combo: 100 µM histamine and 200 U/µL thrombin. The vehicle is DMSO 1:1000. Data is reported as an n/N 1/3 thus no statistical analysis was performed.

5.12 Discussion

The endo-lysosomal cation channels, TPC1, TPC2 and TRPML1, have been identified as being important in the modulation of intracellular Ca^{2+} signals, maintaining lysosomal pH and regulating the trafficking of vesicles through secondary messengers (Grimm et al. 2012; Li et al. 2019; Barbonari et al. 2022). The ER is no longer considered to be the sole source of intracellular Ca^{2+} within mammalian cells with studies such as that by Morgan et al. showing that acidic organelles within the endo-lysosomal system can harness the power to become Ca^{2+} reservoirs, capable of releasing Ca^{2+} upon activation with NAADP (Morgan et al. 2011). From previous work within our lab, it has been highlighted that histamine-evoked Ca^{2+} release initiates a triggering of SOCE through globalising of NAADP-mediated Ca^{2+} signals which evoke release of Ca^{2+} from small endo-lysosomal stores (Miteva et al. 2019). In the case of the two-pore channels, NAADP serves to activate TPC1 and TPC2 binding proteins that have unknown binding sites for NAADP and induce mobilisation of Ca^{2+} from the acidic Ca^{2+} pool, which can then go on to globalise into a much larger Ca^{2+} response through the actions of CICR.

Focussing on the NAADP/TPC axis and taking a closer look at TPC1, it has been highlighted in the literature that this channel may have the capability of modulating lysosomal Ca^{2+} homeostasis through a crosstalk with other small cation channels located on the lysosomal membrane. A recent study highlighted the ability of the NAADP/TPC1 signalling to modulate the endo-lysosomal phenotype and allow for contact site formation between the endosome and the ER through tempering of ER Ca^{2+} signals evoked by activation of IP_3 (Kilpatrick et al. 2017). I have shown via knockdown of TPC1 using Ca^{2+} measurements, that knockdown of TPC1, induces a potentiation of the Ca^{2+} signal, evoked by the TPC2 agonist, TPC2-A1-N. This secondary Ca^{2+} peak that I observed when hAECs were stimulated could be related to the establishment of ER-late endosomal contact sites, allowing for potentiation of the Ca^{2+} signal via TPC2 by TPC2-A1-N when TPC1 is knocked down. A 2022 review highlighted the ability of TPC1 to communicate with mitochondria to influence the release or storage of Ca^{2+} from these stores (Terrar et al. 2022). I did not have the time within the context of this project to consider the effect of these Ca^{2+} signals on

mitochondrial Ca^{2+} release, however, TPC1 and other small cation channels on the lysosomal membrane communicate with the mitochondrial backup Ca^{2+} pool should there be any downregulation of the endolysosomal system. Studies have sought to understand the relationship of ER-mitochondrial Ca^{2+} dynamics, whereby the mitochondria have been elucidated to be ‘firewalls’ or ‘barriers’ toward large intracellular rises in Ca^{2+} and can serve as temporary Ca^{2+} stores to allow cells to survive a Ca^{2+} emergency (Carafoli et al. 2010; Chinopoulos et al. 2010).

The context through which TPC1 mediates the histamine- and TPC2-A1-N -evoked Ca^{2+} release in endothelial cells remains a mystery. However, in this thesis, I have been able to provide a context of how this channel modulates its interactions with these various pharmacological agonists and how the knockdown of the channel affects these processes. It was intriguing to observe that knockdown of TPC1 inhibited the histamine-evoked Ca^{2+} release at low concentrations (0.1 μM) of histamine, potentially highlighting that blockade of the small localised lysosomal Ca^{2+} release could dysregulate NAADP-mediated Ca^{2+} signalling through this channel. At high concentrations of histamine, I observed that the knockdown of TPC1, induced potentiation of the sustained response and this was significantly different from the control. This is indicative that there could be a potential compensatory response from another lysosomal channel or acidic organelle which allows for a further and slower release of Ca^{2+} as compared to control, where ER stores are depleting at a rate faster than the rate of refilling. A 2020 study on anaphylaxis in TPC1-deficient mice, found that the prevalence of hypersensitivity was increased, and mast cell degranulation was abolished in mice not expressing TPC1 (Arlt et al. 2020). This is exciting as mast cells are directly associated with immune responses and my immunogenic amine, histamine here shows reduced efficacy in cells with reduced expression of TPC1. The apparent sustained increase in Ca^{2+} I observed at high concentrations of histamine (30 μM) in TPC1 knockdown cells, could be attributed to a possible delayed activation of CICR acting on ER Ca^{2+} stores, however, without a TPC1 knockout model, it would not be appropriate to fully comment with confidence on this response.

There is unambiguous evidence of the role of TPC2 in Ca^{2+} release mechanisms, in the context of crosstalk with the ER and cell adhesion (although a characteristic observed in cancer phenotypes). TPC2 has been indicated by multiple groups investigating NAADP-mediated Ca^{2+} signalling as the candidate for coordinating Ca^{2+} signals between the lysosome and the ER allowing for local signals to globalise into complete ER signals stimulating release (Patel et al. 2024; Yuan et al. 2024). With the discovery of the direct and potent TPC2 agonist, TPC2-A1-N, it has been possible to delve into the Ca^{2+} dynamics of TPC2 in more detail than has been possible previously. It must be noted that most studies to date investigating the relationship between endolysosomal Ca^{2+} and the NAADP/TPC axis have been conducted using single-cell patch clamp analysis. Although electrophysiology is a powerful and unique tool, I have harnessed the use of techniques that observe thousands of cells over time and although this is mean data, it provides a solid framework for investigating the global effects of the pharmacology on endothelial cell health and function. At the protein level, there was less expression (band was faint) of the TPC2 channel upon knocking down with siRNA specific for TPC2. When I knocked down TPC2, it was clear that at both low (0.1 μM) and high (30 μM) concentrations of histamine, there was significant inhibition of the peak Ca^{2+} response. TPC2 regulates the efflux of Ca^{2+} into the cytosol following stimulation with histamine, and the reduced expression of the channel hinders this response. However, it must be noted that albeit there is reduced expression of the channel in the case of knockdown, there are still residual channels remaining, and due to the nature of these NAADP-mediated responses being so small, it is likely that even with sufficient knockdown there are still enough channels active to allow for a Ca^{2+} signal to propagate. In the case of the TPC2-A1-N agonist, as expected knockdown of TPC2 inhibited, but not completely, intracellular Ca^{2+} release. TPC2 knockdown did not affect the intracellular distribution of Rab46 in hAECs. I had originally hypothesised that the knockdown of TPC2 would induce clustering of Rab46 at the MTOC at low concentrations of histamine, due to the inability of the cell to release Ca^{2+} through this channel. However, the results obtained did not correlate with this and although from this immunofluorescence data it appears TPC2 is not a likely candidate channel for this Rab46 Ca^{2+} dependent dispersal pathway, the Ca^{2+} data highlights that it could be

potentially a combination of channels working as a complex to mediate this dispersal, this remains elusive and double knock-down or knockout cells deficient in both TPC1 and TPC2, may be able shed more light on the Ca^{2+} dynamics through these channels in response to histamine. The distribution analysis here using an ImageJ macro is arbitrary in that it measures particle intensity, and thus, there is no definitive way to distinguish between artefacts of staining and true protein stain. Thus, studying dispersal in live cells would warrant real-time visualisation of the dispersal, versus cells from a Rab46 isogenic KO, however, of note, the generation of Rab46 nanobodies would advance this field, since GFP-tagging alone promotes clustering of Rab46 at the MTOC in the absence of stimuli.

Looking at the functionality of the channels about the release of Ang2 it is clear from my work that knockdown of TPC2 inhibits the histamine-evoked Ca^{2+} release (albeit an n = 1). Ang2 secretion from endothelial cells is complex and context-dependent, with immune responses such as histamine evoking a slight increase in Ang2 secretion, which cannot be increased by increasing the concentration. At high concentrations of histamine, it is not possible to significantly increase Ang2 secretion because there is a brake on secretion (by Rab46) whilst WPBs containing Ang2 are held at the MTOC. If the Ca^{2+} released from this channel is necessary for the release of WPBs from the MTOC, knockdown of the channel would inhibit the response, which I have shown in TPC2. Time restraints prevented exploring the effect of TPC2-A1-N and histamine in co-stimulation to observe the effects on Ang2 secretion.

I observed that there is a self-limiting effect of the histamine-evoked release of Ang2, in that concentrations above 10 μM fail to illicit further release. A recent article investigating the effects of endo-lysosomal Ca^{2+} signalling discussed that in VSMCs, TPCs could promote events that led to the advancement of vasoconstriction and atherosclerosis (Negri et al. 2021). These events are intricately linked with the secretion of Ang2 as in the case of vascular injury there is an upsurge in the release of Ang2 to mediate platelet plug formation and stem clot production and this could in turn be partially mediated through the actions of NAADP and TPC2 before the Ca^{2+} signals are amplified via ER-lysosomal cross-talk. Potentiation of these small localised Ca^{2+} signals via

TPC2 may be globalised through CICR to empty ER stores in response to vascular injury, subsequently leading to a release of Ang2, and that loss of the channel negates this effect, with my findings showing this early in the pathway at the point of trigger before amplification.

Of all the endo-lysosomal Ca^{2+} release channels discussed thus far, TPRML1 remains most elusive, with clear roles identified in the cardiovascular system such as modulation of blood pressure and the ability of localised Ca^{2+} 'sparks' to relax vascular smooth muscle (Thakore et al. 2020). TRPML1 and TPC1 cross-talk have been mentioned more recently in the literature, where TRPML1 plays an active role in maintaining lysosomal pH (crucial for maintenance of lysosomal function). Here, I wished to investigate the effects of histamine-evoked Ca^{2+} release through TPRML1 and what the effects of knockdown of this channel had on this response. High concentrations of histamine (30 μM) potentiated the peak and sustained Ca^{2+} responses. This increase could be attributed to the hypothesis that upon knockdown of TRPML1, TPC2-A1-N could evoke Ca^{2+} release from another lysosomal cation channel (potentially, TPC1/2) evoking a longer sustained Ca^{2+} compared to control. However, there was significant inhibition of the peak Ca^{2+} response at 0.1 μM histamine. Together, with the evidence from TPC1/2 and TPRML1 knockdown, it is clear that reduced expression of these channels significantly negates the histamine-evoked Ca^{2+} response in hAECs at low concentrations of histamine. This alludes to the possibility that these small lysosomal Ca^{2+} channels are responsible, either alone or in combination with one another to coordinate localised Ca^{2+} signals from the lysosome and potentiate them through ER-cross talk. Hence, reduced expression of the channels is enough to impact the trigger response within the lysosome, but global Ca^{2+} amplification may only require a small portion of active channels to potentiate the signal to trigger ER Ca^{2+} release. I have also shown that the knockdown of TRPML1 significantly altered the sustained Ca^{2+} response in hAECs stimulated acutely with TPC2-A1-N. Although the Ca^{2+} traces look remarkably similar, there is a slight potentiation of the knockdown response, in that the release of Ca^{2+} appears to be faster and more sustained in these cells. Compensation from another Ca^{2+} channel of the lysosomal membrane may be allowing for further release, which is in line with current

theories, that due to its fixed location on the lysosomal membrane, TPRML1 could potentially recruit a local channel (TPC1/2) to coordinate the release of Ca^{2+} when its endogenous levels are reduced. However, the exact mechanism through which this is achieved is unknown.

Altogether, the data presented in this chapter highlight three endo-lysosomal Ca^{2+} channels (TPC1, -2 and TRPML1) as potential candidates through which histamine-evoked Ca^{2+} release plays a direct role in Rab46 dispersal from the MTOC. The knockdown of these channels plays a role in both the histamine-evoked Ca^{2+} release and the release of Ang2. I have attempted to use a potent agonist of TPC2, TPC2-A1-N to confer specificity of this compound for TPC2. Although it has been widely published to have exceedingly high specificity for this channel, I have shown that other lysosomal cation channels respond to this compound indirectly and that across all of the pharmacology discussed, there is potential for cross-talk between these channels. After all, it is reported that ER-lysosomal contact sites are pivotal in the response of cells to stimuli that affect NAADP and $PI(3,5)P_2$ signalling, thus it is likely that at the individual channel level, there is a degree of cross-talk allowing for potentiation of localised Ca^{2+} signals in global responses within the cell, and this amplification can be hindered or potentiated when channels are knocked down (Yuan et al. 2023).

Time constraints with knockdown optimisations limited my ability to investigate multiple channel knockdown in combination with the pharmacology applied. I was also unable with time to image the effect of knockdown of TPC1 and TPRML1 on the Rab46 distribution which may have shown differential changes in Rab46 trafficking to and from the MTOC, as the Flexstation data showed altered Ca^{2+} dynamics in the channels. Clinically, suppression of Ca^{2+} signals through endo-lysosomal channels, specifically TPRML1 has been shown *in-vivo* to significantly reduce tumour growth in various cancers of the blood (Yang et al. 2020). However, opposing schools of thought have emphasized favouring TPCs as targets for anti-cancer therapies, due to the nature of TPRML1 distribution within the membrane being spatially restricted (Faris et al. 2018). More work is still needed to fully understand the Ca^{2+} dynamics behind which these channels operate. Only with this, will it answer if and how they are responsible for Rab46 dispersal from the MTOC, however the groundwork

within this thesis, provides a solid foundation. The potential to conduct future studies looking at channel overexpression or multiple channel k/o (or again using a live-cell imaging system) mouse models may provide further evidence for these channels as candidates for Ca^{2+} release channels, through which Rab46 function is dependent.

Chapter. 6

Rab46 single nucleotide polymorphisms are significantly associated with pro-inflammatory diseases.

6.1 Introduction

Single nucleotide polymorphisms (SNPs) are single variations in a nucleotide sequence and are the most generic form of genetic variation in our species, occurring 1 in every 1,000 nucleotides produced (Shen et al. 1999). The prevalence of pro-inflammatory diseases is increasing globally, and the current lifestyles of those individuals suffering from inflammatory disease are determined to be sub-par. A 2011 study into physical inactivity with those suffering from inflammatory disease found that more than 75% of human beings do not meet daily recommended physical exercise needs (Priumboom et al. 2011). Alongside this, our group has shown that in cells where Rab46 was knocked out, there was a significant dysregulation of the degranulation process within mast cells, indicating that the products of this gene could have a role in the immune system. This could have disastrous consequences for those who display the characteristics of mast cell activation syndrome (MCAS) (Pedicini et al. 2024). Our group has also shown that SNPs in EFCAB4b are associated with severe outcomes in COVID-19, a disease whereby severity is characterised by excessive inflammation (Wang et al. 2024). Altogether these data highlight that variations in Rab46 could affect its function and play a pivotal role in the pathophysiology of inflammatory disease.

As the Rab46 signalling pathway controls exocytosis of WPBs which contain pro-migratory, pro-inflammatory, and pro-thrombotic cargo, I questioned if this pathway could contribute to EC-evoked inflammatory disease. Thereby, data from the UK BioBank was extracted to assess the relationship between Rab46 SNPs and five inflammatory diseases: atherosclerosis (Ath), diabetes (Diab), psoriasis (Pso), rheumatoid arthritis (RhA), and urticaria (Urt). These five

diseases are classified as inflammatory due to dysregulated immune responses and the release of pro-inflammatory cytokines leads to functional impairment of cells and tissues, through activation of signalling pathways that perpetuate the inflammatory cascade. The UK BioBank is a regulated, long-term, anonymised database from which patient data can be extracted for downstream analytics. Single nucleotide variant data was extracted from patients with all 5 inflammatory diseases listed and was analysed in the presence of co-variates such as age, sex, and ethnicity. From this data, Leeds Omics ran a candidate gene approach using Plink2 (command-line software for whole genome data analysis) to investigate whether there were Rab46 SNPs significantly associated with the disease types. The analysis identified 38 SNPs (Appendix Table 1) that were significantly associated ($p < 0.0001$) with these diseases. In this chapter, I have further analysed this data to demonstrate the SNPs associated with each disease and those associated with co-variates age, sex, and ethnicity.

Considering all conditions, it is challenging to definitively attribute the identified SNPs solely to the conditions without accounting for potential confounding variables. Therefore, I performed a secondary analysis on the same data including sex, age, and ethnicity as covariates. From this data, I was able to establish if these three covariates exposed any further SNPs within the Rab46 coding sequence that had detrimental consequences for the clinical manifestation of the above diseases. Variant Effect Predictor (VEP) models revealed multiple missenses and synonymous mutations across all the conditions, albeit with no direct clinical consequences as ascertained from ClinVar. However, with this knowledge, SNPs in Rab46 are significantly associated with inflammatory disease and this could help improve our understanding of how genomic changes in this protein could increase the risk of these diseases in certain cohorts of individuals.

6.2 UK BioBank population demographics and highlighting 38 Rab46 SNPs significantly associated with all 5 inflammatory conditions

Firstly, I wanted to extract the control population from the UK BioBank, consisting of 15,300 individuals from the entirety of the bank population that did not have any of the 5 listed conditions. From this, I then produced an overall demographics table (Table. 6.1) summarising the numbers of individuals within each disease cohort, their age range and sex. The Plink2 server was used to analyse this large-scale dataset, to identify genetic variants associated with disease and allow downstream PCA analysis to be performed. There was a discovery of 38 total significant SNPs in the exonic and intronic coding regions of the Rab46 sequence. I imported this data onto a Venn software where I then ran each of the 5 diseases against the same parameters defined in Plink2 and found that across the diseases, repeated SNPs in Rab46 were common amongst the disease cohorts and this has been expressed in the form of a Venn diagram, highlighting the relationships of various SNPs, and identifying if any of them overlapped with multiple conditions (Figure 6.1) These 38 intronic and exonic SNPs are listed (Appendix Table.1). 33 of the 38 total SNPs were significantly associated with all 5 inflammatory diseases. SNP rs56082948 was significantly associated with Ath, Pso, RhA and Urt and is reported to be an intronic variant and results in the substitution of an A > G allele.

Table 6.1 Overall population demographics

Characteristic	Total N.	Atherosclerosis	Urticaria	Psoriasis	Diabetes	Rheumatoid Arthritis	Control
No. Individuals	**76792**	**3856**	**11186**	**15339**	**45169**	**1242**	**15300**
Age (yrs)	**70.1 ± 9.86**	**70.5 ± 9.38**	**69.5 ± 9.96**	**70 ±10.25**	**70 ±10.25**	**70.5 ±9.96**	**59.3 ± 9.45**
Sex							
Male	**41087**	**2617**	**3658**	**7668**	**26789**	**355**	**5823**
Female	**35705**	**1239**	**7528**	**7671**	**18380**	**887**	**9477**

SNP rs17780600 was identified to be associated with Ath and RhA, resulting in a reference allele change from T>A or T>G and is intronic. Across Ath, Diab, and RhA, SNP rs3803135 was identified as being a synonymous variant which a C > T allele change. Finally, across Pso, Urt and Diab, SNPs rs142228158 and rs71534261 were both identified as intronic, non-coding region changes, C > T and T > C respectively. For this analysis, I have only considered exonic SNPs (due to time constraints), within the coding regions of Rab46, however, it is acknowledged that introns can play roles in the phenotypic consequences of SNPs, for example; splice site alterations and enhancers or silencers.

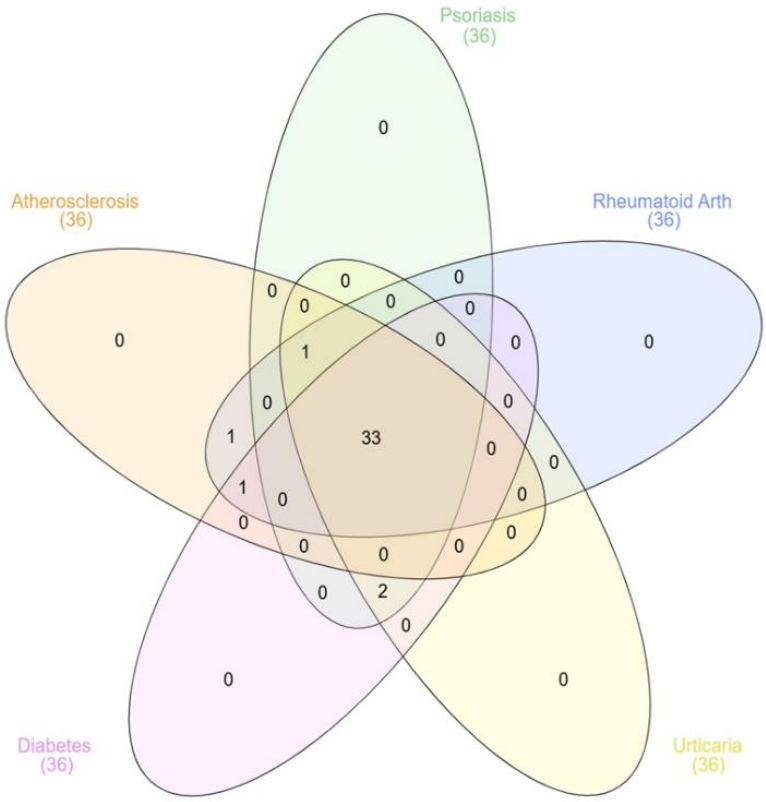

Figure 6.1 38 SNPs within Rab46 are significantly associated with inflammatory disease. (A) Venn diagram highlighting the relationships of the 38 significant exonic and intronic SNPs between the different disease types.

6.3 SNPs significantly associated with the inflammatory disease within the coding regions of Rab46

Here, I assessed exonic SNPs, due to their location within the protein-coding regions of Rab46 and their predicted outcome on the coding sequence, thus they could have a detrimental effect on those expressing these allele changes. The SNPs discussed here (Table 6.2) are purely exonic and are associated with all disease groups. From these 9 SNPs there was a codon change leading to a change in the amino acid coded for. I used the AlphaFold prediction tool (accessible via: alphafold.ebi.ac.uk) to explore the effect of these amino acid changes on the likelihood of observing a pathogenic change and displayed the full protein highlighting the SNPs (Figure 6.2). For 7 out of 9 of these SNPs, the change in amino acid was likely to have little consequence on protein function and was labelled benign. SNPs rs11062745 and rs19697920 displayed an uncertain pathogenic score, indicating that it is probable that amino acid changes in these two regions could infer damage or functional changes to the protein. SNP rs242016 (T > C) lies within the second EF-hand domain, the only functional and crucial Ca^{2+} sensing EF-hand domain in Rab46, as evidenced by recent work in COVID-19 (Wang et al. 2024). I also observed that SNP rs11062745 (C > T) lies within the Rab domain, the crucial domain that confers GTPase activity to the final protein. PolyPhen2 scores for SNPs rs242016 and rs11062 indicated a pathogenic change in the amino acid sequence, thus, these SNPs warrant further investigation.

Table 6.2 Exonic SNPs associated with Rab46 across 5 inflammatory diseases

SNP ID	MAF (ALFA)	REF	ALT	Consequence	Codon Change	Amino Acid Change	AlphaMissense Pathogenicity
rs11062745	0.145	T	C	Missense Variant	**A**CA/**G**CA	T712A	Uncertain
rs71534241	0.025	G	T	Missense Variant	A**C**C/A**A**C	T281N	Likely benign
rs36030417	0.145	A	T	Missense Variant	CA**T**/CA**A**	H212Q	Likely benign
rs17697920	0.146	C	T	Synonymous Variant	CT**G**/CT**A**	L194L	Uncertain
rs242018	0.279	C	T	Missense Variant	**G**AA/**A**AA	E154K	Likely benign
rs3803135	0.120	C	T	Synonymous Variant	AA**G**/AA**A**	K139K	Likely benign
rs242017	0.287	G	A	Missense Variant	G**C**A/G**T**A	A128V	Likely benign
rs242016	0.164	G	A	Synonymous Variant	CA**C**/CA**T**	H115H	Likely benign
rs71582873	None	CCC	del	Inframe Indel	AGATA/ATA	RV7-8I	Likely benign

MAF (ALFA) = Minor allele frequency, rare variant is MAF < 0.01.

REF = Reference allele

ALT = Alternative allele (i.e. the SNP change)

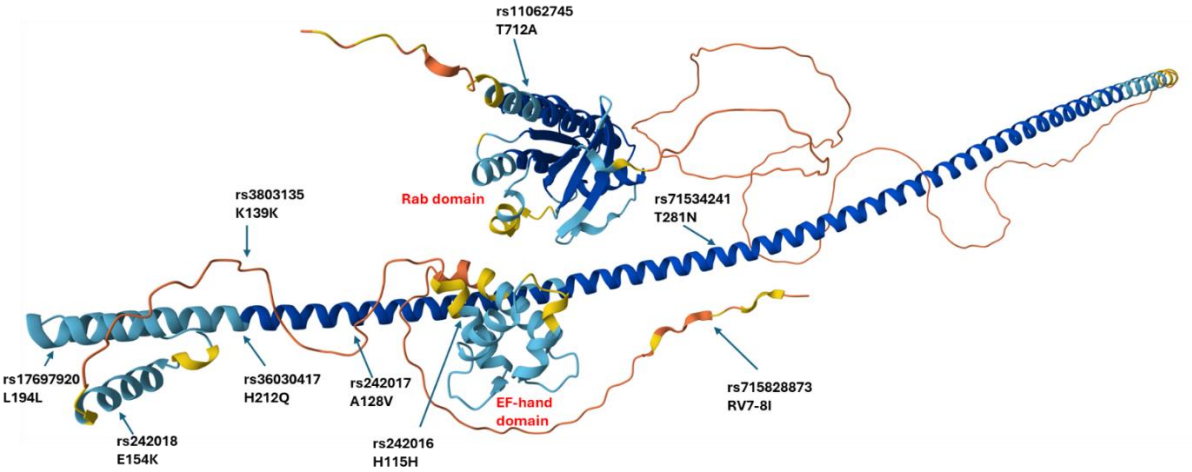

Figure 6.2 AlphaFold predicted the structure of *EFCAB4b* highlighting key SNPs associated with Rab46 across 5 inflammatory conditions. Rs number indicates the SNP variant and associated amino acid changes are noted. Highlighted in red are the Rab domain and EF-hand domains, showing the protein folded along its primary axis. The EF-hand domains are characterised by their loop formation and only EF-hand 2 is responsible for Ca^{2+} binding.

6.4 Principal component analysis (PCA) highlights hetero- and homogeneity within the disease cohorts

To further investigate the distribution of disease cohorts compared to the control population from the UK Biobank, I used principal component analysis (PCA). These PCA plots visualise the homogeneity or heterogeneity of the diseased groups relative to the control group. The PCA outputs display the control population in blue and the disease cohorts in red. For atherosclerosis, there was a large spread of red dots which can infer substantial heterogeneity in the disease group. This suggests that patients with atherosclerosis may have underlying genetic changes driving the disease, with factors like age, genetic predisposition and lifestyle contributing to disease progression (Bjorkegren & Lusis, 2022). Similarly, urticaria had a heterogeneous spread within the disease population. This could imply that factors such as severity, disease duration and immune triggers could be driving forces behind this heterogenous spread. Diabetes was interesting in that there was no clear clustering in the control population versus the disease cohort. This could be down to the fact that diabetes is a multi-factorial condition upon which there are various triggers.

The tight clustering of red dots in both rheumatoid arthritis and psoriasis (Figure 6.3) suggests a homogenous molecular profile amongst both sets of patients. From this, we can infer that it may be possible for RhArt and Pso to have clearly defined molecular profiles involved in the pathogenesis of the conditions. However, it must be noted that homogeneity can be an artefact of the specific data used within the analysis, thus, it must be taken with caution. The discovery of heterogeneity in the atherosclerosis and urticaria groups gives way for future downstream subgroup discovery analysis which could potentially reveal subgroups of patients within the disease that show altered clinical manifestation or respond differently to treatment.

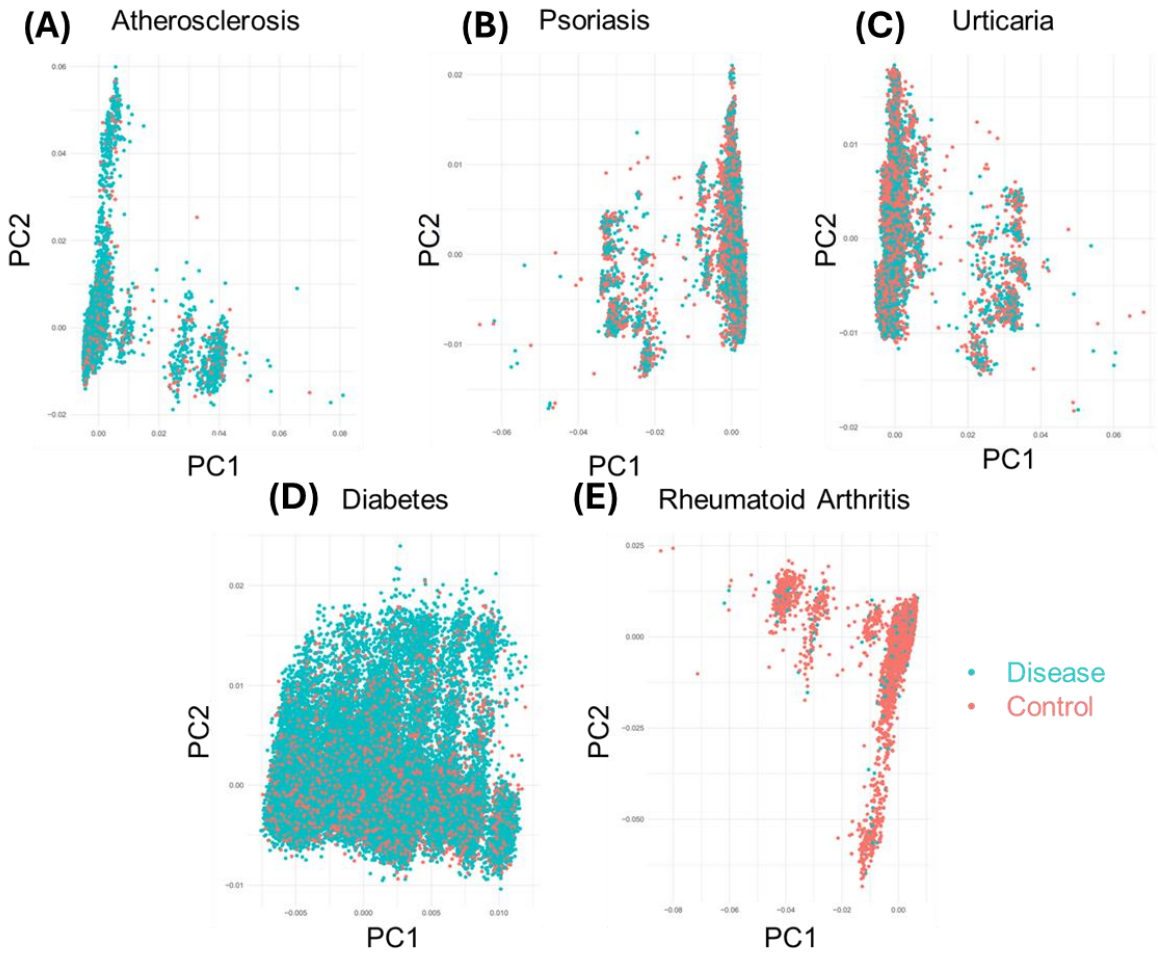

Figure 6.3 PCA plots of patient numbers in the disease cohorts as compared to the control population. (A) PCA plot of atherosclerosis, (B) PCA plot of psoriasis, (C) PCA plot of urticaria, (D) PCA plot of diabetes, (E) PCA plot of rheumatoid arthritis. All data outputs are generated in R Studio. Blue dots represent the control population (sample 15,300 non-disease presenting individuals from the UK BioBank). Red dots illustrate the respective disease cohorts.

6.5 Covariate analysis of age, sex and ethnicity reveals further SNPs significantly associated with inflammatory disease in Rab46

Single variate analysis showed promising heterogenous and homogenous relationships across multiple inflammatory diseases. To explore whether other confounding variables might influence the genetic changes observed in Rab46 SNPs, I included variables such as age, sex, and ethnicity. The control population in the co-variate data was larger (n = 500,000) and consisted of the entirety of the UK BioBank thus when this analysis was run, an additional 3 significant SNPs in Rab46 were discovered which is due to the larger sample size. The 38 significant SNPs are summarised in the appendix (Appendix Table 1) and those 3 additional within the coding regions (Table 6.3) of Rab46 are listed as being missense or synonymous in nature. Thus, these SNPs pose additional concerns, as they are expressed in exonic areas of the genome whereby the protein is coded and could play a role in the inflammatory disease progression.

Table 6.3 SNPs in Rab46 significantly associated with inflammatory disease in the context of covariate analysis.

SNP ID	MAF (ALFA)	REF	ALT	Consequence	Codon Change	Amino Acid Change
rs7138453	0.449	G	T	Missense Variant	**G**AT/**T**AT	A7T
rs76779686	0.023	C	G	Missense Variant	T**C**C/T**G**C	S6C
rs9788233	0.119	T	C	Missense Variant	**A**GG/**G**GG	R7G

MAF (ALFA) = Minor allele frequency, rare variant is MAF < 0.01.

REF = Reference allele

ALT = Alternative allele (i.e. the SNP change)

6.6 Age is a predominant driving force of atherosclerosis and ethnicity contributes to variation in the molecular profile of the disease

Ethnicity contributes to variation in the molecular profile of atherosclerosis, denoted by a shift along PC1 (Figure 6.4A). When examining gender as a covariate, we observe a slight separation between males and females along PC1 (the direction of maximal variance), which captures the most significant source of variation within the sample. This separation could explain biological differences between males and females that contribute to atherosclerosis; however, the separation is not well enough defined, inferring that gender alone is not a strong predictor of disease progression (Figure 6.4B). When considering age as a confounding variable, I observed a clear trend along PC1, with younger (1960) individuals clustering toward the left (Figure 6.4C) and older (1940) individuals toward the right. It can be inferred from this shift that age is a significant factor in the development of atherosclerosis.

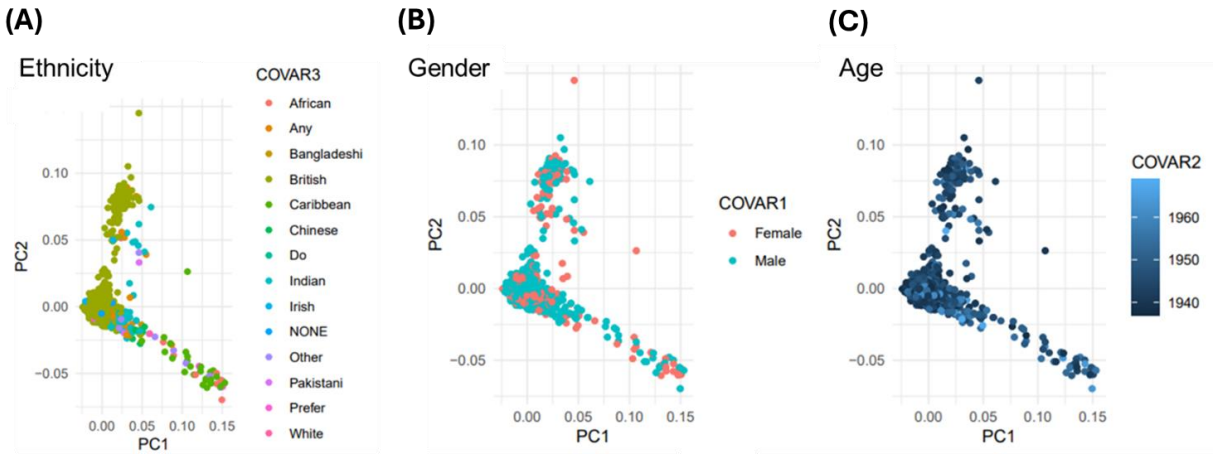

Figure 6.4 PCA plot of atherosclerosis considering age, sex, and ethnicity as covariates. (A) Ethnicity is a co-variate; varying colours determine each ethnic background. (B) Gender as a co-variate, red = females, blue = males. (C) Age as a covariate, increasing age from 1940 birth to 1960> birth. All are plotted as PCA, and output is generated in R Studio.

6.7 Ethnic background is a notable factor in the development of urticaria

Along PC1 when considering ethnicity as a variable, we observe distinct clusters of individual ethnicities (Figure 6.5A). Those of Indian, Irish, and Mixed descent are distinct from British individuals. It could be that those individuals share a common genetic makeup or are exposed to environmental risk factors that heighten their chances of developing the condition. Analysing the distribution of males and females presenting with urticaria, I observe a slight degree of separation between the two sexes along PC1 (Figure 6.5B). This suggests that there may be minor biological differences between males and females that could contribute to ascertaining the condition, but it must be noted that the degree of separation is not large and thus is only arbitrary in use as a predictor of risk for urticaria. In terms of age, there is a trend along PC1 with older individuals (<1940) clustering linearly toward the younger individuals (1970>) toward the left of the x-axis (Figure 6.5C). This suggests that age may be a factor associated with urticaria, however, the separation of the clusters is not as defined as other conditions discussed, which suggests age is not a definitive factor in the development of urticaria.

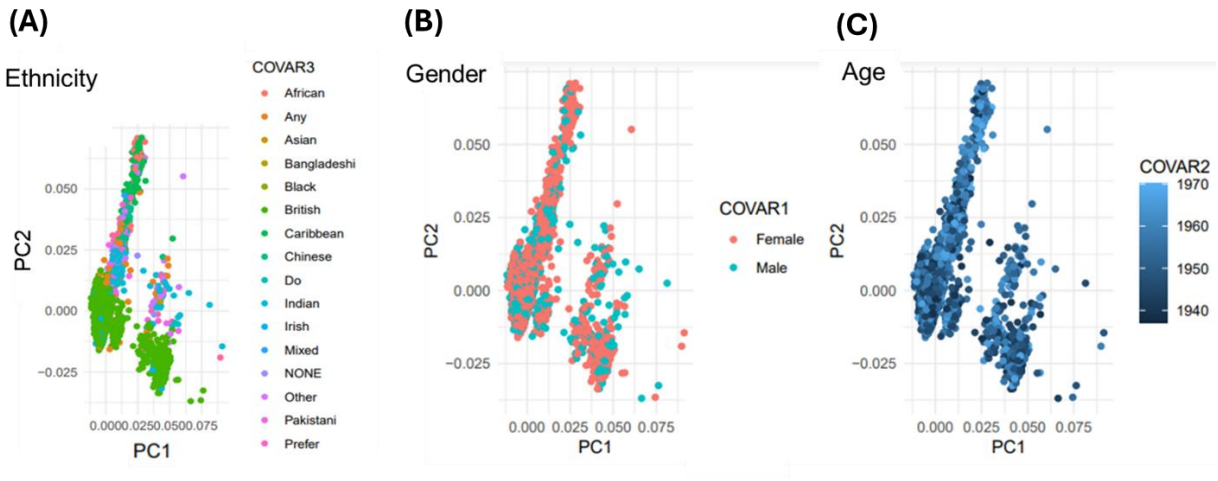

Figure 6.5 PCA plots for urticaria considering age, sex, and ethnicity as covariates. (A) Ethnicity is a co-variate; varying colours determine each ethnic background. (B) Gender as a co-variate, red = females, blue = males. (C) Age as a covariate, increasing age from 1940 birth to 1970 birth date. All are plotted as PCA (PC1 – x-axis, PC2 – y-axis), and output is generated in R Studio.

6.8 Age and ethnic background have a strong influence on the development of diabetes

Diabetes is a chronic condition affecting more than 830 million people globally, with projections suggesting this number will double by 2050 (Hossain et al. 2024). When I explored ethnic differences in individuals with diabetes it was clear that there was a rightward shift for those of British descent and vice versa for other ethnic backgrounds (Figure 6.6A). This highlights that ethnicity plays a role in the molecular profile of diabetes and that ethnic crossover on the plots, suggests potential cross-talk of genetic or environmental risk factors. From this UK BioBank analysis, gender is not a mitigating factor in the manifestation of the condition. The PCA data indicates there is a slight degree of separation between males and females in the disease cohort, however, this is not pronounced, and thus it is not a strong predictor of diabetes risk (Figure 6.6B). Age, however, showed a clear right-shift trend along the PC1 axis, with older individuals clustered toward the right and younger individuals clustered toward the left. This is indicative of a strong link between age and the development of diabetes (Figure 6.6C). It is observed that as age increases, individuals tend to cluster toward a specific right-shifted region of the PCA space, indicating changes in their genetic profile that are associated with diabetes.

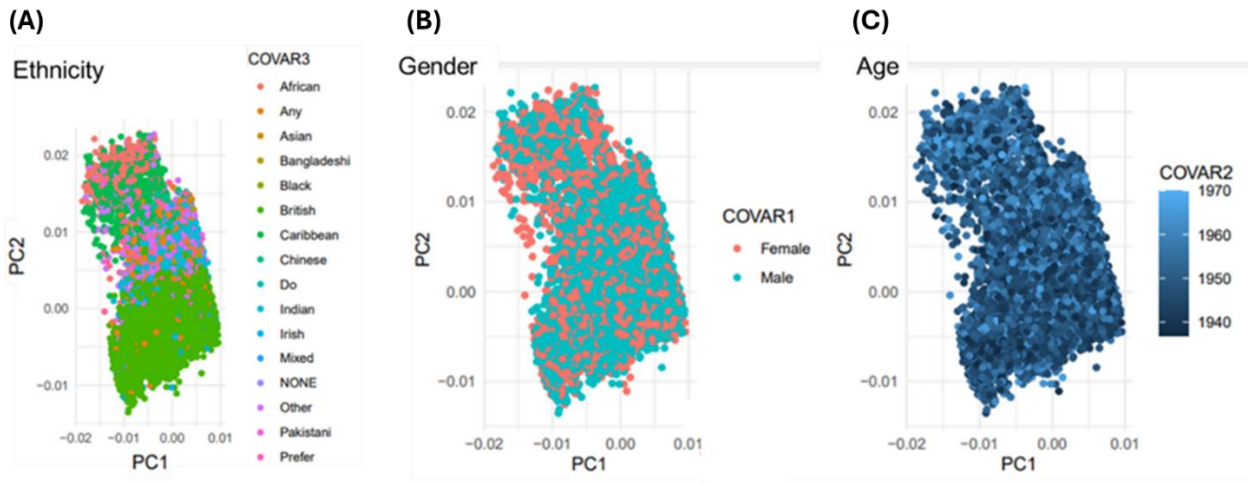

Figure 6.6 PCA analysis of diabetes, considering age, sex, and ethnic background as co-variables. (A) Ethnicity is a co-variate; varying colours determine each ethnic background. (B) Gender as a co-variate, red = females, blue = males. (C) Age as a covariate, increasing age from 1940 birth to 1970 birth date. All are plotted as PCA (PC1 – x-axis, PC2 – y-axis), and output is generated in R Studio.

6.9 Age, sex, and ethnicity are not strong predictors of psoriasis risk

There appears to be a degree of clustering along the PC1 axis when considering ethnicity as a risk factor for psoriasis (Figure 6.7A). These plots establish that there are associations between the three variables, however, they do not establish causation. It is clear from this analysis that there must be other factors, not controlled for here that have a more profound effect on the development of psoriasis, based on its molecular profile. When considering all three variables in the PCA analysis the minimal separation between males and females and the minor separation of the age groups in the psoriasis cohort demonstrates that the pathogenesis of the condition is not influenced by these variables (Figure 6.7B, Figure 6.7C).

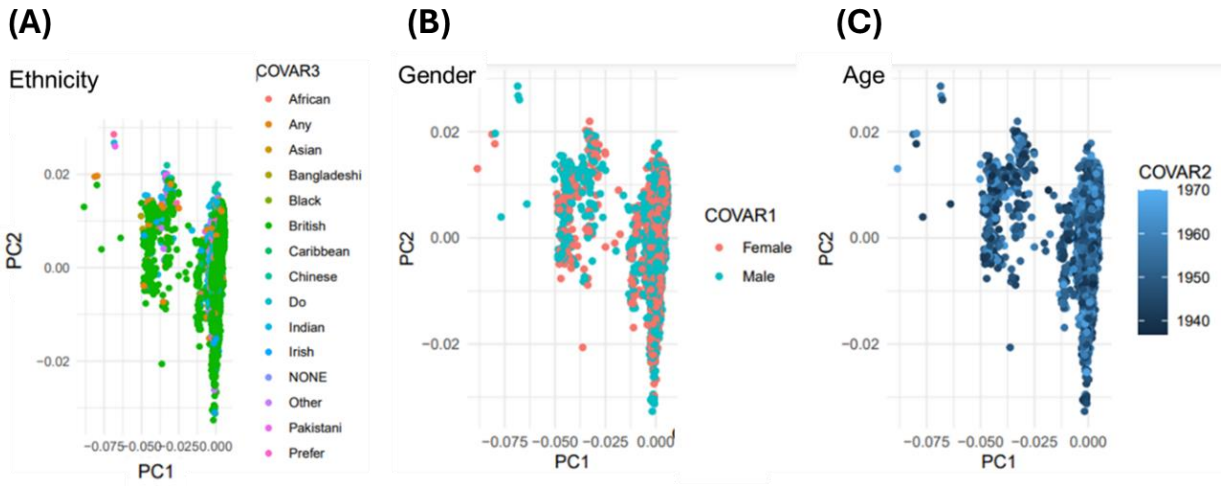

Figure 6.7 PCA plots for psoriasis, highlighting the limited relationship between age, sex, and ethnic background in disease risk. (A) Ethnicity is a co-variate; varying colours determine each ethnic background. (B) Gender as a co-variate, red = females, blue = males. (C) Age as a covariate, increasing age from 1940 birth to 1970 birth date. All are plotted as PCA (PC1 – x-axis, PC2 – y-axis), and output is generated in R Studio.

6.10 Ethnicity may play a notable role in the risks associated with the development of rheumatoid arthritis

Varying ethnicities cluster at different areas along PC1, suggesting that these individual groups may potentially share a genetic makeup or are exposed to environmental risk factors that put them at risk of developing the condition (Figure 6.8A). Conversely, there are 3 groups (Caribbean, Indian, and Chinese) that all demonstrate clear and distinct clustering; hence these populations may possess specific traits that make them more susceptible to the condition. A downstream analysis looking at subgroups may deepen our understanding of how differences in ethnic background may contribute to the heterogeneous nature of RA. Again, in the case of rheumatoid arthritis (RA), sex and age have minimal influence over the development of the condition, like psoriasis (Figure 6.8B, 6.8C). There is slight separation based on sex with this disease cohort along PC1, highlighting that there may be unexplained biological changes within this disease group that affect males and females independently. However, the separation is not well pronounced, hence, sex alone is not a strong predictor of RA in this population. When considering age as a risk factor for the development of RA, there is a left-directional shift along PC1, with older individuals clustering leftwards and vice versa for younger (1960) individuals. This shift might explain that age is a factor involved in altering the molecular profile of RA, however, the separation is not distinctive, thus, age is not-likely to be a mitigating factor in the development of RA.

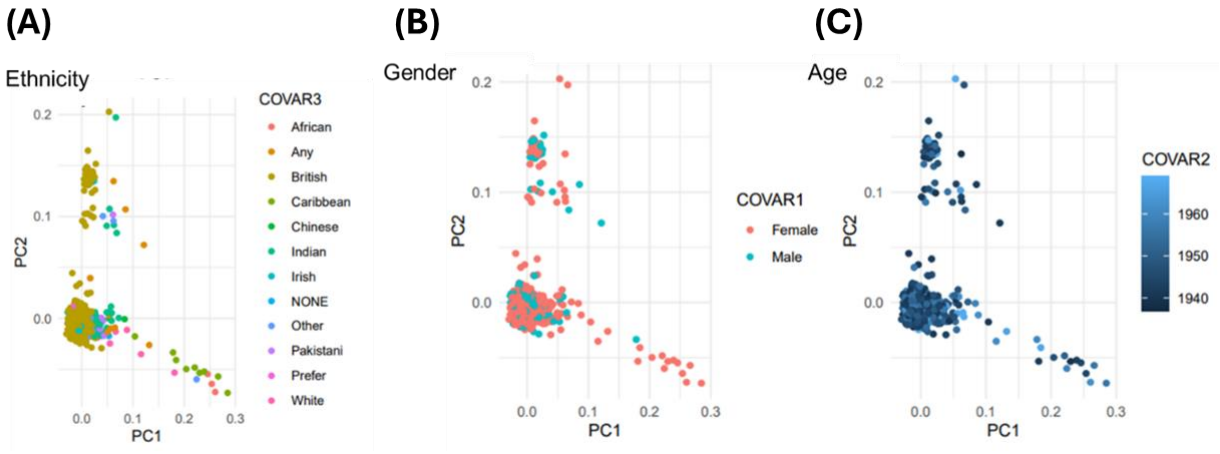

Figure 6.8 PCA plots for rheumatoid arthritis showing age, sex, and ethnicity as co-variables. (A) Ethnicity is a co-variate; varying colours determine each ethnic background. (B) Gender as a co-variate, red = females, blue = males. (C) Age as a covariate, increasing age from 1940 birth to 1960 birth date. All are plotted as PCA (PC1 – x-axis, PC2 – y-axis), and output is generated in R Studio.

6.11 Variant Effect Predictor (VEP) modelling identifies intronic non-coding SNPs as the predominant class in Rab46 associated with inflammatory disease

SNPs located within non-coding regions are not any less important than those that affect the coding sequence of the final protein. Any genetic change at the allele level can be detrimental to protein and cell function. It has been widely reported that transcriptional changes within proteins can induce genotype-phenotype associative change (Nair et al. 2021). One of the main concerns surrounding a volume of intronic, non-coding SNPs is the effects that introns play in gene regulation. Intron retention is whereby introns are mistakenly recognised by mRNA as coding regions to be included in the final sequence and this type of genetic failure is commonly observed in disease models (Wong et al. 2016; Middleton et al. 2017). This can be pathogenic as it can reduce the levels of functioning protein in the cell which then negates the actions of the fully operational protein. Across the 5 inflammatory conditions named in this thesis, the outputs generated by Plink2 analysis have identified non-coding intronic SNPs as the predominant outcome for all diseases (Table 6.4).

Table 6.4 (%) Intronic SNPs associated with Rab46 by disease cohort

Disease	% Intronic SNPs Rab46
Atherosclerosis	52.6
Urticaria	50
Diabetes	47.2
Psoriasis	50
Rheumatoid Arthritis	51.2

I have not taken liberty to analyse the effects of these intronic SNPs here, however, with intronic SNPs also being identified (Appendix Tables 2-6), it is plausible that these could have important roles in changes to gene expression, due to splice site variation for example. Variant effector prediction (VEP) analysis is a powerful tool used by omics researchers to obtain reports on the percentages of the varying types of SNPs observed in certain cohorts. Here, I

employed the use of the Ensembl data base to investigate SNPs significantly associated with Rab46 across the 5 disease groups and produced pie charts to show the distribution and variety of SNP variation (Figure 6.9). This analysis highlights the likelihood and severity of mutation outcomes in each disease. Overall, missense variants are the most commonly observed exonic SNP amongst this group of patients, across the 5 diseases in terms of Rab46. However, it is clear that intronic SNPs affecting non-coding regions of the protein are the predominant class and could still play a role in disease progression or disease risk.

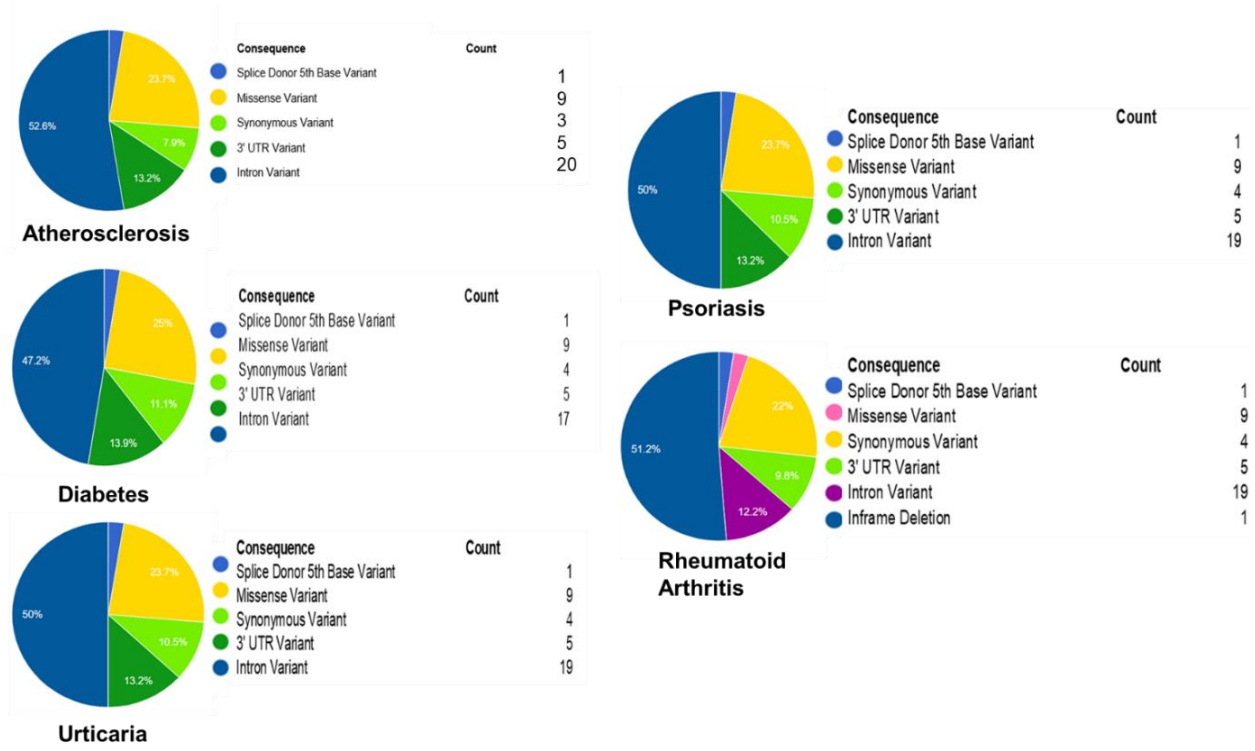

Figure 6.9 Variant effect predictor (VEP) analysis across 5 inflammatory diseases significantly associated with Rab46. VEP outputs for all 5 diseases. All analyses run through Ensembl VEP output software (accessible via: https://tinyurl.com/4nyx48kc, 20.01.25) from the Plink2-byEV input. Graphs are solely generated by the software and tables have been modified to include consequence and count of SNV per SNP.

6.12 Discussion

I have shown that SNPs significantly associated with Rab46 are implicated in inflammatory disease. With the rising incidence of these pro-inflammatory diseases worldwide it has become critical to investigate the potential relationship between genetic mutation on the clinical manifestation of the condition, to deepen our understanding of disease pathophysiology. Firstly, I wanted to identify if possession of any number of these SNPs associated with Rab46, were observed amongst multiple inflammatory diseases. I have shown that multiple SNPs are observed across multiple diseases and that they share a common denominator. The possession of any number of these SNPs does not directly imply that the disease will clinically manifest itself, they are simply markers of the genetic variation within chromosome 12. I have for this thesis, focussed on exonic SNPs, due to their location in the protein-coding regions of Rab46, however, downstream analysis of the intronic variants in the future could be a valuable tool to study these inflammatory diseases.

Although the listed exonic SNPs are not registered on the ClinVar database, variation in the coding sequence of Rab46 could lead to downstream altered signalling and further expansive analysis of these SNPs could reveal cross-talk amongst other diseases, not just inflammatory. An interesting discussion surrounds the relationship between missense SNPs and the response of drugs in the body. These subtle genetic changes can alter how an individual responds to or metabolises a drug, thus, affecting its bioavailability or increasing the risk of developing side effects that might not have been identified as common when compared to the general population of users of said drug. A study looking at major depressive disorder found that individuals with non-synonymous SNPs in the F-G loop of the CYP2D6 protein (rs1065852, rs3810651, and rs117986340) showed reduced enzymatic activity and impairment of commonly used SSRIs to treat the condition (Xin et al. 2020). Overall, it is clear that even non-direct changes in the genomic sequence of coding regions of proteins can influence disease outcomes at the clinical level. I decided to first take each disease and the three associated co-variants (age, sex, and ethnicity) and investigate the effect of these further.

It can be inferred that age is a significant factor in the development of atherosclerosis. This is well published in the literature, with labs identifying increasing age as a well-defined biomarker for the condition. It was originally postulated that atherosclerosis was a condition of the elderly, however, evidence has now come to light highlighting that these pathogenic changes in the vessel microenvironment occur from adolescence and the build-up of fatty streaks serve as clear indicators of future disease progression as age increases (Hong, 2010; McGill et al. 2000; Almohtasib et al. 2024). Looking at the PCA plot (Figure 4.10b) we see that as age increases; individuals tend to cluster at a specific region on the plot indicating there is a change in their molecular makeup associated with the disease. The main ethnic group analysed in Figure 4.10c is British, however, one observes a distinct clustering of the varying ethnic backgrounds along PC1. This is indicative that ethnicity may play a role in the genetic profile associated with atherosclerosis. Groups such as African and Indian appear to cluster tightly together, suggesting shared genetic or risk factors for the condition. Early studies into ischaemic heart disease (IHD) found that an enhanced susceptibility to insulin resistance in South Asians was attributed to poor glucose tolerance and high fasting triglyceride levels (Chaturvedi, 2003). Albeit this study could not conclusively deduce that increased levels of IHD were attributed to ethnicity alone. However, they did report that exposure of South Asian populations to a highly Westernised diet, was a contributing factor to the elevated risk of developing cardiovascular disease in this ethnic minority.

Age is a dominant risk factor in the development of atherosclerosis and ethnicity plays a role in variation of the clinical presentation of the disease and could contribute to remodelling of the molecular profile of the condition. Gender has a less profound effect on the development of the disease; however, it would be interesting to perform further downstream subgroup analysis to look closer at the clustering of African and Indian populations to observe whether sex influences the manifestation of the condition. Multivariate analysis could further explore interactions between the variables; however, it must be noted that these plots are limited in that they do not take socio-economic and lifestyle considerations, which could alter disease profiles.

The global incidence of urticaria is 0.1-3% of the population, with females twice as likely to be affected compared to their male counterparts (Khan et al. 2013). An ongoing study into mixed-ethnicity in Korea, KYRBS, has been collating data on the effects of mixed paternal/maternal race on the susceptibility to developing an allergic disease (asthma, allergic rhinitis, and atopic dermatitis). Univariate analysis of both the paternal and maternal influence found that those individuals with at least one parent from outside Korea, had a significant difference in the prevalence of allergic disease, with urbanity and economic status showing significant odds ratio (OR) across the disease groups (Kim et al. 2020). However, it should be noted that this study is founded on an anonymous survey of high-school students, who may have difficulty in expressing their perceived economic status and degree of urbanity. However, the study has reported a 96.7% response since it began in 2005.

A 2019 study based in Shanghai, China, investigated the relationship between age and the risk of developing pre-diabetes and diabetes, with a participant count of 3540 (2776 after statistical analysis). The prevalence of diabetes was 15.1% and 52.3% for prediabetes (Yan et al. 2023). The results of the study found that the prevalence of diabetes and prediabetes amongst those aged 40-49 was around 11.1% and 40.3%, respectively. This risk rose to 23.9% and 47.6% respectively among those aged between 60-69. Thus, advancing age is a major risk factor for the development of diabetes, however, pre-diabetes is a bidirectional condition and with early detection, normal glucose tolerance can be achieved (Echouffo-Tcheugui & Selvin, 2023; Yan et al. 2023). Multiple studies have agreed with the fact that age is a prominent risk factor in diabetes risk, however, the varying degree of age at the time of diagnosis in older individuals makes it difficult to establish disease outcomes attributed to age alone. A US Health and Retirement Study (HRS) is a population-based longitudinal survey investigating various conditions and age at presentation as a model to study all-cause mortality (Cigolle et al. 2022). They noted that although advancing age is a predominant characteristic in the development of diabetes, a large majority of elderly individuals enter old age with no idea that they have diabetes, thus, the heterogeneous nature of the condition is clinically reinforced and highlights that improvements in disease management are required.

A recent multi-ethnic study investigating the development of psoriasis found that the female sex was a predominant risk factor for the condition (Loo et al. 2024). Of the 330 patients in the study, 83 (25%) went on to develop psoriasis, with 45.8% being Malay, 28.9% Chinese and 25.3% being Indian. One of the most interesting factors driving psoriasis risk was female sex (OR = 3.33, 95% CI 1.78-6.22). The mean age of individuals presenting with psoriasis in our UK BioBank analysis was 70 ± 10.25 years, and when comparing this to the mean age from the Loo et al. study the mean age of individuals at the time of disease presentation regardless of sex was 42.7 years. It could be likely that we do not observe an effect of sex within the PCA analysis, due to the mean age being higher than the typical age of presentation, or that the individuals within our cohort had already undergone therapeutic intervention that could alter disease outcome at that time point. In agreement with the Loo et al. study, the Christophers lab demonstrated that the risk of developing psoriatic arthritis (progressive worsening of psoriasis affecting joints) following diagnosis of psoriasis remained constant irrespective of the age at diagnosis, which agrees with my findings (Christophers et al. 2010).

The COVID-19 pandemic has cast shadows over disease outcomes, and in particular, rheumatic diseases have come under the spotlight as long-term disease outcomes are less favourable in ethnic minority backgrounds (Jordan, 1999; Galloway et al. 2022). However, not all reports on ethnicity in arthritis have reported favourably on this having a strong impact. An observational cohort study in England and Wales was conducted between 2018 and 2020 which quantified the diagnosis of early inflammatory arthritis (Adas et al. 2023). They observed 5 ethnic groups (White, Asian, Mixed, Black, or Other) and from this they found no significant differences in disease onset or progression related solely to ethnicity. However, they noted that those individuals of Mixed, Asian, or Black ethnic backgrounds had lower perceived odds for remission after three months from diagnosis. Another powerful tool used to track whether changes in genomic risk scores affect disease progression was the GENRA case-control study based in South London. It analysed the risk of gene changes in RA from environmental factors. The risk factors associated with RA in European and Asian populations could also be applied to those of African descent (Traylor et

al. 2017). They also found that outcomes associated with smoking and alcohol consumption aligned across the 3 ethnic populations. As a result of these known, harmful environmental risks, the group decided to observe whether alcohol or smoking traits in the European and North American populations and the risks associated with them, could be observed within the African cohort. However, the study lacked sufficient power to detect individual SNPs associated with RA within GENRA. However, they did use a genetic risk score to predict SNV as inflammatory conditions such as RA are polygenic in nature and comprise small-effect mutations.

Firstly, intronic SNPs can be crucial in the dysregulation of splice sites, leading to abnormal mRNA sequences being generated. It is now possible to use these intronic SNPs to identify patterns or predict consequential splice sites. Within these intronic regions of nucleotide sequences certain regions can harbour elements that control the rate of gene expression. SNPs located in the intronic region can help to identify enhancers or silencer sequences of gene expression. An exciting new tool that is currently undergoing improvement is the SpliceAI tool (accessible from: https://spliceailookup.broadinstitute.org/) which can read genetic variations and provide VEP and SIFT score outputs to predict the consequence of SNPs both in the exon and intronic coding region.

Within the exon coding region of Rab46, missense and synonymous variation mutations are also common across all disease cohorts. Large GWAS studies have shown that synonymous mutations in the genome can upset gene regulation for example, via exon skipping or intron retention. Compelling evidence from GWAS shows that there is insufficient published evidence to overrule the already large volume of knowledge that synonymous variants in the genome are majority-neutral and have a negligible effect on disease pathogenesis (Dhindsa et al. 2022). The result of reference allele changes for an alternate (i.e. missense variant) could be neutral, a gain of function (GoF) or loss of function (LoF). All of these can have downstream effects on protein function, which could lead to altered disease outcomes. In the case of Rab46 SNPs, the loss of function within the EF-hand Ca^{2+} binding domain could result in entrapment of the protein at the MTOC, which I have shown earlier can alter Ca^{2+} signalling events related to NAADP within the cell, impacting secretion of

pro-inflammatory cargo such as angiopoietin-2. SNP variation is a common spontaneous event that acts to disrupt the normal functioning of intracellular proteins (Shastry, 2009). GWAS studies have been reporting detrimental outcomes associated with these changes for decades. However, it is only recently with the development of large omics databases that we can determine the clinical repercussions of these small anomalies. Here, I have shown a series of significant SNPs within the coding and non-coding regions of Rab46 and their clinical relevance, as predicted by Plink2 analysis. Disruption to the normal genomic morphology of Rab46 is altered in the 5 disease models discussed above. Globally, diseases such as atherosclerosis and diabetes are significantly on the rise, with an estimated two-fold increase in diagnoses expected by 2050 (Ong et al. 2023). There appears to be significant cross-talk between inflammatory diseases and the cardiometabolic system, thus society must begin to look at these small molecular shifts in allele production to understand whether they play an active role in globalising the pathogenesis of the disease (Poznyak et al. 2020; Xu et al. 2024). Clinically, tools such as cardiometabolic index (CMI) are used to assess all-cause mortality rates within study populations, however, they are arbitrary and confounded by multiple variables that may not be controlled for in the sample. Especially, since all-cause mortality rates tend to be focused on elderly populations. When considering SNP variation, the genetic pool is larger, yes, but it can decipher tiny molecular changes and has the propensity to have direct therapeutic benefits.

It must be noted that there are varying degrees of inconsistencies within the UK BioBank data, be that in sample size amongst disease vs control populations. All efforts were made to ensure that the ratios of males: and females in the study were balanced and that the randomised selection of the control population (n = 15,300) was representative of the total population. Information regarding patient therapeutic status and co-morbidity where not adjusted for in this analysis. Thus, it is difficult to interpret whether co-morbidity or polypharmacy (5 + drugs in a treatment regime across multiple conditions) is affecting the propensity of these observed SNPs across these 5 inflammatory conditions.

Leeds Omics performed Plink2 using a candidate gene approach, thus, it would be beneficial to apply this with other genes to observe any correlation. There

was also no linking analysis performed on the individual SNPs, which poses the question, are they independently associated with the disease or are they linked, i.e. if you possess > 1 SNP are you more likely to develop the condition? It is also possible that there exists an indirect linkage effect, in that can developing one SNP in the candidate gene lead to another. From a pathophysiological perspective, it could be that the development of a small allele change in a protein of interest could indirectly lead to the development of another inflammatory condition downstream of its predicted target.

Overall, this dataset has highlighted that both missense and synonymous SNPs within Rab46 are commonly associated with Rab46 and there is a shared overlap of SNPs between conditions. This predisposes Rab46 to future investigation as a potential candidate protein influencing the pathogenesis of inflammatory disease.

Chapter. 7

Conclusions, limitations & future directions

7.1 Summary of Key Findings

Rab46 is a novel GTPase that typically colocalises with WPBs within the endothelium. This thesis has described the close relationship between Rab46 and differential WPB trafficking of pro-angiogenic cargo in response to vasoactive stimuli highlighting the role of NAADP-mediated Ca^{2+} signals from small, acidic endo-lysosomal stores in this pathway. I have demonstrated in hAECs, that histamine activates Rab46 and triggers a retrograde trafficking along microtubules to the MTOC, where Rab46 selectively mediates the movement of Ang2-positive WPBs, to accumulate at the MTOC. A key role of Rab46 is its ability to operate as a Ca^{2+} sensor in ECs through its two EF-hand Ca^{2+}-binding domains. I have shown in hAECs that the activation of Rab46 in the presence of histamine is independent of Ca^{2+}, but that dispersal of Rab46 and Ang2 from the MTOC is dependent on Ca^{2+} from NAADP-mediated Ca^{2+} channels located on endo-lysosomes. I have evaluated throughout that this NAADP-evoked Ca^{2+} release is likely to be from the TPC2 locale on the lysosomal membrane.

To demonstrate that TPC2 is the functional channel involved in this pathway, I have characterised a specific TPC2 agonist, TPC2-A1-N. This compound mimics the effects of NAADP binding and I have shown that in the presence of co-stimulation of TPC2-A1-N with histamine, I have demonstrated a context-dependent mechanism whereby these compounds can induce dispersal of Rab46 and Ang2 from the MTOC. A key question remains regarding the functional significance of Rab46 and differential WPB dispersal. One possibility is that Rab46 serves as a braking mechanism directing WPBs containing pro-angiogenic cargo toward the MTOC for safe storage to prevent the secretion of irrelevant cargo during an immune response, however, this warrants further investigation. I have also demonstrated that these small NAADP-evoked Ca^{2+} signals can evoke global Ca^{2+} responses through CICR. A key question

remains, in that Rab46 and these Ca^{2+} channels must be spatially and temporally close together and that under histamine stimulation a complex is formed to allow for the Ca^{2+} to bind to the EF-hand domain eliciting dispersal from the MTOC.

7.2 Limitations

Initially, I was using a HUVEC cell model to investigate the distribution of Rab46 under various pharmacological stimuli and to investigate Ca^{2+} signals. However, how these cells are collected by PromoCell® (approx. 10 donors) and pooled led to significant batch-to-batch variability in the data collected. I lost the clustered phenotype at 30 µM histamine and as these cells are obtained from venous cells that are under physiological venous flow *in-vivo* I determined that hAECs would be a more physiologically relevant cell type, due to their morphology, exposure to arterial flow and being from a well-established tissue (aorta) and not a temporary organ, like the umbilical vein from which HUVECs are derived. A limitation of the Ca^{2+} measurements used here was the application of Fura-2. Although possessing ratiometric qualities, which permit the calculation of a ratio between fluorescence intensities at two different wavelengths, there are problems. Variations in the dye concentration within the cell and fluctuations in the signal intensity or optical path length can lead to artefacts of measurements. With NAADP being self-inhibitory at high concentrations, it was determined that NAADP could, itself be used to inherently study its inhibitory effects. However, NAADP even in the -AM ester state, is notoriously difficult to work with as it degrades rapidly in an *in-vitro* setting, thus, I used a well-established antagonist of NAADP, Ned-19 to explore these dynamics, although the use of NAADP-AM may have conferred greater selectivity and/or potency over Ned-19. I devised and wrote an ImageJ macro (see Appendix) for analysing the distribution of Rab46 across three cellular regions, perinuclear, intermediate, and periphery. This macro works based on particle intensity (specifically the intensity of the green, GFP channel) whereby it measures the intensity of the green signal according to a pre-determined particle measurement. I set the particle size from any particle to be detected and mapped between 0.3 µm to infinity. Albeit the macro is an arbitrary method for determining Rab46 distribution, as there is reliance on static, fixed-cell imaging, where the effect of Rab46 distribution is displayed as ‘before

or after' stimulation with the pharmacology. At the time of this thesis, it was possible to ascertain an optimised method to live-cell image Rab46 movement. The reasoning for this was, due to no commercially available secondary antibodies that could live-cell stain that were not GFP-bound. Previous work from the lab has shown that in cells with GFP-bound (at the N-terminus) Rab46, they behave similarly to cells that have under stimulation with 30 μM histamine and thus, upon staining, become clustered at the MTOC and prevent the ability to explore the trafficking of the protein in response to vasoactive stimuli. Regarding the endo-lysosomal channels, I struggled to validate commercially available primary antibodies for TPC1, TPC2 and TPRML1 that would produce meaningful and quantifiable data. One other limitation of this work was not considering the vWF secretome in the context of Rab46 movement, i.e. additional cargo located on WPBs (e.g. endothelin-1, P-selectin) and the effects that these may imply on Rab46 interactions or movement within the cell in response to histamine. This thesis has also not considered the implications of these histamine-evoked Ca^{2+} responses and the distribution of Rab46 in the context of disease states or the potential for developing novel therapeutics, which could warrant further investigation. With the discovery of TPC2-specific agonists, I have been able to explore the effects of Ca^{2+} signalling through this pathway, however, at the point of writing, no direct and specific agonists, or antagonists of TPC1 have been identified in the literature. ML-SA1, a potent agonist of TRPML1 has been reported to be specific, however, time restraints within the lab prevented me from being able to investigate this avenue of work.

7.3 Future Work

The novel data collected in this project opens avenues to explore the context-dependent effects of Rab46 trafficking in response to vasoactive stimuli, with an emphasis on the role of Ca^{2+} signalling from endo-lysosomal stores playing a crucial role in this pathway. It is evident that Rab46 has crucial roles in the vasculature but is implicated in the correct functioning of the immune system. I will now propose an outline of potential future work that is necessary to enable a greater understanding of Rab46's potential as a novel therapeutic target.

7.3.1 Rab46 mechanisms

GTPases are regulated by the actions of multiple effector proteins, which operate spatially and temporally to modulate the activity of the Rab protein. Rab46 is no different and previous work has shown that proteins such as dynein and ATP1α are responsible for the retrograde trafficking of Rab46 to the MTOC following stimulation (Pedicini et al. 2021). Future studies will support these findings, through the identification of further potential effector proteins and more detailed methods such as Ascorbate Peroxidase (APEX) screening (proximity labelling for protein-protein interactions) or Multiple Approaches Combined (Mac-tag) assays which use mass spectrometry to look at bait and prey proteins or through biotin ligation. Crucial to understand how proteins interact with one another and with intracellular cation channels is through the use of live cell imaging techniques. In this thesis, I have used static, plated cells, which were subsequently stimulated and then fixed at a specific time point (normally 10 minutes). At what time within this 10-minute window the trafficking of Rab46 and vWF takes place is unknown, hence, I may have lost valuable evidence in monitoring the spatial dynamics of the protein. As Rab46 is a trafficking GTPase, future studies must investigate these conditions (histamine, TPC2-A1-N) in live cells to observe possible hypothesised complex formation between the protein and the channels on the endo-lysosomal membrane. This will support the preliminary evidence outlined in this thesis that TPC2-mediated Ca^{2+} release is responsible for Rab46 and Ang2 dispersal from the MTOC. To date, our lab has attempted to explore raising nanobodies against Rab46, to allow for live cell imaging due to problems encountered with GTP-bound Rab46 auto-clustering at the MTOC. At the time of writing, these nanobodies are currently under investigation by another member of the lab and will be reported on in due course. Within this thesis, I have touched on the agonising effect of TPC2-A1-N on potentiating the Ca^{2+} release through TPC2. This is only part of the story and analogue screening techniques could be employed to identify specific agonists of TPC1 and TPRML1. In the case of TPC1, this is pivotal, as it is likely that in the context of Ca^{2+} signalling, TPC2-A1-N, although shown to be specific could have potential off-target effects on TPC1 due to the proximity of the channels within the endo-lysosomal system. Live cell imaging with GCaMP proteins could

provide visualisation of Ca^{2+} binding at these proposed complex sites between Rab46 and endo-lysosomal channels. Proving co-localisation will further strengthen the argument that the Ca^{2+} released from these channels is responsible for Rab46/WPB detachment from the MTOC. I attempted to begin work with live-cell imaging of lysosomes; however, it proved difficult in hAECs due to their inability to maintain lysosomal Ca^{2+} dyes within their lumen, thus this area would warrant future study to characterise the distribution of Rab46 and lysosomes in the context on histamine stimulation.

7.3.2 Computational and structural modelling

Within our lab, previous members have created a full-length protein of Rab46 to assess its folding and dynamic properties. However, to date, no structural work has been performed. During the Rab GTPase cycle, Rab's undergo multiple conformational changes to either activate or inactivate, thus removing them themselves from the cycle. As Rab GTPases function as molecular 'on and off' switches, through the hydrolysis or phosphorylation of GTP/GDP, studies investigating these changes could provide insights into how Rab46 modulates its activity in the context of activating or inhibitory signalling. At the centre of Rab46 activity, is its ability to function as a Ca^{2+} sensor, via its two EF-hand domains. Investigating the role of Ca^{2+} and how it links with conformational changes in the overall structure of Rab46 could highlight how the dispersal of the protein and WPBs following stimulation is mediated through the potential complex formation with one or more of the endo-lysosomal cation channels highlighted in this body of work.

The exact binding sites of TPC2-A1-N on TPC2 are currently unknown. Future work should employ the use of AlphaFold or Pymol software to help identify potential binding pockets for these compounds on the channel allowing for a greater understanding of how these agonists operate. There are currently no known binding sites between Rab46 and the three endo-lysosomal Ca^{2+} channels listed in this thesis. Using prediction models would permit the generation of a possible Rab46 interactome that would give further clues as to how these proteins are channels co-localise under the context of stimulus-

induced trafficking and would initiate the search for small molecules that could serve as targets for these binding pockets in the treatment of disease.

7.3.3 TPC1/2 & TRMPL1 transgenic mice

The use of transgenic or knockout mice models has been at the centre of genomic research, providing a crucial tool to investigate the effects of loss of proteins on the normal physiology of the organism. To continue the work generated within this thesis, it is pivotal that work surrounding Ca^{2+} signalling from NAADP-mediated stores is conducted in cells that do not contain TPC1, TPC2 and TPRML1 or in-combination using either 'Cre-lox' or CRISPR genomic editing. I have shown in this thesis that is possible to significantly reduce the expression of these channels in hAEC using specific siRNAs. However, it is clear from my results that even a small expression of these channels may be sufficient to allow for small, localised Ca^{2+} release from endo-lysosomes to globalise into a full ER response via CICR. At the time of writing, there is a lack of an anti-Rab46 antibody commercially available that will recognise Rab46 in the murine model. With the continued work on identifying potential Rab46 nanobodies, it is likely shortly this will be possible.

7.4 Conclusion

The ability of ECs to work together to coordinate cellular machinery to cope with the physiological pressures of multiple vasoactive stimuli is pivotal in its function. This cell type is unique in that is capable of responding to agonist-specific signalling through activation of the vascular 'first-aid kits,' WPBs. I have shown that the large GTPase, Rab46, is crucial in the mediation of differential trafficking of these organelles and their cargo to the MTOC in response to stimuli. WPBs possess an innate plasticity that allows them to store functionally discrete cargo (i.e. Ang2 and P-selectin) and the exocytosis of said cargo is tightly regulated by EC function. The retrograde trafficking of Rab46 to the MTOC is a Ca^{2+} -independent pathway, however, the anterograde dispersal of Rab46 and WPBs containing Ang2 is a Ca^{2+} -mediated response. Herein, I have shown that the Ca^{2+} signalling necessary for this dispersal is from an NAADP-mediated Ca^{2+} store that is functionally separate from the IP_3 ER store,

however, their physiologies do interlink. NAADP-mediated Ca^{2+} signalling is modulated through small, acidic endo-lysosomal cation channels (TPC1/2 and TRPML1), and this describes for the first time a functional mechanism for the role of Rab46 and these channels in their ability to coordinate and distinguish Ca^{2+} signals from distinct vasoactive stimuli. All together the data demonstrates a close relationship between the ability of Rab46 to function as a braking mechanism against the dispersal of pro-angiogenic cargo from WPBs following an immunogenic stimulus. I have shown Rab46 to be a stimulus-coupled regulator of differential trafficking of WPBs containing Ang2 and as a functional Ca^{2+} sensor of Ca^{2+} release from endo-lysosomal stores. These signalling pathways warrant investigation as potential avenues for the discovery of therapeutics that tackle cardiovascular diseases.

References

Adas, M.A., Norton, S., Balachandran, S., Alveyn, E., Russell, M.D., Esterine, T., Amlani-Hatcher, P., Oyebanjo, S., Lempp, H., Ledingham, J., Kumar, K., Galloway, J.B., Dubey, S., 2022a. Worse outcomes linked to ethnicity for early inflammatory arthritis in England and Wales: a national cohort study. Rheumatology 62, 169–180. https://doi.org/10.1093/rheumatology/keac266

Adjambri, A.E., Bouvier, S., N'guessan, R., N'draman-Donou, E., Yayo-Ayé, M., Meledje, M.-F., Adjé, M.L., Sawadogo, D., 2020. Discovery of Type 3 von Willebrand Disease in a Cohort of Patients with Suspected Hemophilia A in Côte d'Ivoire. Mediterranean Journal of Haematology and Infectious Disease 12, e2020019. https://doi.org/10.4084/MJHID.2020.019

Afghah, Z., Chen, X., Geiger, J.D., 2020. Role of endolysosomes and inter-organellar signalling in brain disease. Neurobiology of Disease 134, 104670. https://doi.org/10.1016/j.nbd.2019.104670

Agola, J., Jim, P., Ward, H., BasuRay, S., Wandinger-Ness, A., 2011. Rab GTPases as regulators of endocytosis, targets of disease and therapeutic opportunities. Clinical Genetics 80, 305–318. https://doi.org/10.1111/j.1399-0004.2011.01724.x

Akwii, R.G., Sajib, M.S., Zahra, F.T., Mikelis, C.M., 2019. Role of Angiopoietin-2 in Vascular Physiology and Pathophysiology. Cells 8, 471. https://doi.org/10.3390/cells8050471

Alharbi, A.F., Parrington, J., 2025. TPC2 in drug development: Emerging target for cancer, viral infections, cardiovascular diseases, and neurological disorders. Pharmacological Research 213, 107655. https://doi.org/10.1016/j.phrs.2025.107655

Almohtasib, Y., Fancher, A.J., Sawalha, K., 2024. Emerging Trends in Atherosclerosis: Time to Address Atherosclerosis from a Younger Age. Cureus. https://doi.org/10.7759/cureus.56635

Alzahofi, N., Welz, T., Robinson, C.L., Page, E.L., Briggs, D.A., Stainthorp, A.K., Reekes, J., Elbe, D.A., Straub, F., Kallemeijn, W.W., Tate, E.W., Goff, P.S., Sviderskaya, E.V., Cantero, M., Montoliu, L., Nedelec, F., Miles, A.K., Bailly, M., Kerkhoff, E., Hume, A.N., 2020. Rab27a co-ordinates actin-dependent transport by controlling organelle-associated motors and track assembly proteins. Nature Communications 11, 3495. https://doi.org/10.1038/s41467-020-17212-6

Angiopoietin-2: Development of inhibitors for cancer therapy | Current Oncology Reports [WWW Document], n.d. URL https://link.springer.com/article/10.1007/s11912-009-0017-3 (accessed 11.20.24).

Appelqvist, H., Wäster, P., Kågedal, K., Öllinger, K., 2013a. The lysosome: from waste bag to potential therapeutic target. Journal of Molecular Cell Biology 5, 214–226. https://doi.org/10.1093/jmcb/mjt022

Arendse, L.B., Wyllie, S., Chibale, K., Gilbert, I.H., 2021. *Plasmodium* Kinases as Potential Drug Targets for Malaria: Challenges and Opportunities. American Journal of Cell and Infectious Disease. 7, 518–534. https://doi.org/10.1021/acsinfecdis.0c00724

Arlt, E., Fraticelli, M., Tsvilovskyy, V., Nadolni, W., Breit, A., O'Neill, T.J., Resenberger, S., Wennemuth, G., Wahl-Schott, C., Biel, M., Grimm, C., Freichel, M., Gudermann, T., Klugbauer, N., Boekhoff, I., Zierler, S., 2020. TPC1 deficiency or blockade augments systemic anaphylaxis and mast cell activity. Proceedings of the National Academy of Sciences. U.S.A. 117, 18068–18078. https://doi.org/10.1073/pnas.1920122117

Arndt, H., Bolanowski, M.A., Granger, D.N., 1996. Role of interleukin 8 on leucocyte-endothelial cell adhesion in intestinal inflammation. Gut 38, 911–915. https://doi.org/10.1136/gut.38.6.911

Atkinson, G.C., 2015. The evolutionary and functional diversity of classical and lesser-known cytoplasmic and organellar translational GTPases across the tree of life. British Medical Council Genomics 16, 78. https://doi.org/10.1186/s12864-015-1289-7

Ayagama, T., Bose, S.J., Capel, R.A., Priestman, D.A., Berridge, G., Fischer, R., Galione, A., Platt, F.M., Kramer, H., Burton, R.A.B., 2021. A modified density gradient proteomic-based method to analyze endolysosomal proteins in cardiac tissue. iScience 24, 102949. https://doi.org/10.1016/j.isci.2021.102949

Babich, V., Meli, A., Knipe, L., Dempster, J.E., Skehel, P., Hannah, M.J., Carter, T., 2008. Selective release of molecules from Weibel-Palade bodies during a lingering kiss. Blood 111, 5282–5290. https://doi.org/10.1182/blood-2007-09-113746

Bagshaw, R.D., Mahuran, D.J., Callahan, J.W., 2005. A Proteomic Analysis of Lysosomal Integral Membrane Proteins Reveals the Diverse Composition of the Organelle. Molecular & Cellular Proteomics 4, 133–143. https://doi.org/10.1074/mcp.M400128-MCP200

Bagur, R., Hajnóczky, G., 2017. Intracellular Ca^{2+} Sensing: Its Role in Calcium Homeostasis and Signalling. Molecular Cell 66, 780–788. https://doi.org/10.1016/j.molcel.2017.05.028

Bajaj, L., Lotfi, P., Pal, R., Ronza, A.D., Sharma, J., Sardiello, M., 2019. Lysosome biogenesis in health and disease. Journal of Neurochemistry 148, 573–589. https://doi.org/10.1111/jnc.14564

Banecki, K.M.R.M., Dora, K.A., 2023. Endothelin-1 in Health and Disease. International Journal of Molecular Science 24, 11295. https://doi.org/10.3390/ijms241411295

Barbonari, S., D'Amore, A., Palombi, F., De Cesaris, P., Parrington, J., Riccioli, A., Filippini, A., 2022. Relevance of lysosomal Ca^{2+} signalling machinery in cancer. Cell Calcium 102, 102539. https://doi.org/10.1016/j.ceca.2022.102539

Baumgartner, H.K., Gerasimenko, J.V., Thorne, C., Ferdek, P., Pozzan, T., Tepikin, A.V., Petersen, O.H., Sutton, R., Watson, A.J.M., Gerasimenko, O.V., 2009. Calcium Elevation in Mitochondria Is the Main Ca^{2+} Requirement for Mitochondrial Permeability Transition Pore (mPTP) Opening. Journal of Biological Chemistry 284, 20796–20803. https://doi.org/10.1074/jbc.M109.025353

Beltran, A., Jaramillo, A.P., Vallejo, M.P., Acosta, L., Barberan Parraga, G.C., Guanín Cabrera, C.L., Gaibor, V.G., Cueva, M.G., 2023. Desmopressin as a Treatment in Patients With Von Willebrand Disease: A Systematic Review. Cureus. https://doi.org/10.7759/cureus.44310

Benest, A.V., Kruse, K., Savant, S., Thomas, M., Laib, A.M., Loos, E.K., Fiedler, U., Augustin, H.G., 2013. Angiopoietin-2 Is Critical for Cytokine-Induced Vascular Leakage. PLoS ONE 8, e70459. https://doi.org/10.1371/journal.pone.0070459

Berditchevski, F., Odintsova, E., 1999. Characterization of integrin-tetraspanin adhesion complexes: role of tetraspanins in integrin signalling. Journal of Cell Biology 146, 477–492. https://doi.org/10.1083/jcb.146.2.477

Bergers, G., Hanahan, D., 2008. Modes of resistance to anti-angiogenic therapy. Nature Reviews Cancer 8, 592–603. https://doi.org/10.1038/nrc2442

Bharati, K.P., Prashanth, U.R., 2011. Von Willebrand disease: an overview. Indian Journal of Pharmacology and Science 73, 7–16. https://doi.org/10.4103/0250-474X.89751

Bhattacharjee, A., Abuammar, H., Juhász, G., 2024. Lysosomal activity depends on TRPML1-mediated Ca^{2+} release coupled to incoming vesicle fusions. Journal of Biological Chemistry 300, 107911. https://doi.org/10.1016/j.jbc.2024.107911

Billaud, M., Lohman, A.W., Johnstone, S.R., Biwer, L.A., Mutchler, S., Isakson, B.E., 2014. Regulation of Cellular Communication by Signaling Microdomains in the Blood Vessel Wall. Pharmacological Reviews 66, 513–569. https://doi.org/10.1124/pr.112.007351

Björkegren, J.L.M., Lusis, A.J., 2022. Atherosclerosis: Recent developments. Cell 185, 1630–1645. https://doi.org/10.1016/j.cell.2022.04.004

Boccaccio, A., Scholz-Starke, J., Hamamoto, S., Larisch, N., Festa, M., Gutla, P.V.K., Costa, A., Dietrich, P., Uozumi, N., Carpaneto, A., 2014. The phosphoinositide $PI(3,5)P_2$ mediates activation of mammalian but not plant TPC proteins: functional expression of endolysosomal channels in yeast and plant

cells. Cell Molecular Life Sciences 71, 4275–4283. https://doi.org/10.1007/s00018-014-1623-2

Bonam, S.R., Wang, F., Muller, S., 2019. Lysosomes as a therapeutic target. Nature Reviews Drug Discovery 18, 923–948. https://doi.org/10.1038/s41573-019-0036-1

Bonifacino, J.S., Neefjes, J., 2017. Moving and positioning the endolysosomal system. Current Opinion in Cell Biology 47, 1–8. https://doi.org/10.1016/j.ceb.2017.01.008

Bos, J.L., Rehmann, H., Wittinghofer, A., 2007. GEFs and GAPs: Critical Elements in the Control of Small G Proteins. Cell 129, 865–877. https://doi.org/10.1016/j.cell.2007.05.018

Bourne, H.R., Sanders, D.A., McCormick, F., 1991. The GTPase superfamily: conserved structure and molecular mechanism. Nature 349, 117–127. https://doi.org/10.1038/349117a0

Bourque, S.L., Davidge, S.T., Adams, M.A., 2011. The interaction between endothelin-1 and nitric oxide in the vasculature: new perspectives. American Journal of Physiology 300, R1288-1295. https://doi.org/10.1152/ajpregu.00397.2010

Brighouse, A., Dacks, J.B., Field, M.C., 2010. Rab protein evolution and the history of the eukaryotic endomembrane system. Cell and Molecular Life Science 67, 3449–3465. https://doi.org/10.1007/s00018-010-0436-1

Bright, N.A., Gratian, M.J., Luzio, J.P., 2005. Endocytic Delivery to Lysosomes Mediated by Concurrent Fusion and Kissing Events in Living Cells. Current Biology 15, 360–365. https://doi.org/10.1016/j.cub.2005.01.049

Brunetti, V., Berra-Romani, R., Conca, F., Soda, T., Biella, G.R., Gerbino, A., Moccia, F., Scarpellino, G., 2024. Lysosomal TRPML1 triggers global Ca^{2+} signals and nitric oxide release in human cerebrovascular endothelial cells. Frontiers in Physiology. 15, 1426783. https://doi.org/10.3389/fphys.2024.1426783

Buckley, M.L., Ramji, D.P., 2015. The influence of dysfunctional signalling and lipid homeostasis in mediating the inflammatory responses during atherosclerosis. Biochimica et Biophysica Acta (BBA) - Molecular Basis of Disease 1852, 1498–1510. https://doi.org/10.1016/j.bbadis.2015.04.011

Calcraft, P.J., Ruas, M., Pan, Z., Cheng, X., Arredouani, A., Hao, X., Tang, J., Rietdorf, K., Teboul, L., Chuang, K.-T., Lin, P., Xiao, R., Wang, C., Zhu, Y., Lin, Y., Wyatt, C.N., Parrington, J., Ma, J., Evans, A.M., Galione, A., Zhu, M.X., 2009. NAADP mobilizes calcium from acidic organelles through two-pore channels. Nature 459, 596–600. https://doi.org/10.1038/nature08030

Capel, R.A., Bolton, E.L., Lin, W.K., Aston, D., Wang, Y., Liu, W., Wang, X., Burton, R.-A.B., Bloor-Young, D., Shade, K.-T., Ruas, M., Parrington, J., Churchill, G.C., Lei, M., Galione, A., Terrar, D.A., 2015. Two-pore Channels (TPC2s) and Nicotinic Acid Adenine Dinucleotide Phosphate (NAADP) at Lysosomal-Sarcoplasmic Reticular Junctions Contribute to Acute and Chronic β-Adrenoceptor Signaling in the Heart. Journal of Biological Chemistry 290, 30087–30098. https://doi.org/10.1074/jbc.M115.684076

Carafoli, E., 2010. The fateful encounter of mitochondria with calcium: How did it happen? Biochimica et Biophysica Acta (BBA) - Bioenergetics 1797, 595–606. https://doi.org/10.1016/j.bbabio.2010.03.024

Castonguay, J., Orth, J.H.C., Müller, T., Sleman, F., Grimm, C., Wahl-Schott, C., Biel, M., Mallmann, R.T., Bildl, W., Schulte, U., Klugbauer, N., 2017a. The two-pore channel TPC1 is required for efficient protein processing through early and recycling endosomes. Science Reports 7, 10038. https://doi.org/10.1038/s41598-017-10607-4

Chaturvedi, N., 2003. Ethnic Differences in Cardiovascular Disease. Heart 89, 681–686. https://doi.org/10.1136/heart.89.6.681

Chen, C.-C., Krogsaeter, E., Kuo, C.-Y., Huang, M.-C., Chang, S.-Y., Biel, M., 2022. Endolysosomal cation channels point the way towards precision medicine of cancer and infectious diseases. Biomedicine & Pharmacotherapy 148, 112751. https://doi.org/10.1016/j.biopha.2022.112751

Cheng, C.W., Pedicini, L., Alcala, C.M., Deligianni, F., Smith, J., Murray, R.D., Todd, H.J., Forde, N., McKeown, L., 2025. RNA-seq analysis reveals transcriptome changes in livers from Efcab4b knockout mice. Biochemistry and Biophysics Reports 41, 101944. https://doi.org/10.1016/j.bbrep.2025.101944

Cheng, X., Shen, D., Samie, M., Xu, H., 2010. Mucolipins: Intracellular TRPML1-3 channels. FEBS Letters 584, 2013–2021. https://doi.org/10.1016/j.febslet.2009.12.056

Cherfils, J., Zeghouf, M., 2013. Regulation of Small GTPases by GEFs, GAPs, and GDIs. Physiological Reviews 93, 269–309. https://doi.org/10.1152/physrev.00003.2012

Chi, G., Jaślan, D., Kudrina, V., Böck, J., Li, H., Pike, A.C.W., Rautenberg, S., Krogsaeter, E., Bohstedt, T., Wang, D., McKinley, G., Fernandez-Cid, A., Mukhopadhyay, S.M.M., Burgess-Brown, N.A., Keller, M., Bracher, F., Grimm, C., Dürr, K.L., 2024. Structural basis for inhibition of the lysosomal two-pore channel TPC2 by a small molecule antagonist. Structure 32, 1137-1149.e4. https://doi.org/10.1016/j.str.2024.05.005

Chinopoulos, C., Adam-Vizi, V., 2010. Mitochondrial Ca^{2+} sequestration and precipitation revisited. The FEBS Journal 277, 3637–3651. https://doi.org/10.1111/j.1742-4658.2010.07755.x

Chiu, J.-J., Chien, S., 2011a. Effects of Disturbed Flow on Vascular Endothelium: Pathophysiological Basis and Clinical Perspectives. Physiological Reviews 91, 327–387. https://doi.org/10.1152/physrev.00047.2009

Christophers, E., Barker, J., Griffiths, C., Daudén, E., Milligan, G., Molta, C., Sato, R., Boggs, R., 2010. The risk of psoriatic arthritis remains constant following initial diagnosis of psoriasis among patients seen in European dermatology clinics. Academy of Dermatology and Venereology 24, 548–554. https://doi.org/10.1111/j.1468-3083.2009.03463.x

Churchill, G.C., Okada, Y., Thomas, J.M., Genazzani, A.A., Patel, S., Galione, A., 2002. NAADP Mobilizes Ca^{2+} from Reserve Granules, Lysosome-Related Organelles, in Sea Urchin Eggs. Cell 111, 703–708. https://doi.org/10.1016/S0092-8674(02)01082-6

Cigolle, C.T., Blaum, C.S., Lyu, C., Ha, J., Kabeto, M., Zhong, J., 2022. Associations of Age at Diagnosis and Duration of Diabetes with Morbidity and Mortality Among Older Adults. Journal of the American Medical Association Networks Open 5, e2232766. https://doi.org/10.1001/jamanetworkopen.2022.32766

Daverkausen-Fischer, L., Pröls, F., 2022. Regulation of calcium homeostasis and flux between the endoplasmic reticulum and the cytosol. Journal of Biological Chemistry 298, 102061. https://doi.org/10.1016/j.jbc.2022.102061

de Duve, C., Pressman, B. C., Gianetto, R., Wattiaux, R. & Appelmans, F. 1955. Tissue fractionation studies. 6. Intracellular distribution patterns of enzymes in rat-liver tissue. Biochemical Journal. 60, 604–617. doi: 10.1042/bj0600604.

De Leeuw, H.P.J.C., Fernandez-Borja, M., Reits, E.A.J., Romani De Wit, T., Wijers-Koster, P.M., Hordijk, P.L., Neefjes, J., Van Mourik, J.A., Voorberg, J., 2001. Small GTP-Binding Protein Ral Modulates Regulated Exocytosis of von Willebrand Factor by Endothelial Cells. Atherosclerosis, Thrombosis and Vascular Biology 21, 899–904. https://doi.org/10.1161/01.ATV.21.6.899

De Pablo-Moreno, J.A.D., Serrano, L.J., Revuelta, L., Sánchez, M.J., Liras, A., 2022. The Vascular Endothelium and Coagulation: Homeostasis, Disease, and Treatment, with a Focus on the Von Willebrand Factor and Factors VIII and V. International Journal of Molecular Sciences 23, 8283. https://doi.org/10.3390/ijms23158283

Dhindsa, R.S., Wang, Q., Vitsios, D., Burren, O.S., Hu, F., DiCarlo, J.E., Kruglyak, L., MacArthur, D.G., Hurles, M.E., Petrovski, S., 2022. A minimal role for synonymous variation in human disease. The American Journal of Human Genetics 109, 2105–2109. https://doi.org/10.1016/j.ajhg.2022.10.016

Echouffo-Tcheugui, J.B., Selvin, E., 2021. Prediabetes and What It Means: The Epidemiological Evidence. Annual Reviews in Public Health 42, 59–77. https://doi.org/10.1146/annurev-publhealth-090419-102644

Escopy, S., Chaikof, E.L., 2024. Targeting the P-selectin/PSGL-1 pathway: discovery of disease-modifying therapeutics for disorders of

thromboinflammation. Blood Vessels, Thrombosis & Haemostasis 1, 100015. https://doi.org/10.1016/j.bvth.2024.100015

Esposito, B., Gambara, G., Lewis, A.M., Palombi, F., D'Alessio, A., Taylor, L.X., Genazzani, A.A., Ziparo, E., Galione, A., Churchill, G.C., Filippini, A., 2011. NAADP links histamine H1 receptors to secretion of von Willebrand factor in human endothelial cells. Blood 117, 4968–4977. https://doi.org/10.1182/blood-2010-02-266338

Faris, P., Shekha, M., Montagna, D., Guerra, G., Moccia, F., 2018. Endolysosomal Ca^{2+} Signalling and Cancer Hallmarks: Two-Pore Channels on the Move, TRPML1 Lags Behind! Cancers 11, 27. https://doi.org/10.3390/cancers11010027

Farrell, E.F., Antaramian, A., Rueda, A., Gómez, A.M., Valdivia, H.H., 2003. Sorcin Inhibits Calcium Release and Modulates Excitation-Contraction Coupling in the Heart. Journal of Biological Chemistry 278, 34660–34666. https://doi.org/10.1074/jbc.M305931200

Favia, A., Desideri, M., Gambara, G., D'Alessio, A., Ruas, M., Esposito, B., Del Bufalo, D., Parrington, J., Ziparo, E., Palombi, F., Galione, A., Filippini, A., 2014. VEGF-induced neoangiogenesis is mediated by NAADP and two-pore channel-2–dependent Ca^{2+} signalling. Proceedings of the National Academy of Sciences U.S.A. 111. https://doi.org/10.1073/pnas.1406029111

Feijóo-Bandín, S., García-Vence, M., García-Rúa, V., Roselló-Lletí, E., Portolés, M., Rivera, M., González-Juanatey, J.R., Lago, F., 2017. Two-pore channels (TPCs): Novel voltage-gated ion channels with pleiotropic functions. Channels 11, 20–33. https://doi.org/10.1080/19336950.2016.1213929

Ferraro, B., Leoni, G., Hinkel, R., Ormanns, S., Paulin, N., Ortega-Gomez, A., Viola, J.R., De Jong, R., Bongiovanni, D., Bozoglu, T., Maas, S.L., D'Amico, M., Kessler, T., Zeller, T., Hristov, M., Reutelingsperger, C., Sager, H.B., Döring, Y., Nahrendorf, M., Kupatt, C., Soehnlein, O., 2019. Pro-Angiogenic Macrophage Phenotype to Promote Myocardial Repair. Journal of the American College of Cardiology 73, 2990–3002. https://doi.org/10.1016/j.jacc.2019.03.503

Fiedler, U., Reiss, Y., Scharpfenecker, M., Grunow, V., Koidl, S., Thurston, G., Gale, N.W., Witzenrath, M., Rosseau, S., Suttorp, N., Sobke, A., Herrmann, M., Preissner, K.T., Vajkoczy, P., Augustin, H.G., 2006. Angiopoietin-2 sensitizes endothelial cells to TNF-α and has a crucial role in the induction of inflammation. Nature Medicine 12, 235–239. https://doi.org/10.1038/nm1351

Fiedler, U., Scharpfenecker, M., Koidl, S., Hegen, A., Grunow, V., Schmidt, J.M., Kriz, W., Thurston, G., Augustin, H.G., 2004. The Tie-2 ligand Angiopoietin-2 is stored in and rapidly released upon stimulation from endothelial cell Weibel-Palade bodies. Blood 103, 4150–4156. https://doi.org/10.1182/blood-2003-10-3685

Fill, M., Copello, J.A., 2002. Ryanodine Receptor Calcium Release Channels. Physiological Reviews 82, 893–922. https://doi.org/10.1152/physrev.00013.2002

Galione, A., 2019. NAADP Receptors. Cold Spring Harbour Perspectives in Biology 11, a035071. https://doi.org/10.1101/cshperspect.a035071

Galione, A., Evans, A.M., Ma, J., Parrington, J., Arredouani, A., Cheng, X., Zhu, M.X., 2009. The acid test: the discovery of two-pore channels (TPCs) as NAADP-gated endolysosomal Ca^{2+} release channels. Pflugers Arch - European Journal of Physiology 458, 869–876. https://doi.org/10.1007/s00424-009-0682-y

Galloway, 2022. The National Early Inflammatory Arthritis Audit (NEIAA).

Garrity, A.G., Wang, W., Collier, C.M., Levey, S.A., Gao, Q., Xu, H., 2016. The endoplasmic reticulum, not the pH gradient, drives calcium refilling of lysosomes. eLife 5, e15887. https://doi.org/10.7554/eLife.15887

Genazzani, A.A., Mezna, M., Dickey, D.M., Michelangeli, F., Walseth, T.F., Galione, A., 1997. Pharmacological properties of the Ca^{2+} -release mechanism sensitive to NAADP in the sea urchin egg. British Journal of Pharmacology 121, 1489–1495. https://doi.org/10.1038/sj.bjp.0701295

Gerndt, S., Chen, C.-C., Chao, Y.-K., Yuan, Y., Burgstaller, S., Scotto Rosato, A., Krogsaeter, E., Urban, N., Jacob, K., Nguyen, O.N.P., Miller, M.T., Keller, M., Vollmar, A.M., Gudermann, T., Zierler, S., Schredelseker, J., Schaefer, M., Biel, M., Malli, R., Wahl-Schott, C., Bracher, F., Patel, S., Grimm, C., 2020. Agonist-

mediated switching of ion selectivity in TPC2 differentially promotes lysosomal function. eLife 9, e54712. https://doi.org/10.7554/eLife.54712

Goldberg, J., 1998. Structural Basis for Activation of ARF GTPase. Cell 95, 237–248. https://doi.org/10.1016/S0092-8674(00)81754-7

Gopal Krishnan, P.D., Golden, E., Woodward, E.A., Pavlos, N.J., Blancafort, P., 2020. Rab GTPases: Emerging Oncogenes and Tumor Suppressive Regulators for the Editing of Survival Pathways in Cancer. Cancers (Basel) 12, 259. https://doi.org/10.3390/cancers12020259

Grabarek, Z., 2006. Structural Basis for Diversity of the EF-hand Calcium-binding Proteins. Journal of Molecular Biology 359, 509–525. https://doi.org/10.1016/j.jmb.2006.03.066

Gragnano, F., Sperlongano, S., Golia, E., Natale, F., Bianchi, R., Crisci, M., Fimiani, F., Pariggiano, I., Diana, V., Carbone, A., Cesaro, A., Concilio, C., Limongelli, G., Russo, M., Calabrò, P., 2017. The Role of von Willebrand Factor in Vascular Inflammation: From Pathogenesis to Targeted Therapy. Mediators of Inflammation 2017, 1–13. https://doi.org/10.1155/2017/5620314

Grimm, C., Hassan, S., Wahl-Schott, C., Biel, M., 2012. Role of TRPML and Two-Pore Channels in Endolysosomal Cation Homeostasis. The Journal of Pharmacology and Experimental Therapeutics 342, 236–244. https://doi.org/10.1124/jpet.112.192880

Grimm, C., Tang, R., 2020. Could an endo-lysosomal ion channel be the Achilles heel of SARS-CoV2? Cell Calcium 88, 102212. https://doi.org/10.1016/j.ceca.2020.102212

Guéguinou, M., Chantôme, A., Fromont, G., Bougnoux, P., Vandier, C., Potier-Cartereau, M., 2014a. KCa and Ca^{2+} channels: The complex thought. Biochimica et Biophysica Acta (BBA) - Molecular Cell Research 1843, 2322–2333. https://doi.org/10.1016/j.bbamcr.2014.02.019

Gunaratne, G.S., Brailoiu, E., Kumar, S., Yuan, Y., Slama, J.T., Walseth, T.F., Patel, S., Marchant, J.S., 2023. Convergent activation of two-pore channels

mediated by the NAADP-binding proteins JPT2 and LSM12. Science Signalling 16, eadg0485. https://doi.org/10.1126/scisignal.adg0485

Gut, n.d. Gut, 1996. 38(6):911-5.

Hayashi, S., Watanabe, N., Nakazawa, K., Suzuki, J., Tsushima, K., Tamatani, T., Sakamoto, S., Isobe, M., 2000. Roles of P-Selectin in Inflammation, Neointimal Formation, and Vascular Remodelling in Balloon-Injured Rat Carotid Arteries. Circulation 102, 1710–1717. https://doi.org/10.1161/01.CIR.102.14.1710

Hegab, Z., 2012. Role of advanced glycation end products in cardiovascular disease. World Journal of Cardiology 4, 90. https://doi.org/10.4330/wjc.v4.i4.90

Heister, P.M., Poston, R.N., 2020. Pharmacological hypothesis: TPC2 antagonist tetrandrine as a potential therapeutic agent for COVID-19. Pharmacology Research & Perspectives 8, e00653. https://doi.org/10.1002/prp2.653

Hennigs, J.K., Matuszcak, C., Trepel, M., Körbelin, J., 2021. Vascular Endothelial Cells: Heterogeneity and Targeting Approaches. Cells 10, 2712. https://doi.org/10.3390/cells10102712

Hogan, P.G., Rao, A., 2015. Store-operated calcium entry: Mechanisms and modulation. Biochemical and Biophysical Research Communications 460, 40–49. https://doi.org/10.1016/j.bbrc.2015.02.110

Holash, J., Wiegand, S.J., Yancopoulos, G.D., 1999. New model of tumor angiogenesis: dynamic balance between vessel regression and growth mediated by angiopoietins and VEGF. Oncogene 18, 5356–5362. https://doi.org/10.1038/sj.onc.1203035

Homma, Y., Hiragi, S., Fukuda, M., 2021. Rab family of small GTPases: an updated view on their regulation and functions. The FEBS Journal 288, 36–55. https://doi.org/10.1111/febs.15453

Hong, Y.M., 2010. Atherosclerotic Cardiovascular Disease Beginning in Childhood. Korean Circulation Journal 40, 1. https://doi.org/10.4070/kcj.2010.40.1.1

Hordijk, S., Carter, T., Bierings, R., 2024. A new look at an old body: molecular determinants of Weibel-Palade body composition and von Willebrand factor exocytosis. Journal of Thrombosis and Haemostasis 22, 1290–1303. https://doi.org/10.1016/j.jtha.2024.01.015

Horgan, C.P., McCaffrey, M.W., 2009. The dynamic Rab11-FIPs. Biochemical Society Transactions 37, 1032–1036. https://doi.org/10.1042/BST0371032

Horgan, C.P., McCaffrey, M.W., 2011. Rab GTPases and microtubule motors. Biochemical Society Transactions 39, 1202–1206. https://doi.org/10.1042/BST0391202

Horiuchi, H., Doman, T., Kokame, K., Saiki, Y., Matsumoto, M., 2019. Acquired von Willebrand Syndrome Associated with Cardiovascular Diseases. Journal of Atherosclerosis and Thrombosis 26, 303–314. https://doi.org/10.5551/jat.RV17031

Hossain, Md.J., Al-Mamun, Md., Islam, Md.R., 2024. Diabetes mellitus, the fastest growing global public health concern: Early detection should be focused. Health Science Reports 7, e2004. https://doi.org/10.1002/hsr2.2004

Hu, B., Cheng, S.-Y., 2009. Angiopoietin-2: Development of inhibitors for cancer therapy. Current Oncology Reports 11, 111–116. https://doi.org/10.1007/s11912-009-0017-3

Huang, Y.-Q., Li, J.-J., Hu, L., Lee, M., Karpatkin, S., 2002a. Thrombin induces increased expression and secretion of angiopoietin-2 from human umbilical vein endothelial cells. Blood 99, 1646–1650. https://doi.org/10.1182/blood.V99.5.1646

Hutagalung, A.H., Novick, P.J., 2011. Role of Rab GTPases in Membrane Traffic and Cell Physiology. Physiological Reviews 91, 119–149. https://doi.org/10.1152/physrev.00059.2009

Hyttinen, J.M.T., Niittykoski, M., Salminen, A., Kaarniranta, K., 2013. Maturation of autophagosomes and endosomes: A key role for Rab7. Biochimica et Biophysica Acta (BBA) - Molecular Cell Research 1833, 503–510. https://doi.org/10.1016/j.bbamcr.2012.11.018

Ivanova, A., Atakpa-Adaji, P., Rao, S., Marti-Solano, M., Taylor, C.W., 2024. Dual regulation of IP3 receptors by IP3 and PIP2 controls the transition from local to global Ca^{2+} signals. Molecular Cell 84, 3997-4015.e7. https://doi.org/10.1016/j.molcel.2024.09.009

Jaiswal, J.K., Andrews, N.W., Simon, S.M., 2002. Membrane proximal lysosomes are the major vesicles responsible for calcium-dependent exocytosis in nonsecretory cells. Journal of Cell Biology 159, 625–635. https://doi.org/10.1083/jcb.200208154

Jebari-Benslaiman, S., Galicia-García, U., Larrea-Sebal, A., Olaetxea, J.R., Alloza, I., Vandenbroeck, K., Benito-Vicente, A., Martín, C., 2022. Pathophysiology of Atherosclerosis. International Journal of Molecular Sciences 23, 3346. https://doi.org/10.3390/ijms23063346

Jha, A., Ahuja, M., Muallem, S., 2015. Similarities and Differences in Gating of the Two-Pore Channels TPC1 and TPC2. Biophysical Journal 108, 570a. https://doi.org/10.1016/j.bpj.2014.11.3118

Jha, A., Ahuja, M., Patel, S., Brailoiu, E., Muallem, S., 2014. Convergent regulation of the lysosomal two-pore channel-2 by Mg2+, NAADP, PI(3,5)P2 and multiple protein kinases. The EMBO Journal 33, 501–511. https://doi.org/10.1002/embj.201387035

Jin, X., Zhang, Y., Alharbi, A., Hanbashi, A., Alhoshani, A., Parrington, J., 2020. Targeting Two-Pore Channels: Current Progress and Future Challenges. Trends in Pharmacological Sciences 41, 582–594. https://doi.org/10.1016/j.tips.2020.06.002

Jones, N., Iljin, K., Dumont, D.J., Alitalo, K., 2001a. Tie receptors: new modulators of angiogenic and lymphangiogenic responses. Nature Reviews Molecular Cell Biology 2, 257–267. https://doi.org/10.1038/35067005

Jordan, J.M., 1999. Effect of race and ethnicity on outcomes in arthritis and rheumatic conditions: Current Opinion in Rheumatology 11, 98–103. https://doi.org/10.1097/00002281-199903000-00003

Kadowaki, T., Yamaguchi, Y., Ogawa, K., Tokuhisa, M., Okamoto, K., Tsukuba, T., 2021. Rab44 isoforms similarly promote lysosomal exocytosis but exhibit differential localization in mast cells. FEBS Open Biology 11, 1165–1185. https://doi.org/10.1002/2211-5463.13133

Kang, H., Choi, S.W., Kim, J.Y., Oh, S.-J., Kim, S.J., Lee, M.-S., 2024. ER-to-lysosome Ca^{2+} refilling followed by K+ efflux-coupled store-operated Ca^{2+} entry in inflammasome activation and metabolic inflammation. eLife 12, RP87561. https://doi.org/10.7554/eLife.87561

Kannan, K., Stewart, R.M., Bounds, W., Carlsson, S.R., Fukuda, M., Betzing, K.W., Holcombe, R.F., 1996. Lysosome-associated membrane proteins h-LAMP1 (CD107a) and h-LAMP2 (CD107b) are activation-dependent cell surface glycoproteins in human peripheral blood mononuclear cells which mediate cell adhesion to vascular endothelium. Cell Immunology 171, 10–19. https://doi.org/10.1006/cimm.1996.0167

Karageorgos, L.E., Isaac, E.L., Brooks, D.A., Ravenscroft, E.M., Davey, R., Hopwood, J.J., Meikle, P.J., 1997. Lysosomal biogenesis in lysosomal storage disorders. Experimental Cell Research 234, 85–97. https://doi.org/10.1006/excr.1997.3581

Kaufmann, J.E., Oksche, A., Wollheim, C.B., Günther, G., Rosenthal, W., Vischer, U.M., 2000. Vasopressin-induced von Willebrand factor secretion from endothelial cells involves V2 receptors and cAMP. Journal of Clinical Investigation 106, 107–116. https://doi.org/10.1172/JCI9516

Kawasaki, H., Kretsinger, R.H., 2017. Structural and functional diversity of EF-hand proteins: Evolutionary perspectives. Protein Science 26, 1898–1920. https://doi.org/10.1002/pro.3233

Khaddaj Mallat, R., Mathew John, C., Kendrick, D.J., Braun, A.P., 2017. The vascular endothelium: A regulator of arterial tone and interface for the immune system. Critical Reviews in Clinical Laboratory Sciences 54, 458–470. https://doi.org/10.1080/10408363.2017.1394267

Khan, S., Maitra, A., Hissaria, P., Roy, S., Padukudru Anand, M., Nag, N., Singh, H., 2013. Chronic Urticaria: Indian Context—Challenges and Treatment

Options. Dermatology Research and Practice 2013, 1–8. https://doi.org/10.1155/2013/651737

Kilpatrick, B.S., Eden, E.R., Hockey, L.N., Yates, E., Futter, C.E., Patel, S., 2017. An Endosomal NAADP-Sensitive Two-Pore Ca 2+ Channel Regulates ER-Endosome Membrane Contact Sites to Control Growth Factor Signalling. Cell Reports 18, 1636–1645. https://doi.org/10.1016/j.celrep.2017.01.052

Kim, J.T., Kim, H.S., Chun, Y.H., Yoon, J., Kim, H.H., 2020. Effect of multi-ethnicity and ancestry on prevalence of allergic disease. Journal of Microbiology, Immunology, and Infection 53, 640–646. https://doi.org/10.1016/j.jmii.2018.10.004

Knipe, L., Meli, A., Hewlett, L., Bierings, R., Dempster, J., Skehel, P., Hannah, M.J., Carter, T., 2010. A revised model for the secretion of tPA and cytokines from cultured endothelial cells. Blood 116, 2183–2191. https://doi.org/10.1182/blood-2010-03-276170

Knop, M., Aareskjold, E., Bode, G., Gerke, V., 2004. Rab3D and annexin A2 play a role in regulated secretion of vWF, but not tPA, from endothelial cells. EMBO Journal 23, 2982–2992. https://doi.org/10.1038/sj.emboj.7600319

Kuo, I.Y., Ehrlich, B.E., 2015. Signaling in muscle contraction. Cold Spring Harbour Perspectives in Biology 7, a006023. https://doi.org/10.1101/cshperspect.a006023

Lane, D.A., Philippou, H., Huntington, J.A., 2005. Directing thrombin. Blood 106, 2605–2612. https://doi.org/10.1182/blood-2005-04-1710

Larisch, N., Kirsch, S.A., Schambony, A., Studtrucker, T., Böckmann, R.A., Dietrich, P., 2016. The function of the two-pore channel TPC1 depends on dimerization of its carboxy-terminal helix. Cell and Molecular Life Science. 73, 2565–2581. https://doi.org/10.1007/s00018-016-2131-3

Lee, H.C., 2005. Nicotinic Acid Adenine Dinucleotide Phosphate (NAADP)-mediated Calcium Signalling. Journal of Biological Chemistry 280, 33693–33696. https://doi.org/10.1074/jbc.R500012200

Lee, H.C., Aarhus, R., 1995a. A Derivative of NADP Mobilizes Calcium Stores Insensitive to Inositol Trisphosphate and Cyclic ADP-ribose. Journal of Biological Chemistry 270, 2152–2157. https://doi.org/10.1074/jbc.270.5.2152

Leung, K.F., Baron, R., Seabra, M.C., 2006. Thematic review series: lipid posttranslational modifications. geranylgeranylation of Rab GTPases. Journal of Lipid Research 47, 467–475. https://doi.org/10.1194/jlr.R500017-JLR200

Li, G., Li, P.-L., 2021. Lysosomal TRPML1 Channel: Implications in Cardiovascular and Kidney Diseases, in: Zhou, L. (Ed.), Ion Channels in Biophysics and Physiology, Advances in Experimental Medicine and Biology. Springer Nature Singapore, Singapore, pp. 275–301. https://doi.org/10.1007/978-981-16-4254-8_13

Li, P., Gu, M., Xu, H., 2019a. Lysosomal Ion Channels as Decoders of Cellular Signals. Trends in Biochemical Sciences 44, 110–124. https://doi.org/10.1016/j.tibs.2018.10.006

Li, Y., Xu, S., Mihaylova, M.M., Zheng, B., Hou, X., Jiang, B., Park, O., Luo, Z., Lefai, E., Shyy, J.Y.-J., Gao, B., Wierzbicki, M., Verbeuren, T.J., Shaw, R.J., Cohen, R.A., Zang, M., 2011. AMPK Phosphorylates and Inhibits SREBP Activity to Attenuate Hepatic Steatosis and Atherosclerosis in Diet-Induced Insulin-Resistant Mice. Cell Metabolism 13, 376–388. https://doi.org/10.1016/j.cmet.2011.03.009

Linton, M.F., Yancey, P.G., Davies, S.S., Jerome, W.G., Linton, E.F., Song, W.L., Doran, A.C., Vickers, K.C., 2000. The Role of Lipids and Lipoproteins in Atherosclerosis, in: Feingold, K.R., Anawalt, B., Blackman, M.R., Boyce, A., Chrousos, G., Corpas, E., de Herder, W.W., Dhatariya, K., Dungan, K., Hofland, J., Kalra, S., Kaltsas, G., Kapoor, N., Koch, C., Kopp, P., Korbonits, M., Kovacs, C.S., Kuohung, W., Laferrère, B., Levy, M., McGee, E.A., McLachlan, R., New, M., Purnell, J., Sahay, R., Shah, A.S., Singer, F., Sperling, M.A., Stratakis, C.A., Trence, D.L., Wilson, D.P. (Eds.), Endotext. MDText.com, Inc., South Dartmouth (MA).

Lin-Moshier, Y., Keebler, M.V., Hooper, R., Boulware, M.J., Liu, X., Churamani, D., Abood, M.E., Walseth, T.F., Brailoiu, E., Patel, S., Marchant, J.S., 2014. The

Two-pore channel (TPC) interactome unmasks isoform-specific roles for TPCs in endolysosomal morphology and cell pigmentation. Proceedings of the National Academy of Sciences U.S.A. 111, 13087–13092. https://doi.org/10.1073/pnas.1407004111

Liu, T., Liu, X., Li, W., 2016. Tetrandrine, a Chinese plant-derived alkaloid, is a potential candidate for cancer chemotherapy. Oncotarget 7, 40800–40815. https://doi.org/10.18632/oncotarget.8315

Lobov, I.B., Brooks, P.C., Lang, R.A., 2002. Angiopoietin-2 displays VEGF-dependent modulation of capillary structure and endothelial cell survival in vivo. Proceeding of the National Academy of Sciences U S A 99, 11205–11210. https://doi.org/10.1073/pnas.172161899

Lock, J.T., Parker, I., 2020. IP3 mediated global Ca^{2+} signals arise through two temporally and spatially distinct modes of Ca^{2+} release. eLife 9, e55008. https://doi.org/10.7554/eLife.55008

Loo, W.Y., Tee, Y.C., Han, W.H., Faheem, N.A.A., Yong, S.S., Kwan, Z., Pok, L.S.L., Yahya, F., 2024. Predictive factors of psoriatic arthritis in a diverse population with psoriasis. Journal of International Medical Research 52, 03000605231221014. https://doi.org/10.1177/03000605231221014

Lopes da Silva, M., Cutler, D.F., 2016. von Willebrand factor multimerization and the polarity of secretory pathways in endothelial cells. Blood 128, 277–285. https://doi.org/10.1182/blood-2015-10-677054

López, J.J., Dionisio, N., Berna-Erro, A., Galán, C., Salido, G.M., Rosado, J.A., 2012. Two-pore channel 2 (TPC2) modulates store-operated Ca^{2+} entry. Biochimica et Biophysica Acta (BBA) - Molecular Cell Research 1823, 1976–1983. https://doi.org/10.1016/j.bbamcr.2012.08.002

Lopez, J.J., Jardin, I., Albarrán, L., Sanchez-Collado, J., Cantonero, C., Salido, G.M., Smani, T., Rosado, J.A., 2020. Molecular Basis and Regulation of Store-Operated Calcium Entry, in: Islam, Md.S. (Ed.), Calcium Signalling. Springer International Publishing, Cham, pp. 445–469. https://doi.org/10.1007/978-3-030-12457-1_17

Lugano, R., Ramachandran, M., Dimberg, A., 2020. Tumor angiogenesis: causes, consequences, challenges, and opportunities. Cell Molecular Life Science 77, 1745–1770. https://doi.org/10.1007/s00018-019-03351-7

Luo, G.-P., Ni, B., Yang, X., Wu, Y.-Z., 2012. von Willebrand Factor: More Than a Regulator of Hemostasis and Thrombosis. Acta Haematologica 128, 158–169. https://doi.org/10.1159/000339426

Luzio, J.P., Hackmann, Y., Dieckmann, N.M.G., Griffiths, G.M., 2014. The biogenesis of lysosomes and lysosome-related organelles. Cold Spring Harb Perspectives in Biology 6, a016840. https://doi.org/10.1101/cshperspect.a016840

MacGregor, G.A., 1977. Painless thyroiditis. British Medical Journal 2, 1026. https://doi.org/10.1136/bmj.2.6093.1026-a

Mallmann, R.T., Klugbauer, N., 2020. Genetic Inactivation of Two-Pore Channel 1 Impairs Spatial Learning and Memory. Behavioural Genetics 50, 401–410. https://doi.org/10.1007/s10519-020-10011-1

Maruta, Y., Fukuda, M., 2022. Large Rab GTPase Rab44 regulates microtubule-dependent retrograde melanosome transport in melanocytes. Journal of Biological Chemistry 298, 102508. https://doi.org/10.1016/j.jbc.2022.102508

McEver, R.P., 2015. Selectins: initiators of leucocyte adhesion and signalling at the vascular wall. Cardiovasc Research 107, 331–339. https://doi.org/10.1093/cvr/cvv154

McGill, H.C., McMahan, C.A., Herderick, E.E., Malcom, G.T., Tracy, R.E., Strong, J.P., 2000. Origin of atherosclerosis in childhood and adolescence. The American Journal of Clinical Nutrition 72, 1307s–1315s. https://doi.org/10.1093/ajcn/72.5.1307s

Merten, M., Thiagarajan, P., 2000. P-Selectin Expression on Platelets Determines Size and Stability of Platelet Aggregates. Circulation 102, 1931–1936. https://doi.org/10.1161/01.CIR.102.16.1931

Michaux, G., Pullen, T.J., Haberichter, S.L., Cutler, D.F., 2006. P-selectin binds to the D′-D3 domains of von Willebrand factor in Weibel-Palade bodies. Blood 107, 3922–3924. https://doi.org/10.1182/blood-2005-09-3635

Middleton, R., Gao, D., Thomas, A., Singh, B., Au, A., Wong, J.J.-L., Bomane, A., Cosson, B., Eyras, E., Rasko, J.E.J., Ritchie, W., 2017. IRFinder: assessing the impact of intron retention on mammalian gene expression. Genome Biology 18, 51. https://doi.org/10.1186/s13059-017-1184-4

Mietkowska, M., Schuberth, C., Wedlich-Söldner, R., Gerke, V., 2019. Actin dynamics during Ca^{2+}-dependent exocytosis of endothelial Weibel-Palade bodies. Biochimica et Biophysica Acta (BBA) - Molecular Cell Research 1866, 1218–1229. https://doi.org/10.1016/j.bbamcr.2018.11.010

Miteva, K.T., Pedicini, L., Wilson, L.A., Jayasinghe, I., Slip, R.G., Marszalek, K., Gaunt, H.J., Bartoli, F., Deivasigamani, S., Sobradillo, D., Beech, D.J., McKeown, L., 2019. Rab46 integrates Ca^{2+} and histamine signalling to regulate selective cargo release from Weibel-Palade bodies. Journal of Cell Biology 218, 2232–2246. https://doi.org/10.1083/jcb.201810118

Mojzisch, A., Brehm, M.A., 2021. The Manifold Cellular Functions of von Willebrand Factor. Cells 10, 2351. https://doi.org/10.3390/cells10092351

Montero, M., Alonso, M.T., Albillos, A., García-Sancho, J., Alvarez, J., 2001. Mitochondrial Ca^{2+} -induced Ca^{2+} Release Mediated by the Ca^{2+} Uniporter. MBoC 12, 63–71. https://doi.org/10.1091/mbc.12.1.63

Morgan, A.J., Martucci, L.L., Davis, L.C., Galione, A., 2022. Two-pore channels: going with the flows. Biochemical Society Transactions 50, 1143–1155. https://doi.org/10.1042/BST20220229

Morgan, A.J., Platt, F.M., Lloyd-Evans, E., Galione, A., 2011. Molecular mechanisms of endolysosomal Ca^{2+} signalling in health and disease. Biochemical Journal 439, 349–378. https://doi.org/10.1042/BJ20110949

Müller, M.P., Goody, R.S., 2018. Molecular control of Rab activity by GEFs, GAPs and GDI. Small GTPases 9, 5–21. https://doi.org/10.1080/21541248.2016.1276999

Müller, M., Gerndt, S., Chao, Y.-K., Zisis, T., Nguyen, O.N.P., Gerwien, A., Urban, N., Müller, C., Gegenfurtner, F.A., Geisslinger, F., Ortler, C., Chen, C.-C., Zahler, S., Biel, M., Schaefer, M., Grimm, C., Bracher, F., Vollmar, A.M., Bartel, K., 2021. Gene editing and synthetically accessible inhibitors reveal role for TPC2 in HCC cell proliferation and tumor growth. Cell Chemical Biology 28, 1119-1131.e27. https://doi.org/10.1016/j.chembiol.2021.01.023

Mussbacher, M., Schossleitner, K., Kral-Pointner, J.B., Salzmann, M., Schrammel, A., Schmid, J.A., 2022. More than Just a Monolayer: The Multifaceted Role of Endothelial Cells in the Pathophysiology of Atherosclerosis. Current Atherosclerosis Reports 24, 483–492. https://doi.org/10.1007/s11883-022-01023-9

Nair, V., Sankaranarayanan, R., Vasavada, A.R., 2021. Deciphering the association of intronic single nucleotide polymorphisms of crystallin gene family with congenital cataract. Indian Journal of Ophthalmology 69, 2064–2070. https://doi.org/10.4103/ijo.IJO_3062_20

Naylor, E., Arredouani, A., Vasudevan, S.R., Lewis, A.M., Parkesh, R., Mizote, A., Rosen, D., Thomas, J.M., Izumi, M., Ganesan, A., Galione, A., Churchill, G.C., 2009. Identification of a chemical probe for NAADP by virtual screening. Nature Chemical Biology 5, 220–226. https://doi.org/10.1038/nchembio.150

Negri, S., Faris, P., Moccia, F., 2021. Endolysosomal Ca^{2+} signaling in cardiovascular health and disease, in: International Review of Cell and Molecular Biology. Elsevier, pp. 203–269. https://doi.org/10.1016/bs.ircmb.2021.03.001

Nelson, M.R., Thulin, E., Fagan, P.A., Forsén, S., Chazin, W.J., 2002a. The EF-hand domain: A globally cooperative structural unit. Protein Science 11, 198–205. https://doi.org/10.1110/ps.33302

Ng, C., Motto, D.G., Di Paola, J., 2015. Diagnostic approach to von Willebrand disease. Blood 125, 2029–2037. https://doi.org/10.1182/blood-2014-08-528398

Nguyen, T.T.N., Koerdt, S.N., Gerke, V., 2020. Plasma membrane phosphatidylinositol (4,5)-bisphosphate promotes Weibel-Palade body

exocytosis. Life Science Alliance 3, e202000788. https://doi.org/10.26508/lsa.202000788

Nightingale, T.D., Pattni, K., Hume, A.N., Seabra, M.C., Cutler, D.F., 2009. Rab27a and MyRIP regulate the amount and multimeric state of vWF released from endothelial cells. Blood 113, 5010–5018. https://doi.org/10.1182/blood-2008-09-181206

Nightingale, T., Cutler, D., 2013. The secretion of von Willebrand factor from endothelial cells; an increasingly complicated story. Journal of Thrombosis and Haemostasis 11, 192–201. https://doi.org/10.1111/jth.12225

Noguromi, M., Yamaguchi, Y., Sato, K., Oyakawa, S., Okamoto, K., Murata, H., Tsukuba, T., Kadowaki, T., 2023. Rab44 Deficiency Induces Impaired Immune Responses to Nickel Allergy. International Journal of Molecular Sciences 24, 994. https://doi.org/10.3390/ijms24020994

Nohria, A., Garrett, L., Johnson, W., Kinlay, S., Ganz, P., Creager, M.A., 2003. Endothelin-1 and Vascular Tone in Subjects with Atherogenic Risk Factors. Hypertension 42, 43–48. https://doi.org/10.1161/01.HYP.0000074426.71392.D8

Ogawa, K., Kadowaki, T., Tokuhisa, M., Yamaguchi, Y., Umeda, M., Tsukuba, T., 2020. Role of the EF-hand and coiled-coil domains of human Rab44 in localisation and organelle formation. Science Reports 10, 19149. https://doi.org/10.1038/s41598-020-75897-7

Ong, K.L., Stafford, L.K., McLaughlin, S.A., Boyko, E.J., Vollset, S.E., Smith, A.E., Dalton, B.E., Duprey, J., Cruz, J.A., Hagins, H., Lindstedt, P.A., Aali, A., Abate, Y.H., Abate, M.D., Abbasian, M., Abbasi-Kangevari, Z., Abbasi-Kangevari, M., Abd ElHafeez, S., Abd-Rabu, R., Abdulah, D.M., Abdullah, A.Y.M., Abedi, V., Abidi, H., Aboagye, R.G., Abolhassani, H., Abu-Gharbieh, E., Abu-Zaid, A., Adane, T.D., Adane, et al. 2023. Global, regional, and national burden of diabetes from 1990 to 2021, with projections of prevalence to 2050: a systematic analysis for the Global Burden of Disease Study 2021. The Lancet 402, 203–234. https://doi.org/10.1016/S0140-6736(23)01301-6

Pafumi, I., Favia, A., Gambara, G., Papacci, F., Ziparo, E., Palombi, F., Filippini, A., 2015. Regulation of Angiogenic Functions by Angiopoietins through Calcium-

Dependent Signaling Pathways. Biomed Res Int 2015, 965271. https://doi.org/10.1155/2015/965271

Palsuledesai, C.C., Distefano, M.D., 2015. Protein prenylation: enzymes, therapeutics, and biotechnology applications. ACS Chemical Biology 10, 51–62. https://doi.org/10.1021/cb500791f

Park, S., Ahuja, M., Kim, M.S., Brailoiu, G.C., Jha, A., Zeng, M., Baydyuk, M., Wu, L., Wassif, C.A., Porter, F.D., Zerfas, P.M., Eckhaus, M.A., Brailoiu, E., Shin, D.M., Muallem, S., 2016. Fusion of lysosomes with secretory organelles leads to uncontrolled exocytosis in the lysosomal storage disease mucolipidosis type IV. EMBO Reports 17, 266–278. https://doi.org/10.15252/embr.201541542

Patel, S., Ramakrishnan, L., Rahman, T., Hamdoun, A., Marchant, J.S., Taylor, C.W., Brailoiu, E., 2011. The endo-lysosomal system as an NAADP-sensitive acidic Ca^{2+} store: Role for the two-pore channels. Cell Calcium 50, 157–167. https://doi.org/10.1016/j.ceca.2011.03.011

Patel, S., Yuan, Y., Chen, C.-C., Jaślan, D., Gunaratne, G., Grimm, C., Rahman, T., Marchant, J.S., 2022a. Electrophysiology of Endolysosomal Two-Pore Channels: A Current Account. Cells 11, 2368. https://doi.org/10.3390/cells11152368

Patel, S., Yuan, Y., Gunaratne, G.S., Rahman, T., Marchant, J.S., 2022b. Activation of endo-lysosomal two-pore channels by NAADP and PI(3,5)P2. Five things to know. Cell Calcium 103, 102543. https://doi.org/10.1016/j.ceca.2022.102543

Patel, S., Zissimopoulos, S., Marchant, J.S., 2023. Endo-Lysosomal Two-Pore Channels and Their Protein Partners. Handbook of Experimental Pharmacology 278, 199–214. https://doi.org/10.1007/164_2022_601

Pedicini, L., Smith, J., Savic, S., McKeown, L., 2024. Rab46: a novel player in mast cell function. Discovery Immunology 3, kyad028. https://doi.org/10.1093/discim/kyad028

Pedicini, L., Wiktor, S.D., Simmons, K.J., Money, A., McKeown, L., 2021. Affinity-based proteomics reveals novel binding partners for Rab46 in

endothelial cells. Science Reports 11, 4054. https://doi.org/10.1038/s41598-021-83560-y

Petersen, O.H., Fedirko, N.V., 2001. Calcium signalling: Store-operated channel found at last. Current Biology 11, R520–R523. https://doi.org/10.1016/S0960-9822(01)00309-8

Pitt, S.J., Funnell, T.M., Sitsapesan, M., Venturi, E., Rietdorf, K., Ruas, M., Ganesan, A., Gosain, R., Churchill, G.C., Zhu, M.X., Parrington, J., Galione, A., Sitsapesan, R., 2010. TPC2 Is a Novel NAADP-sensitive Ca^{2+} Release Channel, Operating as a Dual Sensor of Luminal pH and Ca^{2+}. Journal of Biological Chemistry 285, 35039–35046. https://doi.org/10.1074/jbc.M110.156927

Pitt, S.J., Lam, A.K.M., Rietdorf, K., Galione, A., Sitsapesan, R., 2014. Reconstituted Human TPC1 Is a Proton-Permeable Ion Channel and Is Activated by NAADP or Ca^{2+}. Science Signalling. 7. https://doi.org/10.1126/scisignal.2004854

Pols, M.S., Ten Brink, C., Gosavi, P., Oorschot, V., Klumperman, J., 2013. The HOPS Proteins hVps41 and hVps39 Are Required for Homotypic and Heterotypic Late Endosome Fusion. Traffic 14, 219–232. https://doi.org/10.1111/tra.12027

Poznyak, A., Grechko, A.V., Poggio, P., Myasoedova, V.A., Alfieri, V., Orekhov, A.N., 2020a. The Diabetes Mellitus–Atherosclerosis Connection: The Role of Lipid and Glucose Metabolism and Chronic Inflammation. International Journal of Molecular Sciences 21, 1835. https://doi.org/10.3390/ijms21051835

Prashar, A., Schnettger, L., Bernard, E.M., Gutierrez, M.G., 2017. Rab GTPases in Immunity and Inflammation. Frontiers in Cell Infectious Microbiology 7, 435. https://doi.org/10.3389/fcimb.2017.00435

Pruimboom, L., 2011. Physical inactivity is a disease synonymous for a non-permissive brain disorder. Medical Hypotheses 77, 708–713. https://doi.org/10.1016/j.mehy.2011.07.022

Puertollano, R., Kiselyov, K., 2009. TRPMLs: in sickness and in health. American Journal of Physiology-Renal Physiology 296, F1245–F1254. https://doi.org/10.1152/ajprenal.90522.2008

Pylypenko, O., Hammich, H., Yu, I.-M., Houdusse, A., 2018. Rab GTPases and their interacting protein partners: Structural insights into Rab functional diversity. Small GTPases 9, 22–48. https://doi.org/10.1080/21541248.2017.1336191

Rahman, T., Cai, X., Brailoiu, G.C., Abood, M.E., Brailoiu, E., Patel, S., 2014a. Two-pore channels provide insight into the evolution of voltage-gated Ca^{2+} and Na^{+} channels. Science Signalling. 7. https://doi.org/10.1126/scisignal.2005450

Rajendran, P., Rengarajan, T., Thangavel, J., Nishigaki, Y., Sakthisekaran, D., Sethi, G., Nishigaki, I., 2013a. The vascular endothelium and human diseases. International Journal of Biological Sciences 9, 1057–1069. https://doi.org/10.7150/ijbs.7502

Rathnakumar, K., Savant, S., Giri, H., Ghosh, A., Fisslthaler, B., Fleming, I., Ram, U., Bera, A.K., Augustin, H.G., Dixit, M., 2016. Angiopoietin-2 mediates thrombin-induced monocyte adhesion and endothelial permeability. Journal of Thrombosis and Haemostasis 14, 1655–1667. https://doi.org/10.1111/jth.13376

Rondaij, M.G., Sellink, E., Gijzen, K.A., ten Klooster, J.P., Hordijk, P.L., van Mourik, J.A., Voorberg, J., 2004. Small GTP-binding protein Ral is involved in cAMP-mediated release of von Willebrand factor from endothelial cells. Arteriosclerosis Thrombosis and Vascular Biology 24, 1315–1320. https://doi.org/10.1161/01.ATV.0000131267.13425.45

Rosen, D., Lewis, A.M., Mizote, A., Thomas, J.M., Aley, P.K., Vasudevan, S.R., Parkesh, R., Galione, A., Izumi, M., Ganesan, A., Churchill, G.C., 2009. Analogues of the Nicotinic Acid Adenine Dinucleotide Phosphate (NAADP) Antagonist Ned-19 Indicate Two Binding Sites on the NAADP Receptor. Journal of Biological Chemistry 284, 34930–34934. https://doi.org/10.1074/jbc.M109.016519

Ruas, M., Chuang, K.-T., Davis, L.C., Al-Douri, A., Tynan, P.W., Tunn, R., Teboul, L., Galione, A., Parrington, J., 2014. TPC1 Has Two Variant Isoforms, and Their Removal Has Different Effects on Endo-Lysosomal Functions

Compared to Loss of TPC2. Molecular and Cellular Biology 34, 3981–3992. https://doi.org/10.1128/MCB.00113-14

Russo, T.A., Banuth, A.M.M., Nader, H.B., Dreyfuss, J.L., 2020. Altered shear stress on endothelial cells leads to remodeling of extracellular matrix and induction of angiogenesis. PLoS ONE 15, e0241040. https://doi.org/10.1371/journal.pone.0241040

Rusu, L., Minshall, R.D., 2018. Endothelial Cell von Willebrand Factor Secretion in Health and Cardiovascular Disease, in: Lenasi, H. (Ed.), Endothelial Dysfunction - Old Concepts and New Challenges. InTech. https://doi.org/10.5772/intechopen.74029

Rybalchenko, V., Ahuja, M., Coblentz, J., Churamani, D., Patel, S., Kiselyov, K., Muallem, S., 2012. Membrane Potential Regulates Nicotinic Acid Adenine Dinucleotide Phosphate (NAADP) Dependence of the pH- and Ca^{2+}-sensitive Organellar Two-pore Channel TPC1. Journal of Biological Chemistry 287, 20407–20416. https://doi.org/10.1074/jbc.M112.359612

Saftig, P., Schröder, B., Blanz, J., 2010a. Lysosomal membrane proteins: life between acid and neutral conditions. Biochemical Society Transactions 38, 1420–1423. https://doi.org/10.1042/BST0381420

Saharinen, P., Eklund, L., Alitalo, K., 2017. Therapeutic targeting of the angiopoietin–TIE pathway. Nature Reviews Drug Discovery 16, 635–661. https://doi.org/10.1038/nrd.2016.278

Sakurai, Y., Kolokoltsov, A.A., Chen, C.-C., Tidwell, M.W., Bauta, W.E., Klugbauer, N., Grimm, C., Wahl-Schott, C., Biel, M., Davey, R.A., 2015. Ebola virus. Two-pore channels control Ebola virus host cell entry and are drug targets for disease treatment. Science 347, 995–998. https://doi.org/10.1126/science.1258758

Samie, M., Xu, H., 2011. Studying TRP Channels in Intracellular Membranes, in: Zhu, M.X. (Ed.), TRP Channels. CRC Press/Taylor & Francis, Boca Raton (FL).

Sandoo, A., van Zanten, J.J.C.S.V., Metsios, G.S., Carroll, D., Kitas, G.D., 2010. The endothelium and its role in regulating vascular tone. Open Cardiovascular Medicine Journal 4, 302–312. https://doi.org/10.2174/1874192401004010302

Schiffrin, E., 2001. Role of endothelin-1 in hypertension and vascular disease. American Journal of Hypertension 14, S83–S89. https://doi.org/10.1016/S0895-7061(01)02074-X

Schillemans, M., Karampini, E., Kat, M., Bierings, R., 2019. Exocytosis of Weibel-Palade bodies: how to unpack a vascular emergency kit. Journal of Thrombosis and Haemostasis 17, 6–18. https://doi.org/10.1111/jth.14322

Schillemans, Maaike, Kat, M., Westeneng, J., Gangaev, A., Hofman, M., Nota, B., van Alphen, F.P.J., de Boer, M., van den Biggelaar, M., Margadant, C., Voorberg, J., Bierings, R., 2019. Alternative trafficking of Weibel-Palade body proteins in CRISPR/Cas9-engineered von Willebrand factor–deficient blood outgrowth endothelial cells. Research and Practice in Thrombosis and Haemostasis 3, 718–732. https://doi.org/10.1002/rth2.12242

Schmiege, P., Fine, M., Blobel, G., Li, X., 2017. Human TRPML1 channel structures in open and closed conformations. Nature 550, 366–370. https://doi.org/10.1038/nature24036

Scholz, A., Lang, V., Henschler, R., Czabanka, M., Vajkoczy, P., Chavakis, E., Drynski, J., Harter, P.N., Mittelbronn, M., Dumont, D.J., Plate, K.H., Reiss, Y., 2011. Angiopoietin-2 promotes myeloid cell infiltration in a β_2-integrin-dependent manner. Blood 118, 5050–5059. https://doi.org/10.1182/blood-2011-03-343293

Shasby, D.M., Ries, D.R., Shasby, S.S., Winter, M.C., 2002. Histamine stimulates phosphorylation of adherens junction proteins and alters their link to vimentin. American Journal of Physiology Lung Cell Molecular Physiology 282, L1330-1338. https://doi.org/10.1152/ajplung.00329.2001

Shastry, B.S., 2009. SNPs: Impact on Gene Function and Phenotype, in: Komar, A.A. (Ed.), Single Nucleotide Polymorphisms, Methods in Molecular Biology. Humana Press, Totowa, NJ, pp. 3–22. https://doi.org/10.1007/978-1-60327-411-1_1

Shen, L.X., Basilion, J.P., Stanton, V.P., 1999. Single-nucleotide polymorphisms can cause different structural folds of mRNA. Proceedings of the National Academy of Sciences U.S.A. 96, 7871–7876. https://doi.org/10.1073/pnas.96.14.7871

Shim, W.S.N., Ho, I.A.W., Wong, P.E.H., 2007a. Angiopoietin: A TIE(d) Balance in Tumor Angiogenesis. Molecular Cancer Research 5, 655–665. https://doi.org/10.1158/1541-7786.MCR-07-0072

Shinde, S.R., Maddika, S., 2018. Post translational modifications of Rab GTPases. Small GTPases 9, 49–56. https://doi.org/10.1080/21541248.2017.1299270

Shintani, M., Tada, M., Kobayashi, T., Kajiho, H., Kontani, K., Katada, T., 2007. Characterization of Rab45/RASEF containing EF-hand domain and a coiled-coil motif as a self-associating GTPase. Biochemical Biophysical Research Communications 357, 661–667. https://doi.org/10.1016/j.bbrc.2007.03.206

Srikanth, S., Jung, H.-J., Kim, K.-D., Souda, P., Whitelegge, J., Gwack, Y., 2010. A novel EF-hand protein, CRACR2A, is a cytosolic Ca^{2+} sensor that stabilizes CRAC channels in T cells. Nature Cell Biology 12, 436–446. https://doi.org/10.1038/ncb2045

Srikanth, S., Woo, J.S., Gwack, Y., 2017. A large Rab GTPase family in a small GTPase world. Small GTPases 8, 43–48. https://doi.org/10.1080/21541248.2016.1192921

Stenmark, H., 2009. Rab GTPases as coordinators of vesicle traffic. Nature Reviews Molecular Cell Biology 10, 513–525. https://doi.org/10.1038/nrm2728

Stenmark, H., Olkkonen, V.M., 2001. The Rab GTPase Family. Genome Biology 2, reviews3007.1. https://doi.org/10.1186/gb-2001-2-5-reviews3007

Suárez-Cortés, P., Gambara, G., Favia, A., Palombi, F., Alano, P., Filippini, A., 2017. Ned-19 inhibition of parasite growth and multiplication suggests a role for NAADP mediated signalling in the asexual development of Plasmodium falciparum. Malaria Journal 16, 366. https://doi.org/10.1186/s12936-017-2013-7

Terrar, D.A., 2022. Endolysosomal calcium release and cardiac physiology. Cell Calcium 104, 102565. https://doi.org/10.1016/j.ceca.2022.102565

Texier, A., Lenting, P.J., Denis, C.V., Roullet, S., Christophe, O.D., 2023a. Angiopoietin-2 binds to multiple interactive sites within von Willebrand factor. Research and Practice in Thrombosis and Haemostasis 7, 102204. https://doi.org/10.1016/j.rpth.2023.102204

Thakore, P., Pritchard, H.A.T., Griffin, C.S., Yamasaki, E., Drumm, B.T., Lane, C., Sanders, K.M., Feng Earley, Y., Earley, S., 2020. TRPML1 channels initiate Ca^{2+} sparks in vascular smooth muscle cells. Science Signalling. 13, eaba1015. https://doi.org/10.1126/scisignal.aba1015

Thillaiappan, N.B., Chavda, A.P., Tovey, S.C., Prole, D.L., Taylor, C.W., 2017. Ca^{2+} signals initiate at immobile IP3 receptors adjacent to ER-plasma membrane junctions. Nature Communications 8, 1505. https://doi.org/10.1038/s41467-017-01644-8

Tirapelli, C.R., Fukada, S.Y., De Godoy, M.A.F., De Oliveira, A.M., 2006. Analysis of the mechanisms underlying the vasorelaxant action of angiotensin II in the isolated rat carotid. Life Sciences 78, 2676–2682. https://doi.org/10.1016/j.lfs.2005.10.031

Titus A, Marappa-Ganeshan R. Physiology, Endothelin. [Updated 2023 May 1]. In: StatPearls [Internet]. Treasure Island (FL): StatPearls Publishing; 2025 Jan-. Available from: https://www.ncbi.nlm.nih.gov/books/NBK551627/

Traylor, M., Curtis, C., Patel, H., Breen, G., Hyuck Lee, S., Xu, X., Newhouse, S., Dobson, R., Steer, S., Cope, A.P., Markus, H.S., Lewis, C.M., Scott, I.C., 2017. Genetic and environmental risk factors for rheumatoid arthritis in a UK African ancestry population: the GENRA case–control study. Rheumatology 56, 1282–1292. https://doi.org/10.1093/rheumatology/kex048

Valentijn, K.M., Valentijn, J.A., Jansen, K.A., Koster, A.J., A new look at Weibel-Palade body structure in endothelial cells using electron tomography., Journal of Structural Biology, 2008, vol. 161 3(pg. 447-458)

Valentijn, K.M., Sadler, J.E., Valentijn, J.A., Voorberg, J., Eikenboom, J., 2011. Functional architecture of Weibel-Palade bodies. Blood 117, 5033–5043. https://doi.org/10.1182/blood-2010-09-267492

Van Breevoort, D., Van Agtmaal, E.L., Dragt, B.S., Gebbinck, J.K., Dienava-Verdoold, I., Kragt, A., Bierings, R., Horrevoets, A.J.G., Valentijn, K.M., Eikenboom, J.C., Fernandez-Borja, M., Meijer, A.B., Voorberg, J., 2012. Proteomic Screen Identifies IGFBP7 as a Novel Component of Endothelial Cell-Specific Weibel-Palade Bodies. Journal of Proteome Research. 11, 2925–2936. https://doi.org/10.1021/pr300010r

Vandendries, E., Furie, Barbara, Furie, Bruce, 2004. Role of P-selectin and PSGL-1 in coagulation and thrombosis. Journal of Thrombosis and Haemostasis 92, 459–466. https://doi.org/10.1160/TH04-05-0306

Van Hinsbergh, V.W.M., 2012. Endothelium—role in regulation of coagulation and inflammation. Semin Immunopathology 34, 93–106. https://doi.org/10.1007/s00281-011-0285-5

Venkatachalam, K., Van Rossum, D.B., Patterson, R.L., Ma, H.-T., Gill, D.L., 2002. The cellular and molecular basis of store-operated calcium entry. Nature Cell Biology 4, E263–E272. https://doi.org/10.1038/ncb1102-e263

Vigil, D., Cherfils, J., Rossman, K.L., Der, C.J., 2010. Ras superfamily GEFs and GAPs: validated and tractable targets for cancer therapy? Nature Reviews Cancer 10, 842–857. https://doi.org/10.1038/nrc2960

Wagner, D.D., Saffaripour, S., Bonfanti, R., Sadler, J.E., Cramer, E.M., Chapman, B., Mayadas, T.N., 1991. Induction of specific storage organelles by von Willebrand factor propolypeptide. Cell 64, 403–413. https://doi.org/10.1016/0092-8674(91)90648-I

Walseth, T.F., Guse, A.H., 2021. NAADP: From Discovery to Mechanism. Frontiers in Immunology 12, 703326. https://doi.org/10.3389/fimmu.2021.703326

Wandinger-Ness, A., Zerial, M., 2014. Rab Proteins and the Compartmentalization of the Endosomal System. Cold Spring Harbor

Perspectives in Biology 6, a022616–a022616. https://doi.org/10.1101/cshperspect.a022616

Wang, X., Zhang, X., Dong, X., Samie, M., Li, X., Cheng, X., Goschka, A., Shen, D., Zhou, Y., Harlow, J., Zhu, M.X., Clapham, D.E., Ren, D., Xu, H., 2012. TPC Proteins Are Phosphoinositide- Activated Sodium-Selective Ion Channels in Endosomes and Lysosomes. Cell 151, 372–383. https://doi.org/10.1016/j.cell.2012.08.036

Waschbüsch, D., Khan, A.R., 2020. Phosphorylation of Rab GTPases in the regulation of membrane trafficking. Traffic 21, 712–719. https://doi.org/10.1111/tra.12765

Weibel, E.R., Palade, G.E., 1964. New Cytoplasmic Components In Arterial Endothelia. Journal of Cell Biology 23, 101–112. https://doi.org/10.1083/jcb.23.1.101

Wiktor, S, University of Leeds PhD Thesis, 2024, The dynamic structure of Rab46 - a novel endothelial protein

Wilson, L.A., McKeown, L., Tumova, S., Li, J., Beech, D.J., 2015. Expression of a long variant of CRACR2A that belongs to the Rab GTPase protein family in endothelial cells. Biochemical and Biophysical Research Communications 456, 398–402. https://doi.org/10.1016/j.bbrc.2014.11.095

Wong, J.J. -L., Au, A.Y.M., Ritchie, W., Rasko, J.E.J., 2016. Intron retention in mRNA: No longer nonsense: Known and putative roles of intron retention in normal and disease biology. BioEssays 38, 41–49. https://doi.org/10.1002/bies.201500117

Wu, M.D., Atkinson, T.M., Lindner, J.R., 2017. Platelets and von Willebrand factor in atherogenesis. Blood 129, 1415–1419. https://doi.org/10.1182/blood-2016-07-692673

Wu, Y.-W., Tan, K.-T., Waldmann, H., Goody, R.S., Alexandrov, K., 2007. Interaction analysis of prenylated Rab GTPase with Rab escort protein and GDP dissociation inhibitor explains the need for both regulators. Proceeding of

the National Academy of Sciences. U.S.A. 104, 12294–12299. https://doi.org/10.1073/pnas.0701817104

Xin, J., Yuan, M., Peng, Y., Wang, J., 2020. Analysis of the Deleterious Single-Nucleotide Polymorphisms Associated with Antidepressant Efficacy in Major Depressive Disorder. Frontiers in Psychiatry 11, 151. https://doi.org/10.3389/fpsyt.2020.00151

Xiong, J., Zhu, M.X., 2016. Regulation of lysosomal ion homeostasis by channels and transporters. China Life Science 59, 777–791. https://doi.org/10.1007/s11427-016-5090-x

Xu, B., Wu, Q., La, R., Lu, L., Abdu, F.A., Yin, G., Zhang, W., Ding, W., Ling, Y., He, Z., Che, W., 2024. Is systemic inflammation a missing link between cardiometabolic index with mortality? Evidence from a large population-based study. Cardiovascular Diabetology 23, 212. https://doi.org/10.1186/s12933-024-02251-w

Yamaguchi, S., Jha, A., Li, Q., Soyombo, A.A., Dickinson, G.D., Churamani, D., Brailoiu, E., Patel, S., Muallem, S., 2011. Transient Receptor Potential Mucolipin 1 (TRPML1) and Two-pore Channels Are Functionally Independent Organellar Ion Channels. Journal of Biological Chemistry 286, 22934–22942. https://doi.org/10.1074/jbc.M110.210930

Yan, Z., Cai, M., Han, X., Chen, Q., Lu, H., 2023. The Interaction Between Age and Risk Factors for Diabetes and Prediabetes: A Community-Based Cross-Sectional Study. DMSO Volume 16, 85–93. https://doi.org/10.2147/DMSO.S390857

Yang, C., Wang, X., 2021. Lysosome biogenesis: Regulation and functions. Journal of Cell Biology 220, e202102001. https://doi.org/10.1083/jcb.202102001

Yang, J., Zhao, Z., Gu, M., Feng, X., Xu, H., 2019. Release and uptake mechanisms of vesicular Ca^{2+} stores. Protein Cell 10, 8–19. https://doi.org/10.1007/s13238-018-0523-x

Yang, Y., Zhai, X., El Hiani, Y., 2020. TRPML1—Emerging Roles in Cancer. Cells 9, 2682. https://doi.org/10.3390/cells9122682

Young, M.R., 2012. Endothelial cells in the eyes of an immunologist. Cancer Immunology and Immunotherapy 61, 1609–1616. https://doi.org/10.1007/s00262-012-1335-0

Yuan, Y., Arige, V., Saito, R., Mu, Q., Brailoiu, G.C., Pereira, G.J.S., Bolsover, S.R., Keller, M., Bracher, F., Grimm, C., Brailoiu, E., Marchant, J.S., Yule, D.I., Patel, S., 2024. Two-pore channel-2 and inositol trisphosphate receptors coordinate Ca^{2+} signals between lysosomes and the endoplasmic reticulum. Cell Reports 43, 113628. https://doi.org/10.1016/j.celrep.2023.113628

Zannettino, A.C.W., Holding, C.A., Diamond, P., Atkins, G.J., Kostakis, P., Farrugia, A., Gamble, J., To, L.B., Findlay, D.M., Haynes, D.R., 2005. Osteoprotegerin (OPG) is localized to the Weibel-Palade bodies of human vascular endothelial cells and is physically associated with von Willebrand factor. Journal of Cell Physiology 204, 714–723. https://doi.org/10.1002/jcp.20354

Zhang, J., Jiang, Z., Shi, A., 2022. Rab GTPases: The principal players in crafting the regulatory landscape of endosomal trafficking. Computational Structural Biotechnology Journal 20, 4464–4472. https://doi.org/10.1016/j.csbj.2022.08.016

Zhang, X., Chen, W., Li, P., Calvo, R., Southall, N., Hu, X., Bryant-Genevier, M., Feng, X., Geng, Q., Gao, C., Yang, M., Tang, K., Ferrer, M., Marugan, J.J., Xu, H., 2019. Agonist-specific voltage-dependent gating of lysosomal two-pore Na+ channels. eLife 8, e51423. https://doi.org/10.7554/eLife.51423

Zheng, T., Huang, L., Chen, N., Xue, H., Ni, P., Huang, G., 2021. Rab25 acts as an oncogene and participates in the regulation of aerobic glycolysis via PKM2 in gastric adenocarcinoma. Translational Cancer Research 10, 790–805. https://doi.org/10.21037/tcr-20-2597

Zografou, S., Basagiannis, D., Papafotika, A., Shirakawa, R., Horiuchi, H., Auerbach, D., Fukuda, M., Christoforidis, S., 2012. Rab-genome analysis reveals novel insights in Weibel-Palade body exocytosis. Journal of Cell Science 104174. https://doi.org/10.1242/jcs.104174

Appendix

ImageJ Macro Code: Rab46 Cellular Distribution

```
imageTitle=getTitle();                    //returns a string with the image title
run("Split Channels");
selectWindow("C1-"+imageTitle);
close();
selectWindow("C2-"+imageTitle);
run("Subtract Background...", "rolling=3 sliding");
run("Duplicate...", " ");
rename("DUPLICATE");
selectWindow("C3-"+imageTitle);
rename("nuclei");
run("Command From Macro", "command=[de.csbdresden.stardist.StarDist2D],
args=['input':'nuclei', 'modelChoice':'Versatile (fluorescent nuclei)',
'normalizeInput':'true', 'percentileBottom':'1.0', 'percentileTop':'99.8',
'probThresh':'0.5', 'nmsThresh':'0.4', 'outputType':'Both', 'nTiles':'1',
'excludeBoundary':'2', 'roiPosition':'Automatic', 'verbose':'false',
'showCsbdeepProgress':'false', 'showProbAndDist':'false'], process=[false]");
selectWindow("Label Image");
setOption("ScaleConversions", true);
run("8-bit");
run("Auto Local Threshold", "method=Contrast radius=15 parameter_1=0
parameter_2=0 white");
setOption("BlackBackground", true);
```

```
run("Convert to Mask");

run("Invert LUTs");

run("Distance Map");

run("Invert LUTs");

selectWindow("C2-" +imageTitle);

//run("Brightness/Contrast...");

setMinAndMax(60, 255);

run("Apply LUT");

selectWindow("C2-" +imageTitle);

run("Auto Threshold", "method=MaxEntropy white");

run("Set Measurements...", "area mean min integrated redirect=[Label Image]
decimal=3");

selectWindow("C2-" +imageTitle);

run("Analyze Particles...", "size=0.01-Infinity display");

saveAs("Results", "\\C:\\ + imageTitle + ".txt");          // Insert file path location

close("Results");

selectWindow("C2-"+imageTitle);

run("Set Measurements...", "area mean min integrated redirect=DUPLICATE
decimal=3");

selectWindow("C2-"+imageTitle);

run("Analyze Particles...", "size=0.01-Infinity display");

saveAs("Results","\\C:\\ + imageTitle + ".txt");          // Insert file path location

close();

close("Results");

close("ROI Manager");
```

```
close("DUPLICATE");
```

ImageJ Macro Code: WPB Counts

```
imageTitle=getTitle();                    //returns a string with the image title
run("Split Channels");
selectWindow("C1-"+imageTitle)
close();
selectWindow("C2-"+imageTitle);
setOption("ScaleConversions", true);
run("8-bit");
run("Subtract Background...", "rolling=3 sliding");
run("Auto Local Threshold", "method=Bernsen radius=15 parameter_1=0
parameter_2=0 white");
run("Analyze Particles...", "size=0.1-3.00 show=Masks clear add");
run("Set Measurements...", "area perimeter feret's redirect=Nondecimal=9");
roiManager("Measure");
saveAs("Results", "C:\\Users\\umamo\\OneDrive - University of Leeds\\4-Year
PhD Project\\Flow Experiments\\"+imageTitle+".txt");
selectWindow("C2-"+imageTitle);
close();
selectWindow("Mask of C2-"+imageTitle);
close();
close("Results");
close("ROI Manager");
```

Table.1 38 SNPs significantly associated with Rab46

SNP ID	SNP ID2	SNP ID3	SNP ID4	SNP ID5
All Diseases	Ath, Pso, Rh Arth, Urt	Ath, Rh Arth	Ath, Diab, Rh Arth	Pso, Urt, Diab
rs7138453	rs56082948	rs17780600	rs3803135	rs142228158
rs887304				rs71534261
rs877554				
rs242017				
rs242018				
rs10848899				
rs12826025				
rs7297853				
rs10848894				
rs10848893				
rs887305				
rs10848906				
rs35179033				
rs11062752				
rs242016				
rs17836183				
rs11062745				
rs61907258				
rs36030417				
rs17697920				
rs71579245				
rs7299033				
rs61537702				
rs57335133				
rs17836273				
rs80119105				
rs11062767				
rs71534241				
rs76779686				
rs7350575				
rs150013368				
rs17770235				
rs9788233				

Table.2 Rab46 SNPs significantly associated with atherosclerosis

RSID	REF	ALT	LOG(OR)	P
rs7138453	T	C	0.654119	3.32E-29
rs887304	T	C	0.654151	3.32E-29
rs877554	A	T	0.654162	3.33E-29
rs242017	G	A	0.656673	5.13E-29
rs242018	C	T	0.6578	6.22E-29
rs10848899	G	A	0.665439	2.22E-28
rs12826025	G	A	0.666729	2.89E-28
rs7297853	T	C	0.680982	6.64E-28
rs10848894	T	C	0.685183	1.20E-27
rs10848893	C	T	0.679074	1.93E-27
rs887305	A	C	0.687817	7.22E-27
rs10848906	C	A	0.717167	1.11E-25
rs35179033	C	CA	0.812311	4.18E-22
rs11062752	G	C	0.834054	2.00E-21
rs242016	G	A	0.799896	3.14E-21
rs17836183	C	T	0.813104	9.87E-21
rs11062745	T	C	0.814824	1.11E-20
rs61907258	A	G	0.832045	4.46E-20
rs36030417	A	T	0.832302	4.56E-20
rs17697920	C	T	0.832522	4.63E-20
rs71579245	A	G	0.854129	5.55E-20
rs7299033	T	C	0.854189	5.88E-20
rs3803135	C	T	0.934846	9.76E-20
rs17780600	T	G	0.849241	1.52E-19
rs61537702	G	C	0.853778	2.00E-19
rs57335133	G	A	0.853862	2.01E-19
rs17836273	C	T	0.854634	2.11E-19
rs80119105	A	C	0.877523	3.29E-19
rs56082948	A	G	0.867023	3.46E-19
rs11062767	C	T	0.875525	3.48E-19
rs71534241	G	T	0.883223	5.36E-19
rs76779686	A	G	0.883752	5.61E-19
rs7350575	A	G	0.882551	6.39E-19
rs150013368	C	T	0.887578	7.25E-19
rs17770235	T	C	0.878917	7.63E-19
rs9788233	T	C	0.961322	1.68E-17
rs71579245	A	G	1.36011	0.003588
rs7299033	T	C	1.33783	0.003823
rs3803135	C	T	1.19817	0.008892

Table.3 Rab46 SNPs significantly associated with diabetes

RSID	REF	ALT	LOG(OR)	P
rs877554	A	T	0.710452	3.86E-37
rs7138453	T	C	0.710587	3.93E-37
rs242017	G	A	0.710727	4.11E-37
rs10848894	T	C	0.710758	4.13E-37
rs10848906	C	A	0.710643	4.16E-37
rs242018	C	T	0.710818	4.20E-37
rs7297853	T	C	0.711193	4.55E-37
rs887304	T	C	0.713436	7.09E-37
rs12826025	G	A	0.715744	1.22E-36
rs35179033	C	CA	0.718017	1.84E-36
rs10848893	C	T	0.718949	2.20E-36
rs10848899	G	A	0.72374	5.67E-36
rs11062752	G	C	0.72403	6.07E-36
rs887305	A	C	0.751694	9.91E-34
rs242016	G	A	0.87639	2.36E-26
rs17836183	C	T	0.883823	5.18E-26
rs11062745	T	C	0.889429	8.76E-26
rs36030417	A	T	0.897278	1.88E-25
rs61907258	A	G	0.89746	1.89E-25
rs17697920	C	T	0.900241	2.55E-25
rs7299033	T	C	0.924925	4.90E-25
rs57335133	G	A	0.925402	2.10E-24
rs3803135	C	T	0.927889	2.59E-24
rs17836273	C	T	0.927947	2.62E-24
rs80119105	A	C	0.944337	2.84E-24
rs61537702	G	C	0.928284	2.89E-24
rs71534261	C	T	0.952598	4.91E-24
rs71579245	A	G	0.9527	5.18E-24
rs142228158	G	A	0.957383	7.59E-24
rs150013368	C	T	0.96608	1.97E-23
rs76779686	A	G	0.966416	2.02E-23
rs17770235	T	C	0.958892	2.43E-23
rs7350575	A	G	0.966191	2.64E-23
rs11062767	C	T	0.971149	3.20E-23
rs9788233	T	C	1.03411	1.68E-21
rs71534241	G	T	1.06658	4.18E-21
rs71579245	A	G	1.44536	0.002442
rs71534261	C	T	1.4493	0.002527
rs71534241	G	T	1.37168	0.00285
rs142228158	G	A	1.49551	0.002944
rs7299033	T	C	1.25845	0.002982
rs80119105	A	C	1.33231	0.008085

Table.4 Rab46 SNPs significantly associated with urticaria

RSID	REF	ALT	LOG(OR)	P
rs887304	T	C	0.807214	1.51E-32
rs877554	A	T	0.807228	1.52E-32
rs7138453	T	C	0.80725	1.52E-32
rs10848894	T	C	0.807279	1.52E-32
rs10848899	G	A	0.807554	1.59E-32
rs10848893	C	T	0.807644	1.61E-32
rs11062752	G	C	0.807885	1.67E-32
rs10848906	C	A	0.808093	1.77E-32
rs242017	G	A	0.809632	2.21E-32
rs242018	C	T	0.810595	2.56E-32
rs12826025	G	A	0.810826	2.83E-32
rs887305	A	C	0.823603	1.86E-31
rs7297853	T	C	0.888979	3.12E-28
rs35179033	C	CA	0.952397	3.29E-25
rs242016	G	A	0.989066	1.81E-23
rs17836183	C	T	1.00096	4.71E-23
rs11062745	T	C	1.00271	5.22E-23
rs36030417	A	T	1.02405	2.56E-22
rs61907258	A	G	1.02409	2.57E-22
rs17697920	C	T	1.02439	2.64E-22
rs71534261	C	T	1.04885	3.14E-22
rs142228158	G	A	1.04888	3.16E-22
rs71579245	A	G	1.05398	4.47E-22
rs7299033	T	C	1.05358	4.62E-22
rs61537702	G	C	1.05398	1.76E-21
rs17836273	C	T	1.05414	1.76E-21
rs57335133	G	A	1.05432	1.80E-21
rs9788233	T	C	1.06202	2.77E-21
rs56082948	A	G	1.06926	3.24E-21
rs80119105	A	C	1.08278	3.32E-21
rs11062767	C	T	1.08092	3.57E-21
rs71534241	G	T	1.08981	5.83E-21
rs76779686	A	G	1.08993	5.93E-21
rs7350575	A	G	1.08961	7.04E-21
rs150013368	C	T	1.09449	7.84E-21
rs17770235	T	C	1.0842	8.04E-21
rs3803135	C	T	1.25096	3.46E-17
rs142228158	G	A	1.37204	0.002962
rs71534261	C	T	1.37453	0.003028
rs71579245	A	G	1.36013	0.003588
rs7299033	T	C	1.33776	0.003831

Table.5 Rab46 SNPs significantly associated with psoriasis

RSID	REF	ALT	LOG(OR)	P
rs7138453	T	C	0.81635	1.43E-33
rs10848894	T	C	0.81671	1.51E-33
rs877554	A	T	0.816715	1.51E-33
rs242017	G	A	0.816746	1.52E-33
rs35179033	C	CA	0.816937	1.59E-33
rs12826025	G	A	0.816727	1.62E-33
rs887304	T	C	0.81728	1.65E-33
rs242018	C	T	0.817296	1.65E-33
rs10848893	C	T	0.823207	4.26E-33
rs887305	A	C	0.82439	5.13E-33
rs11062752	G	C	0.826726	7.33E-33
rs7297853	T	C	0.854456	2.49E-31
rs242016	G	A	0.851059	2.75E-31
rs10848899	G	A	0.873458	3.84E-30
rs10848906	C	A	0.894885	3.39E-29
rs17836183	C	T	0.998837	3.12E-24
rs11062745	T	C	1.00479	4.98E-24
rs61907258	A	G	1.02208	1.94E-23
rs17697920	C	T	1.02415	2.27E-23
rs36030417	A	T	1.02417	2.27E-23
rs7299033	T	C	1.06124	7.77E-23
rs142228158	G	A	1.06754	1.37E-22
rs71534261	C	T	1.06774	1.37E-22
rs71579245	A	G	1.07852	2.56E-22
rs57335133	G	A	1.06415	3.54E-22
rs17836273	C	T	1.06605	4.01E-22
rs61537702	G	C	1.06673	4.31E-22
rs56082948	A	G	1.07905	6.82E-22
rs80119105	A	C	1.09546	8.38E-22
rs76779686	A	G	1.09455	8.89E-22
rs150013368	C	T	1.09718	1.05E-21
rs71534241	G	T	1.0999	1.26E-21
rs11062767	C	T	1.10047	1.41E-21
rs7350575	A	G	1.10149	1.74E-21
rs17770235	T	C	1.09532	1.92E-21
rs9788233	T	C	1.14637	6.03E-20
rs3803135	C	T	1.29136	6.64E-17
rs7299033	T	C	1.30466	0.00355
rs71579245	A	G	1.51906	0.006254
rs142228158	G	A	1.64652	0.009743
rs71534261	C	T	1.64978	0.009978

Table.6 Rab46 SNPs significantly associated with rheumatoid arthritis

RSID	REF	ALT	LOG(OR)	P
rs7138453	T	C	0.428019	7.36E-26
rs877554	A	T	0.428079	7.46E-26
rs7297853	T	C	0.428225	7.76E-26
rs10848894	T	C	0.428418	8.06E-26
rs887304	T	C	0.42874	8.67E-26
rs10848906	C	A	0.429069	9.54E-26
rs887305	A	C	0.429918	1.14E-25
rs242017	G	A	0.433706	2.67E-25
rs242018	C	T	0.435088	3.62E-25
rs17836183	C	T	0.503962	1.02E-24
rs10848899	G	A	0.443204	2.03E-24
rs12826025	G	A	0.448304	5.95E-24
rs10848893	C	T	0.450664	9.05E-24
rs3803135	C	T	0.548184	4.65E-22
rs35179033	C	CA	0.511605	1.42E-20
rs11062752	G	C	0.540144	2.86E-19
rs242016	G	A	0.520608	4.73E-19
rs11062745	T	C	0.530942	1.54E-18
rs17697920	C	T	0.537084	3.07E-18
rs36030417	A	T	0.537345	3.15E-18
rs61907258	A	G	0.53759	3.24E-18
rs71579245	A	G	0.558768	7.15E-18
rs7299033	T	C	0.558734	7.50E-18
rs17780600	T	G	0.553863	1.61E-17
rs61537702	G	C	0.555675	1.80E-17
rs57335133	G	A	0.555809	1.83E-17
rs17836273	C	T	0.556116	1.87E-17
rs9788233	T	C	0.609975	2.12E-17
rs80119105	A	C	0.57402	3.34E-17
rs11062767	C	T	0.572966	3.56E-17
rs56082948	A	G	0.567037	3.60E-17
rs71534241	G	T	0.577325	5.16E-17
rs76779686	A	G	0.577453	5.27E-17
rs7350575	A	G	0.577308	6.04E-17
rs150013368	C	T	0.58019	6.76E-17
rs17770235	T	C	0.575255	7.44E-17
rs71579245	A	G	1.36005	0.003587
rs7299033	T	C	1.33777	0.003823
rs3803135	C	T	1.11718	0.003974